



Influence of high dose irradiation on core structural and fuel materials in advanced reactors

*Proceedings of a Technical Committee meeting
held in Obninsk, Russian Federation, 16–19 June 1997*



INTERNATIONAL ATOMIC ENERGY AGENCY

IAEA

The originating Section of this publication in the IAEA was:

Nuclear Power Technology Development Section
International Atomic Energy Agency
Wagramer Strasse 5
P.O. Box 100
A-1400 Vienna, Austria

INFLUENCE OF HIGH DOSE IRRADIATION ON CORE STRUCTURAL
AND FUEL MATERIALS IN ADVANCED REACTORS

IAEA, VIENNA, 1998
IAEA-TECDOC-1039
ISSN 1011-4289

© IAEA, 1998

Printed by the IAEA in Austria
August 1998

The IAEA does not normally maintain stocks of reports in this series.
However, microfiche copies of these reports can be obtained from

INIS Clearinghouse
International Atomic Energy Agency
Wagramerstrasse 5
P.O. Box 100
A-1400 Vienna, Austria

Orders should be accompanied by prepayment of Austrian Schillings 100,—
in the form of a cheque or in the form of IAEA microfiche service coupons
which may be ordered separately from the INIS Clearinghouse.

FOREWORD

The IAEA's *International Working Group on Fast Reactors (IWGFR)* periodically organizes meetings to discuss and review important aspects of fast reactor technology. The fifth meeting in the series, held in Obninsk, Russian Federation, 16–19 June 1997, was devoted to the influence of high dose irradiation on the mechanical properties of reactor core structural and fuel materials.

The IAEA wishes to thank all the participants of the Technical Committee meeting for their valuable contributions, especially the Chairman L. Zabudko. The IAEA officer responsible for this work is A. Rinejski of the Division of Nuclear Power.

EDITORIAL NOTE

In preparing this publication for press, staff of the IAEA have made up the pages from the original manuscripts as submitted by the authors. The views expressed do not necessarily reflect those of the IAEA, the governments of the nominating Member States or the nominating organizations.

Throughout the text names of Member States are retained as they were when the text was compiled.

The use of particular designations of countries or territories does not imply any judgement by the publisher, the IAEA, as to the legal status of such countries or territories, of their authorities and institutions or of the delimitation of their boundaries.

The mention of names of specific companies or products (whether or not indicated as registered) does not imply any intention to infringe proprietary rights, nor should it be construed as an endorsement or recommendation on the part of the IAEA.

The authors are responsible for having obtained the necessary permission for the IAEA to reproduce, translate or use material from sources already protected by copyrights.

CONTENTS

SUMMARY	1
Current status of studies on FR fuel and structural materials in the Russian Federation ... <i>V.M. Poplavsky, L.M. Zabudko</i>	7
Neutron irradiation effects in fusion or spallation structural materials: Some recent insights related to neutron spectra	15
<i>F.A. Garner, L.R. Greenwood</i>	
Status and possibility of fuel and structural materials experimental irradiation in BN-600 reactor. Stages of BN-600 reactor core development	37
<i>B.A. Vasiljev, A.I. Zinovjev, A.I. Staroverov, V.V. Maltsev, A.N. Ogorodov</i>	
Performance of FBTR mixed carbide fuel	47
<i>S. Govindarajan, P. Puthiyavinayagam, S. Clement Ravi Chandar, S.C. Chetal, S.B. Bhoje</i>	
Post-irradiation examination of mixed (Pu, U)C fuels irradiated in the fast breeder reactor	57
<i>R. Baldev, K.V. Kasiviswanathan, V. Venugopal, N.G. Muralidharan, A. Ramabathiran, N. Raghu, J. Joseph, S. Kurien, B. Venkataraman, M.T. Shyamsunder, S. Murugan, K.A. Gopal, P.V. Kumar, P. Kalyanasundaram</i>	
Development of vibropac MOX fuel pins serviceable up to superhigh burnups	69
<i>A.A. Mayorshin, G.I. Gadzhiev, V.A. Kisly, O.V. Skiba, V.A. Tzykanov</i>	
Assemblies and fuel pin behaviour under irradiation in FBR BN-350	93
<i>V.N. Karaulov, A.P. Blynski, I.L. Yakovlev, E.V. Kononova</i>	
In-pile tests and post-reactor investigations of fuel pins with U-Pu fuel	107
<i>L.I. Moseev, A.N. Vorobyev, L.M. Zabudko, B.S. Kiryanov, S.I. Porollo, S.V. Shulepin, S.A. Antipov, T.S. Menshikova</i>	
Inner wall attack and its inhibition method for FBR fuel pin cladding at high burnup	119
<i>Xu Yongli, Long Bin, Li Jingang, Wan Jiaying</i>	
Material properties of a high-dose irradiated martensitic wrapper: Steel 1.4914	129
<i>E. Materna-Morris, K. Ehrlich</i>	
The performance of type EP-450 ferritic-martensitic steel under neutron irradiation at low temperatures	139
<i>V.S. Khabarov, A.M. Dvoriashin, S.I. Porollo</i>	
Post-irradiation examination of Ti or Nb stabilized austenitic steels irradiated as BN-600 reactor fuel pin claddings up to 87 dpa	145
<i>S.I. Porollo, A.N. Vorobyev, S.V. Shulepin</i>	
Influence of swelling and creep data on PFBR core design	153
<i>P. Puthiyavinayagam, S. Gopal, S.J. Winston, S. Govindarajan, S.C. Chetal, S.B. Bhoje</i>	
Development of martensitic steels for high neutron damage applications	169
<i>D.S. Gelles</i>	
Irradiation creep of austenitic steels irradiated up to high fluence in the BOR-60 reactor	179
<i>V.S. Neustroev, V.K. Shamardin</i>	
Influence of high dose irradiation on structure and fracture of the C0.1-Cr16-Ni15-Mo3-Nb steel	189
<i>S.A. Averin, A.V. Kozlov, E.N. Shcherbakov</i>	

Variability of irradiation creep and swelling of HT9 irradiated to high neutron fluence at 400–600°C	197
<i>M.B. Toloczko, F.A. Garner</i>	
A problem to determine short term mechanical properties changes of ferrite-martensite and austenitic steels as materials of fuel assembly of fast reactors under high dose neutron irradiation	211
<i>A.V. Kozlov, A.S. Averin, S.V. Brushkova, G.V. Kalashnic</i>	
Swelling and in-pile creep of neutron irradiated 15Cr15NiTi austenitic steels in the temperature range of 400 to 600° C	223
<i>R. Hübner, K. Ehrlich</i>	
In-pile strength of austenitic steels for fast reactors fuel pin cladding	231
<i>V.V. Popov</i>	
A re-evaluation of helium/dpa and hydrogen/dpa ratios for fast reactor and thermal reactor data used in fission-fusion correlations	239
<i>F.A. Garner, L.R. Greenwood, B.M. Oliver</i>	
LIST OF PARTICIPANTS	251

SUMMARY

1. FUEL MATERIALS

Over 40 years of intensive multinational development, considerable experience with highly irradiated MOX fuel has been accumulated. In Europe, about 8000 fuel pins have reached burnup values of 15 at.%. Some experimental pins have attained burnup levels of 23.5 at.% in PFR and 16.9 at.% in PHENIX. More than 4000 fuel pins with pellet MOX fuel were irradiated in BN-350 and BN-600. The maximum burnup in BN-600 is ~12 at.%. Experience is being acquired with MOX fuel with high Pu content for its use as actinide burner. From the irradiation results obtained from BOR-60, BN-350, and BN-600, it may be concluded that there are no significant differences in performance among UO_2 , PuO_2 and MOX fuels, but additional experimental support for such a conclusion is required.

In addition, MOX fuel has been studied in vibro-packed form in The Russian Federation and in the United Kingdom, where vibro-packed fuel was used extensively in DFR, principally in granular form at very high burnup levels, often in excess of 20 at.%. While this fuel was found to give satisfactory performance at reference ratings up to 450–500 W/cm, its use at high ratings in excess of 500 W/cm was often associated with abnormally high cladding corrosion rates. The latter were attributed to loss of fuel stability at high power ratings, and a parametric study of the data failed to reveal any sensitivity to O/M ratio, clad composition or Pu content. After the repetition of these observations in PFR vibro fuel, the UK abandoned further development of this fuel type in favour of the use of annular MOX pellet fuel, which was eventually taken successfully to burnups in excess of 23% in PFR, with no problems being attributed to the fuel itself. Their excellent performance allowed high irradiation exposures of advanced cladding material and wrappers.

In The Russian Federation, for BOR-60 applications, techniques have been found to maintain stable MOX vibro-packed fuel densities and to reduce the O/M ratios in this fuel type — two features identified as contributing to high cladding corrosion values — primarily through the use of uranium getter. Use of these modifications has allowed some vibro-packed fuel pins, clad in ferritic-martensitic material, to reach record burnups of about 35 at.% over a 10 year period, with ratings of ~450 W/cm at the start of irradiation. This performance must be maintained when the fuel is exposed under commercial conditions at high flux/ratings.

In India, the use of mixed carbide fuel with 70 at.% PuC used as driver fuel for FBTR Mark 1 cores will continue, following the successful operation of FBTR Mark 1 carbide fuel to 30 000 MW·d/t without fuel failure. The post-irradiation examinations of this fuel indicates that exposure could be comfortably increased to 50 000 MWd/t, with linear ratings as high as 400 W/cm. However, the MOX fuel for India's prototype fast reactor will be used with a power output of 500 MWe.

Work on high burnup fuel in the United States of America was terminated when the LMR programme was discontinued.

2. STRUCTURAL MATERIALS

The primary limitation for attainment of high burnup is associated with the integrity of the cladding, and not with any inherent properties of the fuel. When the cladding is breached

to allow release of fission gas and solid isotopes, as well as fuel to the reactor coolant, this requires further burnup to be terminated. A number of persistent themes have emerged as common observations and developments in all countries. Each of these themes are presented separately in the following sections.

2.1 Variability of response in nominally similar materials and environments

There was often a great difference in the amount of data scatter from various types of experimental sources. With a single, well controlled variable, the data scatter was minimal and the fundamental dependences were easy to identify and model. In other data collections from real operating components there was often a wide amount of scatter that sometimes precluded the definite identification of the principle variables and degradation mechanisms responsible for the response to the irradiation environment. While the results of the controlled single variable experiments can be used to help analyse such complex data fields, the origin of such large scatter is uncertain.

Many of the simultaneously contributing processes involved in fuel pin evolution are inherently stochastic in nature and cannot be defined with precision. Crack propagation and corrosion fit this description. Second, there are large spatial and temporal variations in all important environmental variables across each structural and fuel component, and also between components. Therefore, a complex interaction in stress and other variables arises between each of the components in any given structural ensemble. Results of analysis of BN-350 creep and swelling data have been interpreted in the light of such variations. It may be noted that the larger amount of data scatter often was directly correlated to the variability of microstructure and microchemistry in the steels arising from insufficiently well controlled production processes.

A major conclusion is that the highest priority be given to development of both stringent material specifications and production process control.

2.2 Paths toward improved structural material

With one significant exception, most countries are following one or both branched paths in the development of improved materials. On the first branch, the attempt is being made to extend the duration of the incubation period of void swelling in low nickel ($\leq 18\%$) austenitic steel. In all countries with such programmes this approach has resulted in significant delay of the onset of swelling, often to doses on the order of 80–100 dpa (displacement per atom). Given the inherent phase instability of these steels under irradiation, such an approach entails some uncertainty, since the microchemical and microstructural evolution is often found to be very sensitive to details of reactor operational histories, not all aspects of which can always be anticipated. Once the transient regime of swelling is terminated, austenitic steels have the potential to swell at $\sim 1\%$ /dpa and failure arising from swelling-related problems.

The second branch of material development has often been pursued simultaneously with the first branch in many countries and relies on the significantly lower swelling rate inherent in ferritic and ferritic/martensitic alloys. In this path, the major limiting property now becomes radiation-induced embrittlement rather than void swelling.

In both branches, the major focus of research and development activity has been the development and maintenance of stable phases and microstructures, a requirement that has been found to be strongly associated with maintenance of desirable properties. There is some concern that incompatibility might develop at very high burnup if austenitic cladding is to be included in a martensitic or ferritic-martensitic wrapper.

The single most significant exception to these two branches was that of the use of the high nickel Nimonic PE16 alloy in the UK. Based on a long prior history with this alloy, the UK fortunately found a microstructurally-stable, swelling resistant alloy early in its material development effort. In the UK, this material and its production have been optimized, and very high burnup (~25%) levels have been achieved with very low failure rates at doses approaching ~150dpa.

2.3 Voids

Once the void swelling value reaches levels in excess of several per cent, it dominates not only the dimensional stability, but controls the creep rate, phase stability, embrittlement characteristics and, to a lesser extent, properties such as elastic modules, and the thermal and electrical conductivity. Some investigations have shown that the electrical conductivity could be used to measure the void swelling. *It may be concluded that deviations of the resistance change from the theoretically predicted values could be used to estimate the microchemical contributions to resistivity change as well.*

Most significantly, the primary concern resulting from void swelling was that of void related extreme embrittlement or EES. In many cases the life-limiting factor for fuel pins and other structural components was the EES phenomenon. The EES is most likely also going to be a major end-of-life concern for austenitic near core internal components. It has been shown that the irradiation creep of martensitic steels is lower than that of austenitic steels, primarily due to the lower swelling rate of these steels. The creep-swelling relationship, however, appears to be independent of the differences in the crystal structure.

2.4. Environmental interactions with EES

A number of investigations have been devoted to the deleterious influence of corrosion and intergranular attack resulting from fission products that accumulate during high neutron exposure. A Chinese study explored such effect in a simulated environment. Russian studies have shown that such attack would provide extreme cracks on the inner surface of cladding, and that these cracks can initiate the EES failure mechanism. It has been of particular concern whether such corrosion attack problems would accelerate at higher burnup levels.

2.5. Inherent superiority of martensitic steels

A number of investigations have concentrated on the performance of ferritic-martensitic steels. Although the compositional paths taken in such development varied from country to country, the performance of high dpa dose was generally superior to that of austenitic steels. However, there are several qualifications to this statement. First such steels must be limited to somewhat lower temperature ranges since their strength falls off strongly at high temperatures. The "Achilles heel" of martensitic steels is the development of large shifts in ductile to brittle transition temperature at lower irradiation temperatures. This can be

partially avoided by the use of a higher inlet temperature, but in BN-350 such steel has served very well in spite of the low inlet temperature. One study showed that in one such steel there was an initial period in which the steel was most brittle and then some recovery ensued at higher exposure. This behaviour suggests that the steel is not completely phase-stable under irradiation. Smaller levels of instability have been observed in other austenitic steels. *In terms of actual demonstrated performance however, martensitic steels are clearly the superior path to high dpa exposure*

2.6. Technique development

Innovative ways to assess the performance of fuel pins are continually being developed. Studies have explored the limits of currently available techniques to adequately predict such performance.

The study of the influence of high dose irradiation on performance of reactor materials must also be developed in terms of such fundamental processes as evolution of microstructure and radiation defects in materials. Experimental validations must be supported by fundamental investigations to provide the proper understanding of the material performance.

3. USE OF FAST REACTOR DATA FOR OTHER REACTOR CONCEPTS

Fast reactor data have provided and will continue to provide most of the high dose data that can be applied to light water power reactors, fusion reactors and accelerator-driven spallation neutron devices. Combined with data from some high flux thermal test reactors, such as SM-2 and HFIR, these data must form the bases of predictions for the other reactor systems.

In some cases, the data from fast reactors can be directly applied to the other systems, but in general the differences in neutron flux-spectra must be considered and some adjustments must be made prior to the application of the data to the new environment. The most important features of such "translations" involve solid and gaseous transmutation products and related differences in the displacement rate.

Given the continuing trend of experimental reactor shutdowns world-wide (EBR-II, FFTF, RAPSODIE, DFR, PFR, KNK-2, etc.), it is particularly important that current operation of reactor facilities be maintained, and that their irradiation services be made available to these other reactor programmes.

4. CONCLUSIONS

1. Within the span of 40 years of intensive multinational development, great experience on fast reactor MOX fuel pins has been accumulated.
2. It is apparent that the cladding, rather than the fuel or the wrapper material, provides the greatest potential limitation to reaching high dpa levels, and thereby hinders high fuel burnup. The major degradation problems are void swelling for austenitic and, to a lesser extent, embrittlement at low temperatures for martensitic and ferritic-martensitic steels. The maintenance of desirable properties is directly coupled with maintaining a stable microstructure against the action of neutron induced displacements. The most important

requirements for such stability are well-defined specifications and well-controlled production methods.

3. There are three paths to achievement of high fuel burnup: (1) low nickel austenitic steel; (2) martensitic and ferritic-martensitic alloys, and (3) high nickel nimonic PEI6 alloy. Of these, the lower-nickel austenitics are inherently unstable during irradiation, and eventually must swell. If fuel burnups of >20% are to be achieved in fast reactors, the combination of austenitic cladding and the use of one of the other two swelling resistant materials for wrappers may pose a problem.

**NEXT PAGE(S)
left BLANK**

CURRENT STATUS OF STUDIES ON BN FUEL AND STRUCTURAL MATERIALS IN THE RUSSIAN FEDERATION

V.M. POPLAVSKY, L.M. ZABUDKO
Institute of Physics and Power Engineering,
Obninsk, Russian Federation



XA9848037

Abstract

Review is made on the principle factors which restrict the BN fuel life time: dimensional changes of wrappers and cladding due to steel swelling and irradiation creep; fuel-cladding mechanical and chemical interaction, fuel mass transfer, deterioration of mechanical properties of cladding steel under irradiation. The information on the programs of structural materials development is given. The main results on the advanced BN fuel development are presented.

1. The main limiting features of life time of fuel elements with oxide fuel

Calculational investigations confirmed by the BN reactor operational experience allow the following principle factors affecting the endurance reliability of fuel elements and sub-assemblies (SA) in general, to be recognized:

- a strong dimensional change of SAs elements in the result of steel swelling and irradiation creep;
- processes which occur inside fuel elements (mechanical and chemical interaction of fuel with cladding, fission gas pressure, fuel mass transfer).

1.1. Dimensional changes of the SA wrapper and fuel pin cladding

Swelling and irradiation creep of wrapper materials result in wrapper elongation, increase of cross-sectional dimensions, changes in a cross-section shape, SA bending and thus, in significant contact interacting forces. At the initial stage of BN-350 and BN-600 reactors operation the limits in fuel burn-up were related to these very dimensional changes of wrappers made of steel 16Cr-IIINi-3Mo in its austenitized state. After the wrapper steel had been replaced with steel 16Cr-IIINi-3Mo in its cold-worked state the maximum fuel burn-up in the BN-600 reactor achieved 8,3 % h.a. According to the results calculated analysis based on post irradiation measurements of the wrapper geometry in cooling ponds as well as some measurements of SA removal forces in the course of refuelling the wrapper changes didn't make any effect on the burn-up restriction in the BN-600 core, at least under the values of 9,5 - 10at.%. However it was definitely decided to replace the previous steel with the steel of ferritic-martensitic type, EP-450. Thus solving the problem of wrapper deformation even at higher burn-up values. Nowadays the third type of the core is implemented in the BN-600 reactor with SAs' wrapper made of the EP-450 steel.

The mechanical interaction between the fuel bundle and the wrapper is one of the most serious reasons for a high burn-up restriction until refractory low-swelling cladding steels are created. In order to decrease contact forces between fuel pins with a wire spacer some design changes are possible. They are related to a certain change in a wire pitch as well as in a relative diameter of a wire spacer. It is possible also to reduce the wrapper rigidity by making its wall thinner. However all these measures proved to be inefficient.

Besides the problem of mechanical interaction of fuel pin bundle and wrapper the severe degradation (loss of strength and ductility) of cladding mechanical properties was observed for fuel pins with maximum dose higher than 75 - 80 dpa when the cladding deformation was 4 - 7%. The only way-to solve these two problems is to develop low-swelling cladding steel.

1.2. In-fuel pin processes

1.2.1. In the BN-600 core of the first loading type, to be more precise, in the zone of high enrichment actually each run resulted in unsealed fuel pins in terms of gas and delayed neutron signals when the burn-up values exceeded 5,5 -6 at.%. The work on finding out the reasons for loss of tightness in fuel pins of the high enrichment zone (HEZ) consisted in a calculated analysis of the impact of operational conditions on fuel pins strength, a post-reactor study of fuel pins in the hot cell laboratory, an analysis of the results obtained. The main specific feature for the HEZ SAs, in contrast to SAs of the low enrichment zone (LEZ), was their scheduled reshuffling after each run in the direction closer to the center of the core with their rotation by 180°. At that very time fuel elements were subjected to a certain power ramp which caused additional mechanical interaction between fuel and cladding in the course of reactor coming up to power. Besides it turned out that in many fuel elements of the HEZ SAs there was mass transfer in the form of a fuel column rupture thus resulting in the enhanced aggressive fission yield and corrosion cracking of cladding under stress. We carried out the analysis and saw that there is a direct relationship between fuel column ruptures, initial linear rating (before reshuffling), power ramp and probability of fuel element failure. The following conclusions were made:

- if maximum linear rating before reshuffling was less than 400 - 410 W/cm, SAs reshuffling and rotation are allowable only if power ramp is less than 50 W/cm,
- if initial linear rating was high enough (more than 400 - 410 W/cm), SAs reshuffling is allowable even in the case when power ramp is up to 80 - 90 W/cm.

With the aim to eliminate unsealed fuel pins in the BN-600 core certain measures were taken. The organizations OKBM (N.Novgorod), VNIINM (Moscow), IPPE (Obninsk) and BN-600 participated in the work. First of all, the practice of SA reshuffling and rotation accompanied by a power ramp was ruled out. Though the analysis of reasons for loss of tightness didn't reveal a definite impact of high linear power values ($q = 540$ W/cm) on fuel pins loss of tightness, the decision was taken to decrease the maximum value of linear power. In this case the foreign experience was taken into consideration. In order to create more beneficial conditions for fuel operation three zones of enrichment were introduced instead of the previous two ones to flatten power density field. And finally, structural materials used for wrappers and clads were changed for austenitic steel in its cold-worked state, thus increasing burn-up. So in the core of the second loading type loss of fuel pins tightness was eliminated.

1.2.2. According to the numerous calculated and experimental investigations, in case of no reshuffling which can result in fuel mass transfer and power ramp, by choosing a proper value of the smeared density it is possible to avoid considerable increase in clad damage caused by the mechanical impact of the fuel up to the burn-up value of 20 at.% with allowance for the scheduled transient conditions.

To hold the clad integrity in the hottest cross-sections under the fission-gas conditions is a more complicated task at high burn-up levels. In this case the approach consists in development of high-temperature strength steel types and optimization of a fuel element design (increase in a clad wall thickness and extension of gas plenum sizes). However as the high burn-up core physics requires reduction in its steel fraction, there is no definite opinion on the most optimum ratio of a cladding wall thickness and its diameter. Everything will be determined by the progress in development of low-swelling types of steel with high level of high-temperature strength.

It is reasonable to increase the clad wall thickness even from the point of view of resistance to cladding corrosion often happened on its fuel side. The post-reactor study of BN-600 fuel pins with uranium oxide as a fuel performed in the hot-cell laboratory of the IPPE showed an insignificant value of the clad corrosion damage. For instance, for fuel elements irradiated up to the burn-up of 11 at.% (irradiation dose of 87,5 dpa) the corrosion depth didn't exceed 30 μm , the interaction nature was intercrystalline. There was no notice of any relationship between the depth of corrosion interaction and fuel burn-up (with the values equal to 7,4- 11,8at.%). As for the results of investigations of pins with MOX fuel irradiated in BN-350 and BOR-60 (the maximum burn-up value was 12,6 at.%), they showed a more serious corrosion damage of cladding (up to 100 μm). In all the cases clads were made of austenitic steel. Additional investigations are necessary to confirm the feasibility to achieve the burn-up of 20 at.% from the point of view of corrosion damage of cladding with MOX fuel.

2. The main trends of improvement of fuel clad and SA wrapper structural materials

2.1. In 1987 the first comprehensive program on the development of structural materials was implemented /1/. It was performed under the supervision of the R&D Institute of Inorganic Materials (VNIINM), Moscow. The principle goal of the Program consisted in choosing of materials for cores with the maximum burn-up of 10 at.% of the BN-350 and BN-600 reactors. Their chemical composition is presented in Table 1.

Table 1. Chemical composition of the materials for BN-350 and BN-600 standard SAs.

Steel type	N	Si	Mn	P	Cr	Ni	Mo	Nb	Ti	A
ChS-68 (cladding)	0,05-0,08	0,3-0,6	1,3-2,0	0,45-0<3	15-16,5	14-15,5	1,9-2,5	-	0,2-0,3	0,001-0,005
EP-450 (wrapper)	0,1-0,15	0,6	0,6	0,03	12-14	0,3	1,2-1,8	0,25-0,55	-	0,004

Since 1992 the materials indicated in Table I are adopted as standard in the cores of these reactors.

By now more than 400 SAs with the EP-450 steel wrapper have been irradiated in the BN-600 reactor. The swelling and irradiation creep of the steel was investigated using statistical analysis of dimensional measurements conducted on spent subassembly wrappers located in the storage pool after irradiation in the BN-600 reactor. We analysed the results of wrappers geometry measurements which were carried out on the BN-600 reactor with spent SA (50 SAs). The following results were obtained on irradiation creep data of EP-450 steel :

- the creep modulus increases in the temperature range of 480 - 490 C, that can be explained by a superposition of thermal creep deformation upon the irradiation creep deformation;
- the mean value of the modulus is equal to $0.25 \times 10^{-6} (\text{MPa} \times \text{dpa})^{-1}$, the maximum modulus value is equal to $B = (0.7-1) \times 10^{-6} (\text{MPa} \times \text{dpa})^{-1}$ (in the temperature range of $T < 480\text{C}$);
- there is some trend to an irradiation creep modulus increase at $T = 350 \text{ C}$.

The following results were obtained on EP-450 swelling:

- very smooth temperature dependence of steel swelling,
- the dose dependence of swelling is rather low at $\approx 0.004\% / \text{dpa}$.

The results of post-irradiation study of EP-450 wrappers confirmed its high irradiation stability.

In accordance with a special decisions in the BN-600 more than 27 000 fuel pins with ChS - 68 CW cladding have been irradiated up to maximum burn-up more than 10 at.%, more than 2500 fuel pins reached doses more than 80 dpa (the maximum dose of 93,7 dpa). The irradiation preformance of all fuel pins was good enough, but PIE revealed high swelling of cladding steel and degradation of cladding mechanical properties.

2.2. The second comprehensive program includes several trends of the development of new structural materials for cladding with the aim to achieve 15% h.a. They are as follows:

- further improvement of austenitic stainless steel in order to increase its strength and to decrease its swelling by means of optimization of dope composition; improvement of metallurgical and technological processes,
- improvement of ferritic-martensitic steel with the aim to be used in cladding,
- development of ODS ferritic-martensitic steels, with satisfactory strength properties at the temperatures of 700 °C.

As it was mentioned earlier, austenitic steel swelling which results in thermomechanical interaction with a non-swelling wrapper can become an insuperable obstacle in achieving the burn-up higher than 15at.%. One of the principle ways to solve this problem consists in using ferritic-martensitic steel for cladding as well. By now two SAs (127 fuel pins in each, uranium dioxide as a fuel) have been irradiated in the BN-350 reactor, with the maximum burn-up being 12 at.% and the maximum dose of 45 dpa. In the BOR-60 reactor 13 SAs have been irradiated (each contains 37 fuel pins with a vibro-compact MOX fuel) with the maximum burn-up of 15- 26 at.% and the maximum dose up to 144 dpa. The maximum fuel burn-up achieved in experimental fuel pins in dismountable subassembly is 30.3 at%. In both reactors the initial temperatures of cladding were rather high for the steel of this type (680 - 700°C). The results of irradiation and PIE are positive.

In accordance with this program another group of fuel pins with their clads made of steel EP-450 has been prepared to be irradiated in the BN-600 reactor. 5 Sas with EP-450 cladding pis in outer row of assembly were loaded in the core in 1996. Additional experimental verification of the steel corrosion and high-temperature strength is required, with the steel being irradiated at the maximum clad temperatures of 680 - 690 °C under the conditions of a power reactor.

For a number of years the work on the technology and investigation of a set of properties of the ODS steel as advanced cladding materials for BN reactor fuel element is being performed in the Institute of Physics and Power Engineering. A considerable amount of work has been carried out on development and investigation of the model ODS steel based on steel 13Cr-2Mo. The effect of this steel alloying with vanadium, titanium, aluminium, tungsten, niobium has been studied. Oxides of yttrium, titanium, calcium were used as hardening particles.

The transition from the ODS steel with its ferritic structure to the steel with a two-phase ferritic-martensitic structure is of great interest. Based on new developments of the ODS steel technology steel samples with the ferrite content of 40 - 60% were obtained. Nowadays steel 12Cr-2Mo-Nb-B-P-Y₂O₃ (CaO) accepted as the basic one. The samples of this steel were irradiated in BR-10 at temperatures of about 700 C in order to investigate their high-temperature strength . Now the PIE of samples is under way.

3. Development of fuel materials

At present two reactors, BN-350 and BN-600 operate with a uranium oxide fuel, the MOX vibro-compact fuel is used in the BOR-60 reactor and uranium nitride is used as a fuel in the BR-10 reactor.

3.1. MOX-fuel

A special program of work has been developed and implemented with an aim to introduce the MOX fuel. The BN-800 core has been designed on the basis of the MOX fuel since the very beginning. As for the MOX-fuelled BN-600 core its improved design is under development now. Two technologies were suggested and are supported for the MOX-fuel fabrication, a pellet technology and a vibro-compact one. The information on SAs with the MOX fuel is given in table 2.

Table 2. MOX-fuelled SAs irradiated in the BN-350, BN-600 and BOR-60 reactors (end of 1996).

Reactors	Number of SAs	Max burn-up % h.a.	Max dose, dpa
BOR-60	350(vibropack fuel)	30.3	≈160
	10 (pellet fuel)	16.7	87
BN-350	14 (pellet)/2(vibro)	10.8/7.2	65/43
BN-600	6(vibropack fuel)	9.6	76,7
	12 (pellet fuel)	11.8	80.7

3.2. Carbide and nitride fuels

The experimental study of the carbide fuel was started in the BR-5 reactor. The core with uranium monocarbide was in operation from 1965 to 1971. The maximum burn-up amounted to 6.2at.% .

Now the second loading of BR-10 core with uranium mononitride fuel is under operation, the maximum burn-up - 8 at%. In first mononitride fuel loading several fuel pins were successfully irradiated up to 9at.%. This time a special decision is preparing to increase maximum burn-up up to 10at.% .

In the BOR-60 6 subassemblies with UC, UNC, UPuC were irradiated up to 10 at.% . Successful tests confirmed the feasibility to achieve 10at.% in He-bonded fuel elements with carbonitride fuel [2,3].

3.3. Fuels for fast reactor - actinide burner

In Russia extensive study on fast reactor cores which can efficiently burn plutonium and minor actinides is under way in order to demonstrate the possibility of actinide utilization in BN-600 and BN-800 reactors. Technological study on development and fabrication of MOX fuel with high Pu content and fuels without Pu content (inert matrix fuels) are carried out .

3.3.1. MOX with high Pu content

First experience with high Pu content oxide fuel (100%) was obtained in BR-10 where two core loadings with PuO₂ were irradiated . The results of PIE on PuO₂ fuel rods

performed which were irradiated up to 12 at.% and traditional MOX fuel rods which were irradiated in BOR-60, BN-350 and BN-600 reactors allowed to make the following conclusions on irradiation behavior of high Pu oxide fuel/4/.

- There is no difference between PuO_2 or UO_2 or MOX fuels for swelling, gas release, fission products behavior, microstructural changes. These properties changes depend on fuel burn-up and temperature.

- Fuel cladding interaction increases with the Pu content increase. The lowering of the initial O/M ratio in the PuO_2 fuel and the utilization of improved cladding steel could probably decrease cladding corrosion damage to the level of UO_2 fuel pins. But this conclusion needs to be confirmed by experiments.

One experimental subassembly (19 pins) with 40% Pu was irradiated in BOR-60 up to 4.7at.% /6/. The fuel pins were fabricated using vibropac technology. The specific feature of the irradiation behavior of fuel pins is its increased concentration of Pu in the periphery of fuel in middle plane that caused the corrosion damage of the inner cladding surface to the depth of 70mm. It should be noted that this vibropac fuel had low value of O/M ratio (1.94 - 1.95).

Beginning on 1994 the laboratory study on MOX fuel with 45% Pu fabrication is carried out in the VNIINM, Moscow. The fabrication techniques of chemical coprecipitation and mechanical mixing of oxide powders are studied /5/. It is shown that as for mechanical mixed so for coprecipitated powder it is possible to obtain the homogeneous fuel from powder and the solid solution after the sintering. The pellet solubility of fuel was studied also. Now 4 fuel pins are manufactured to be irradiated together with 4 vibropacked MOX fuel (with 45% Pu also) in BOR-60.

In conclusion, there is hope on available irradiation results, that there is no principal difference in irradiation behavior of MOX fuel with high Pu content. However the performance has to be confirmed at higher burn-up levels on a larger statistics mainly in respect of corrosion behavior. Some new decisions in fuel design (particularly, large pellet central hole) has to be confirmed also.

3.3.2. Inert matrix fuels

Use of Pu without U fuel allows the higher Pu consumption rates to be reached. In fuel pin manufacturing, the use of such materials is still a highly innovative concept . Basic research is being conducted on this subject and consideration is being given to ways of identifying all potential and promising uses of the concept.

The development of the PuO_2+MgO fuel is carried out in the IPPE, Obninsk /8/. At the first stage the work was carried out with Th and U, as simulators. The chemical precipitation techniques was used. The most optimum parameters of fabrication process were chosen. The following out-of-pile properties have been studied:

- homogeneity of UO_2 distribution,
- hardness, ultimate strength
- thermal conductivity, melting temperature
- fuel-matrix-clad interaction, phase changing.

Several pellets were reprocessed, the optimum solution parameters have been determined. Two fuel pins were fabricated for the BR-10 irradiation, the loading is expected to be in the nearest reactor shut-down.

Several pellets of PuO_2+MgO have been fabricated using the same techniques .

One of the principal criterion of fuel with inert matrix its reprocessing ability. From this point of view solid solutions of plutonium carbides, plutonium nitrides and inert matrix ZrC, ZrN are seems to be the best candidates.

Two synthesis processes of UC-ZrC and PuC+ZrC were developed in VNIINM, Moscow /7/:

- from initial metals,
- from the initial oxides.

Using these techniques the following fuels were fabricated and irradiated in the BOR-60 reactor:

- 56%UC +44%ZrC, 55% PuC+45%ZrC for the core region,
- 15%UC +85%ZrC for the blanket region

The subassembly with 19 fuel pins was irradiated in the BOR-60 , 7 fuel pins contained 55%PuC+45%ZrC fuel , 12 fuel pins contained 56%UC+44%ZrC. Irradiation parameters are shown in Table 3.

Table 3. Irradiation parameters of inert matrix fuel in BOR-60

Parameter	Value
Max.burn-up,% at.	8.
Max.fluence,cm ⁻² ,E>0.1Mev	4.43*10 ²²
Max. linear rating,kW/m	40.2
Max clad temperature, C	635±25

All fuel pins were intact.

The principal PIE results of inert matrix fuel are the following:

- no deformation of cladding (measurement error ±0.01 mm),
- gas release from the fuel less than 2%,
- fuel swelling is equal to 1% per 1% of fuel burn-up,
- the fine-grain structure and round-form voids uniformly distributed over fuel volume (as for the unirradiated fuel),
- instead of initial two phases only one phase was observed , which seems to be rather favourable factor for fuel performance,
- homogeneous distribution of Pu,
- local carburization of cladding only in the upper part of pins.

Technological research on synthesis of solid solution of UN+ZrN from initial oxides and fabrication of fuel columns with different density , shape and size was performed also. The properties of PuC+ZrC are close to the properties of PuN+ZrN solid solution. This fact and existing experience of UN+ZrN fabrication proved the feasibility of carbothermal synthesis of PuN +ZrN from the initial oxides. The feasibility of fabrication of UN+ZrN, PuN+ZrN solid solution from the initial metals was demonstrated also.

Today the PuO₂+MgO and PuN+ZrN fuels are preparing for the irradiation in the BOR-60 reactor in dismountable subassembly.

In conclusion, even if small irradiation experience with inert matrix fuel allows to hope that irradiation behavior of some fuel types with inert matrix will be satisfactory numerous study will be neede to check this concept.

REFERENCES

- [1] F.G.Reshetnikov, Yu.K.Bibilashvili, et al. Development of structural materials and problem of increasing fuel burn-up. Proc. of Int.Conf.on Fast Reactors and Related Fuel Cycles, 1991, Kyoto, Japan, v.1, p.7.6-1.
- [2] V.M.Murogov, V.M.Poplavski, L.M.Zabudko. Fast reactor endurance reliability and experience of fuel element and subassembly operation in Russia. Proc. of an Advisory Group meeting , Vienna, December 1994.
- [3] A.A.Mayorshin , Yu.K.Bibilashvili L.M.Zabudko et al. Use of carbide - nitride fuel in the USSR : a review. Proc. of IAEA TCM, Vienna, 1987.
- [4] V.M.Poplavski, L.M.Zabudko, L.I.Moseev et al. Some results on development, irradiation and post-irradiation examination of fuels for fast reactor - actinide burner. Proc. of IAEA TCM, Vienna, November 1995.
- [5] F.G.Reshetnikov, S.A.Antipov, V.A.Astafjev et al.Proc. of Int.Conf.on Evaluation of Emerging Nuclear Fuel Cycle Systems, Clobal 1995, Sept. 1995, France, p.320.
- [6] A.A.Mayorshin, G.I.Gadzhiev, V.A.Kisly et al. Proc. of Int.Conf.on Evaluation of Emerging Nuclear Fuel Cycle Systems, Clobal 1995, Sept. 1995, France, p.1417.
- [7] B.D.Rogozkin, N.M.Stepennova, Yu.E.Fedorov et al. IAEA TCM on Research of Fuel Aimed at Low Fission Gas Release, Moscow, Oct.1996.
- [8] I.S.Kurina, N.N.Shevchenko et al. IAEA TCM on Research of Fuel Aimed at Low Fission Gas Release, Moscow, Oct.1996.



NEUTRON IRRADIATION EFFECTS IN FUSION OR SPALLATION STRUCTURAL MATERIALS: SOME RECENT INSIGHTS RELATED TO NEUTRON SPECTRA

F A GARNER, L R GREENWOOD
Pacific Northwest National Laboratory,
Richland, WA, USA

Abstract

A review is presented of recent insights on the role of transmutation in the development of radiation-induced changes in dimension or radiation-induced changes in physical or mechanical properties. It is shown that, in some materials and some neutron spectra, transmutation can significantly affect or even dominate a given property change process. When the process under study is also sensitive to displacement rate, and especially if it involves radiation-induced segregation and precipitation, it becomes much more difficult to separate the transmutation and displacement rate dependencies. This complicates the application of data derived from "surrogate" spectra to predictions in other flux-spectra environments. It is also shown in this paper that one must be sensitive to the impact of previously-ignored "small" variations in neutron spectra within a given reactor. In some materials these small variations have major consequences.

1 INTRODUCTION

As the fusion materials program continues to investigate the response of various candidate materials to neutron irradiation, it becomes increasingly more obvious that additional attention must be paid to the consequences of differences in neutron flux and spectra, especially in situations where transmutation exerts a significant influence.

A similar realization has developed recently in the various spallation neutron programs currently under consideration[1]. Whereas the elemental and isotopic changes induced by neutron absorption are well-defined, transmutation caused by collisions with very high energy (~ 1 GeV) protons and/or the resultant spallation neutrons produces a complex shower of all possible isotopic species of lesser mass than the original. These new isotopes in turn are subject to both radioactive decay and further transmutation. Thus, accelerator-driven spallation devices will produce changes in material composition and changes in behavior that are correspondingly harder to analyze or predict.

If a given radiation damage process is sensitive to both displacement rate and transmutation-induced or spallation-induced compositional changes, then it may be difficult to identify and separate the individual effects of these two variables. If the transmutant or its precursor also tends to segregate via a flux-dependent process, then additional complexity arises in the translation of data generated in the "surrogate" spectra to produce predictions for the fusion or spallation application.

The problem lies not only in translating data from one reactor spectra to another, but has also been found to sometimes affect the interpretation of data collected from various locations in a given reactor. This

latter concern arises because differences in displacement rate across a reactor core are usually accompanied by spectral variations, which in some alloys are large enough that they can exert a strong influence on transmutation rates per neutron. In stainless and ferritic steels irradiated in fast reactors it was possible to ignore such "minor" variations in spectra, providing the damage was expressed in displacements per atom or "dpa".

Whereas stainless and ferritic steels irradiated in fast reactor spectra experience a relatively small amount of transmutation to solid and gaseous species, the shift to other spectral environments and other materials has led to the realization that solid transmutation products in particular must be studied in more depth, even in fast reactors for some materials of current interest.

This paper addresses some of the recent insights on the impact of both solid and gaseous transmutation products, focusing on a number of material groups that exhibit a strong transmutant response to variations in neutron spectra. Some fraction of this material was reviewed earlier in ref. 2.

With a few exceptions, this paper will not focus on the isotopic details of the various transmutation processes, but will focus only on the chemical and physical consequences of the resultant elemental changes. The isotopic details are contained in the various references cited, however. Solid transmutants will be discussed first, followed by gaseous transmutants.

2. Mo-Re ALLOYS

Molybdenum and its alloys, especially those of the Mo-Re system, have been proposed as potential fusion candidates because of their inherently high melting point and strength, room temperature fabricability, and possession of an acceptable match with the coefficients of thermal expansion of carbon and tungsten[3,4].

Garner, Greenwood and Edwards have shown that Mo-Re alloys will strongly transmute to Mo-Re-Os-Ru-Tc alloys even in the FFTF fast reactor spectra[5,6]. The most important and initially surprising observation of this work is that the transmutation rate per dpa changes strongly across the fast reactor core, as shown in Figures 1 and 2. If transmutation-sensitive data for different irradiation temperatures or different dpa levels are derived from different core positions, this can introduce an uncontrolled and highly synergistic variable into the data analysis.

Even more significantly, the transmutation rate of Re is an especially strong function of the thermal neutron fluence, and in highly-thermalized neutron spectra can lead to the near-total replacement of rhenium with osmium, as shown in Figure 3 for the HFIR reactor. The correlation of data from different test reactors and the extrapolation of such correlations to fusion-relevant spectra is obviously more difficult under such conditions.

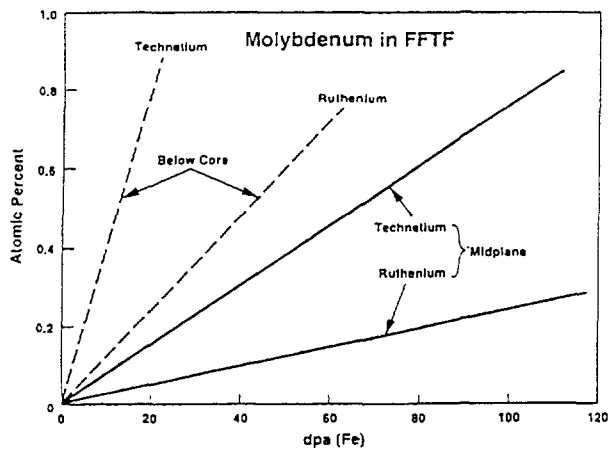


FIGURE 1. Predictions of technetium and ruthenium formation in pure molybdenum during irradiation in FFTF at the core midplane and the center of the below-core basket [5].

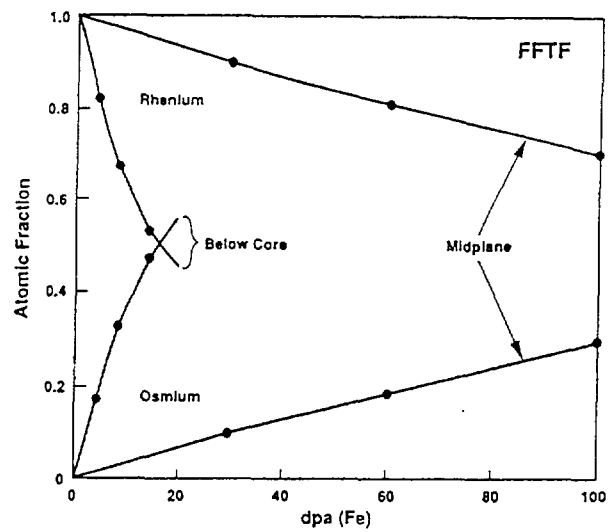


FIGURE 2. Prediction of osmium formation in rhenium during irradiation in FFTF at the core midplane and the center of the below-core basket [5].

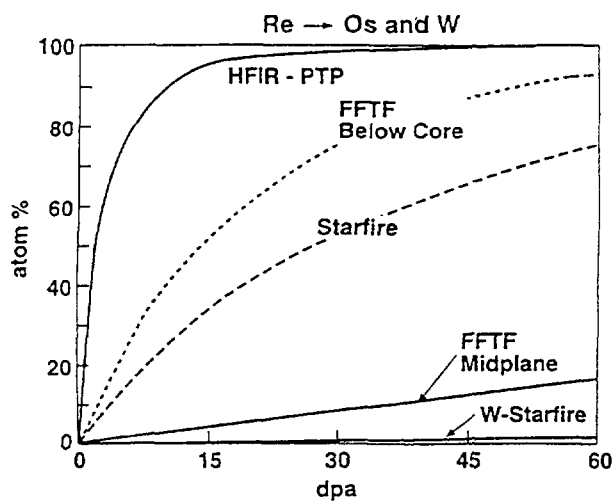


FIGURE 3. Transmutation of rhenium to osmium in various irradiation facilities. Production of tungsten is also shown for the STARFIRE fusion concept; however, tungsten production is negligible in HFIR and FFTF [6].

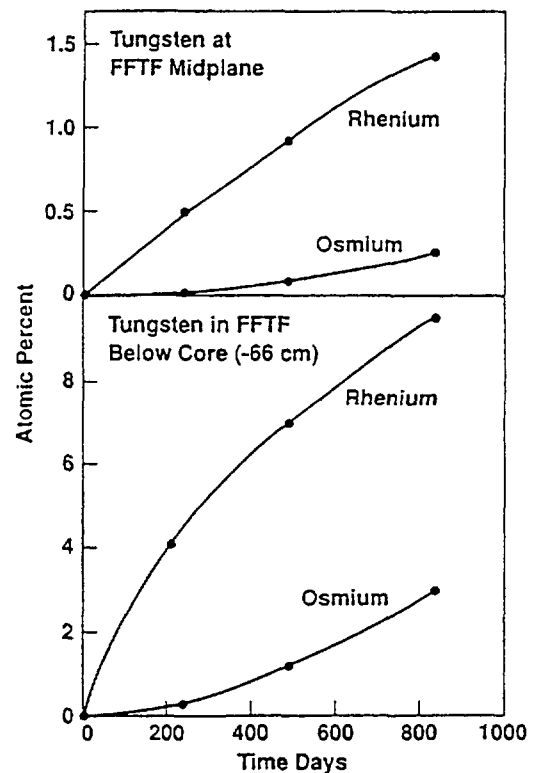


FIGURE 4. Predicted formation of rhenium and osmium from pure tungsten irradiated in FFTF at both the core midplane and below-core basket positions [6].

An additional level of complexity arises from the fact that both Re and Os segregate very strongly during irradiation of Mo-Re alloys. The tendency toward radiation-driven segregation is so pronounced that the equilibrium bcc chi-phase is completely bypassed in Mo-41Re, leading to the formation of a very high density of thin platelets. These platelets are a hexagonal phase, consisting almost entirely of Re and Os[5,7]. Separation of the influence of displacement rate and transmutation rate is thus even more difficult. This problem may be only of academic interest, however, since one consequence of such segregation is a strong embrittlement, that probably disqualifies Mo-Re alloys for most uses in nuclear systems. For instance, studies by Gorynin et al. [8] and Fabritsiev et. al.[9] have shown that relatively low levels of irradiation in the SM-2 mixed spectrum reactor lead to a severe embrittlement and also to a strong loss of electrical conductivity in a wide range of Mo-Re alloys. Hasegawa et. al. showed that, after irradiation of Mo-5Re in FFTF to 7-34 dpa, it was possible to see the encroaching impact of radiation-induced precipitation on ductility even at that low level of Re[10].

3. TUNGSTEN AND TUNGSTEN-CONTAINING ALLOYS

Tungsten is currently being used as a substitute for molybdenum in "low-activation" ferritic steels[11-13]. Pure W or W-Re alloys have also been suggested for plasma-facing components[14,15]. A material produced with a copper matrix reinforced with thin tungsten wires has been irradiated in FFTF as part of a study of potential high heat flux materials[16]. Porous tungsten impregnated with copper is planned for irradiation in HFIR[17] and has been proposed as a material for Tokamak divertor plates[18].

However, low-activation does not imply low-transmutation. All of the various transmutant-related problems discussed earlier for Re are even more pronounced for W, which first transmutes to Re and then to Os, as shown in Figures 4 and 5. Note the large differences in transmutation rate per dpa that exist in typical test positions in FFTF. At only 20 dpa in the HFIR mixed spectrum reactor, 30% of the W will transmute to Re and Os, demonstrating the strong sensitivity of W to thermal neutrons[6].

In some design studies such transmutation is thought to be beneficial, since Re additions to W before irradiation actually improve strength, ductility, recrystallization resistance and machinability, as reviewed in ref. 19. This expectation is judged by the authors of this paper to be rather optimistic, however, since most of the available irradiation data on W and its alloys were developed in fast reactors, (as reviewed in ref. 20) where the impact of transmutation is relatively smaller. Two studies have directly addressed the effects of transmutation due to thermal neutrons[8,21] and focused on resultant losses in ductility.

Garner and Megusar reported that dynamically-compacted tungsten densified 2-3% during fast reactor irradiation to 32-60 dpa in the range 423-600°C[22]. They noted that while such densification may have reflected only a recovery of original porosity, it may have also involved the strong role of transmutation. More importantly, the specimens were found to have become exceptionally brittle during irradiation, which might also arise in part from the influence of transmutation.

No data are known to the authors on the possible role of segregation or precipitation of Re and Os in W alloys, but parallels drawn to the observed behavior of Mo-Re-Os alloys are suggestive of the possibility.

4. COPPER, COPPER ALLOYS AND COPPER-BASED BRAZES

Copper alloys have been proposed for service as high-heat flux components in fusion reactors primarily because of their high thermal conductivity, even though copper is not low-activation in nature[23-25]. Since the electrical conductivity is easier to measure than the thermal conductivity, most experimental studies on highly radioactive copper alloys focus on electrical conductivity measurements. Since the two conductivities are related, it is possible to make predictions of the thermal conductivity.

Transmutation of Cu forms relatively large amounts of Ni and Zn, and smaller amounts of cobalt, all of which strongly decrease the electrical and thermal conductivity[26-32]. On a per atom basis, nickel has the strongest effect. Unfortunately, the Ni/Zn ratio increases at the very high neutron energies characteristic of fusion spectra[27] such that fast reactor data underestimate the conductivity loss for fusion application.

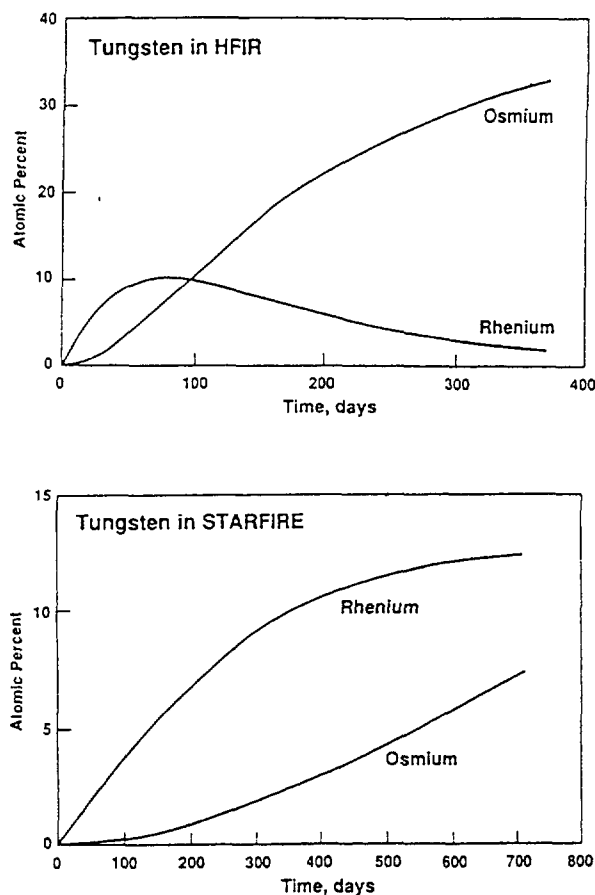


FIGURE 5. Predicted formation of rhenium and osmium irradiated in (a) the PTP position of HFIR at 85 MW, and (b) the first wall position of STARFIRE at 3.8 MW/m² [6]. Note that the relative amounts of osmium and rhenium are reversed in the two reactors after 100 days.

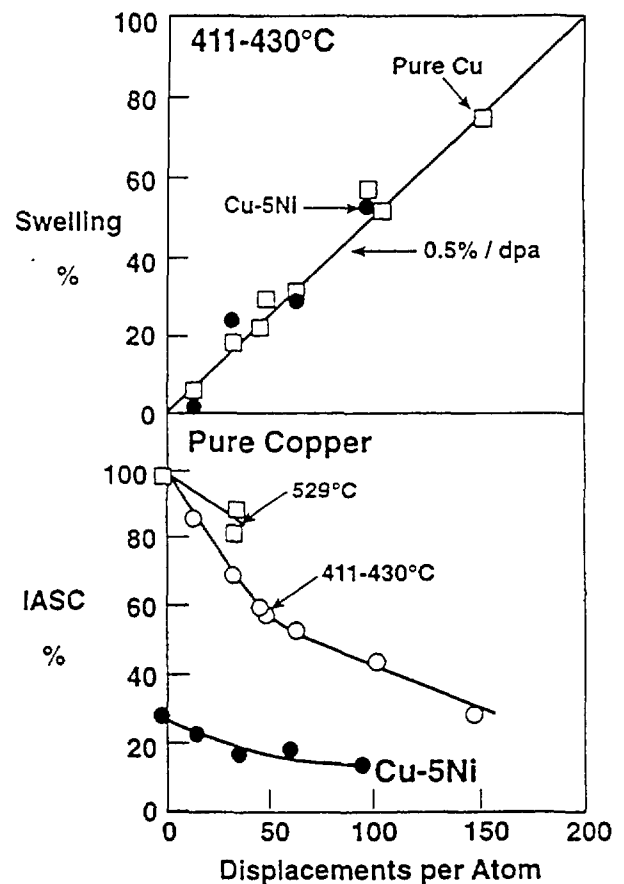


FIGURE 6. Nickel introduced as either an alloy or as a transmutant does not appear to affect the steady-state swelling behavior observed in FFTF, but both voids and transmutants (Ni, Zn, Co) lead to a decrease in the electrical conductivity [29]. Void swelling is less at 520°C.

Interestingly, however, the substantial addition of Ni, and presumably Zn, does not affect the steady-state swelling rate of Cu at $\sim 400^{\circ}\text{C}$, as shown in Figure 6, which also shows the irradiation-induced decrease in electrical conductivity. Voids also contribute to the decrease in thermal and electrical conductivities, however.

Once again there is a substantial variation of transmutation rates for copper, both within and between reactors, significantly complicating the application to fusion spectra of data developed from surrogate spectra. Edwards, Garner and Greenwood[31] have shown, however, that it is possible to separate the influence of voids and transmutants on the electrical conductivity of pure copper. This separation allows the prediction of conductivity losses in other spectra if it can be assumed that the swelling rate of copper is largely insensitive to Ni and Zn concentration, and if it can also be assumed that segregation plays no role in either the void growth or the conductivity change.

Muroga and Garner showed that transmutant nickel segregates to void surfaces in pure copper but zinc does not[33]. In another study Muroga and coworkers showed a similar behavior at grain boundaries during electron irradiation of Cu-Ni and Cu-Ni-Zn alloys[34]. No precipitation occurred as a consequence of this irradiation-induced redistribution, and it therefore appears appropriate to assume that segregation has no net consequences on the change in either electrical or thermal conductivity of pure copper.

Pure copper is a relatively simple system, however, and the potential exists for more complicated interactions between transmutation, segregation and precipitation in more complex alloys. For example, Edwards, Garner and Grant have shown that HfO_2 dispersoids in a copper powder-metallurgy alloy absorb transmutant nickel as the irradiation proceeds[35]. This continuous absorption fortuitously causes a plateau to develop in the electrical conductivity, while the conductivity of other dispersion-hardened alloys continues to decline, as shown in Figure 7a. The HfO_2 dispersoids also are affected by displacive radiation, with the larger particles slowly shrinking, and a new population of thin crystalline platelets of HfO_2 forming in the alloy matrix. This once again demonstrates that radiation-induced segregation and precipitation reactions can have a significant impact on a material's response to transmutation.

Other transmutation-sensitive examples can easily be found in the copper alloy systems described in references 28-30. For example, when considering the relative response of Cu-2Be and Cu-1.8Ni-0.3Be, it is important to remember that the purpose of the nickel in the latter alloy was to more effectively precipitate the beryllium, thereby requiring less Be for a given strength level and also yielding a higher conductivity matrix. Transmutation of Cu to Ni will therefore drive Be from solution. In Cu-2Be the initially rather low conductivity at such high Be levels is increased slightly during irradiation but quickly reaches a plateau as shown in Figure 7b[29]. This plateau is thought to arise from the formation of $(\text{Cu},\text{Ni},\text{Co})\text{Be}$ beryllide precipitates. Segregation and precipitation thus balance the concurrent effects of nickel transmutants and Be removal. This alloy does not swell significantly.

In Cu-1.8Ni-0.3Be most, but not all, of the Be was already out of solution before irradiation, and the full influence of both void swelling and transmutants in solution reduces the conductivity from its initially much higher value. Depending on the preirradiation heat treatment, the action of radiation-induced segregation can initially increase the conductivity somewhat, as also shown in Figure 7b.

Copper-based brazes usually contain one or more of Ag, Au, Sn, Ni and Ti. As shown in Figure 8, Au and Ag quickly transmute to Hg and Cd respectively, exhibiting once again a strong sensitivity to differences in neutron spectra both within and between reactors[36]. An irradiation program initiated by Garner, Hamilton and Edwards to study the influence of irradiation on brazes was conducted in the FFTF fast reactor[37,38]. In examination of specimens from this experiment it was demonstrated that the combined effects of transmutation, diffusion, segregation and displacement damage in fast reactors can have a strong influence on braze microstructure, strength and integrity, and in some cases, can disqualify some brazes for nuclear applications[38]. In a highly thermalized spectra the impact would have been even stronger. In HFIR, for instance, the loss of gold proceeds at a rate of ~13% per month[39].

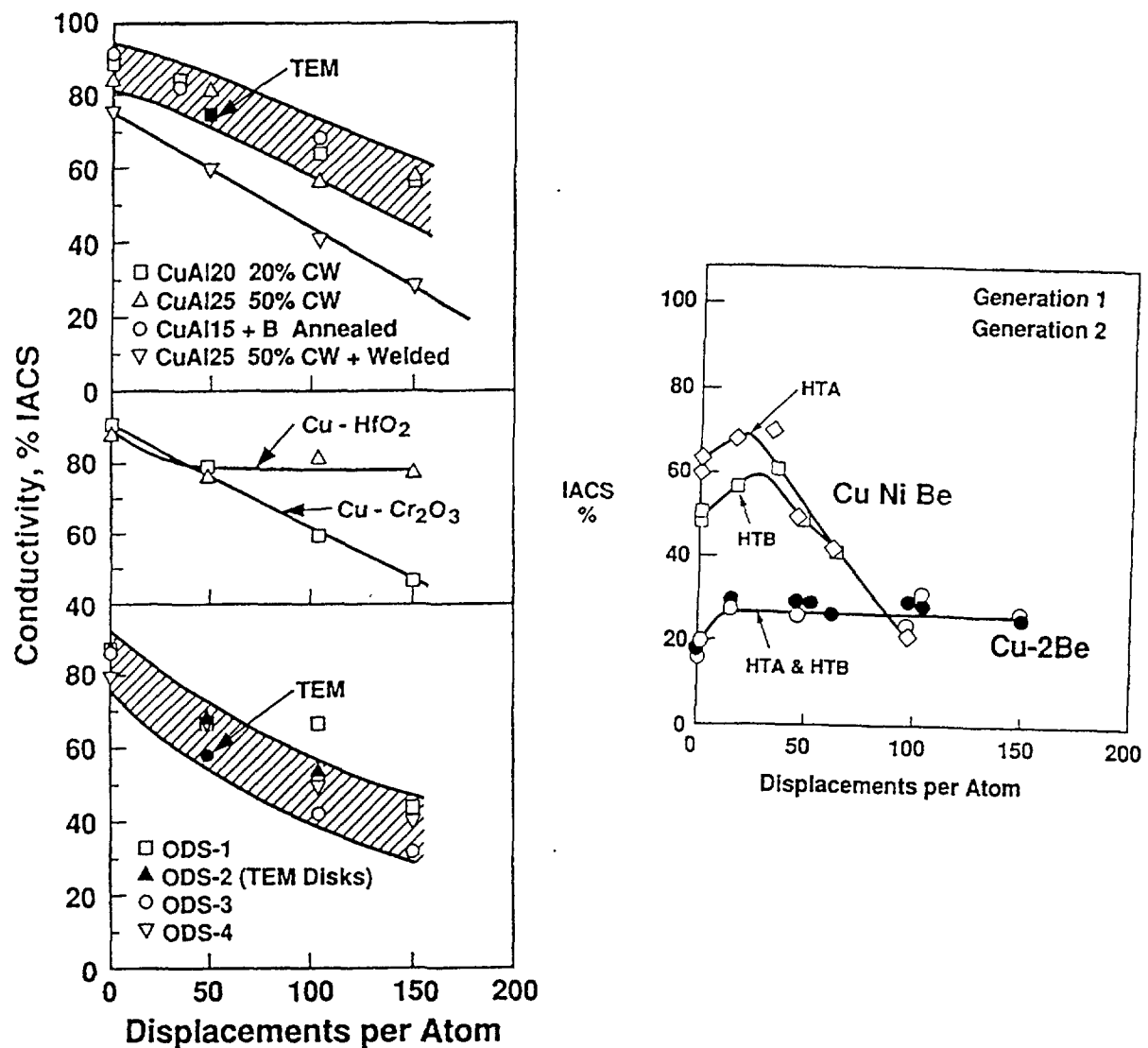


FIGURE 7. (a) Electrical conductivity of mechanically-alloyed copper alloys irradiated in FFTF [30]. Most dispersion-strengthened alloys, with the exception of Cu-Hf₂, continue to decline in conductivity as the irradiation proceeds; (b) comparison of conductivity changes of CuNiBe and CuBe alloys irradiated in several heat treat conditions in FFTF [29].

5. ALUMINUM AND ITS ALLOYS

While Al has not been considered for many fusion applications, its alloys are candidate materials for some components in spallation systems. The swelling, phase stability and mechanical properties of aluminum alloys irradiated in HFIR have been shown by Farrell to be very sensitive to both their original solute content and transmutation-produced silicon, the latter reaching 7.1% at 270 dpa[40]. Figure 9 shows the pronounced effect of the original and subsequent solute content on void swelling. Evolution of mechanical properties was shown to be particularly sensitive to the level of transmutation-produced silicon.

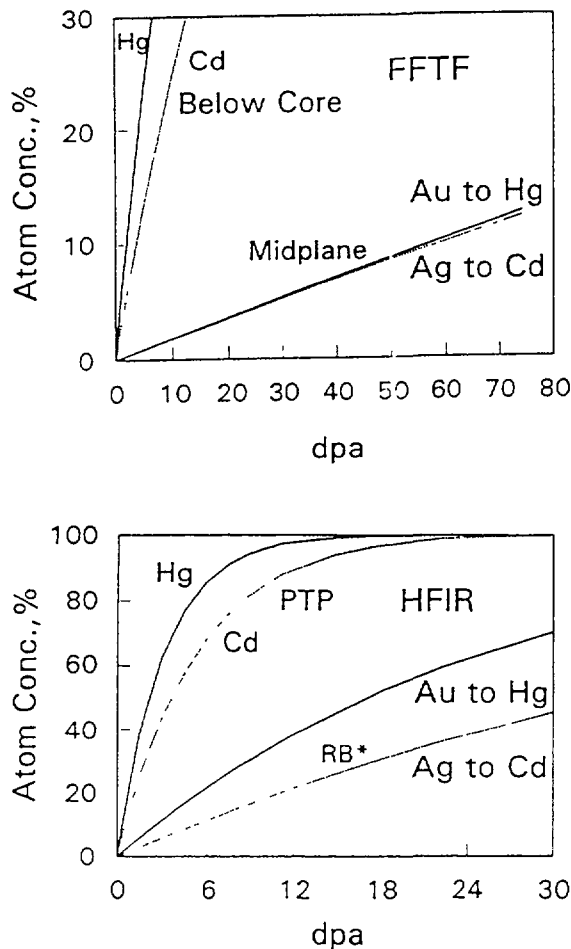


FIGURE 8. Production of mercury and cadmium from gold and silver in FFTF at the mid-plane and at ~66 cm, which is the middle of the below-core basket in MOTA, and the PTP and RB* positions in HFIR [36].

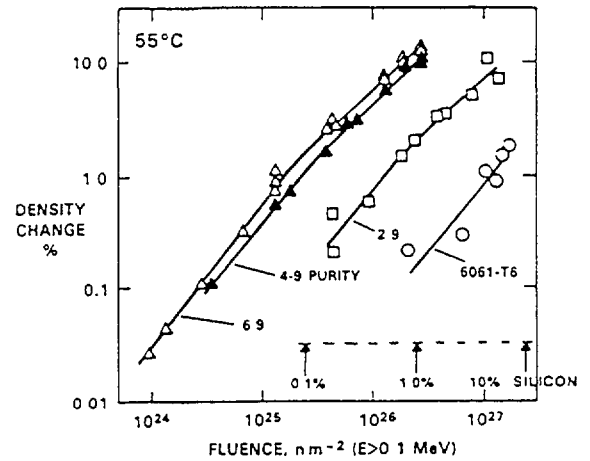


FIGURE 9. Swelling of aluminum and aluminum alloy 6061-T6 during irradiation in HFIR at 55°C [40]. Alloy 6061-T6 contains 1.0 wt% Mg and 0.6 wt% Si. Additional silicon forms continuously by transmutation as shown on the lower right.

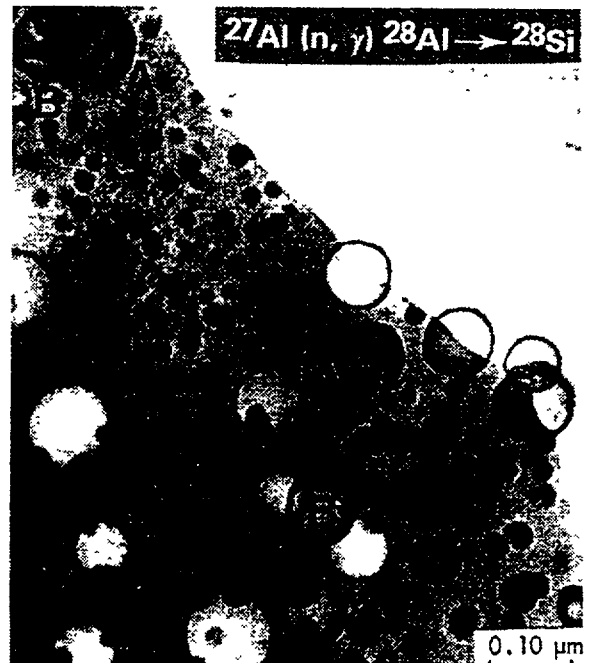


FIGURE 10. Silicon coated cavities and silicon precipitates observed by Farrell in 1100 grade aluminum after irradiation at 55°C for three years in HFIR [40].

Since silicon is insoluble in aluminum, it precipitates out as discrete particles and also as shells on radiation-induced voids, as shown in Figure 10. It is probably reasonable to assume that such coatings must influence the growth rate of voids. These considerations introduce an additional level of complexity into the interpretation and extrapolation of the data, since the rate of silicon formation is determined by the thermal-to-fast neutron flux ratio, but the segregation rate is probably dependent only on the fast flux. Helium production, which may be important for void formation in aluminum, also arises only from the fast flux. These various factors have shown by Weeks and coworkers to lead to significant differences in hardening in the HFIR and HFBR reactors[41], as well as differences arising from spectral variations within HFBR, as shown in Figure 11.

6. VANADIUM AND ITS ALLOYS

Once again, a "low-activation" material, namely vanadium, is shown not to imply low- transmutation. Ohnuki, Garner and their coworkers have shown that there are significant consequences to the fusion-relevant testing of vanadium alloys in surrogate spectra[6, 42-45]. Again, here is a neutron-induced transmutation reaction (producing Cr from V) that is strongly spectra-sensitive (Figure 12). The situation is further complicated in that there is a smaller reverse reaction (Cr to V) reaction with different spectral sensitivity. In addition, the fusion-relevant (n,2n) reaction producing V from Cr is quite different in response from the (n, γ) reaction with thermal neutrons.

Chromium not only segregates at microstructural sinks but participates in a variety of precipitation reactions involving other alloying elements such as Ti. When a large amount of transmutant Cr is formed and significant segregation occurs near grain boundaries, a unique form of transmutation-induced embrittlement occurs, as shown in Figure 13, in which every grain boundary becomes a preexisting crack, leading to failure for even the smallest physical insult[42,43]. Part of the failure mechanism appears to be associated with the relatively strong but opposite influences of Cr and Ti on the lattice parameter of vanadium alloys[44].

The void swelling of vanadium is also very sensitive to small amounts of chromium, such that significant transmutation to chromium converts a relatively slow swelling, pure metal into a high swelling alloy[44,45]. Figure 14 shows the strong impact of small preirradiation additions of chromium on the swelling of vanadium in FFTF[44].

7. STAINLESS STEELS

In earlier publications it was shown that the major solid transmutation reactions that occur in stainless steels were of no significant consequence in fast reactor spectra and were of only minor consequence in highly thermalized reactor spectra[46,47]. The near-total loss of the minor alloying element Mn by (n, γ) reactions in HFIR was thought not to affect void swelling, although the conclusion was actually based on the behavior of a range of Mn-modified variants of 316 steel studied in the EBR-II fast reactor[46]. The slower

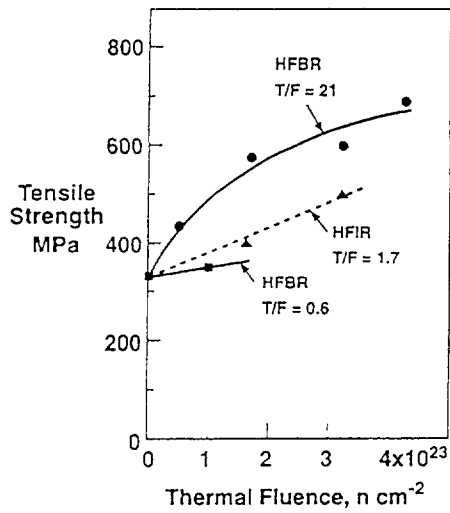


FIGURE 11. Influence of thermal-to-fast (T/F) neutron ratio on evolution of tensile strength of 6061-T6 aluminum irradiated at 50°C [41].

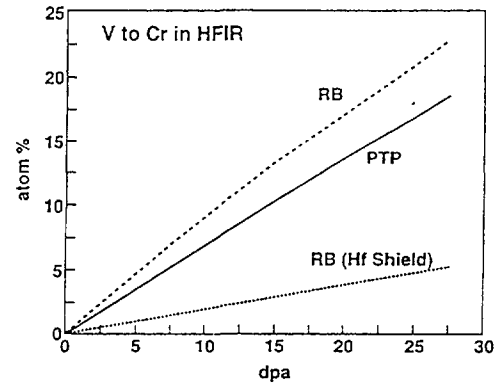
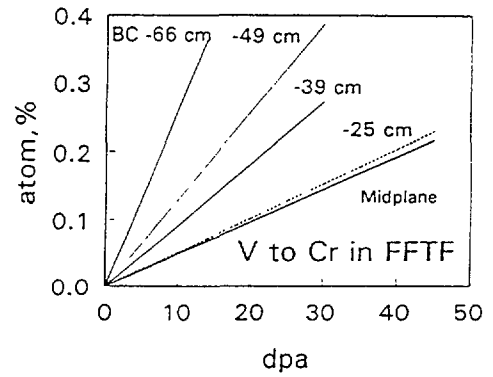


FIGURE 12. Calculated transmutation rates for pure vanadium irradiated in various neutron spectra [6].

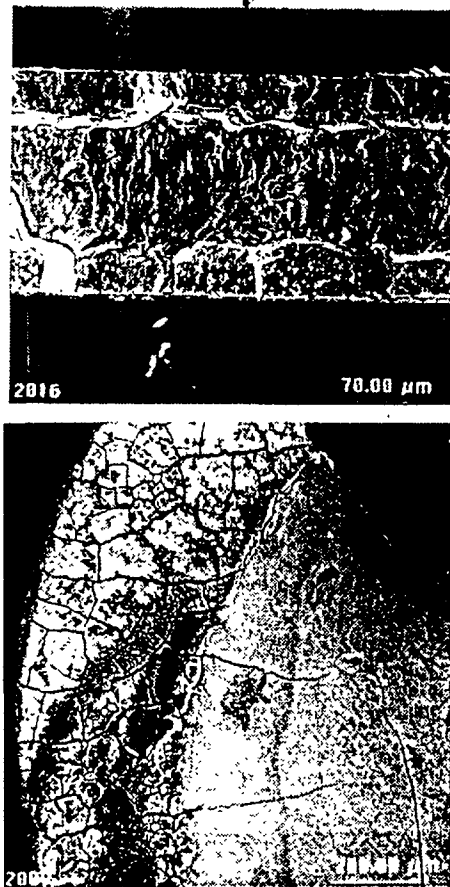


FIGURE 13. (a) Fracture surface of a V-10Ti-1Ni TEM disk irradiated in HFIR to 30 dpa at 500°C. The disk was broken by hand with two tweezers. Preexisting cracks were found to surround every grain on both specimen surfaces, as shown in (b) for another partially electropolished disk. Note that cracks propagate easily into the polished area. These cracks arose from transmutation to form 22% Cr, followed by segregation of both Cr and Ti to grain boundaries. The fracture mode is intergranular in nature for the depth of one grain and transgranular beyond one grain depth [43].

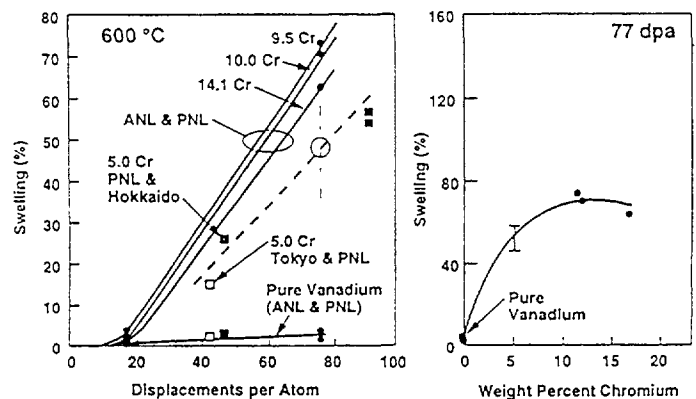


FIGURE 14. Compilation of neutron-induced swelling data of V-Cr alloys irradiated in FFTF-MOTA at 873 K (600°C), showing the largest influence on swelling at low chromium levels [44].

tendency in fusion spectra to increase Mn content by (n,p) and (n,2n) reactions was also thought to be of no real consequence.

The formation in HFIR of small amounts of V from Cr in stainless steels was found by Brager and Garner[47] to be balanced by segregation of the V into various carbide phases that form in irradiated steel, once again demonstrating the role of segregation. Therefore, it has been generally assumed that stainless steels are not directly sensitive to V and Mn solid transmutants, although such a conclusion is only strictly applicable to void swelling and not to other possible damage mechanisms.

The possibility of transmutation having some significant effect on stainless steels has recently been revisited, however. In addition to gaseous transmutations discussed in the next section, several significant new insights on solid transmutation have arisen. Whereas Mn is usually a minor element (1-2%) in stainless steels (used primarily to remove sulphur and other troublesome trace solutes from the alloy matrix), there was for some years a large effort directed toward the development of "low activation" steels, in which Ni was to be replaced by Mn[48,49]. Some of these alloys were also strengthened with W and V. Although the Mn content will increase in fusion-relevant neutron spectra, the presence of thermal neutrons in test reactors can cause a very strong depletion of manganese. In HFIR ~80% of the original manganese is removed by 80 dpa[46]. In light water power reactors the thermal-to-fast neutron ratio is lower by a factor of ~4, and the loss of Mn in a pressurized water reactor baffle bolt has been calculated by the authors to be ~46% at 100 dpa. There would also be large reductions in W and V contents of such alloys.

Since it is now known that radiation-induced segregation of Mn away from microstructural sinks predisposes austenitic Fe-Cr-Mn base alloys to a pronounced instability toward ferrite and sigma phase formation[50-55], further transmutation-induced reductions in manganese content are seen to be very counterproductive, leading to largely ferritic alloys after irradiation. This sensitivity to transmutation precludes the confident testing of Fe-Cr-Mn alloys in highly thermalized spectra such as found in HFIR.

Chung, Sanecki, and Garner have recently explored the possibility that MnS precipitates might be unstable and slowly dissolve under irradiation, especially in highly thermalized spectra, and thereby release S, F and other deleterious trace elements back into the alloy matrix[56]. Such a release of trace elements would arise from a combination of Mn to Fe transmutation, cascade mixing at the precipitate interface, and the inverse Kirkendall effect acting as a pump to export Mn away from the precipitate. Chung and coworkers demonstrated that such an indirect consequence of transmutation and inverse segregation indeed occurs in 304 and 316 stainless steels irradiated in a boiling water reactor. They postulated that this instability might in part contribute to the phenomenon of irradiation assisted stress corrosion cracking.

8. REDUCED ACTIVATION FERRITIC STEELS

As noted earlier, a number of national programs were initiated to develop a low activation ferritic alloy for fusion application[11-13], with most of the current effort being conducted in an international

program[57]. All of these programs have one feature in common, however. All candidate alloys have had Mo replaced with W, Ta and V in varying amounts, all of which are elements that transmute strongly. Tantalum transmutes to W and Hf[58], both of which are also subject to strong transmutation.

One of these alloys, F82H, has been irradiated in HFIR[59] and comparisons have been made with FFTF data[57]. It should be expected, however, that results from the two reactors are not strictly comparable due to the large differences in transmutation.

9. GASEOUS TRANSMUTANTS

Most early attention on gas effects in the fusion community has been addressed toward helium production in materials, but emphasis has been progressively shifting to focus also on hydrogen production and transport, and potential interactions of hydrogen with helium.

Early helium-oriented studies in steels focused on the (n,α) reactions occurring only at high neutron energies, as shown in Figure 15. It was later recognized that much more helium could be produced by the two-step $^{58}\text{Ni}(n,\gamma)^{59}\text{Ni}(n,\alpha)^{56}\text{Fe}$ reaction sequence [60], which operates at much lower neutron energies, as demonstrated in Figure 16. Note in each case, however, that nickel is the major contributor to helium production in Fe-Cr-Ni base alloys. Garner and coworkers have recently demonstrated in several fast reactors that the measured helium concentration indeed scales directly with the nickel content, independent of the spectral balance of the high energy and low energy contributions[61,62]. Note also in Figure 16 that there is a $^{59}\text{Ni}(n,\gamma)$ reaction producing ^{60}Ni whose cross-section is significantly larger than that of the $^{59}\text{Ni}(n,\alpha)$ reaction, and a somewhat smaller cross-section for the $^{59}\text{Ni}(n,p)$ reaction that produces hydrogen. As shown in Figure 17 these three reactions, as well as the (n,γ) reactions with ^{58}Ni and ^{60}Ni , operate to produce a dramatic time-dependent evolution in the balance of nickel isotopes.

As shown in Figure 18, nickel in Fe-Cr-Ni alloys is also the major source of hydrogen via a variety of reactions at neutron energies above ~ 1 MeV. Generally overlooked, however, has been the generation of hydrogen via the $^{59}\text{Ni}(n,p)$ reaction. Greenwood and Garner have shown that in highly thermalized neutron spectra this contribution cannot be overlooked[61,63]. There is approximately one hydrogen atom produced by this reaction for every six helium atoms produced from ^{59}Ni .

Due to the different high energy thresholds (~ 1 MeV vs. ~ 6 MeV), the (n,p) reactions occurring from fast neutrons in Fe-Cr-Ni alloys initially produce hydrogen at higher rates than the helium-producing (n,α) reactions. As the ^{59}Ni inventory builds up in mixed neutron spectra, however, the production rates of both gases increase, but helium eventually surpasses the hydrogen in generation rate, as demonstrated in Figure 19. When the thermal-to-fast neutron ratio is much larger, however, it is possible to pass over the peak in the ^{59}Ni concentration shown in Figure 17. In such cases the rates of gas production eventually decline, but only after very large levels of gas have been generated, as shown in Figure 20.

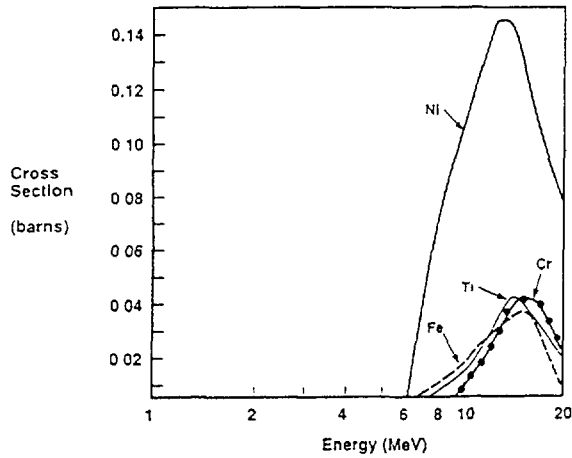


FIGURE 15. Cross sections for (n,α) reactions as a function of neutron energy for common elements used in structural steels.

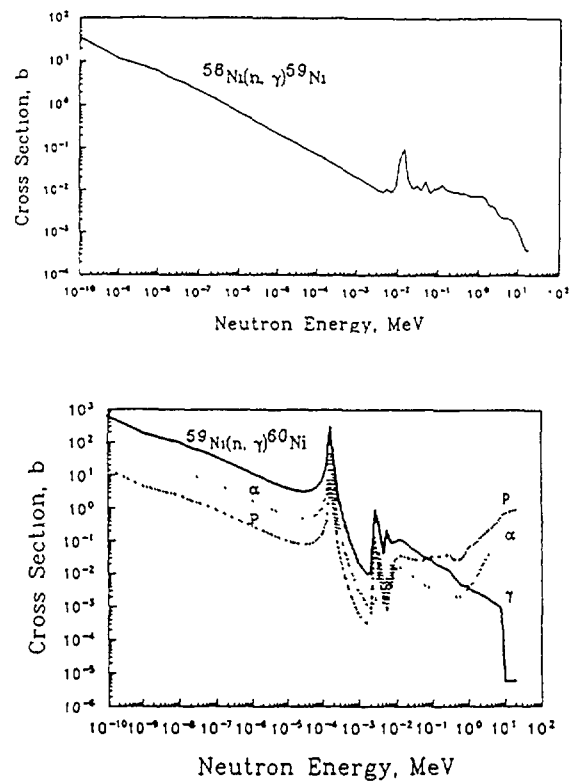


FIGURE 16. (top) Cross section for production of ^{59}Ni from naturally occurring ^{58}Ni . (bottom) Cross sections for production via ^{59}Ni of hydrogen (n,p), helium (n,α), and stable ^{60}Ni (n,γ).

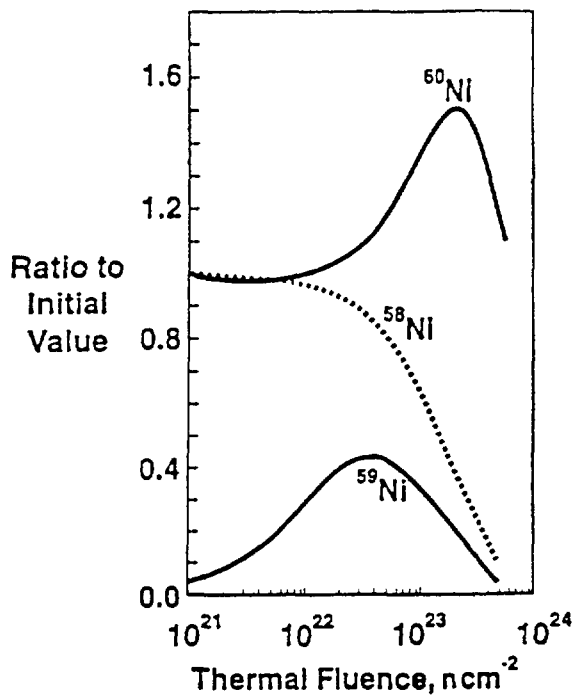


FIGURE 17. Isotopic alteration of major nickel isotopes during thermal neutron irradiation. ^{58}Ni and ^{60}Ni are naturally occurring isotopes, but ^{59}Ni is only formed by transmutation.

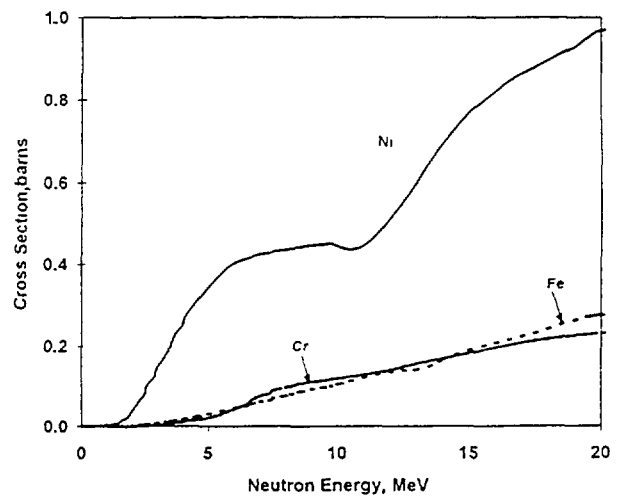


FIGURE 18. Cross sections for (n,p) reactions as a function of neutron energy for common elements used in structural steels.

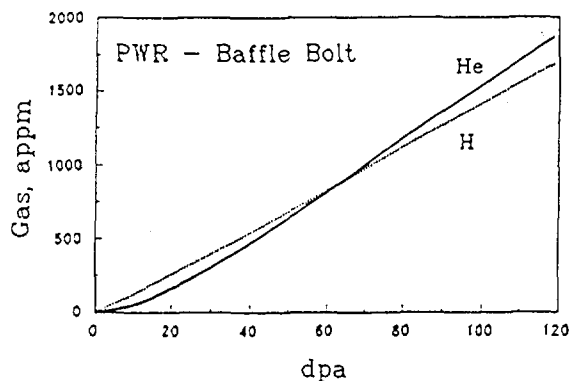


FIGURE 19. Helium and hydrogen generated in 316 stainless steel when subjected to the PWR baffle bolt spectrum. The initially slower rate of helium production compared to that of hydrogen arises from high energy neutron interactions. The slow buildup of ^{59}Ni eventually leads to a higher production rate of both helium and hydrogen arising from low energy neutrons, but helium eventually passes hydrogen.

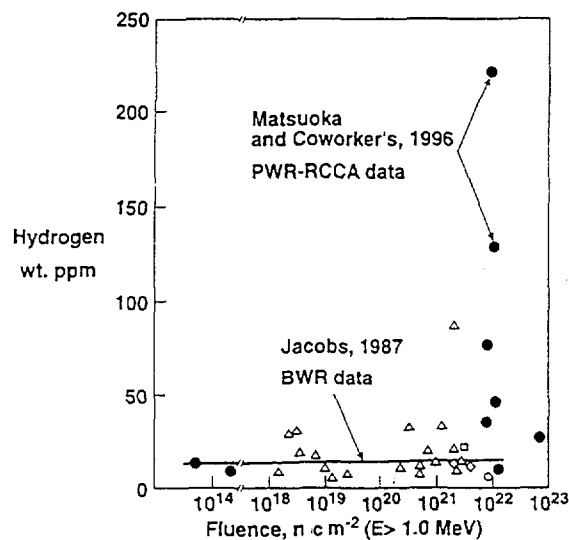


FIGURE 21. Comparison of residual hydrogen levels measured by Jacobs [65] in type 304 stainless steel irradiated in hardware from five different BWRs and that of Matsuoka and coworkers [66] in RCCA cladding irradiated just above the top of a PWR core.

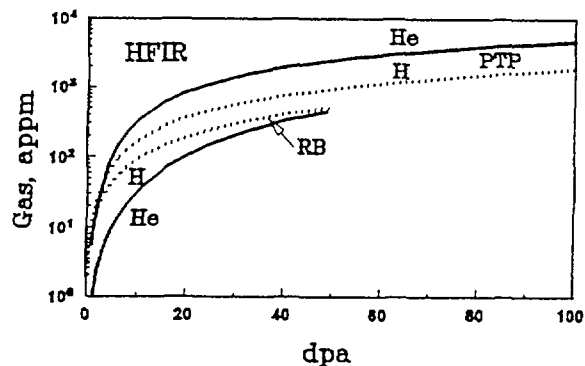


FIGURE 20. Hydrogen and helium production are shown as a function of dpa for the PTP and RB* positions in HFIR. Note the reversal in relative importance between the two positions. The RB* position has a hafnium liner to reduce the thermal neutron population.

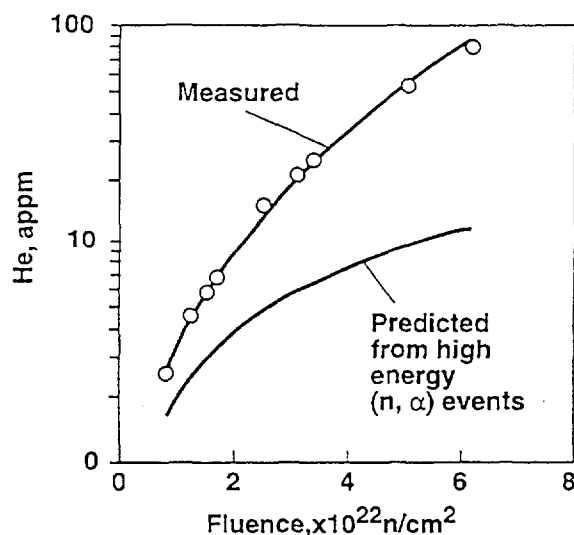


FIGURE 22. Measured vs. predicted helium production in copper vs. thermal fluence [78]. The calculation assumes a thermal to fast ratio of 1.2.

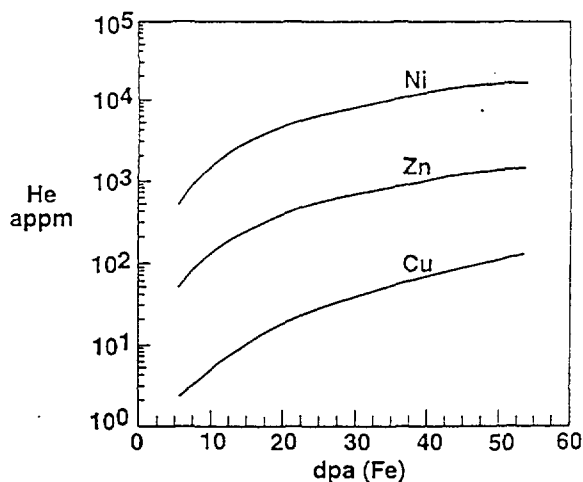


FIGURE 23. Helium production rates of copper and its two major transmutants, calculated for HFIR-PTP position.

It is normally assumed that while helium is insoluble in all metals of interest and also relatively immobile, hydrogen is quite mobile in metals and cannot build up to any significant fraction of the concentrations than can be reached by helium. While this conclusion was quite reasonable for fast reactors operating at temperatures in the range 400-650°C, there is a growing concern by the authors of this paper that hydrogen may be able to accumulate in metals under some reactor-relevant conditions. These conditions are high levels of concurrent helium and hydrogen generation, such as arises from large inventories of ^{59}Ni in highly-thermalized neutron spectra, and low temperatures ($\leq 350^\circ\text{C}$) characteristic of water cooled reactors. It is felt that under these conditions, hydrogen diffusion can be retarded enough by the high microstructural densities characteristic of these temperatures and may be stored as H_2 in small bubbles initially nucleated by helium. Garner has proposed that such a mechanism may act to cause voids to form at very low temperatures (250-350°C) in high nickel alloys irradiated in light water reactors[64].

Possible evidence for helium-hydrogen interactions in cavities may have been provided by Matsuoka and coworkers[65]. Whereas Jacobs[66] had previously shown that residual hydrogen measurements in 304 stainless steel were relatively independent of both fast neutron flux and fluence at 10-30 wppm in BWR irradiation to $\leq 4 \times 10^{21} \text{ n cm}^{-2}$ ($E > 1.0 \text{ MeV}$), Matsuoka showed that irradiation of RCCA (a strong thermal neutron absorber in a safety rod cluster) cladding in a PWR to $\sim 10^{22} \text{ n cm}^{-2}$ ($E > 1.0 \text{ MeV}$) sometimes yielded very large residual hydrogen levels at positions close to the core. The apparent large scatter in Matsuoka's data shown in Figure 21 is most probably a reflection of the very large fluctuations in thermal-to-fast neutron ratio that exist just above the core and around the RCCA absorber rods. While the range of hydrogen concentrations is very large, it was also found by Matsuoka to be very reproducible for a given position on the RCCA.

In the $10^{21} - 10^{22} \text{ n cm}^{-2}$ ($E > 1.0 \text{ MeV}$) range the ^{59}Ni concentration is most likely beginning to dominate both the hydrogen and helium generation. Note that Matsuoka's data are plotted vs. fast fluence, which does not reflect the degree of ^{59}Ni formation. The authors of this paper note that the highest levels of hydrogen found by Matsuoka appear to reside in the region of highest thermal-to-fast ratio. The high retention levels of hydrogen in Matsuoka's experiment may reflect an increased level of trapping in small helium bubbles or possibly even voids that were stimulated to form by the high levels of both helium and hydrogen.

It is particularly important to emphasize that alloys containing much higher levels of nickel, such as the Inconels and Hastelloys, will generate proportionally higher levels of both hydrogen and helium, and therefore may be much more susceptible to problems arising from the action of gaseous transmutation products.

The $^{59}\text{Ni}(n,\alpha)$ reaction is highly exothermic compared to most nuclear reactions. It involves a very large energy release of $\sim 5.1 \text{ MeV}$, shared between the helium atom and the ^{56}Fe atom at 4.76 MeV and 340 KeV, respectively. The 340 KeV recoil is much larger than the average neutron-induced energy transfer to atoms resulting from fast neutron collisions. While the helium atom loses most of its energy via electronic

processes that produce only 62 displacements on the average, the highly energetic recoiling ^{56}Fe atom loses much of its energy via nuclear interactions and creates 1701 displacements on the average[67]. Greenwood and Garner have recently noted that the (n,p) and (n, γ) reactions of ^{59}Ni are also exothermic in nature, but only contribute an additional 3% to the atomic displacement process[63].

In some spectra this enhanced damage process can also lead to a substantial increase in displacement rate over that calculated using the internationally-accepted NRT displacement model. It should be noted that this damage contribution increases directly with nickel content of the alloy. While pure nickel in the very highly thermalized (1:1) HFIR reactor will experience an enhanced displacement rate that is almost twice that predicted by the standard NRT dpa model, AISI 316 stainless steel in the PWR baffle bolt position experiences an enhancement of only several percent. This enhanced dpa contribution might be significant for nickel-base alloys irradiated at higher thermal-to-fast ratios, however.

One of the most difficult processes to study during neutron irradiation is the separate and possibly synergistic effects of helium and displacement damage. The major problem is that it is very difficult to conduct a truly one-variable experiment for helium. Almost all techniques employed to study helium introduce some other concurrent variable, or are subject to unavoidable variations in neutron flux-spectra and reactor history.

Recently, however, a truly one-variable approach has evolved that has yielded very successful results in both austenitic and ferritic alloys. As reviewed by Odette, one can alter the isotopic balance of isotopes in nickel to produce varying amounts of helium production[68]. In fast reactor spectra, the side-by-side irradiation of specimens that are doped with ^{59}Ni and specimens that are not doped yields a very successful one-variable helium effects experiment. A series of papers on this subject by Garner and coworkers have shown that the influence of helium on microstructure, void swelling and tensile properties of model austenitic steels is very much smaller than previously anticipated. This experimental series is summarized in ref. [69].

For highly thermalized spectra it is better to alter the $^{58}\text{Ni}/^{60}\text{Ni}$ ratio and also add ^{59}Ni to achieve a range of helium production schedules. Gelles, Hankin and Hamilton recently reported the results of a test on ferritic alloys irradiated in HFIR[70]. They demonstrated that when Fe-12Cr and Fe-12Cr-1.5Ni, the latter with three different isotopic mixtures for the nickel, were irradiated side by the side, the resultant changes in shear tensile properties and microstructures were mostly dependent on the mere presence of nickel, rather than being significantly dependent on the helium generation rate.

In retrospect, this conclusion is not unexpected, since two earlier ion bombardment studies by Johnston et al. on Fe-Cr binaries[71] and Ayrault et al. on HT-9[72] demonstrated that addition of 2% nickel as a chemical additive changed the swelling behavior more than did additions of helium. Kleueh and coworkers have irradiated in HFIR several ferritic alloys, both doped and undoped with natural nickel, to hopefully simulate the effects of helium on microstructural evolution and mechanical properties[73-75]. Gelles, however, has argued that these experiments cannot be used to convincingly demonstrate the role of

helium but only demonstrate that nickel itself dictates the final results. Based on the results from his isotopic tailoring studies, it appears that Gelles is most likely correct[76,77].

There is another possible isotopic doping procedure that can be used for copper alloys. It is not as dramatic as that of the $^{58}\text{Ni} - ^{59}\text{Ni}$ sequence, however, because an extra step is required. This is the $^{63}\text{Cu}(n,\gamma)^{64}\text{Cu}(\beta)^{64}\text{Zn}(n,\gamma)^{65}\text{Zn}(n,\alpha)^{62}\text{Ni}$ sequence, which in highly thermalized spectra can produce much more helium than would be produced from (n,α) fast neutron reactions, as demonstrated in Figure 22.

By predoping alloys with Zn, a natural transmutant, it might be possible to produce higher levels of helium by skipping over the first two steps in the isotopic chain. There is another approach that would be even more effective, however. Since both nickel and zinc are transmutants in copper, and nickel generates even more helium (and hydrogen) per atom than does zinc, as shown in Figure 23, it might be possible to develop a suitable matrix of Cu-Ni-Zn alloys, and then irradiate one set without shielding against thermal neutrons and another set with shielding. If the nickel was isotopically altered, this would also provide additional flexibility in helium and hydrogen generation schedules. Such an experiment might cast significant light on the separate and possibly synergistic effects of solid and gaseous transmutants in copper alloys.

10. PHASE STABILITY CONSIDERATIONS

If the stability of a given precipitate is sensitive to both displacement rate and alloy composition, its existence in a given radiation environment can depend on transmutation and displacement rate, as demonstrated earlier for the Mo-Re and Al-Si systems, where new elements are produced during irradiation. If, however, an existing element is removed by transmutation during irradiation, a precipitate can disappear if the composition drops below the solubility limit characteristic of the particular displacement rate. Platov and Pletnev[79] have developed the general formulism for this situation and then applied it to the two phase alloy Al-0.058% Sc containing ScAl_3 precipitates. They show that in a fusion neutron spectrum the burnout of scandium, occurring by a high energy $(n, 2n)$ reaction, would lead to complete dissolution of the precipitates by $5 \times 10^{23} \text{ n cm}^{-2}$. While this is a rather high exposure, it is expected that alloy systems sensitive to transmutation via thermal or epithermal neutrons might lead to dissolution at much lesser exposures.

11. CONCLUSIONS

It now appears that transmutation to either solid or gaseous products must be considered as a strong potential contributor to any radiation-induced damage process. Not only might transmutation rates per dpa vary between reactors, but for some materials and damage processes, the usually-ignored spectral variations within a reactor core might be significant. When flux-driven processes involving segregation or precipitation occur, the need to identify and separate the effects of transmutation and displacement rate becomes even more important.

REFERENCES

- [1] F. A. Garner and W. F. Sommer, "Radiation Damage Issues in Accelerator-Driven Spallation Neutron Systems", Proceedings of 2nd Inter. Conf. on Accelerator-Driven Transmutation Technologies and Applications, Kalmar, Sweden, 1996, in press.
- [2] F. A. Garner and L. R. Greenwood, Mater. Trans. JIM, 34 (1993) 985.
- [3] G. M. Kalinin, J. Nucl. Mater. 179-181 (1991) 1193.
- [4] V. V. Rybin and D. L. Smith, J. Nucl. Mater. 191-194 (1992) 30.
- [5] F. A. Garner, L. R. Greenwood and D. J. Edwards, J. Nucl. Mater. 212-125 (1994) 426.
- [6] L. R. Greenwood and F. A. Garner, J. Nucl. Mater., 212-215 (1994) 635.
- [7] D. J. Edwards, F. A. Garner and D. S. Gelles, J. Nucl. Mater., in press.
- [8] I. V. Gorynin, V. A. Ignatov, V. V. Rybin, S. A. Fabritsiev, V. A. Kazakov, V. P. Chakin, V. A. Tsykanov, V. R. Barabash and Y. G. Prokofyev, J. Nucl. Mater. 191-194 (1992) 421.
- [9] S. A. Fabritsiev, V. A. Gosudarenkova, V. A. Potapova, V. V. Rybin, L. S. Kosachev, V. P. Chakin, A. S. Pokrovsky and V. R. Barabash, J. Nucl. Mater. 191-194 (1992) 426.
- [10] A. Hasegawa, K. Abe, M. Satou, and C. Namba, J. Nucl. Mater. 225 (1995) 259.
- [11] D. S. Gelles, Reduced Activation Materials for Fusion Reactors, ASTM STP 1047, American Society for Testing and Materials, 1990, p. 113.
- [12] F. Abe, T. Noda, H. Araki and M. Okada, Reduced Activation Materials for Fusion Reactors, ASTM STP 1047, American Society for Testing and Materials, 1990, p. 130.
- [13] R. Kleuh and P. J. Maziasz, Reduced Activation Materials for Fusion Reactors, ASTM STP 1047, American Society for Testing and Materials, 1990, p. 140.
- [14] A. Tobin, J. Nucl. Mater. 85-86 (1979) 197.
- [15] D. Murphy, S. Warren and G. J. Butterworth, Fusion Eng. Des. 22 (1993) 379.
- [16] F. A. Garner, M. L. Hamilton, D. J. Edwards, B. N. Singh, J. F. Stubbins, T. Shikama, S. J. Zinkle and P. Samal, Fusion Reactor Materials Semiannual Progress Report DOE/ER-0313/10, 1991, 186.
- [17] I. Šmid, K. Satoh, M. Akiba, M. Araki, M. Dairaku, E. Kny, K. Nakamura, S. Suzuki and K. Yokoyama, presented at ICFRM-6, 1993, in Stresa, Italy.
- [18] L. N. Bystrov, L. I. Ivanov, V. I. Markushev, S. A. Maslyayev, K. B. Povarova, M. E. Reznitskii, Yu. O. Tolstobrov and A. B. Tsepelev, Fiz. Khim. Obrab. Mater. 4 (1991) 38.
- [19] I. Šmid, H. D. Pacher, G. Vieder, U. Mszanowski, Y. Igitkhanov, G. Janeschitz, J. Schlosser and L. Plöchl, J. Nucl. Mater. 233-237 (1966) 701.

- [20] H. Ullmaier and F. Carsughi, Nucl. Instr. and Meth. in Physics Res. B, 101 (1995) 406.
- [21] F. D. Kingsbury and J. Moteff, Effects of Radiation on Structural Metals, ASTM STP 426, American Society for Testing and Materials, (1967) p. 512.
- [22] F. A. Garner and J. Megusar, Fusion Reactor Materials Semiannual Progress Report for period ending Sept. 30, 1993, DOE/ER-0313/15, p. 201.
- [23] H. R. Brager, H. L. Heinisch and F. A. Garner, J. Nucl. Mater. 133 & 134 (1985) 676.
- [24] R. W. Conn, V. A. Chuyanov, N. Inoue and D. R. Sweetman, Sci. Am. (April 1992) 103.
- [25] G. Vieider, A. Cardella, M. Akiba, R. Matera and R. Watson, Fusion Eng. Des. 16 (1991) 23.
- [26] H. M. Frost and J. C. Kennedy, J. Nucl. Mater. 141-143 (1986) 169.
- [27] F. A. Garner, H. L. Heinisch, R. L. Simons and F. M. Mann, Rad. Eff. and Defects in Solids, 113 (1990) 229.
- [28] F. A. Garner, H. R. Brager and K. R. Anderson, J. Nucl. Mater. 179-181 (1991) 250.
- [29] F. A. Garner, M. L. Hamilton, T. Shikama, D. J. Edwards and J. W. Newkirk, J. Nucl. Mater., 191-194 (1992) 386.
- [30] D. J. Edwards, K. R. Anderson, F. A. Garner, M. L. Hamilton, J. F. Stubbins and A. S. Kumar, J. Nucl. Mater., 191-194 (1992) 416.
- [31] D. J. Edwards, F. A. Garner and L. R. Greenwood, J. Nucl. Mater., 212-215 (1994) 404.
- [32] S. A. Fabritsiev, A. S. Pokrovsky, S. J. Zinkle, A. F. Rowcliffe, D. J. Edwards, F. A. Garner, V. A. Sandakov, B. N. Singh and V. R. Barabash, J. Nucl. Mater., 233-237 (1996) 526.
- [33] T. Muroga and F. A. Garner, J. Nucl. Mater. 207 (1993) 327.
- [34] T. Muroga, E. Ishimaru, and N. Yoshida, Proc. 16th Inter. Symp. on Effects of Radiation on Materials, ASTM STP 1175, American Society for Testing and Materials, (1993) p. 1013.
- [35] D. J. Edwards, F. A. Garner and D. J. Grant, to be submitted to J. Nucl. Mater., also "The Properties and Microstructure of Neutron Irradiated, Oxide Dispersion Strengthened Copper Alloys", Ph.D. Dissertation, University of Missouri-Rolla, 1993.
- [36] F. A. Garner, L. R. Greenwood and D. J. Edwards, Fusion Reactor Materials Semiannual Progress Report for period ending March 31, 1994, DOE/ER-0313/16, p. 47.
- [37] F. A. Garner, M. L. Hamilton, D. J. Edwards, B. N. Singh, J. F. Stubbins, T. Shikama and S. J. Zinkle, Fusion Reactor Materials Semiannual Progress Report for Period Ending March 31, 1991, DOE/ER-0313/10, p. 186.
- [38] D. J. Edwards, M. L. Hamilton, F. A. Garner and J. D. Troxell, to be published in Proceedings of 18th Inter. Symp. on Effects of Radiation on Materials, ASTM STP 1325, American Society for Testing and Materials; also in DOE/ER-0313/18, p. 299.

- [39] L. R. Greenwood, J. Nucl. Mater. 216 (1994) 29.
- [40] K. Farrell, Dimensional Stability and Mechanical Behavior of Irradiated Metals and Alloys, Brit. Nucl. Eng. Soc. London, 1983, Vol. 1, p. 73.
- [41] J. R. Weeks, C. J. Czajkowski, and K. Farrell, Effects of Radiation on Materials: 16th Inter. Symp. ASTM STP 1175, American Society for Testing and Materials, 1993, p. 1168.
- [42] S. Ohnuki, H. Takahashi, K. Shiba, A. Hishinuma, J. E. Pawel and F. A. Garner, J. Nucl. Mater. 218 (1995) 217.
- [43] S. Ohnuki, H. Takahashi, F. A. Garner, J. E. Pawel, K. Shiba and A. Hishinuma, J. Nucl. Mater. 233-237 (1996) 411.
- [44] F. A. Garner, L. R. Greenwood, B. A. Loomis, S. Ohnuki and N. Sekimura, J. Nucl. Mater. 233-237 (1996) 406.
- [45] F. A. Garner, D. S. Gelles, H. Takahashi, S. Ohnuki, H. Kinoshita and B. A. Loomis, J. Nucl. Mater. 191-194 (1992) 948.
- [46] J. F. Bates, F. A. Garner and F. M. Mann, J. Nucl. Mater. 103-104, 999 (1981).
- [47] H. R. Brager and F. A. Garner, J. Nucl. Mater. 117 (1983) 159.
- [48] R. L. Klueh and P. J. Maziasz, Reduced Activation Materials for Fusion Reactors, ASTM STP 1047, American Society for Testing and Materials, 1990, p. 7.
- [49] F. A. Garner and J. M. McCarthy, Reduced Activation Materials for Fusion Reactors, ASTM STP 1047, American Society for Testing and Materials, 1990, p. 19.
- [50] F. A. Garner, H. R. Brager, D. S. Gelles and J. M. McCarthy, J. Nucl. Mater. 148 (1987) 294.
- [51] F. A. Garner, F. Abe and T. Noda, J. Nucl. Mater. 155-157 (1988) 870.
- [52] J. M. McCarthy and F. A. Garner, J. Nucl. Mater. 155-157 (1988) 877.
- [53] J. M. McCarthy, J. Nucl. Mater. 179-181 (1991) 626.
- [54] F. A. Garner, H. R. Brager and H. Takahashi, J. Nucl. Mater. 179-181 (1991) 633.
- [55] K. Miyahara, F. A. Garner and Y. Hosoi, J. Nucl. Mater. 191-194 (1992) 1198.
- [56] H. M. Chung, J. E. Sanecki and F. A. Garner, Effects of Radiation on Materials: 18th Inter. Symp., ASTM STP 1325, American Society for Testing and Materials, in press.
- [57] A. Kohyama, A. Hishinuma, D. S. Gelles, R. L. Klueh, W. Dietz and K. Ehrlich, J. Nucl. Mater. 233-237 (1996) 138.
- [58] C. B. A. Forty, G. J. Butterworth and J.-Ch. Sublet, J. Nucl. Mater. 212-215 (1994) 640.

- [59] D. J. Alexander, J. E. Pawel, M. L. Grossbeck, A. F. Rowcliffe and K. Shiba, Effects of Radiation on Materials: 17th Inter. Symp., ASTM STP 1270, American Society for Testing and Materials, 1996, p. 945.
- [60] L. R. Greenwood, D. W. Kneff, R. P. Skowronski and F. M. Mann, J. Nucl. Mater. 122-123 (1984) 1002.
- [61] F. A. Garner, L. R. Greenwood and B. M. Oliver, Effects of Radiation on Materials: 18th Inter. Symp. ASTM STP 1325, American Society for Testing and Materials, in press.
- [62] L. R. Greenwood, F. A. Garner and B. M. Oliver, J. Nucl. Mater. 212-215 (1994) 492.
- [63] L. R. Greenwood and F. A. Garner, J. Nucl. Mater. 233-237 (1996) 1530.
- [64] F. A. Garner, Proc. of Inter. Workshop on Defect Production, Accumulation and Materials Performance in Irradiation Environments, Davos, Switzerland, Oct. 2-8, 1996, in press.
- [65] T. Matsuoka, T. Yonezawa, K. Nakamura, H. Myojin, J. Shimizu and T. Nagata, "Life Time Estimation of Cladding Tube Cracking by Absorber Swelling of PWR RCCA Rodlets", 1996, proc. of ICONE-4, to be published.
- [66] A. J. Jacobs, Influence of Radiation on Material Properties: 13th Inter. Symp. (Part II), ASTM STP 956, American Society for Testing and Materials, 1987, p. 239.
- [67] L. R. Greenwood, J. of Nucl. Mater., 115 (1983) 137.
- [68] G. R. Odette, J. Nucl. Mater. 141-143 (1986) 1011.
- [69] F. A. Garner, M. L. Hamilton, L. R. Greenwood, J. F. Stubbins and B. M. Oliver, Effects of Radiation on Materials: 16th Inter. Symp., ASTM STP 1175, American Society for Testing and Materials, 1993, 921.
- [70] D. S. Gelles, G. L. Hankin and M. L. Hamilton, Proc. of Inter. Workshop on Defect Production, Accumulation and Materials Performance in Irradiation Environments, Davos, Switzerland, Oct. 2-8, 1996, in press.
- [71] W. G. Johnston, T. Lauritzen, J. H. Rosolowski and A. M. Turkalo, Effects of Radiation on Materials: Eleventh Conference, ASTM STP 782, American Society for Testing and Materials, 1982, p. 809.
- [72] G. Ayrault, Damage Analysis and Fundamental Studies Quarterly Progress Report, Oct.-Dec. 1981, DOE/ER-0046/8, vol. 1, 1982, p. 182.
- [73] R. L. Klueh and D. J. Alexander, J. Nucl. Mater. 218 (1995) 151.
- [74] R. L. Klueh and D. J. Alexander, J. Nucl. Mater. 187 (1992) 60.
- [75] R. L. Klueh, J. M. Vitek, W. R. Corwin and D. J. Alexander, J. Nucl. Mater. 155-157 (1988) 973.
- [76] D. S. Gelles, J. Nucl. Mater. 230 (1996) 187.

- [77] D. S. Gelles, Proc. 18th Inter. Symp. on Effects of Radiation on Materials, ASTM STP 1325, American Society for Testing and Materials, in press.
- [78] D. W. Kneff, L. R. Greenwood, B. M. Oliver, R. P. Skowronski, and E. L. Callis, Rad. Effects 93 (1986) 217.
- [79] Yu. M. Platov and M. N. Pletnev, J. Nucl. Mater. 211 (1994) 95-100.

STATUS AND POSSIBILITY OF FUEL AND STRUCTURAL MATERIALS EXPERIMENTAL IRRADIATION IN BN-600 REACTOR. STAGES OF BN-600 REACTOR CORE DEVELOPMENT

B.A. VASILJEV, A.I. ZINOVJEV, A.I. STAROVEROV
Experimental Machine Building Bureau,
Nizhny Novgorod



V.V. MALTSEV, A.N. OGORODOV
NPP BN-600,
Zarechny

Russian Federation

Abstract

The results of the irradiation of standard and experimental fuel subassemblies (SA) in BN-600 reactor are presented. The prospects of further tests on experimental SAs and on standard SAs up to 12 % h.a. burnup and damage doses ≥ 90 dpa are also analyzed.

1. INTRODUCTION

The BN-600 reactor (Fig.1) was put into operation as the 3rd power unit of Beloyarskaya NPP. The mean load factor was 0.69 to 0.74 for a period of 17 years operation without taking account of the 2 year period spent in commissioning .

Pertaining to BN-600 reactor the following three cores were developed and subsequently installed:

- since 1980-1986 - initial core (type 1);
- since 1986-1991 - core of 1st modernisation (type M);
- since 1991 - core of 2nd modernisation (type M1) (Fig.2).

At present the following fuel SAs (Fig.3) irradiation parameters are attained in BN-600 reactor with M1 core: maximum fuel burnup (B_{max}) - 10 % h.a., maximum damage dose (D_{max}) - 75 dpa, SAs lifetime - 480 effective full power days (efpd). Austenitic cold-worked (CW) steel ChS-68 and ferritic steel EP-450 are used as the structural materials for cladding and for wrapper, respectively.

During the reactor operation with M1 core, one or two cases of loss of SAs leak-tightness were observed and the load factor was 0.77.

Further transition of BN-600 reactor to a core of 3rd modernisation (M2) is planned with the existing structural materials.

Irradiation parameters: B_{max} - 11.3 % h.a., D_{max} - 84 dpa, SAs lifetime- 540 efpd.

2. RESULTS OF BN-600 REACTOR M1 CORE STANDARD SAs IRRADIATION

Within a programme of experimental confirmation of engineering decisions and neutronic characteristics of the M2 core project, tests of about 35 thousand standard fuel elements (FEs) for increased lifetime were carried out starting from 27th to 34th reactor runs. The following parameters were attained: B_{max} - 12 % h.a. (for SAs of high enrichment zone), D_{max} - 94 dpa (for SAs of low enrichment zone). The following parameters were attained for a lot of standard SAs: B_{max} - 9.5 % h.a. (depending on fuel enrichment), D_{max} - 75-80 dpa, SAs lifetime - 540 efpd. Practically all FEs remained leak-tight.

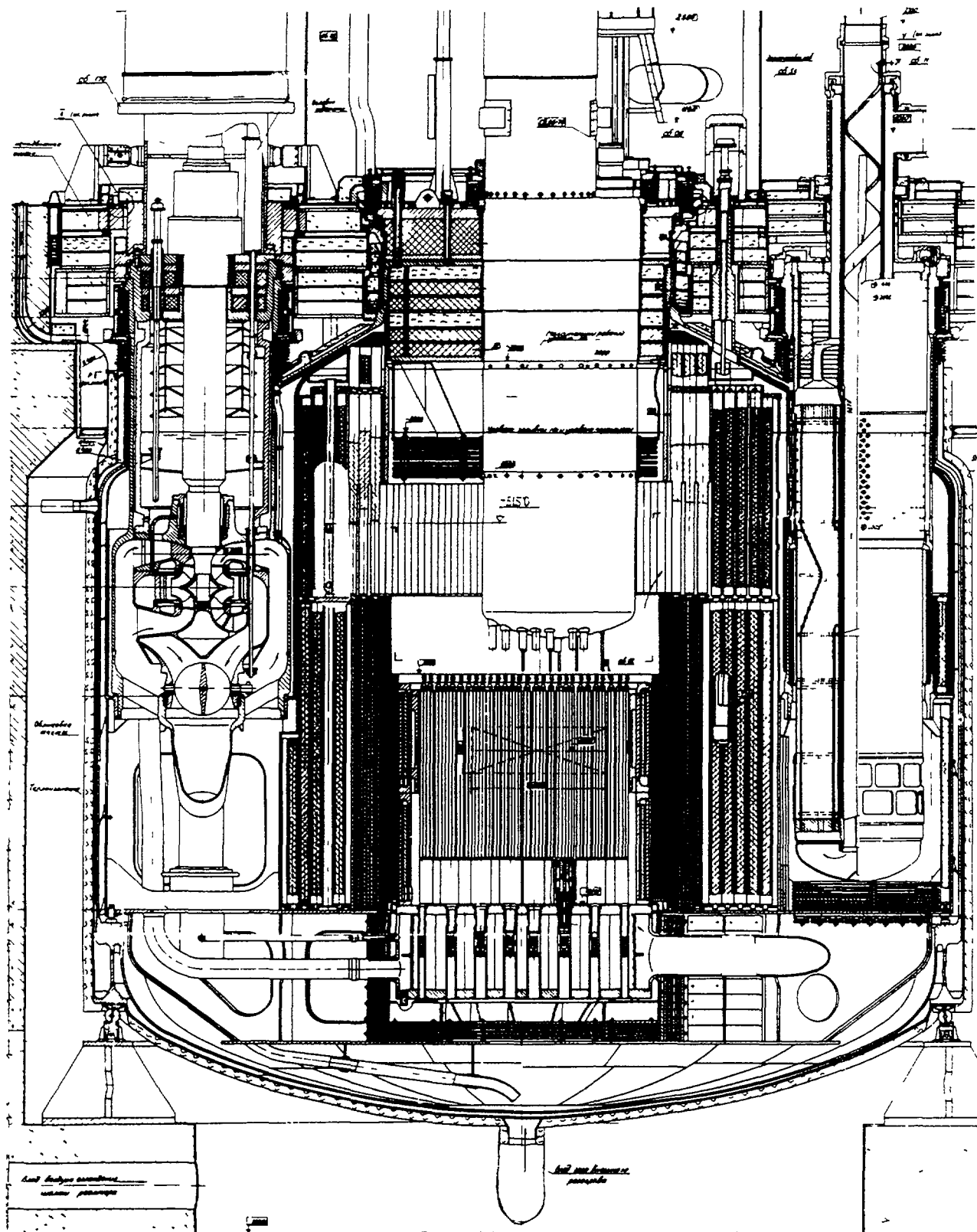


Fig 1 - BN-600 reactor

In total, about 37 thousand FEs have been successfully operated and about 3 thousand of them accumulated damage dose of more than 80 dpa.

It is planned to carry out additional testing of standard SAs for increased lifetime up to 540 efpd within 36th, 37th and 38th runs.

3. RESULTS OF EXPERIMENTAL SAs WITH MOX FUEL IRRADIATION IN BN-600 REACTOR

From the 20th (1988) to the start of the 36th (June 1997) runs, 6 experimental SAs with vibrocompacted MOX fuel and 18 experimental SAs with pelletized MOX fuel containing plutonium with a low Pu-240 content were tested in BN-600 reactor.

Proceeding from the minimisation of power perturbation in the core and additional margin of reactivity inserted when installing the experimental SAs with MOX fuel into uranium core, the experimental SAs were placed at the periphery of low and medium enrichment zones with a pitch not less than two positions and in a number not more than 12 SAs (12 experimental SAs were in the core within 27th run).

All experimental SAs tested had upper and lower axial blankets. Austenitic steels ChS-68 CW, EP-172 CW and ferritic steel EP-450 were used as structural materials for cladding and for wrapper, respectively.

The following irradiation parameters were reached:

for SAs with vibrocompacted MOX fuel :

Bmax - 10.9% h.a., Dmax - 79 dpa, SAs operation time is 510 efpd ;

for SAs with pelletized MOX fuel :

Bmax - 11-11.8 % h.a., Dmax 75-81 dpa , SAs operation time - 540 efpd.

There are no claims on experimental SAs performance, all FEs remained leak-tight.

At present two experimental SAs with pelletized MOX fuel are installed in the reactor to be tested from the beginning of the 36th run.

After accepting in 1992 for the BN-800 reactor to have a core with zero sodium void reactivity effect as standard, an experimental SA was developed modelling to the optimum extent (in BN-600 reactor conditions) the BN-800 standard SA operation conditions: experimental SA wrapper size - 94.5 x 2 mm, FE size - 6.6 x 0.4 mm; boron carbide and steel elements instead of upper axial blanket.

In addition, new experimental SAs with pelletized MOX fuel were developed like those of BN-600 reactor standard SA and intended for substantiation of technical and engineering decisions made for the proposed BN-600 "hybrid" core with uranium and MOX fuel.

The experimental SAs described above (of BN-800 SAs and of new experimental SAs with pelletized MOX fuel) are planned to be installed in the reactor for irradiation in 1998 - 1999.

4. PROSPECTIVE REVIEW OF TESTS PLANNED IN BN-600 REACTOR

For assuring further increase of SAs lifetime (B_{\max} - 12% h.a. and $D_{\max} \geq 90$ dpa) it is necessary to use new structural materials with increased irradiation stability for FE claddings. It is necessitated by the need to reduce the mechanical interaction between the swelling FE bundle and the wrapper, which now is the main factor limiting the fuel burnup.

At present work on this problem is being carried out in several areas.

1). Low swelling ferritic steel EP-450, used for standard SAs wrappers, will be used for FE claddings.

An experimental SA with FE bundle of EP-450 steel is planned to be tested in 1998-1999. The experimental SA is similar to a standard SA and differs only in the FE size: 6.9×0.55 mm (previous one was 6.9×0.4 mm). It is expected to attain the following irradiation parameters: B_{\max} - 13.8 % h.a., D_{\max} - 100 dpa, SAs irradiation time - 4 runs.

5 experimental SAs with a "hybrid" FE bundle were installed in the reactor for testing within 36 run.

2). It is planned to use prospective cold-worked austenitic steels of increased irradiation stability as structural materials:

- a) steel ChS-68 CW with increased phosphorus content ;
- b) steel EK-164 with optimised proportion of chrome, nickel and alloying additions.

It is expected that the use of these steels for FEs claddings will allow the following parameters to be attained: B_{\max} - 12-15 % h.a., D_{\max} - 90-120 dpa.

At present these steels are going through the stage of industrial implementation in metallurgical and tube production. Irradiation of experimental SAs with FEs of these steels is planned for 1998-1999.

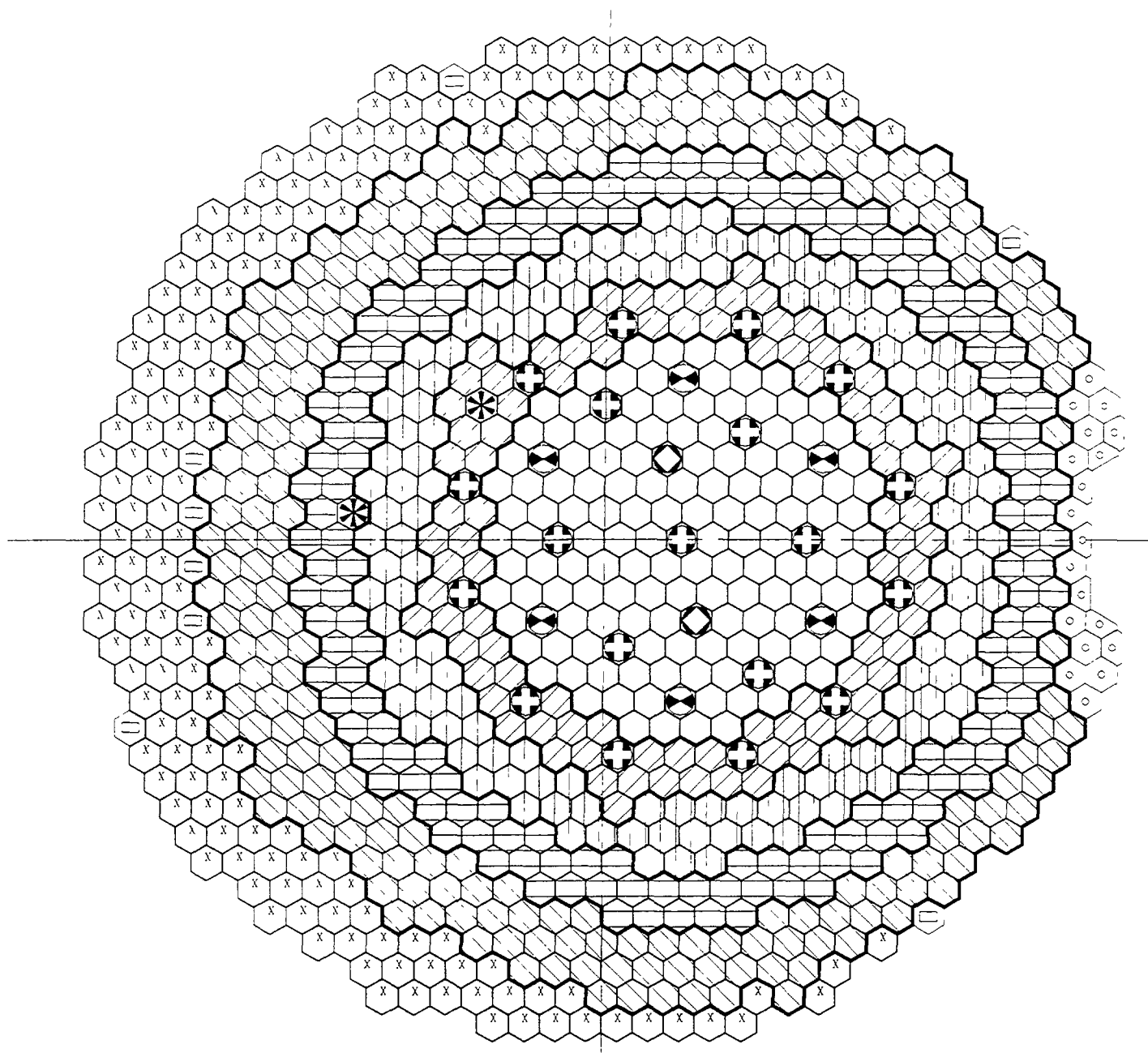
3). Improved steels ChS-68 CW and EP-172 CW with optimised fabrication technology are used as structural materials for FEs claddings.

Experimental SAs are developed with improved cladding steels ChS-68 CW and EP-172 CW that are structurally similar to standard SAs and differing in the FE size: 6.8×0.5 mm (previous one was 6.9×0.4 mm). Now, 6 SAs of this type are installed in the reactor.

It is expected that the use of these steels for FEs claddings will allow the following parameters to be attained: B_{\max} - 13.8 % h.a. , D_{\max} - 90 dpa, irradiation time - 4 runs.

Along with the development of new experimental SAs for the BN-600 reactor, an experimental irradiation device (ID) for testing individual experimental FEs to high burnups (to 20% h.a.) and a material testing assembly (MTA) for testing samples of prospective materials to high damage doses (150 dpa) have been developed (Fig.4,5).

The ID and MTA are similar and were developed on the basis of a standard SA which instead of having central FEs (31 in number) has a hexagonal channel along the entire FE bundle height. Into the channel, through a specially designed SA head , a removable container shaped as a



	136 SAs of inner core		19 shim rods
	94 SAs of intermediate core		2 control rods
	139 SAs of outer core		2 neutron sources
	161 SAs of inner radial blanket		163 in-vessel storage cells
	217 SAs of outer radial blanket		19 steel shield SAs
	6 emergency protection rods		8 service positions

Fig 2 – BN-600 core layout (type M1)

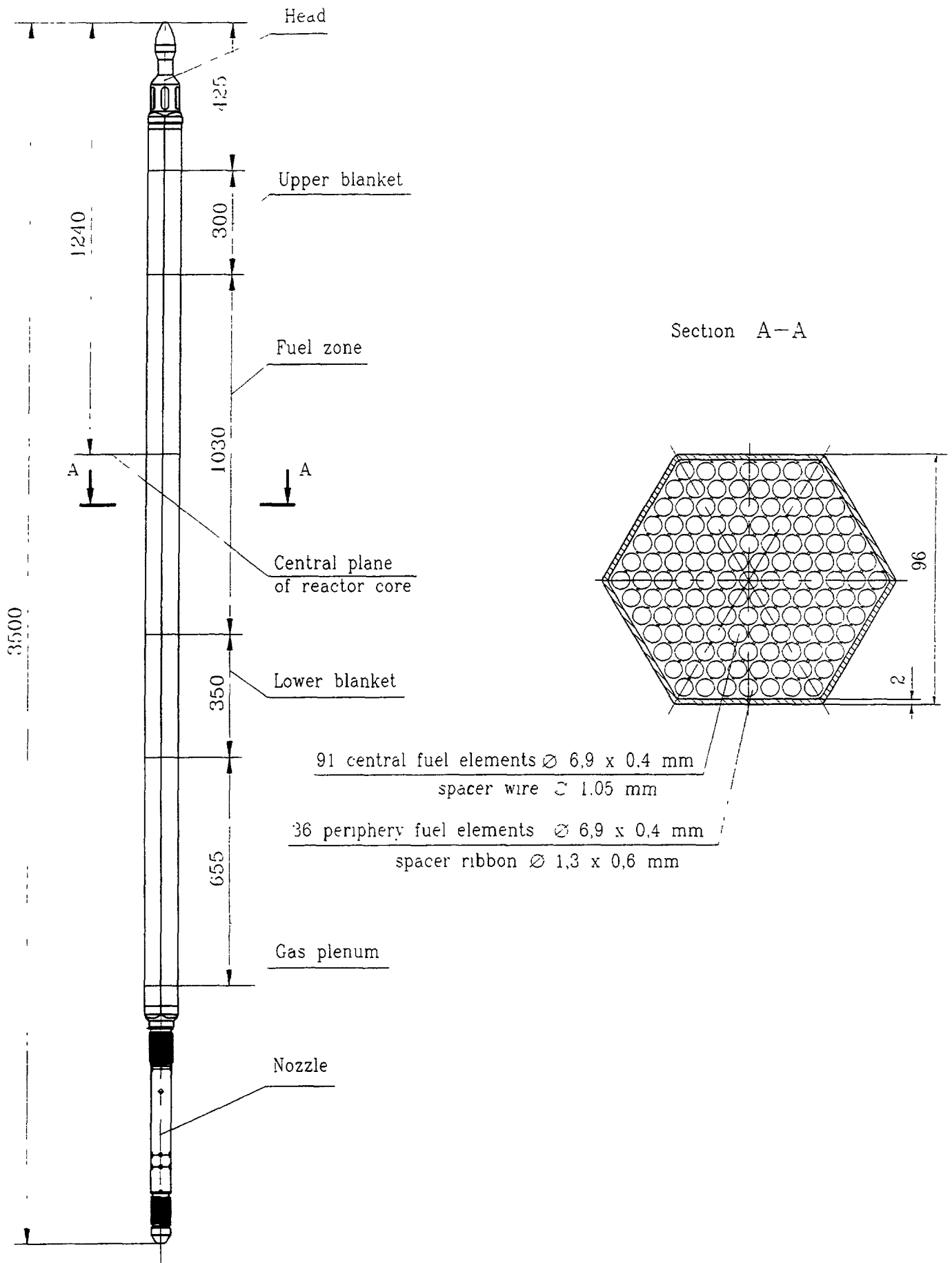


Fig 3 - BN-600 fuel sub-assembly

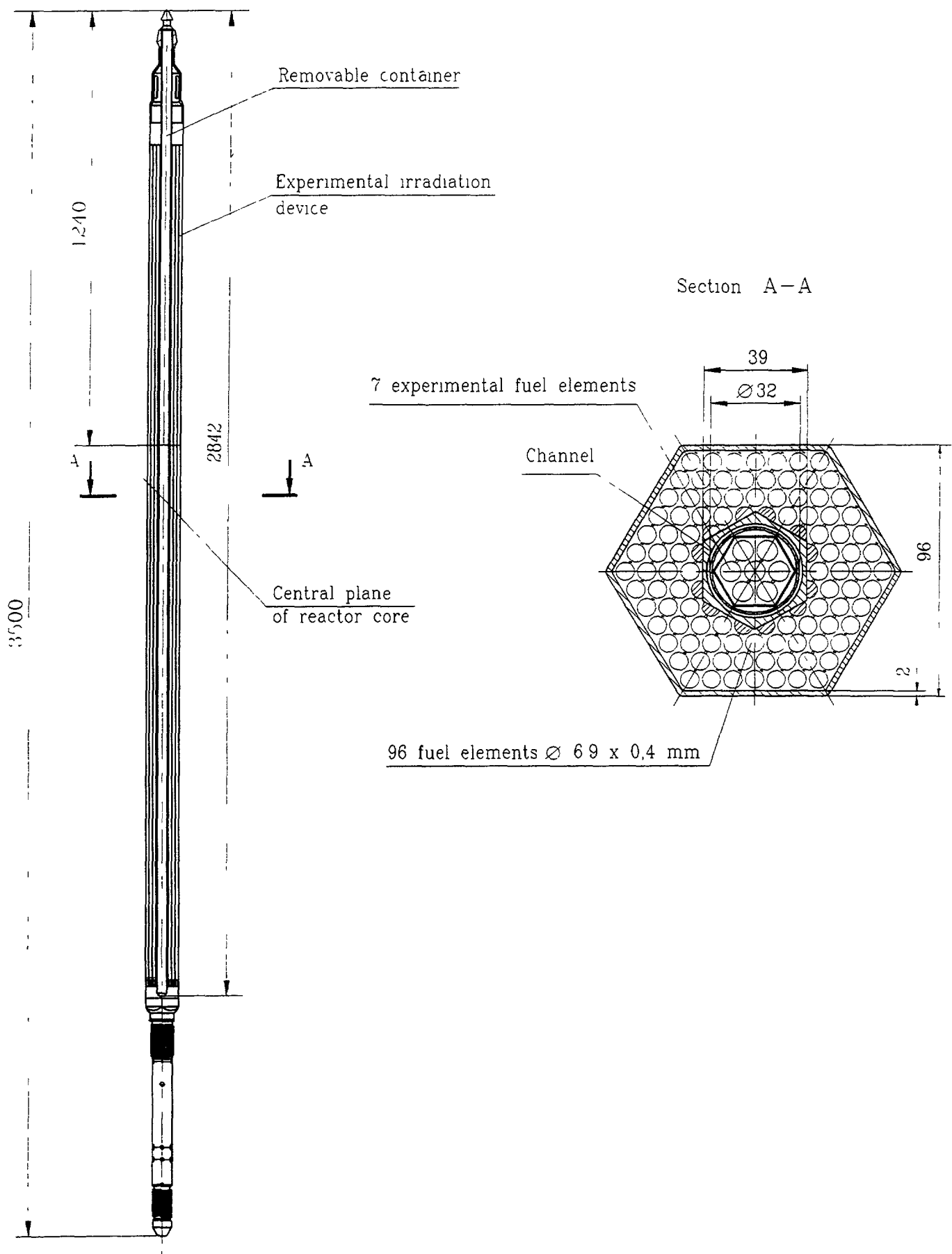


Fig 4 - Experimental irradiation device with removable container

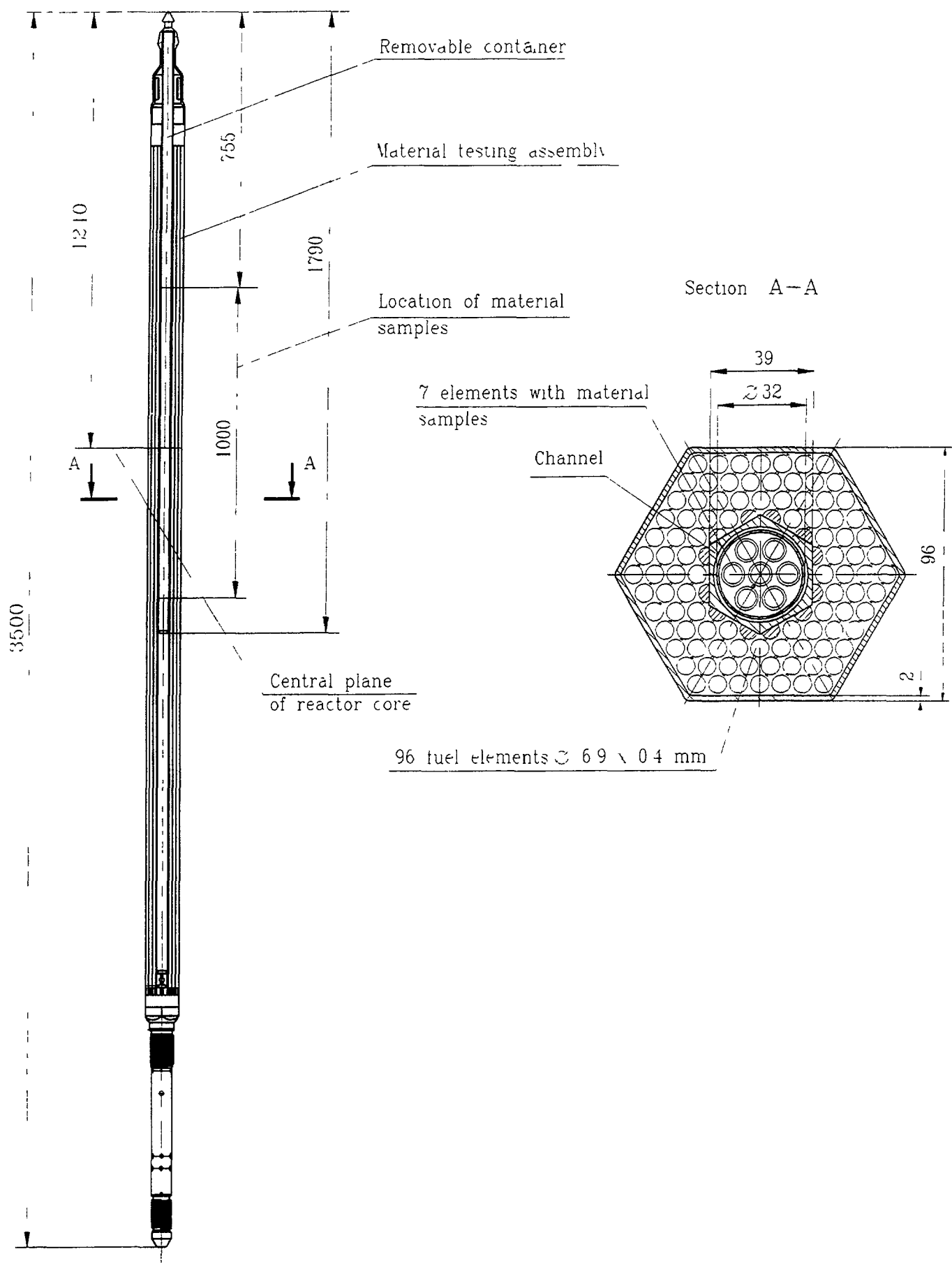


Fig 5 - Material testing assembly with removable container

tube provided with a head and plug is installed. Structural material of the channel and container is steel EP-450.

The hexagonal channel and the container have openings for cooling the assembly (ID or MTA). The container together with ID (or MTA) are of the same geometry as that of standard SA and, so, can be handled using the standard reactor refuelling path.

The ID and MTA design allows remote removal of the container under the protection of inert gas or under the sodium layer (in a spent fuel drum) from the irradiated assembly and its insertion into a "fresh" assembly for continued irradiation.

The ID container can hold up to 7 experimental full-scale FEs. The container head and plug have mesh filters for limiting the possible escape of fuel particles beyond the container boundary.

Depending on MTA type, the MTA with container allows the testing of 8 to 49 samples of structural materials (plate-type, tubular, pressure loaded or non-loaded) in a wide range of temperatures up to 700°C. For assuring stable temperature conditions during irradiation, the MTAs are arranged in the central core positions remote from the absorber rods.

Due to the possibility of continuing the irradiation of the removable container in "fresh" assemblies at ID and MTAs irradiation time within three runs, the container of each assembly can be irradiated for six runs. The following irradiation parameters are planned for this case:

- for container of ID: Bmax - 15-20 % h.a., Dmax - 150 dpa;
- for container of MTA: Dmax - 150 dpa.

5. CONCLUSION

Since the start of operation three cores (1st type, M and M1) were subsequently installed in BN-600 reactor. As a further step it is planned to install the 4th M2 core with maximum fuel burnup of 11.3 % h.a.

In the BN-600 reactor, tests are carried out to increase the lifetime of BN-600 standard SAs and to irradiate experimental SAs with MOX fuel in support of BN-600 and BN-800 core projects using MOX fuel.

Now the main direction for increasing the lifetime of SAs and fuel burnup is the development and study of new structural materials with increased irradiation stability for FEs claddings. Materials for future consideration in Russia are steel EP-450, steel ChS-68 CW with increased phosphorus content, steel EK-164 and improved steels ChS-68 CW and EP-172 CW.

For BN-600 reactor an irradiation device (ID) and a material testing assembly (MTA) are developed with a removable container allowing irradiation of prospective fuel compositions (to burnup of 15-20 % h.a.) and of structural materials (to a damage dose of 150 dpa at a temperature of up to 700°C).

S. GOVINDARAJAN, P. PUTHIYAVINAYAGAM,
S. CLEMENT RAVI CHANDAR, S.C. CHETAL, S.B. BHOJE
Indira Gandhi Centre for Atomic Research,
Kalpakkam, India

Abstract

Mixed carbide fuel of 70% PuC content is being used as driver fuel in the Fast Breeder Test Reactor (FBTR) for the first time in the world. When it was first proposed for FBTR small core, its performance potential had to be assessed based upon extrapolated data. High Pu content of the fuel reduces the thermal conductivity and melting point. Also, small diameter of FBTR fuel results in high heat flux at fuel-clad gap. A conservative initial estimate limited the linear power to 250 W/cm and the burnup to 25,000 MWd/t. Subsequently, detailed analyses were performed with the use of measured as well as data from literature. Based on this, the linear power has been upgraded to 320 W/cm. Also analyses indicate that the fuel is capable of sustaining a peak burnup of 50,000 MWd/t. Recently, the central fuel subassembly was unloaded for post irradiation examination (PIE) after the initial target burnup of 25,000 MWd/t. Preliminary results from PIE indicate that the analysis is well supported by the results.

1. INTRODUCTION

The Mark I small carbide core of the Fast Breeder Test Reactor (FBTR) employs mixed (U-Pu)C of 70% PuC composition. At the time of installation of the core, the targets set for the fuel were 250 W/cm for peak linear heat rating and 25,000 MWd/t for peak fuel burnup. These targets were revised after rigorous analysis to 320 W/cm and 50,000 MWd/t respectively. The fuel has reached a peak burnup of 30,000 MWd/t so far without any fuel failure. The central subassembly of the core was discharged after a burnup of 25,000 MWd/t for post-irradiation examination (PIE). This paper discusses the details of analysis carried out to upgrade the performance targets of the fuel and also compares the swelling data obtained from PIE with the data used for analysis. The design specification for the Mark I core fuel is given in Table I.

2. LINEAR HEAT RATING

The design criteria followed in fixing the allowable operating heat rating of the fuel is that there should be a margin of at least 15% between operating linear heat rating and the safety limit. The safety limit is defined as the rating at which incipient melting occurs after taking into account all uncertainties in properties, operation etc. It is also to be ensured that the overpower trip threshold is set well within safety limit to take care of overshoot under transients. This design approach is illustrated in Fig. 1.

The data used for determining safety limits of the fuel is given in Table II. Maximum uncertainty in determining safety limit is caused by the fuel-clad gap conductance. Because of the tolerances specified on clad O.D., clad thickness and pellet diameter, the cold diametral gap varies over the range of 0.06 - 0.30 mm for fresh fuel. The gap conductance also varies with the linear heat rating because of temperature dependence of hot gap and thermal conductivity of helium. In reality, there could be restructuring of fuel in the reactor due to cracks developing owing to thermal stress and this could reduce the gap to some extent.

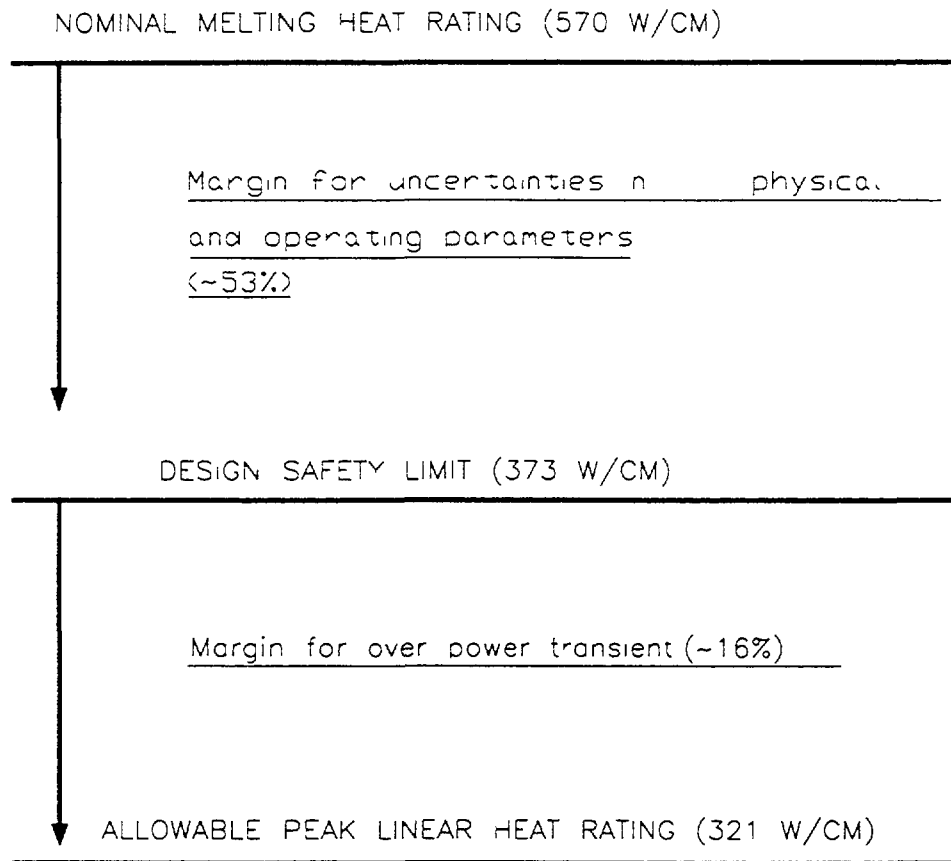


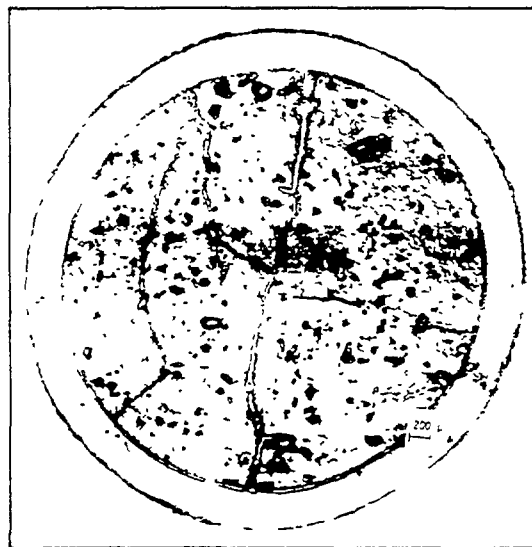
FIG Design approach for allowable heat rating.

TABLE I. DESIGN SPECIFICATION FOR MARK I CORE FUEL

Fuel	:	(U - Pu) C
PuC content	:	70 w/o
M ₂ C ₃ content	:	6 - 12 w/o
Clad OD	:	5.1 mm
Clad thickness	:	0.37 mm
Pellet diameter	:	4.18 mm
Pellet density	:	90% of T.D.
Smeared density	:	83% of T.D



a) OUT-PILE TEST (320 W/cm)



b) PIE MICROGRAPH (300 W/cm, 25000 MWd/t)

FIG. 2. View of fuel cross section.

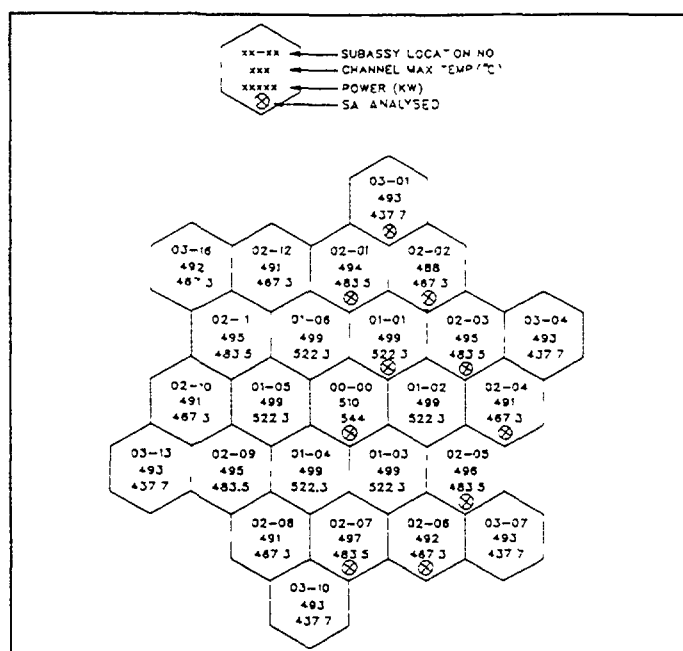


FIG. 3. FBTK mark I core configuration.

Out-pile tests were carried out in the Radiochemistry laboratory at the **Indira Gandhi Centre for Atomic Research** to understand the thermal behaviour of the fuel. The fuel specimens were heated by electrical resistance heating upto a rating of 500 W/cm in the set up. The cross section of the fuel at a rating of 320 W/cm is shown in Fig.2. For comparison, the cross section showing the microstructure obtained by PIE is also shown adjacently.

The theoretical analysis without taking into account restructuring gave a design safety limit of 373 W/cm on linear power for fresh fuel and a value of 800 W/cm for fuel fully in contact with clad and reaching a saturated value of gap conductance of 1.5 W/cm²-K. With this safety limit, the operating heat rating was limited to 320 W/cm for the Mark I core fresh fuel. As the linear heat rating has significant influence on the burnup of fuel, both in free swelling phase and the Fuel Clad Mechanical Interaction (FCMI) phase, it was decided to keep the linear heat rating at 320 W/cm itself, till some data on the swelling rate of fuel is obtained.

3. BURNUP

Since carbide fuel of this composition is being used for the first time in the world, there are no data available on the burnup capability of this fuel. In the analysis for the estimation of fuel capability in terms of its achievable burnup at a given linear power, swelling and thermal and irradiation creep of both the fuel and the clad play important roles. The unavailability of data on swelling and creep of the FBTR fuel composition enhances the uncertainty of predictions. An attempt has however been made based on data available for other mixed carbide fuels. Most of the data available for carbide fuel in the open literature are only for the standard mixed carbide fuel containing 15-20% PuC. Hence all the data concerning the fuel material have been suitably modified and adopted for FBTR fuel. Also data on clad irradiation creep available in the literature is used in the analysis. For thermal creep and out-pile rupture life of clad material the data generated in-house [1] have been considered along with those published in the literature. The analysis covers the entire core as linear power varies both radially and axially in the core.

The analysis was carried out for both nominal and hotspot conditions. The attainable burnup values for the maximum rated fuel pin of all the subassemblies are presented. The Mark I core configuration is shown in Fig.3. The subassembly ring number, its serial number, thermal power and maximum channel temperature are shown in the same figure. There are 10 subassemblies having a distinct combination of thermal power and coolant channel temperature for which analysis has been carried out and they are indicated by a circle mark in the same figure and these assemblies are representatives of the entire core.

3.1. Fuel Material Properties

The properties involved in the analysis are thermal conductivity, melting point, coefficient of linear thermal expansion, volumetric swelling rate, thermal and irradiation creep rate etc. The melting point and mean coefficient of thermal expansion are measured/estimated to be 2100 K and 11.2×10^{-6} respectively [2]. The average thermal conductivity corresponding to the smeared density of 83% is 10.575 W/m-K which is derived from the measured data [3]. The swelling rate is a strong function of fuel centre temperature and literature data is for standard mixed carbide fuel [4]. The melting point of the standard mixed carbide fuel is reported as 2743 K. The temperature data points in the available literature on swelling of reference fuel were normalised, using the ratio of melting points, in order to get the temperature data points for FBTR fuel. The percentage volumetric swelling rate for the FBTR fuel as a function of fuel centre temperature, derived by the above procedure, is shown in Fig.4. The equation for thermal

creep rate for this fuel is modified in the same way from the correlation published in the literature [5] and is given below.

$$\dot{\epsilon}_i = 1.49 \times 10^{10} \times \sigma^{2.44} \times \exp(-50000/T)$$

The irradiation creep of fuel is almost independent of temperature and is a function of stress and fission density rate [6]. Many correlations have been published in the literature. Among them the one proposed by Muller-Lyda and Dienst is found to be close to the experimental results observed and hence the same was adopted for this analysis.

$$\dot{\epsilon}_i = 1.37 \times 10^{-27} \times \sigma \times F$$

3.2. Clad Material Properties

For the clad material, in addition to the properties discussed for fuel, both in-pile and out-pile creep rupture life of clad play a dominant role in determining the burnup capability of the fuel. The thermal conductivity at the middle and top column of fuel pin are worked out as 20.6 and 21.7 W/m-K respectively and the mean coefficient of thermal expansion is 18.5×10^{-6} /K based on in-house data. The irradiation creep behaviour of this material adopted in this study is due to Puigh et al [7] and only the secondary creep term is employed for simplicity. The correlation thus becomes

$$\dot{\epsilon}_i (\%) = 7.25 \times 10^{-4} \times \sigma \times \phi$$

With regard to thermal creep, measurements have been made on 20% CW 316 SS tubes inhouse [1]. With the data available, the following correlation for creep strain rate has been derived as a function of rupture life.

$$\dot{\epsilon}_i = 0.000293728 (t_{ro})^{-1.53687}$$

The rupture life at the working temperature is to be obtained from Larson-Miller-Parameter (LMP) which in turn could be obtained from correlations linking LMP and stress. For out-pile rupture life and in-pile rupture life, the following correlations are derived using LMP approach based on measured data and FFTF data [8,9]. A value of 13.5 is assumed for the constant.

For out-pile rupture life,

$$\log t_r = (4.3800 - \log \sigma) / (1.4087 \times 10^{-4} \cdot T) - 13.5 \quad \text{for } \sigma > 200 \text{ MPa}$$

$$\log t_r = (6.4515 - \log \sigma) / (2.8120 \times 10^{-4} \cdot T) - 13.5 \quad \text{for } \sigma < 200 \text{ MPa}$$

For in-pile rupture life,

$$\log t_r = (5.4832 - \log \sigma) / (2.2506 \times 10^{-4} \cdot T) - 13.5 \quad \text{for } \sigma > 145 \text{ MPa}$$

$$\log t_r = (6.4377 - \log \sigma) / (2.8972 \times 10^{-4} \cdot T) - 13.5 \quad \text{for } \sigma < 145 \text{ MPa}$$

3.3. Analytical Modelling

This study pertains only to the steady-state operation of the fuel. The calculation of attainable burnup is carried out for fuel pin at two axial locations viz., fuel column middle and top. The analysis is carried out for a peak linear heat rating of 320 W/cm. The various hot spot factors are given in the following table and they are assumed to be same for all SA. Various data used in the analysis such as radial power factors, average linear power and the linear power at the fuel middle and top column positions for all SA are given in the table below. Clad wastage due to sodium corrosion is negligible for reactor grade sodium.

HOT SPOT FACTORS:

SA	Fuel	Fuel-Clad gap	Clad	Film	Coolant
1 - 10	1.3077	1.1924	1.3131	1.5749	1.1795

DATA FOR ANALYSIS:

Sl.no	SA location	Radial power factor	Linear power (W/cm)		
			Average	Fuel middle	Fuel top
1	00-00	1.0035	278.7	320.0	214.2
2	01-01	1.0142	267.6	310.5	207.9
3	02-04	1.0269	239.4	281.3	188.3
4	02-03	1.0249	247.7	290.5	194.5
5	02-02	1.0269	239.4	281.3	188.3
6	02-01	1.0249	247.7	290.5	194.5
7	02-07	1.0249	247.7	290.5	194.5
8	02-06	1.0269	239.4	281.3	188.3
9	02-05	1.0249	247.7	290.5	194.5
10	03-01	1.0072	224.2	258.4	173.0

The analysis is divided into two phases. In each phase different phenomena dominate and the total achievable burnup is the sum of the two. The first phase is known as free swelling phase in which the initial gap provided between clad and fuel pellet closes on account of fuel swelling due to irradiation. The achievable burnup in this is governed by linear power. Among the data needed for finding the temperature distribution, the gap conductance is an important one and it varies with the fuel-clad gap. As the fuel burns, the fuel swells and hence the gap reduces. On account of improvement in the gap conductance, the temperature drop in the gap too decreases which in turn reduces the fuel centre temperature. Gap conductance keeps on increasing as the burnup proceeds and reaches a steady-state value as the fuel-clad contact occurs. The time taken to reach this point determines the attainable burnup in the free swelling phase. For finding the temperature distribution, the fuel pellet is modelled as a set of concentric cylinders.

TABLE II. DATA FOR DETERMINING LINEAR RATING

Specific Heat of Sodium	: 1266 J/ kg - K
Thermal Conductivity of Sodium	: 64.9 W/ m - K
Thermal Conductivity of SS 316 clad	: 21.0 W/ m - K
Thermal Conductivity of fuel	: $6.253 - 2.8604 \times 10^{-3} T (K)$ $+ 1.879 \times 10^{-6} T^2 + 1.1559 \times 10^{-18} T^3$ $- 4.55618 \times 10^{-12} T^4$ W/ m - K
Film Heat Transfer coefficient between Sodium and Clad	: 120000 W/ m ² - K
Fuel Thermal expansion coefficient	: $6.95 \times 10^{-6} + 5 \times 10^{-9} T (K)$ $- 0.1134 \times 10^{-11} T^2$ / K
Clad Thermal expansion coefficient	: $1.789 \times 10^{-5} + 2.398 \times 10^{-9} T (K)$ $- 3.269 \times 10^{-13} T^2$ / K
Porosity correction factor	: $(1 - P) / (1 + P)$ P - porosity factor
Density of fuel	: 92 % T.D.
Melting point of fuel	: 2123 K (1850 ° C)

The second phase of the analysis is known as Fuel-Clad Mechanical Interaction phase (FCMI). In this phase, once the pellet and clad make physical contact with each other, any further swelling of fuel exerts pressure on clad. This pressure is exerted on both fuel and clad resulting in various stresses on these components. Under the influence of these stresses both fuel and clad start creeping. FCMI pressure goes on increasing till a steady state equilibrium is attained between fuel swelling, clad creep and fuel creep. The steady-state value of gap conductance is assumed to be 1.5 W/cm²/K. The swelling rate of fuel becomes a constant when the gap conductance saturates at the steady-state value. The life of the fuel pin achievable in FCMI phase depends on creep rupture life of clad corresponding to the FCMI steady-state pressure.

The attainable burnup in FCMI phase is mainly governed by creep rupture life of clad which in turn depends on the clad midwall temperature. In some cases where the clad stresses are very low, the rupture life would obviously be very high. However, there is a physical limitation to the creep of fuel as dictated by the available porosity in the fuel. Hence in such cases where stresses are low, the burnup is governed by the available space. For finding the stresses in the clad, the clad is modelled as a thin cylinder. The fuel pellet is modelled as a solid thick cylinder. For the fuel pellet, various properties used in the analysis are derived for a volume averaged temperature.

TABLE III . ATTAINABLE BURNUP

SA LOCATION		Nominal temperature					Hot spot temperature				
		00-00	01-01	02-04	02-03	03-01	00-00	01-01	02-04	02-03	03-01
TOP OF FUEL COLUMN											
Linear Power	W/Cm	214 2	207 9	188 3	194 5	173 0	214 2	207 9	188 3	194 5	173 0
Clad midwall temp	deg C	533 4	521 7	511 6	516 3	511 9	576 7	562 7	550 2	555 9	550 2
Fuel centre temp	deg C	811 2	791 3	755 8	768 4	736 2	928 0	903 6	859 0	874 8	833 9
Free swell burnup	MWd/Kg	48 1	50 6	55 8	54 0	59 6	38 1	41 2	47 2	45 2	51 1
FCMI burnup	MWd/Kg	20 6	30 8	41 5	38 5	42 8	23 2	16 3	12 9	12 6	11 6
Total burnup	MWd/Kg	68 7	81 4	97 3	92 5	102 4	61 3	57 5	60 2	57 9	62 7
Clad stress - FCMI	MPa	240 7	247 2	246 8	246 6	241 2	160 5	193 1	211 0	212 3	222 0
Allowable stress	MPa	311 2	339 9	364 8	353 3	364 0	270 4	281 1	290 7	286 3	290 7
MIDDLE OF FUEL COLUMN											
Linear power	W/Cm	320 0	310 5	281 3	290 5	258 4	320 0	310 5	281 3	290 5	258 4
Clad midwall temp	deg C	454 0	447 4	440 1	443 2	438 6	486 1	478 1	468 7	472 5	466 2
Fuel centre temp	deg C	869 9	851 0	805 7	820 7	774 4	1012 2	988 6	931 1	950 0	891 0
Free swell burnup	MWd/Kg	33 4	35 6	41 7	39 6	46 3	22 7	25 0	31 8	29 5	37 5
FCMI burnup	MWd/Kg	35 2	36 1	38 5	37 7	40 3	24 5	26 6	30 2	28 9	33 4
Total burnup	MWd/Kg	68 6	71 7	80 2	77 3	86 6	47 2	51 6	62 0	58 4	70 9
Clad stress - FCMI	MPa	286 2	291 4	285 1	290 1	273 2	115 6	142 7	224 2	196 0	267 8
Allowable stress	MPa	467 6	475 0	483 2	479 8	485 0	427 3	440 5	451 1	446 8	453 9

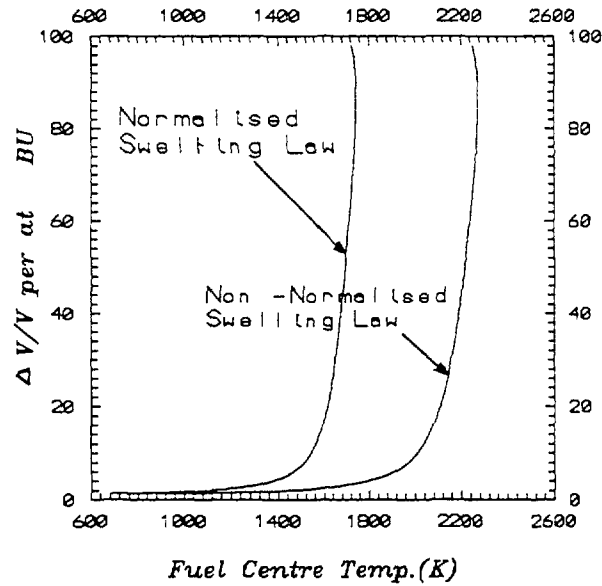


FIG. 4. Fuel Swelling Rate

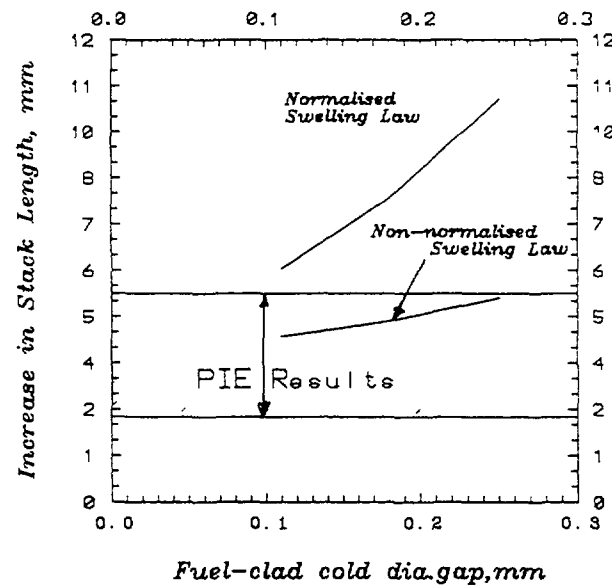


FIG. 5. Elongation of fuel pellet stack length.

3.4. Burnup estimates

The attainable burnup for Mark I core fuel of FBTR have been estimated for the entire core for a peak linear heat rating of 320 W/cm in order to consider the enhancement of burnup. The results are given at two axial locations viz. fuel column top and middle at both nominal and hot spot temperature conditions. The attainable burnup values for nominal temperature conditions and hot spot temperature conditions are presented in Table III. The study shows that burnup attainable at the fuel middle column is the limiting one for nominal temperature conditions. But under hot spot temperature conditions, for subassemblies in ring 2 and beyond, the burnup attainable at fuel top column appears to be the limiting one. The total attainable

burnup is well above 50,000 MWd/t for all the SA under both nominal as well as hot spot conditions except in the case of central subassembly in hot spot condition where it is 47,200 MWd/t

4. FREE SWELLING RATE

As earlier mentioned, the free swelling rate of the fuel has been derived from the data on (U-20%Pu)C fuel. Recently PIE carried out on the central SA removed from the FBTR after it had reached a burnup of 25,000 MWd/t has given data on the length increase in the pellet stacks of nine pins. This data has been compared with the expected stack elongation. The swelling of fuel as calculated using the data on (U-20%Pu)C fuel (non-normalised) and that using the normalised data are plotted in Fig.5. It appears that the data on (U-20%Pu)C is directly applicable for the FBTR fuel.

5. CONCLUSION

The performance of FBTR Mark I core carbide fuel is good. Based on the analyses carried out, its linear heat rating has been raised from 250 W/cm to 320 W/cm and the fuel has seen a peak burnup of 30,000 MWd/t so far without any fuel failure. PIE performed on the central SA removed from the core after the initial target burnup of 25,000 MWd/t reveals that the Pu rich carbide fuel swelling behaviour is more or less the same as the (U-20%Pu)C fuel. The target burnup is enhanced to 50,000 MWd/t based on the estimates. Further enhancement of linear heat rating upto 400 W/cm will be considered.

REFERENCES

- [1] MATHEW, M. D., et al., Creep rupture properties of solution annealed and cold worked type 316 stainless steel cladding tubes, IGC-117, 1990.
- [2] SENGUPTA, A. K., et al., Melting temperature of mixed carbide fuel for FBTR, Seminar on Fast Reactor Fuel Cycle, Kalpakkam, 1986.
- [3] GANGULY, C., Communication on observed Thermal conductivity data, Ref. No. RMD/(11.6.4)/93/105, BARC.
- [4] MIKAILOFF, H., L'element combustible carbure a joint helium pour la filiere a neutrons rapides: problems poses par le gonflement du combustible, BIST 196 (1974).
- [5] PREUSSER, T., Modelling of carbide fuel rods. Nucl. Tech. 57 (1982) pp 343-371.
- [6] MULLER-LYDA, I., DIENST, W., A measurement of the irradiation induced creep of mixed carbide nuclear fuel. Journal of Nuclear Materials 90 (1980) pp 232-239.
- [7] PUIGH, R. J., et al., An in-reactor creep correlation for 20% cold worked AISI 316 stainless steel. Proc. Symp. on Effects of radiation on materials. Scottsdale, June 1982 (ASTM STP 782, pp 108-121).
- [8] PUIGH, R. J., HAMILTON, M.L., In-Reactor creep rupture behaviour of the D9 and 316 alloys. ASTM STP 956, pp 22-29.
- [9] LOVELL, A. J., et al., In-Reactor creep rupture of 20% CW AISI 316 stainless steel. Journal of Material Science. 16 (1981) pp 870-876.

POST-IRRADIATION EXAMINATION OF MIXED (Pu, U)C FUELS IRRADIATED IN THE FAST BREEDER REACTOR

R. BALDEV, K.V. KASIVISWANATHAN, V. VENUGOPAL,
N.G. MURALIDHARAN, A. RAMABATHIRAN, N. RAGHU, J. JOSEPH,
S. KURIEN, B. VENKATARAMAN, M.T. SHYAMSUNDER,
S. MURUGAN, K.A. GOPAL, P.V. KUMAR, P. KALYANASUNDARAM
Metallurgy and Materials Group,
Indira Gandhi Centre for Atomic Research,
Kalpakkam, India



Abstract

The Fast Breeder Test Reactor (FBTR) at Indira Gandhi Centre for Atomic Research (IGCAR), Kalpakkam, India, using mixed (Pu,U)C fuel has completed eleven years of operation. One fuel subassembly which has seen more than 25,000 MWd/t burn-up has been discharged from this reactor taken up for post-irradiation examination. The PIE carried out on this fuel subassembly has established that the fuel has performed satisfactorily and it is capable of being taken to higher levels of burn-up and linear heat ratings. The facilities available for PIE of advanced fuels and the PIE work carried out are discussed in detail in this paper.

1. INTRODUCTION

The Fast Breeder Test Reactor (FBTR) with a small core, using mixed plutonium-uranium carbide (70% PuC, 30% UC) as its driver fuel, has achieved a maximum power of 10.5 MWt, and the fuel has seen a peak linear heat rating of 320 W/cm. This fuel has so far achieved more than 30,000 MWd/t burn-up, without any failure.

Post-Irradiation Examination (PIE) was carried out on a fuel subassembly discharged from the reactor, after reaching a burn-up of more than 25,000 MWd/t. In addition, PIE excluding metallography has been carried out on four experimental fuel pins irradiated in FBTR. These fuel pins contain fuels with the present core composition as well as the proposed expanded core composition (55% PuC, 45% UC). The irradiation experiments are undertaken to understand the beginning of life performance of these fuels, compare the performance of the fuel compositions of the present core and of the proposed expanded core. This paper discusses in detail the PIE done on the driver fuel discharged after 25,000 MWd/t burn up. Results of PIE on experimental fuel pins irradiated in FBTR are also briefly touched upon. A brief description of the PIE facilities for metallurgical examinations at Radiometallurgy Laboratory (RML), IGCAR is also given in this paper.

2. DESCRIPTION OF PIE FACILITY

PIE facilities at RML, IGCAR can remotely handle and examine highly irradiated advanced fuels in the inert gas (nitrogen) atmosphere hot cells where the temperature, pressure and cell atmosphere are closely monitored and controlled. The PIE facilities consist of seven concrete shielded hot cells and a few lead shielded cells. The concrete shielded hot cells have walls made of high density concrete (density 3.5 gm/cc, wall thickness 1200mm), and the lead shielded cells have walls of lead (250/200mm thick). The hot cells are equipped with



FIG 1 A view of the operating area of the hot cells

master-slave-manipulators for carrying out operations in the hot cells. The cells are also equipped with power manipulators for handling loads up to 50 kg, and in-cell cranes for handling heavier loads up to one tonne. Lead glass windows are provided on the cell wall for viewing into the cells. These concrete shielded hot cells are designed to handle irradiated material with radioactivity up to 3.7×10^7 GBq. and the lead cells up to 3.7×10^4 GBq. Fig.1 shows a view of the operating area of the hot cells.

The hot cells have a high purity nitrogen gas atmosphere, with provisions for changing over to air atmosphere during examinations when inert atmosphere is not required or during man entry into the cells. This recirculatory nitrogen gas system with provisions for cooling, filtration and purification, maintains the hot cells at a negative pressure (-25mm water column nominal), and at very low levels of moisture and oxygen.

A remotely operated trolley, mounted with a shielded flask is used for the transport of plutonium rich fuel subassemblies and irradiated objects from FBTR to RML. A Vertical Transfer System installed in the hot cell floor is used for transfer of irradiated subassemblies from this shielded flask into the hot cell. It has a vertical double door alpha-tight transfer system (150mm diameter), specially adapted for this purpose.

A horizontal transfer system installed in the RML hot cell wall is used for transferring dismantled irradiated fuel and structural materials from RML to other laboratories for radiochemical analysis, reprocessing or waste disposal. The horizontal transfer system also is a double door alpha-tight transfer system (270mm diameter).

RML hot cells have state-of-the-art techniques for metallurgical examination of the irradiated materials. The PIE techniques cover a wide spectrum of examination methods, nondestructive as well as destructive. The techniques have been chosen to extract maximum information with reliability and accuracy. The details of in-cell equipments and other PIE facilities are described below.

The sodium removal system provided in the hot cell consists of a leak-tight chamber to house the subassembly and two tanks containing ethanol, which is used as a cleaning fluid, with provision for pumping the liquid from one tank to the other through the chamber, using compressed nitrogen. This system is used to remove the residual deposits of sodium from the external as well as internal surfaces of the subassemblies.

A remotely operated CNC drilling and milling machine provided in the hot cell is used to dismantle the subassembly without damaging the fuel pins. It can also machine tensile test specimens from the wrapper material of the subassembly. It has an inductive type probe attached to it, to facilitate dimensional measurements of the subassembly, with an accuracy of ± 20 microns.

A 30 kW(Th) swimming pool type reactor (KAMINI) installed below the hot cells, provides the neutron beam required for taking the neutron radiography of the fuel subassemblies and fuel pins. The reactor is capable of giving a collimated neutron beam of flux 107 n/sq.cm/sec at the radiography site. A precise positioning and indexing mechanism (0.5 degree steps) facilitate neutron tomography of fuel pins and fuel subassemblies. Pin-to-pin spacing, plutonium redistribution, depletion of boron in the control rods etc. can be studied using this system.

Leak testing of the fuel pins are being carried out using a glycol leak test system, with a sensitivity of 100 microns through hole.

Diameter measurements of the fuel pins are done on a profilometer which has provisions for holding the pin vertically and to move a carriage holding two LVDTs (accuracy of measurement $\pm 2 \mu\text{m}$) against the pins in diametrically opposite directions to scan the diameter along the length of the fuel pins. Data acquired through a computer gives the diametrical profile of the fuel pins.

Eddy current testing (ECT) of the fuel pins is done with the pin held vertically and by moving the encircling ECT probe along the length of the pins. A PC based data acquisition system is used and the results are compared with those from calibrated pins having known defects in the clad tube. ECT can detect abnormalities on the cladding tube as well as on the cladding tube-fuel pellet interface (sensitivity 7% wall thickness).

A 420-KV industrial X-ray machine is used to radiograph the fuel pins. This technique is complimentary to the neutron radiography technique. Special techniques have been developed to get the desired sensitivity by reducing the effect of fogging of film due to gamma rays from the pins. Radiographs are studied using image enhancement techniques. Dimensional measurements are made from the radiographs applying suitable correction factors, to get information such as pin diameter, pellet-clad-gap, pellet-to-pellet gap, stack length, spring compression etc. (accuracy of measurements in the radial direction of pins is 0.05mm, and in the axial direction of the pins is 0.5mm). X-radiography can also reveal chipping of pellets, major clad defects etc.

A micro gamma scanning system is provided to evaluate the fissile column length, distribution of fission products and burn-up. This system consists of a bench with stepper motor controlled X,Y movements and rotation for positioning the fuel pin with respect to any of the four collimators which are provided in a turret mechanism. The turret brings

the required collimator in line with the fuel pin and the detector positioned outside the hot cell. This facilitates measurement of gamma spectrums, in the radial as well as axial direction of the fuel pins using the detector and multichannel analyser combination.

The metallographic specimen preparation and examination facilities include a fuel pin sectioning device, a vacuum impregnation system to impregnate the fuel pin with a liquid epoxy resin in order to immobilize the fuel column inside the clad tube before sectioning, remote mounting of specimens, polishing, etching and replica making arrangements, and a metallograph for taking metallographic pictures of the cut sections of the fuel pins. The metallographic pictures are subjected to image processing to evaluate the metallographic structures.

A mechanical testing facility is being established to evaluate the mechanical properties of the cladding tube as well as structural materials. This includes tensile testing, miniature specimen testing, dynamic testing and burst testing.

3. PIE OF FBTR FUEL SUBASSEMBLY

The central fuel subassembly from FBTR with the following irradiation data was discharged in July 1996 and taken up for PIE.

TABLE I. IRRADIATION DATA OF FUEL SUBASSEMBLY

Total burn-up	: 25,036 MWd/t
Peak linear heat rating	: 320 W/cm
Peak power	: 10.5 MWt
Fuel theoretical density	: 90%
Fuel smear density	: 83%
Type of bond	: Helium
<i>Geometry</i>	
outer diameter of pin	: 5.1mm
inner diameter of pin	: 4.36mm
effective stack length	: 321 mm

Visual examination of the fuel subassembly before sodium cleaning did not show any corrosion or surface defects. The subassembly was washed in the alcohol recirculatory system to remove the residual sodium deposits from the external as well as internal surfaces of the subassembly. The shining appearance of the hexagonal sheath after cleaning indicated that excellent purity of sodium has been maintained in the reactor. Fig.2 shows a view of the subassembly kept on the visual examination bench.

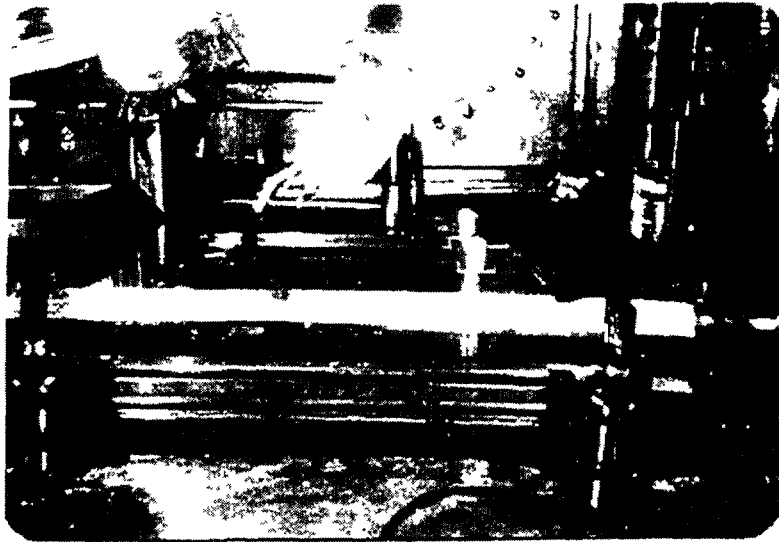


FIG.2 A view of fuel subassembly on visual examination bench

Dimensional measurements on the fuel subassembly indicated that the hexagonal sheath in the fuel region of the subassembly did not have any swelling or bulging. The width across-flat of the hexagonal sheath was found to be generally within the original limits of tolerances. Fig.3 shows a view of the fuel subassembly held on the work table of the CNC machine. Fig.4 shows an image of the subassembly reconstructed using the numerous dimensional measurements carried out along its entire length, using the machine.

The subassembly was dismantled using the CNC remote milling and drilling machine. Fuel pins extracted from the assembly, did not show any corrosion or deformation on visual examination. However, the central fuel stack regions of the clad appeared coloured due to the

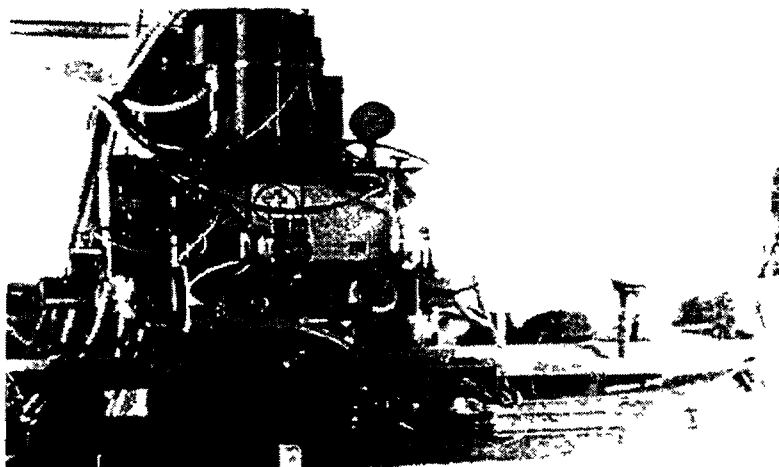


FIG. 3. A view of fuel subassembly during dimensional measurements

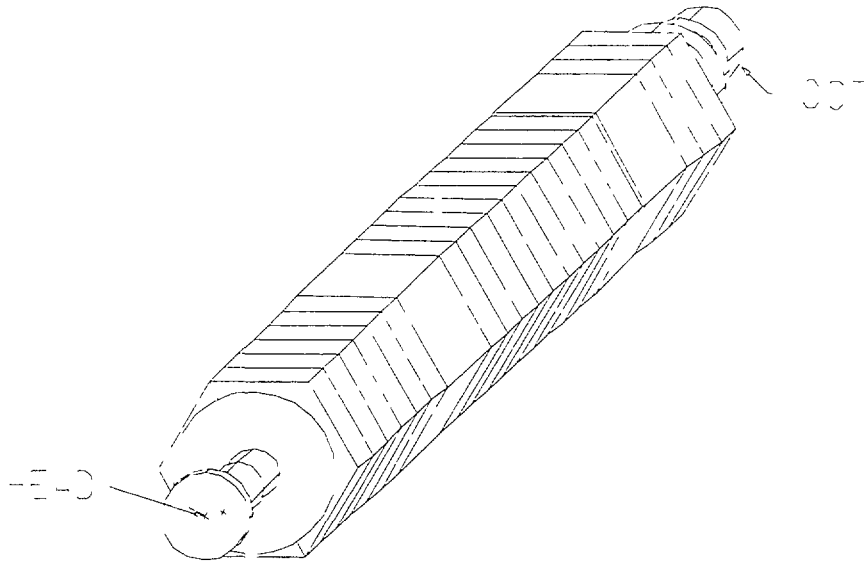


FIG. 4. Reconstructed view of the fuel subassembly

effect of temperature. Fig.5 shows a view of the dismantled pins stacked in a rack. Glycol leak testing of the fuel pins did not indicate any identifiable leaks. Nine fuel pins which lie in a line on the cross section of the subassembly as indicated in Fig.6 were selected for further detailed examinations.

Diameter and length measurements carried out on nine pins indicated that the diameters and lengths are generally within the original limits of tolerance and that there is no clad deformation. Fig.7 shows a typical diameter profile of the fuel pins.

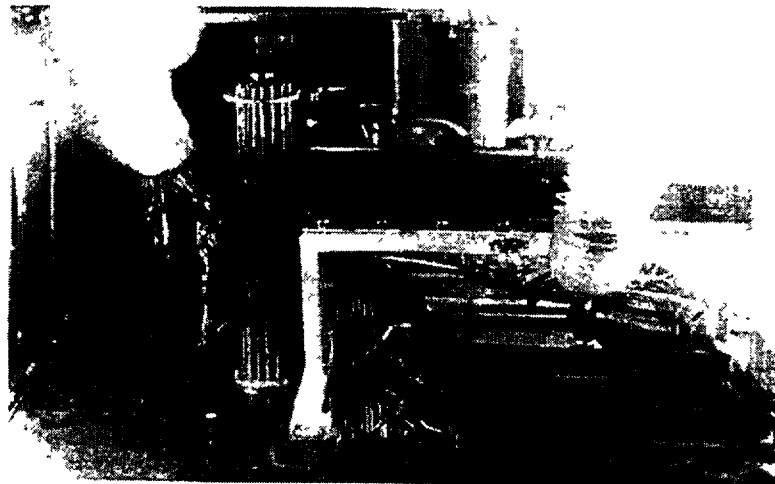


FIG. 5. A view of the fuel pins dismantled from the subassembly

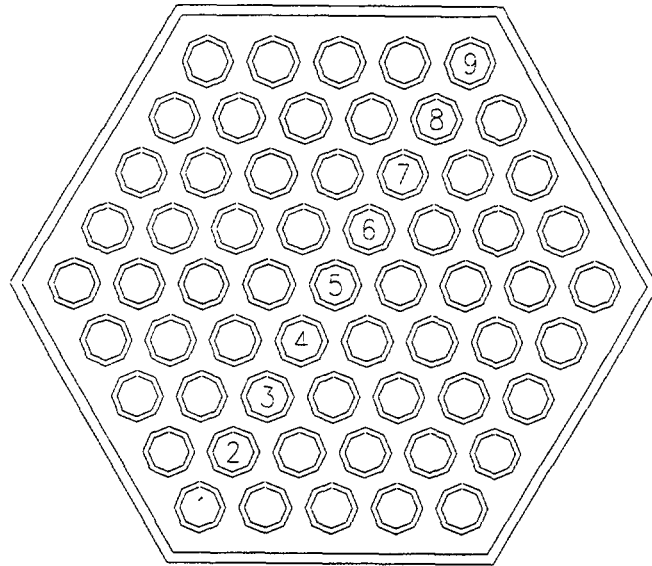


FIG. 6. Sketch showing cross section of fuel subassembly indicating pins selected for detailed examinations.

Eddy current testing of the fuel pins did not indicate any surface defect or abnormality on the clad tube. Analysis of signals indicated that the spring support inside the pins was touching the clad and that this location was varying for the nine pins. The accuracy of location is within $\pm 2\text{mm}$. The location of spring support determined using ECT indicated that the pellet stack length have increased due to swelling of the fuel. These results correlate well with that of X-radiography which followed ECT. Fig.8 shows a typical ECT output.

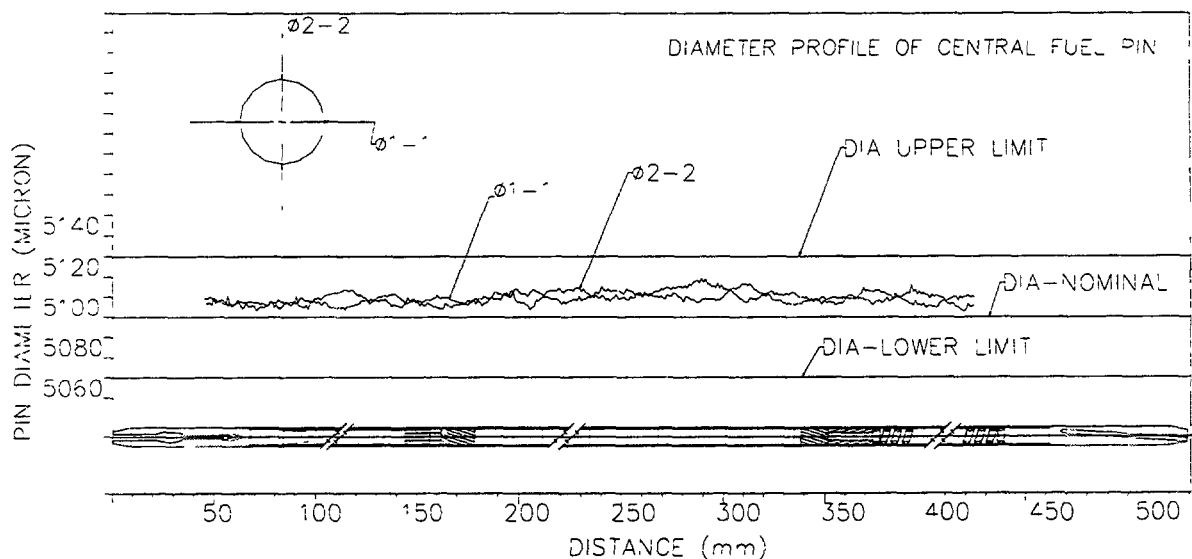


FIG. 7. Typical diameter profile of a fuel pin

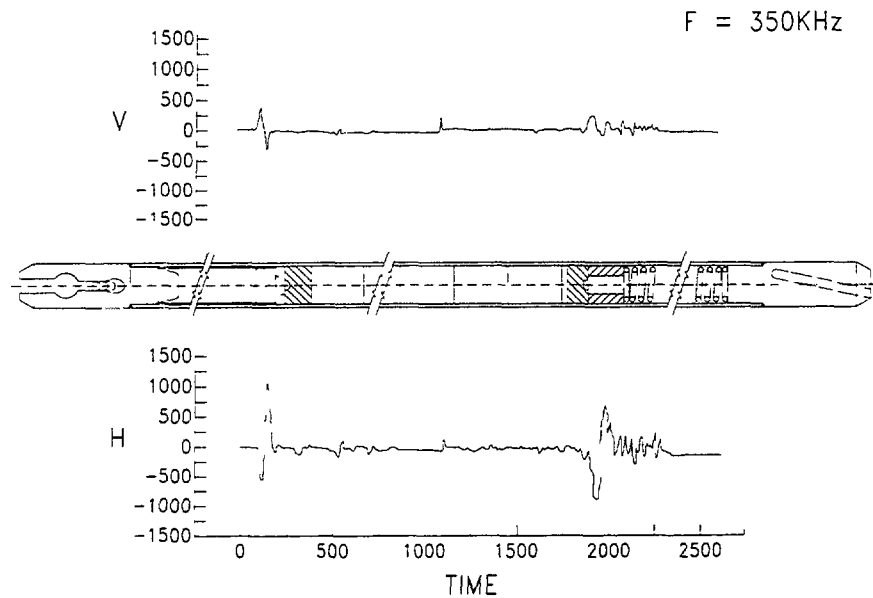


FIG. 8 Eddy current signal output of a typical fuel pin

X-radiography of the fuel pins revealed that the pellet-clad gap and the pellet-to-pellet gaps are too small to be measured. Original pellet-clad gaps were in the range 0.110mm to 0.250mm. An increase in fuel stack length was noticed. This varies from 2.17mm to 5.35mm (0.68% to 1.67%). This is in agreement with the eddy current test results which detected

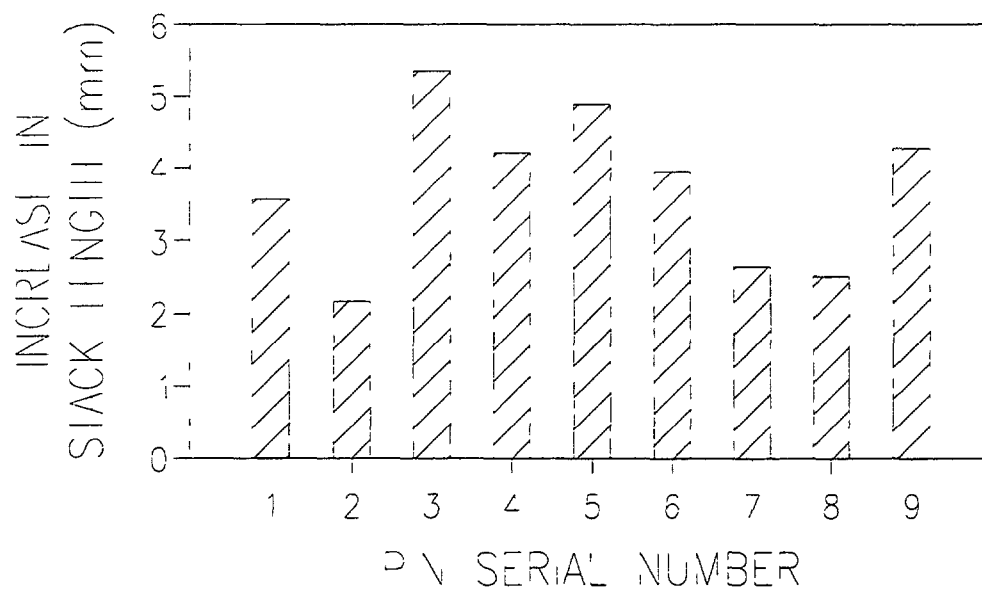


FIG 9. Chart showing increase in fuel stack lengths estimated using x-radiography

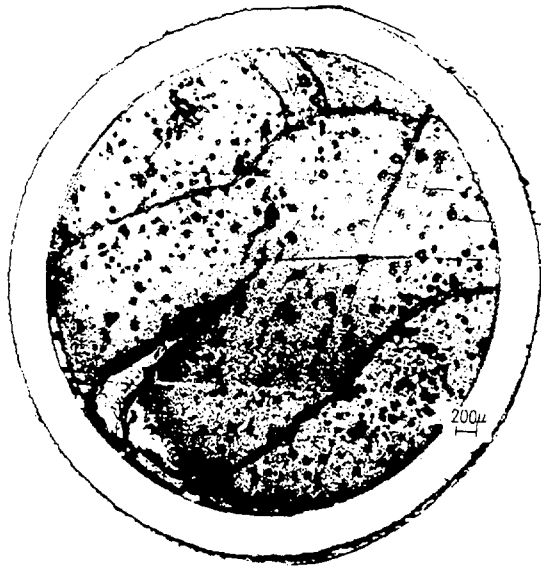
the variation in the location of the spring support. No gross abnormalities were observed. Fig.9 shows the variation in stack length measured from X-radiographs for the nine selected pins.

Two of the pins showing a stack length increase of 0.825% and 1.67% were taken up for carrying out sectioning and metallography. Fig.10 shows the metallographic pictures of the cut sections of fuel. Fig.11 shows photo micrographs of etched structure of the fuel at a section at the centre of the fissile column. An etched structure of as fabricated fuel is also included in this figure. The results of metallographic examinations revealed the following.

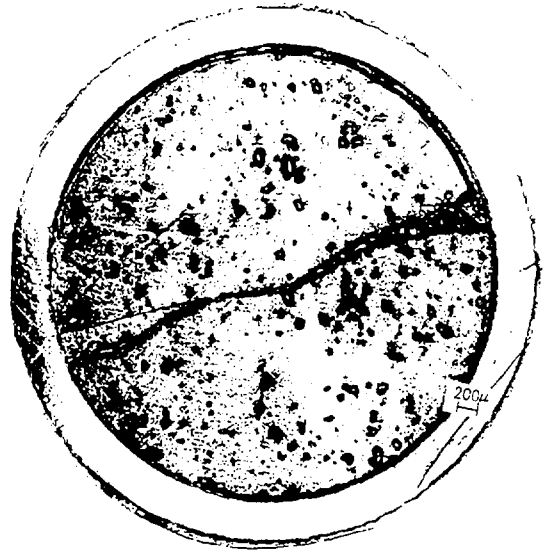
- (1) The fuel was seen to have several cracks in the cut section taken at the centre of the fuel column, whereas at the end, the extent of cracking was relatively less. The etched structure of the fuel cross section did not indicate any evidence of restructuring (fig.11).
- (2) The fuel-clad gap was seen to be closing due to cracking, as well as swelling of the fuel. The fuel clad gap was less at the centre of the fuel column, compared to the end, as expected.

The swelling rate of the fuel is a strong function of the fuel centerline temperature. The metallographic results show that the fuel is cracking, facilitating early closure of the fuel clad gap, resulting in reduction of the fuel centre line temperature. The swelling rate of carbide fuels of a different composition (8% PuC, 92% UC) as a function of fuel centerline temperature has been reported by Mikailoff [1]. Since swelling data for FBTR fuel composition (70% PuC, 30% UC) is not known, a modified swelling rate has been arrived at for this fuel, after normalisation using ratios of melting points of the two fuel compositions [2]. The two swelling rates are compared in Fig.12. From fig.12 it can be seen that the swelling rate is very low at centre line temperature of about 1300 K for FBTR fuel composition. The average swelling rate estimated from X-radiography results of the nine pins, as well as measured from the metallographic cross-sections, is approximately 1.2% per atom percent burnup, which indicates that the swelling rate for FBTR fuel has been lower than the predicted values shown in Fig.12. Hence the PIE results shows that the linear heat rating can be safely increased for this fuel to 400 w/cm. The presence of fuel clad gap seen in the metallographic cross sections (Fig.10) as well as the gap available in the fuel due to cracks, indicate that, space is still available to accommodate further swelling of the fuel. Hence it can be also concluded that the fuel can be safely taken to higher levels of burnup say 50,000 Mwd/t.

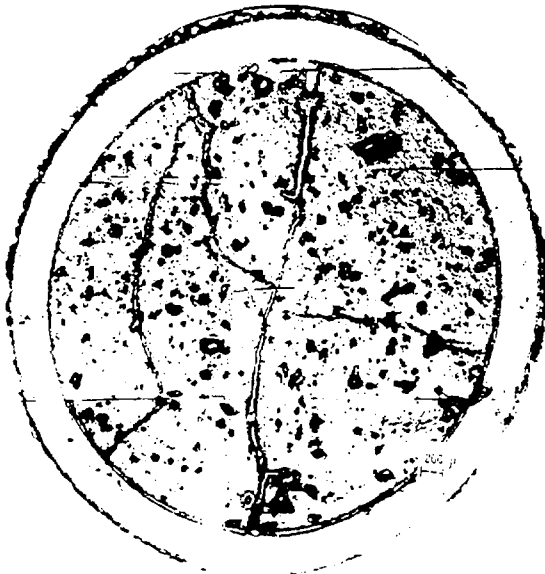
In addition to the driver fuel subassembly PIE four experimental fuel pins, irradiated to very low level of burn up (15 to 25 effective full power days) in the reactor is also being carried out. These fuel pins were having the same geometry of the driver fuel pins and were irradiated in a special capsule assembled in carrier assembly. The pins had pellets both 70% PuC 30%UC (driver fuel composition) and 55% PuC 45%UC composition thought for an expanded core configuration, stacked in separately, with an insulation pellet (UC) in between. The results of PIE carried out so far indicates satisfactory performance of these pins.



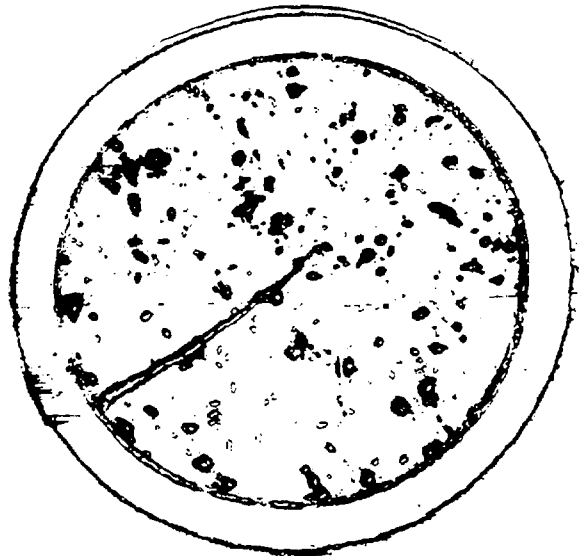
(a) Centre of fissile column, 300 W/cm,
25,000 MWd/t



(b) Top of fissile column, 210 W/cm,
18,000 MWd/t



(c) Centre of fissile column, 300 W/cm,
25,000 MWd/t



(d) Top of fissile column, 210 W/cm,
18,000 MWd/t

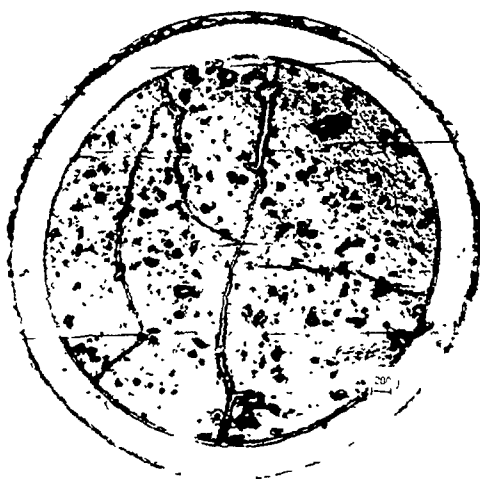
FIG. 10. Photomicrographs of cut cross sections of fuel pins. Figs. a & b show the cross sections at the middle and end of fuel column for pin number 3 and Figs. c & d for pin number 7 respectively (refer fig. no. 6)



(a) At the edge



(b) At the centre



(c) Unirradiated

FIG.11. Photo micrographs showing etched structure of the irradiated and a typical unirradiated fuel.

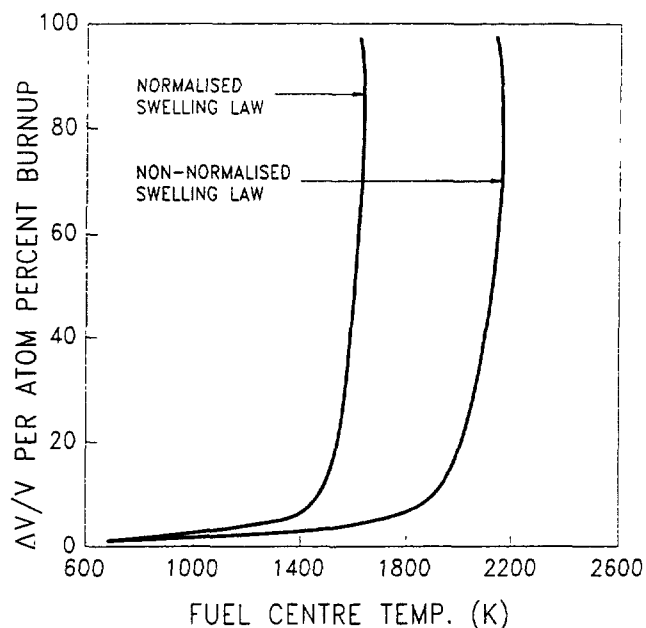


FIG.12. Free swelling of mixed carbide fuels as a function of centre line temperature

4. CONCLUSION

The performance of the carbide fuel chosen as driver fuel for FBTR has been found to be excellent with no indication of fuel failure up to 30,000 Mwd/t of burn up. Detailed PIE carried out on the fuel which has seen burn up in excess of 25,000 Mwd/t did not also reveal any abnormalities. The fuel clad gap was seen to be closing, due to cracking of the fuel. However, marginal fuel clad gap in the range of 10 to 20 μm is seen to be still existing in addition to gaps available in the fuel due to cracks, to accommodate further swelling. These results clearly indicate that the fuel can be safely taken to higher levels of burnups and higher linear heat ratings.

ACKNOWLEDGEMENTS

The authors are thankful to Dr. Placid Rodriguez, Director, IGCAR for his constant encouragements and support. Authors also gratefully acknowledge the keen interest shown by Shri S.B. Bhoje, Director, Reactor Group, IGCAR. The authors are also thankful to various colleagues at Radiometallurgy Division, Bhabha Atomic Research Centre, Mumbai where the fuel was fabricated, for giving many useful data. The contributions of number of colleagues of Reactor Operations Division, IGCAR and Nuclear Systems Division, IGCAR are also gratefully acknowledged.

REFERENCES

- [1] MAIKAILOFF, H., L'element combustible carbure a joint helium pour la filiere a neutrons rapides: problems poses par le gonflement du combustible, BIST 196 (1974).
- [2] GOVINDRAJAN, S., Attainable linear power and burnup of the mixed carbide fuel for FBTR, Internal Report, FBTR/FRG/31411/DN/21



DEVELOPMENT OF VIBROPAC MOX FUEL PINS SERVICEABLE UP TO SUPERHIGH BURNUPS

A.A. MAYORSHIN, G.I. GADZHIEV,
V.A. KISLY, O.V. SKIBA, V.A. TZYKANOV
Research Institute of Atomic Reactors,
Dimitrovgrad, Russian Federation

Abstract

The main results on investigations of fast reactor fuel pins with (UPu) O_2 vibropac fuel to substantiate their serviceability up to the super-high burnups are presented. The BOR-60 reactor fuel pins radiation behaviour in stationary, transient and designed emergency conditions has been determined from the fuel pins dimensional stability analysis having regard to the results of investigation fuel and cladding swelling as well as estimations of fuel and cladding thermal-mechanical and physico-chemical interactions. It is shown that the change of the outer diameter is minimum in fuel pins with VMOX fuel with a getter-metallic uranium powder and ferrito-martensite steel cladding, and the corrosion damage of the cladding inner surface is absent up to 26% h.a. The experiments with over-heating of the irradiated fuel pins cladding up to 850°C did not lead to any changes in pins integrity. The availability of the periphery area of the vibropac fuel core initial structure provides the minimum level of the thermal-mechanical stress at transient conditions of reactor operation.

Introduction

The most efficient way for improving the technique and economical characteristics of fast reactors fuel cycle is the increase of fuel burnup.

According to the estimations to compensate the high cost of fast reactor fuel component the maximum burnup must make up 20÷25 % h.a. When solving this task two problems are the most significant:

- choice of structural materials for fuel pins cladding and fuel assembly wrappers, possessing necessary level of heat-resistance and an acceptable value of radiation swelling;

- provision of the minimum physical-chemical and thermal-mechanical effect of fuel column on cladding.

To realize this problems among the well-known grades of steels preference apparently should be given to ferrito-martensite class materials which demonstrate rather high size stability at moderate temperature levels of the cladding. As appears from the data of fig.1 where there is presented the dependence of the main cladding materials swelling on fluence, the best characteristics shows the American steel HT-9 [1,2].

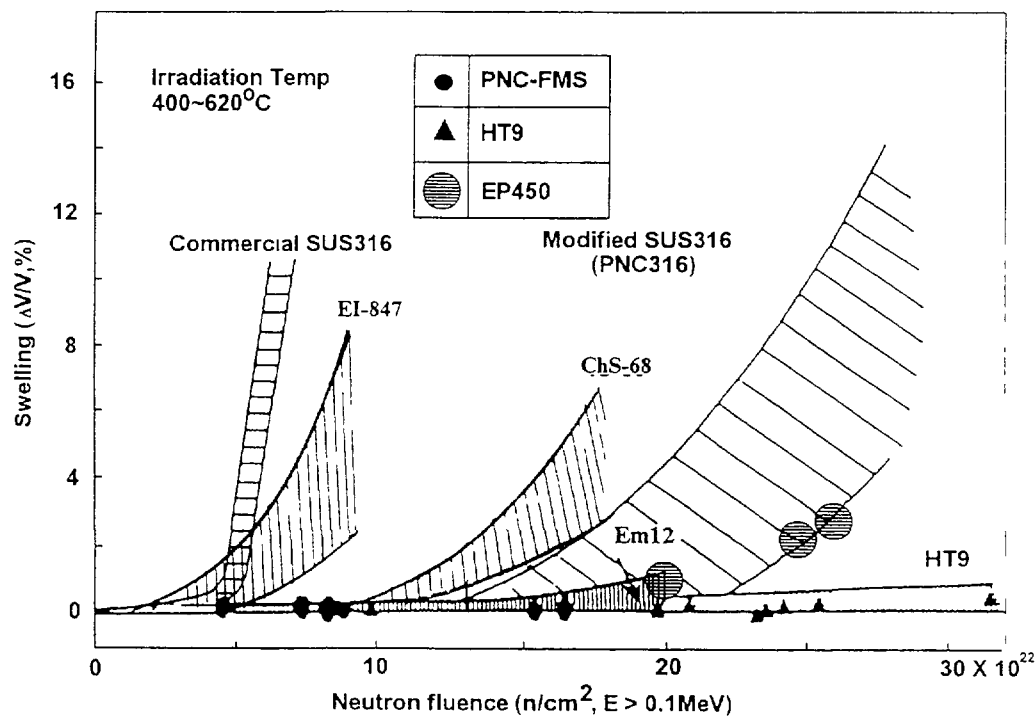


Fig 1. Swelling of structural materials for FBR fuel pins.

EP-450 = Cr13Mo2NbVB,
EI-847 = Cr16Ni15Mo3Nb,
ChS-68 = Cr16Ni15Mo2Mn2TiBV,
Em12 = Cr10Mo2Mn,
HT9 = Cr12Mo1.

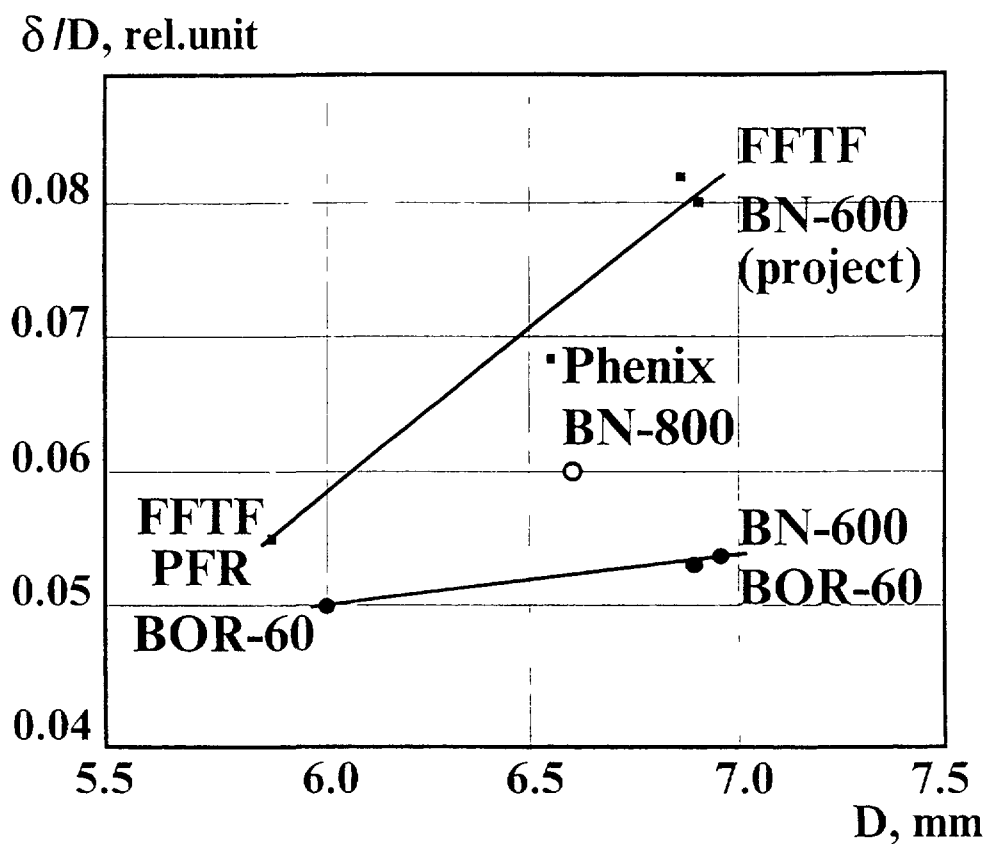


FIG. 2. Dependence the cladding relative thickness vs fuel pin diameter.

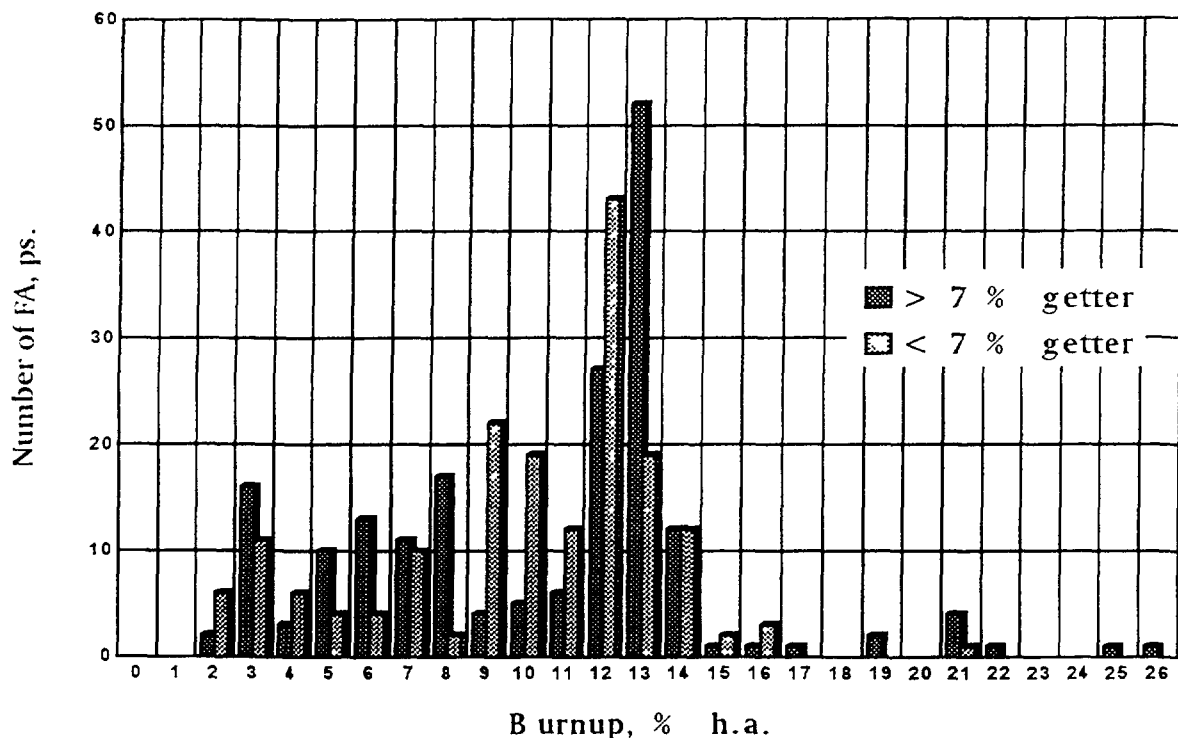


FIG 3 FA distribution of the BOR-60 reactor versus burnup
(wrapper Cr18Ni10, cladding Cr16Ni15Mo3Nb)

As for the problem of thermal-mechanical effect of the fuel column on cladding with minimum chemical interaction of U-Pu oxide fuel and cladding, then to increase the fuel size stability in the case of pellet fuel, the main accent is done on the cladding thickness increase, fig.2 [3,4] (FFTF, HT-9 cladding, burnup - 23,8 %, $\sigma/d = 0,56/6,86$ mm; PFR, cladding PE-16, burnup - 21,0 %, $\sigma/d = 0,38/5,84$ mm; BN-600, there is scheduled the cladding transfer from 6,9 x 0,55 mm of diameter and wall thickness). It is anticipated that the increase of cladding structural strength at the expense of its thickness increase 100 μ m on the average, allows to minimise the corrosion factor effect.

For the last 15 years in RIAR in the range of the closed fuel cycle, based on the use of dry methods for nuclear fuel performed the intensive investigations on the creation of fuel pin design, adapted to the automated remotely-controlled technological process and possessing high operating

Table 1.1

Granulated Fuel UPuO_2 Features

Parameter	Value
Particle density, g/cm^3	$10,7 \div 10,8$
Fraction number	5
Particle size, mm	$-1,00 + 0,63$ $-0,63 + 0,40$ $-0,40 + 0,25$ $-0,25 + 0,10$ $-0,10$
Smear density, g/cm^3	
- fuel pin of FBR	$9,1 \pm 0,2$
- fuel pin of PWR	$9,6 \pm 0,2$
Content mass PuO_2 , %	≈ 30
Isotope mass fraction, %	
^{238}Pu	$0,2 \div 1,7$
^{239}Pu	$64,0 \div 98,5$
^{240}Pu	$3,3 - 21,5$
^{241}Pu	$0,4 \div 9,0$
^{242}Pu	$0,2 - 4,0$
Enrichment UO_2 , %	$45 - 90$

Table 1.2

Production of Granulated Fuel

Type of facility	Fuel	Quantity	Period	Reactor
Granulated UO_2 fuel Facility	UO_2	900	1976-1983	BOR-60
	UO_2	365	1983	BN-350
Granulated UPuO_2	PuO_2	100	1980-1982	BOR-60
	UPuO_2	550	1983-1987	BOR-60
	UPuO_2	75	1984	BN-350
	UPuO_2	70	1987	BN-600
Pilot plant (Granulated Fuel Facility)	UO_2	120	1988	BN-600
	UO_2	535	1988-1989	RPT-10
	UO_2	330	1989-1994	BOR-60
	UO_2	374	1993	BN-350
	UPuO_2	325	1989-1992	BOR-60
	UPuO_2	277	1989-1992	FPS
	UPuO_2	300	1990	BN-600

characteristics. The result of these investigations has been vibropac fuel pin conception. The problems of thermal-mechanical and physical-chemical fuel - cladding interactions have been solved in this conception at the expense of vibropac fuel column.

This column is a mechanical mixture of structural properties based on polydispersed nonregular granular form and powder metallic uranium getter. The technological process of production and control of vibropac fuel pins from granulated UPuO_2 fuel is fully automated and is performed in hot cells RF-1 and RF-2 of the experimental-investigating complex of SSC RIAR [5]. In the reactor BOR-60, which has been operating with vibropac MOX fuel since 1981, there was achieved stable work of standard fuel pins with Cr16Ni15Mo3Nb steel cladding up to planned burnup 12-15 %, fig.3. Basing on fuel pins with VMOX fuel testings in the BOR-60, BN-350 and BN-600 reactors and their material science

Table 2.1.

The main features of BOR-60 fuel
assembly with vibropac $(\text{UPu})\text{O}_2$ fuel

Parameter	Values
Fuel composition	$\text{UO}_2 + \text{PuO}_2$ + U $(\text{UPu})\text{O}_2$
PuO_2 content, %	20-28
Getter mass fraction, %	3.....10
Clad diameter and thickness, mm	6.0 x 0.3; 6.9 x 0.4
Cladding material	Cr16Ni15Mo3Nb (befor 1994) $\text{Cr16Ni15Mo2Mn3TiVB}$ (after 1994)
Maximum linear power, kW/m	(after 1994)
Maximum clad temperature, C	52.0
Maximum fuel burnup, % h.a.:	720
- standard fuel assembly	
- experimental fuel pins	15.6
Fuel pins number, pieces,	28.0
having burnup:	
10-15 %	
15-20 %	6031
more than 20 %	185
	296

Table 2.2

Test Conditions in the BOR-60
Vibropacked Fuel Elements with
Promising Cladding Materials.

Cladding Material	Number of the pins	Heat rate, kW/m	Temperature cladding, °C	Fluens, 10^{22} cm^{-2}	Burnup, % h.a.
Cr16Ni15Mo3NbB	214	44	610	24,3	21,6
Cr16Ni15Mo3NbB+C	10	37	660	11,1	9,9
Cr15Ni16Mo23MnTiVB	993	49	710	15,6	~ 16
Cr20Ni45Mo23MnTiVB	37	37	660	12,1	9,9
Cr20Ni45Mo4B+Y	37	40	690	10,6	12,9
Cr20Ni45Mo4NbBZr	443	48	690	28,2	~ 28
Cr13Mo2NbVB	74	46	670	3,3	4,3
Cr15Ni16Mo-3MnTiNb	19	45	680	10,2	11,6

investigations there was created and varified the calculated program "VICONd" to predict their serviceability.

In this report there are presented the main investigation results for the progress of fuel pins with VMOX fuel program, referred to the super-high burnups achievement and substantiality of their seviceability in emergency conditions of reactor operation.

1. Granulated Fuel Features

The polydispers granulate obtained in the result of cathode deposite crushing after pyroelectrochemical reprocessing of nuclear fuel in malten salts on the base of alkali metal chlorides [6]. The main granulate characterictics and its operating time are presented in tables 1.1 and 1.2 respectively.

To realize the investigation programs, including Pu utilization, the experiments on obtaining granulate fuel with higher power Pu content were also carried out:

- 3,5 kg with 40 % of PuO_2 content (for testing in BOR-60 reactor);

- 0,2 kg with 56 % of PuO_2 content (for technological investigations);

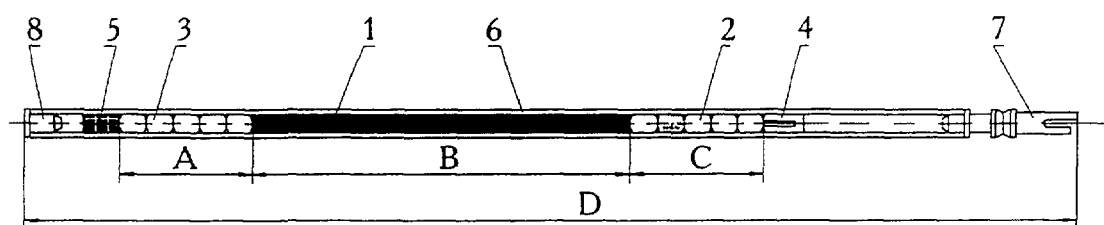
- 0,2 kg 70 % of PuO_2 (for technological investigations).

The quality of granulate with high Pu content practically did not differ from the standard one.

2. The Desing of the Fuel Vibropac Oxide Fuel (VMOX) for Fast Reactor

The design of the fuel pin with VMOX fuel for fast reactor is presented on fig. 2.1, the main technological and operating parameters of the BOR-60 reactor fuel pin are in table 2.1.

The base design of the fuel pin with VMOX fuel includes side areas of the blanket consisting of depleted or natural UO_2 isotope content pellets and U or U-Pu oxide vibropac fuel core. As the fuel pin design allows the avaiability of the compensation



Pos.	Designation
1	Fuel column
2	Lower blanket
3	Upper blanket
4	Supporting bushing
5	Holder
6	Cladding
7	Lower end plug
8	Upper end plug

REACTOR	Dimensions, mm			
	A	B	C	D
BOR-60	100	450	150	1083
BN-350	—	1060	400	1790
BN-600	350	950	350	2400

FIG. 2.1. The fast reactor fuel pin with vibropac $[\text{UPu}]\text{O}_2$ fuel.



FIG 3 I Microstructure of $UPuO_2$ vibropac fuel with burnup 26% of h.a.

volume in the fuel column is separated from the pellets of the blanket side area by gas-permeable element, preventing from granulate spill into the compensation volume when vibropacking.

Practically all the steels of different classes developed for fast reactors have been tested as the experimental fuel pins cladding material (Table 2.1).

More than 27000 of fuel pins have been produced during the whole period of accomplishing the complex program on fuel pins with VMOX fuel development (Table 2.3).

3. The Main Results of Tests and Investigations of Fuel Pins with VMOX Fuel

3.1. Fuel Pins Serviceability in Basic Conditions

The main factors influencing characteristics of fuel pins serviceability when reactor operates in stationary conditions are: fission gas products pressure, swelling fuel pressure and fuel - cladding chemical interaction as a result of formation of corrosive fission gas products and oxygen, disengaged at U and Pu fission.

The analysis of fuel pins with vibropac MOX fuel serviceability has shown [7,9], that:

- the use of fuel composition with the addition of a getter - metallic uranium powder in the amount of 3-10 % mass allowed completely eliminated corrosion processes, induced by the presence of fission products such as Cs, I and processing impurities as Cl, F, CO₂. This fact practically removes the burnup limit because of physical-chemical fuel-cladding interaction. In none of the investigated fuel pin cross-sections up to 26 % burnup there were found any corrosion damage of the cladding inner surface, fig.3.1;

- the outlet of fission gas products from the oxide fuel under cladding at standard operation conditions of fast reactor fuel pins averages 50-70 % and practically does not depend on the type of fuel composition;

- the change of the fuel pin cladding diameter is induced in general by swelling of structural material. The contribution of inelastic deformation did not exceed 0,5 %. The change of the

diameter of fuel pin cladding of steel Cr13Mo2 at doses up to 144 a.p.a. was ~ 1-2 %;

- the rate of pre-stoichiometric composition swelling, estimated by the fuel microstructure at 21, 24 and 26 % burnups was 0,6 \pm 0,1 %/% burnup.

- the fuel column abnormal effective density ($>9,0$ g/cm³), which is provided by the selection of optimal granulometric content at very high pictometric particles density (table 1.1, allows to have sufficient temperature supply up to the melting temperature (more than 400 °C, (fig.3.2)).

3.2. Fuel Pins Serviceability in Transient Conditions

To study the influence of transient conditions on fuel pins serviceability in BOR-60 reactor there have been performed experiments on replacing of fuel assembly with pellets as well as vibropac fuel (table 3.1).

The experiments of fuel pins with UO₂ pellet fuel shown [10]:

- all the 18 fuel assemblies, transferred from the centre to periphery were tight when having reached 10 - 12 % burnup they were unloaded;

Table 3.1

Test Conditions of Subassemblies which
were transferred in the core of BJR-60

Type of the transference	Pellet fuel			Vibropac fuel		
	Number of the SA	Burnup, % h.a.	Number of the un-tight	Number of the SA	Burnup, % h.a.	Number of the un-tight
In the limit of one radius	4	10-12	2	9	8-24	2
From centre to periphery	18	10-12	-	23	7-22	-
From periphery to centre	4	12-17	3	31	8-18	-

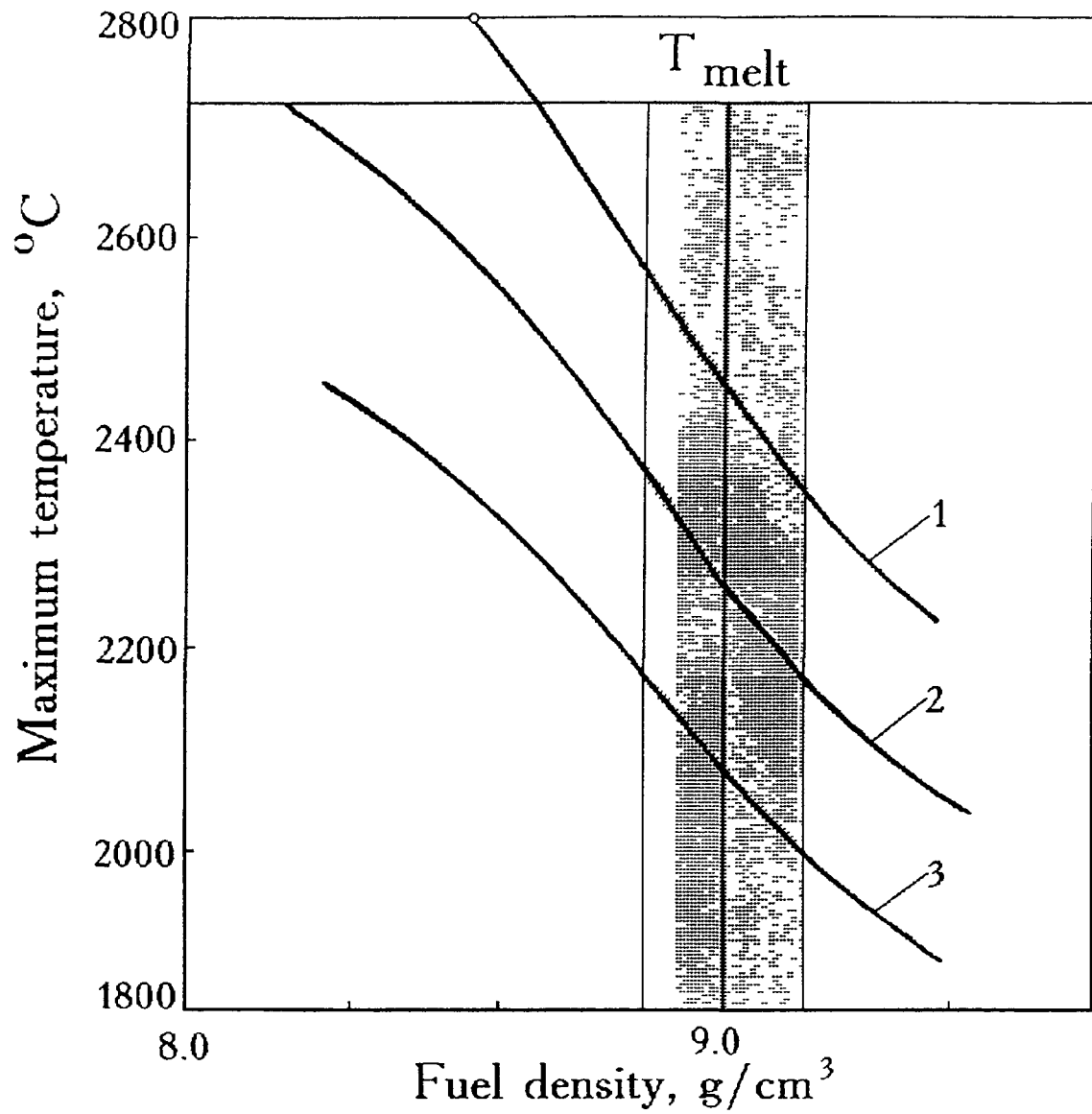
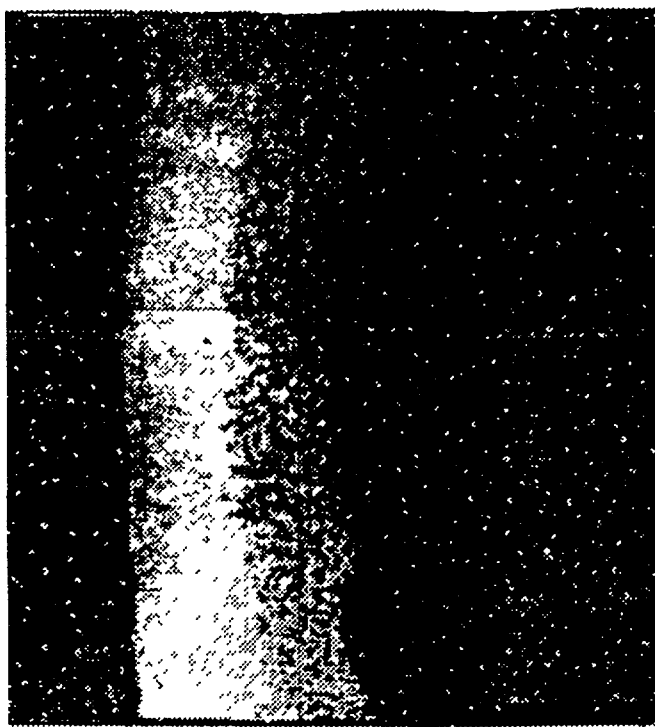
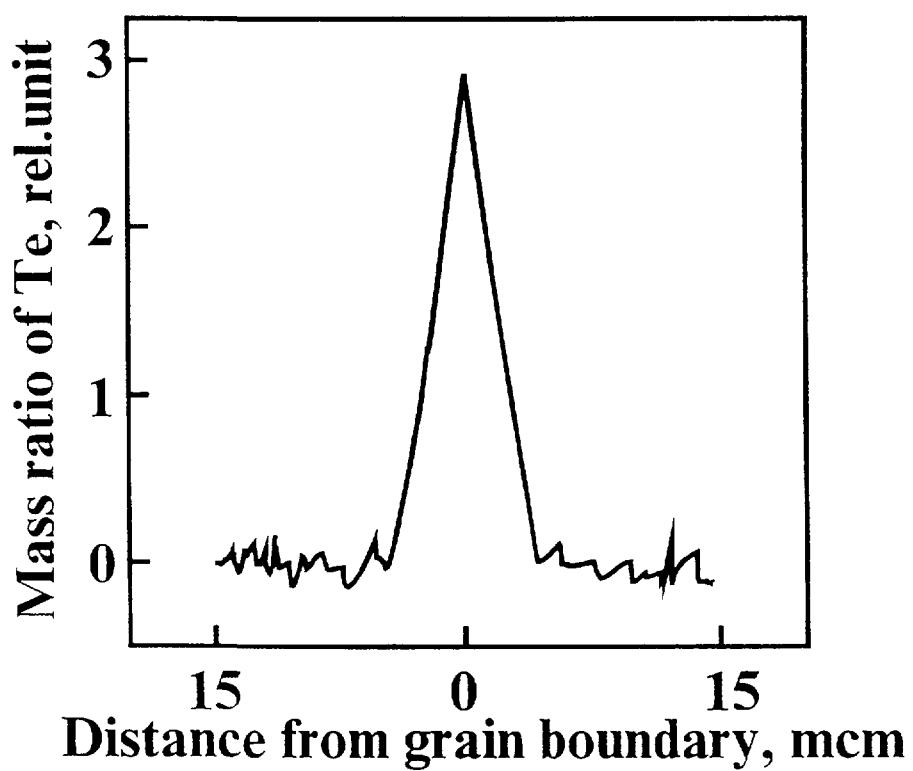


FIG 3.2 Maximum fuel temperature versus the density of vibropac core and fuel element linear power

- 1 - $q_1 = 55$ kW/m,
- 2 - $q_1 = 50$ kW/m,
- 3 - $q_1 = 45$ kW/m,
- - permissible range of the density change



a



b

FIG 3 3 Corrosion of the cladding (Cr20Ni45Mo4Nb):

a - macrostructure, x100;

b - distribution of Te.

- when one fuel assembly was transferred from the fourth row to the sixth one and then back it remained tight;
- four fuel assemblies were transferred in the limit of one radius, where they were installed, two of them turned out to be untight;
- four fuel assemblies were transferred from periphery rows to the centre and three of them turned out to be untight. Two fuel assemblies of this serie have been studied (Table 3.2).

The reasons of cladding untightness of these fuel assemblies, for which the liner power excess was up to 36 % of the initial level were investigated. The investigations have shown the availability of considerable intergrains corrosion with great Te and also Cs content on the corroded grain boundaries, fig.3.3. This type of corrosion was observed on cross-sections with the maximum temperature of fuel pin core surface. The untightness of two fuel pins with vibropac fuel at 20 and 24 % burnup (one from each assembly) was not connected with the change of power since it was detected two campaigns after fuel elements transfer. As the material science investigation have shown the untightness was caused by the exhaustion of cladding material resource characteristics due to its excessive radiation swelling and creep.

Parameters of 17 standard fuel assemblies with vibropac fuel, which were transferred from periphery to the central rows are presented in table 3.3. The transfers in the reactor core with the power increase up to 80 % do not influence on the vibropac fuel pins serviceability. This fact testifies that the lowed temperature of the periphery layer does not allow tellurium

Table 3.2
Tests Conditions Examined
Subassemblies of the
BOR-60 with Pellet UO₂ Fuel

Number of the SA	Cladding Material	Burnup, % h.a	Cladding temperature, °C	Heat rate, kW/m
A-613	Cr16Ni15Mo3NbB	12,6	670	37-46
II-30	Cr20Ni45Mo4Nb	16,9	700	31-49

Table 3.3

Tests Conditions of the Subassemblies with Vibropac Fuel, with were transferred in the core of the BOR-60

Num-ber of the SA	Bur-nup, % h.a.	Heat rate, kW/m	Change of the row	Heat rate, kW/m		State of SA
				initi-al	finish	
I-215	8,1	131	6 → 1 6	202	333	herm.
I-220	13,0	111	→ 2	224	335	herm.
IÃ-31	12,8	211	6 → 2	264	475	herm.
IÃ-44	12,0	169	5 → 2	311	480	herm.
IÃ-50	11,5	136	5 → 2	350	486	herm.
IÃ-52	11,9	170	5 → 1	312	486	herm.
IÃ-53	12,1	143	6 → 3	279	422	herm.
IÃ-55	11,2	176	6 → 1	288	464	herm.
IÃ-56	12,5	174	5 → 1	320	494	herm.
IÃ-57	12,7	172	6 → 2	289	461	herm.
IÃ-59	11,7	155	5 → 1	351	506	herm.
IÃ-60	11,7	154	5 → 1	350	504	herm.
IÃ-65	11,5	157	5 → 1	356	513	herm.
IÃ-66	11,5	183	5 → 1	332	515	herm.
IÃ-71	13,9	113	5 → 1	330	443	herm.
IÃ-72	11,7	158	5 → 2	354	512	herm.
IÃ-77	12,7	118	6 → 4	293	411	herm.

"to reach" cladding and the presence of the initial structure of this layer provides "soft" thermo-mechanical fuel column effect on cladding at transient conditions. The typical vibropac fuel structure, perfect from the point of view of minimum thermo-mechanical effect on cladding, is presented in fig.3.4.

3.3. Serviceability of Fuel Pins at Cladding Overheating

Two types of experiment have been performed: in-pile, when the claddings had high temperature and after irradiation - to study the reliability of pins at emergency over-heatings.

The main parameters of the experiments are presented in table 3.4.

The post-irradiation examinations of the cladding of fuel pins with pellet fuel from OP-25 assembly have shown matrix and

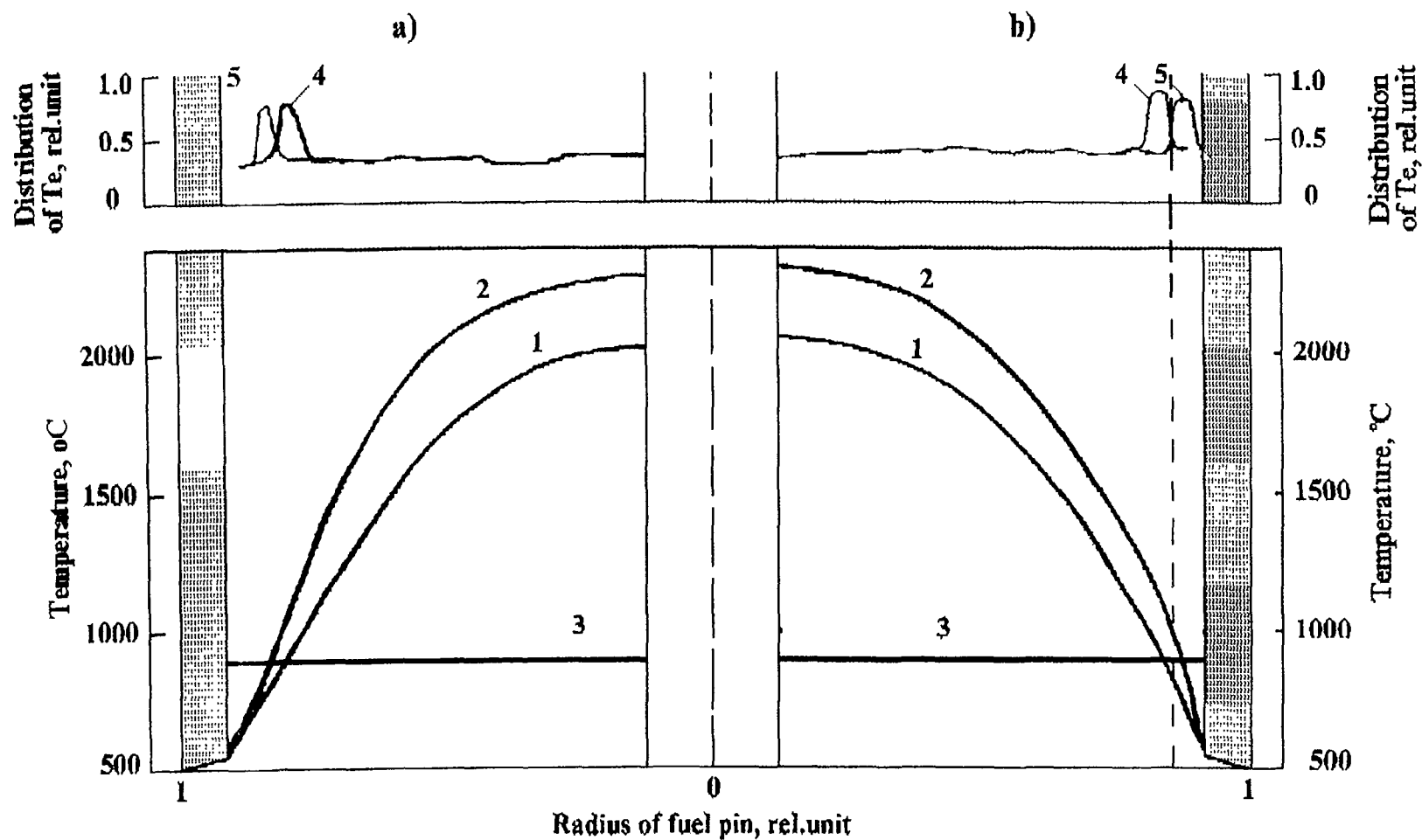


FIG. 3.4. Behaviour of Tc in the vibropac (a) and pellet (b) fuel:

- 1,4 - temperature and Te distribution in the basic regime;
- 2,5 - temperature and Te distribution at 20 % power ramp;
- 3 - initial temperature of Te vaporization (990°C).

Table 3.4

Tests Conditions of the BOR-60 Subassemblies under Higher Parameters

Number of the SA	Materials		Burnup, % h.a.	Heat rate, kW/m	Cladding temperature, °C	Postreactor tests conditions		Depth of the corrosion, mkm
	Fuel	Cladding				T _{clad.}	t _{min}	
II-25	UO ₂ pellet	Cr13Mo2NbVB	12,6	44,4	740	-	-	200
IA-35	UPuO ₂ vibro	Cr16Ni15Mo3Nb	5,4	60,0	740	-	-	-
IA-73	UPuO ₂ vibro	Cr15Ni15Mo3Nb	7,0	40,1	661	850	90	-
IA-115	UPuO ₂ vibro	Cr13Mo2NbVP	21,0	48,2	687	850	90	-

intergranular corrosion in the upper sections of the column part, caused by cesium and iodine interaction. A large amount of tellurium was also observed in the interaction products. The results obtained testify that high temperature of the cladding of pellet fuel pin causing high temperature of the column periphery zone influences greatly on the tellurium radial distribution and thus on its with cladding interaction. The irradiation of fuel pins with a vibropac UPuO₂ + U (10 % mass) fuel composition under very hard conditions (Q_1 up to 60 kW/m, $T_{clad.}=740$ °C) did not involve any chemical fuel-cladding interaction. The same result was obtained when fuel pins with vibropac UPuO₂+U fuel irradiated in BOR-60 reactor up to 21 % burnup were heated up to 800-850°C for 1-1,5 hour not in reactor. At these testing conditions also there were not found any evidence of corrosion damage of the inner cladding surface.

3.4. Serviceability of Fuel Pins with High Plutonium Content.

To study radiation aspects of plutonium utilisation there was developed the granulate production technology and were fabricated experimental fuel pins with UPuO₂+U fuel composition containing 40% of Pu. The fuel assembly was tested in the BOR-60

reactor up to 4,7 % burnup at maximum linear rate 46 kW/m and cladding temperature up to 650 °C [11].

Plutonium isotope composition, % : 238; 239; 240; 241; 242 = 0,5; 71; 19; 7,5; 2,0 , U-235 enrichment was 64,5.

Post-irradiation material science examinations showed that the radiation behaviour peculiarity of the fuel pin with ~ 40 % Pu content is the increase of its concentration on periphery in the central maximum linear rate part of the column. This became the reason of cladding frontal corrosion damage 70mm depth in some fuel pins. There were not founded chemical fuel-cladding interaction in the high-temperature part. Taking into account the importance of this problem, additional testings and investigations on parameters optimisation and fuel column initial characteristics up to superhigh burnups are scheduled.

3.5. The BOR-60 Reactor Fuel Pins to Study Superhigh Burnups

Successful tests of standard fuel pins with Cr16Ni15Mo3Nb steel cladding and Cr18Ni10Ti steel wrapper tube up to 15% h.a. burnup, solution of the thermal-mechanical and physical-chemical vibropac fuel pin core-cladding interaction allowed to begin to realise qualitatively new stage - the study of the limit burnup

Table 3.5.

Program to Achieve Super High Burnups and Damage Doses in the BOR-60

No	Material		Number of fuel pins	Burnup(forecast), % h.a.							
	Fuel pin cladding	FA Wrapper		1995			1996				
				2	3	4	1	2	3	4	
1	Cr13Mo2NbVB	Cr13Mo2N- bVB	185	19...24				24...29			
3											
2	Cr13Mo2NbVB	Cr13Mo2N- bVB	74	26							
	Cr16Ni15Mo3VB c.w.										
3	Cr13Mo2NbVB		6*	28 (155 dpa)		29...31		33		35 (190 dpa)	

* Refabricated fuel pins having the burnup from 21 to 26 % of h.a. in dismountable FAs

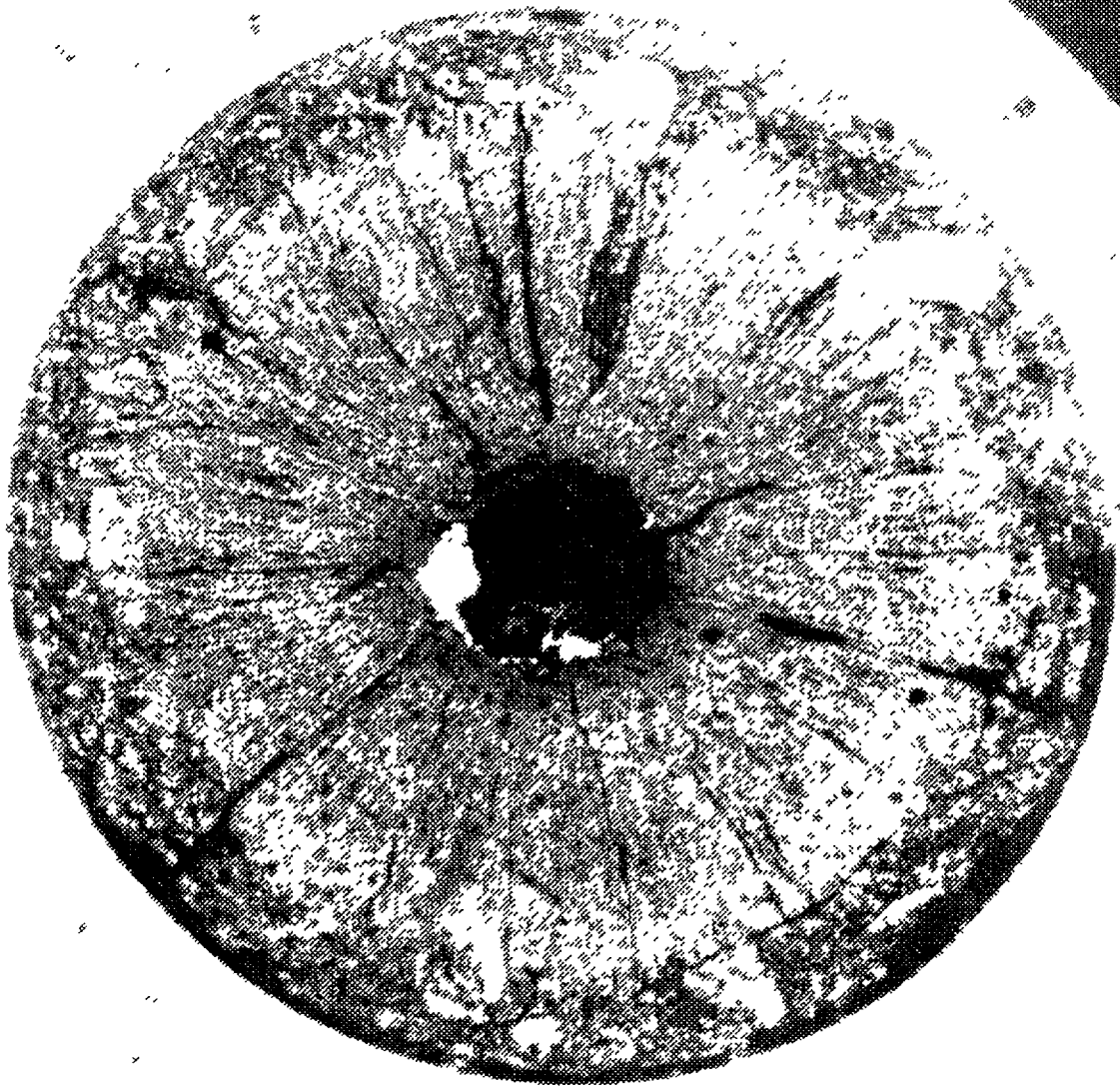


FIG 3 5 Macrostructure of the central cross-section of the BN-600 fuel pin (x25)

and dose characteristics of fuel pins and structural materials. The program of experiments on the base of standard design as well as on the base of the BOR-60 reactor dismantlable fuel assembly was developed for this purpose. The program provides testings of standard fuel assemblies with promising structural materials and additional irradiation of refabricated fuel pins in a dismantlable assembly (Table 3.5).

The results of cladding materials swelling (see Fig.1) illustrate the best size stability of ferrito-martensite steels,

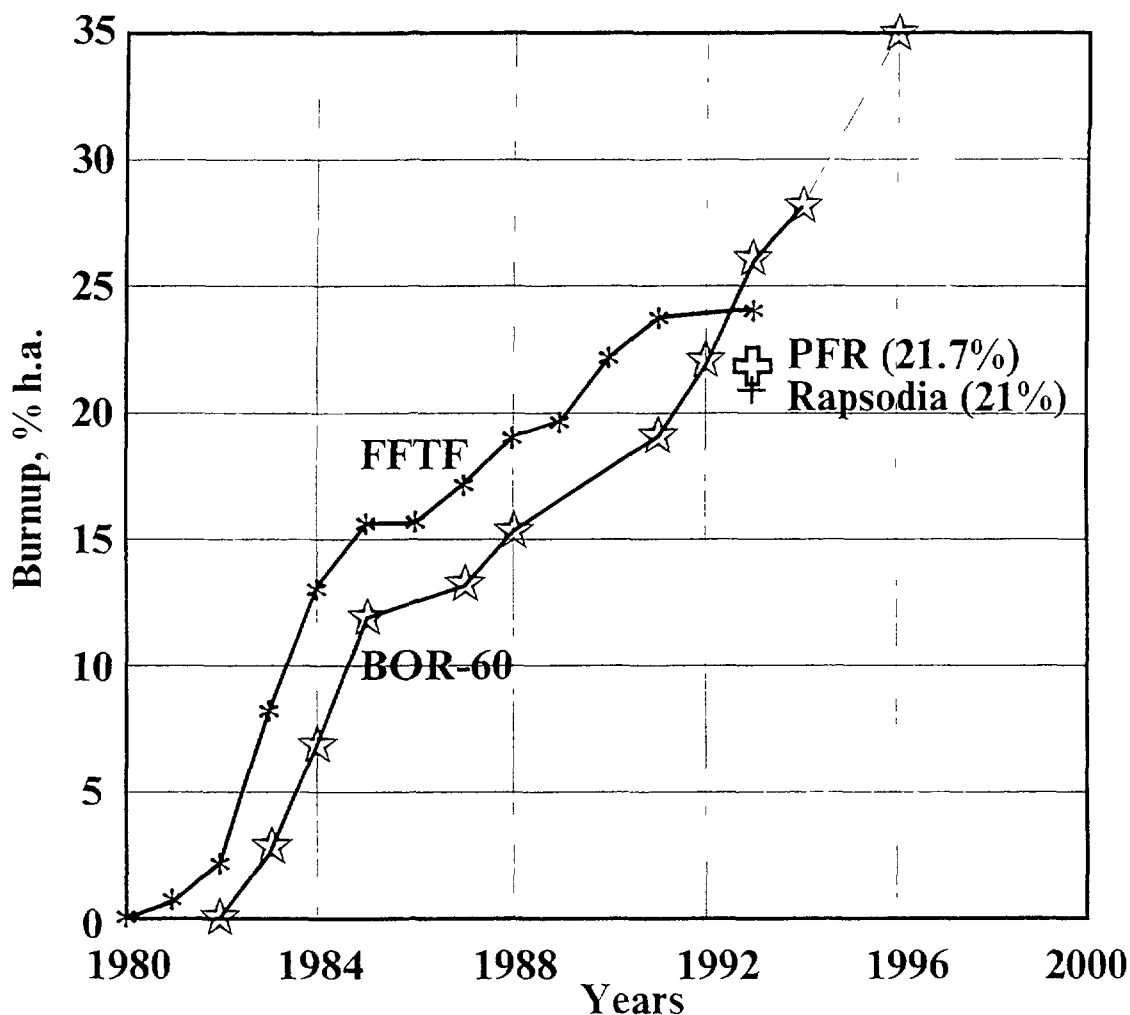
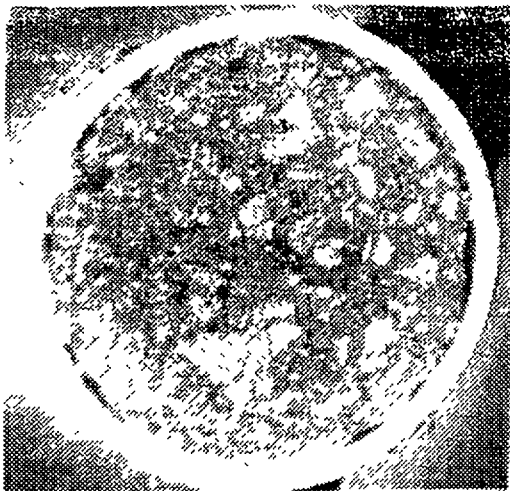


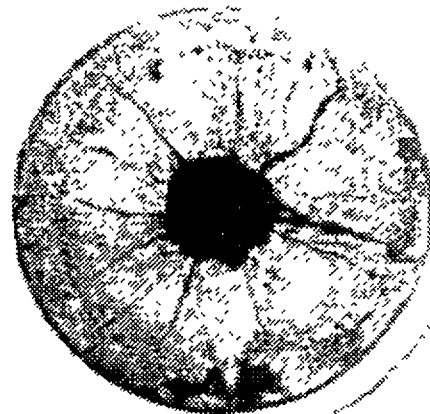
FIG. 3.6. Burnup achievements in $UPuO_2$ fuel in fast breeder reactors.

$Cr_{13}Mo_2NbVB$ Russian steel in particular. That is why the main emphasis was given to ferrito-martensite steels, despite the fact of their relatively low heat-resistance in the experiments on achieving super-high burnups of vibropac oxide fuel. Data are as of May, 1995 when there was achieved the world record burnup 28% on the experimental fuel pins with $Cr_{13}Mo_2NbVB$ steel cladding in the reactor BOR-60, (Fig. 3.5). The tests of these fuel pins are continued.

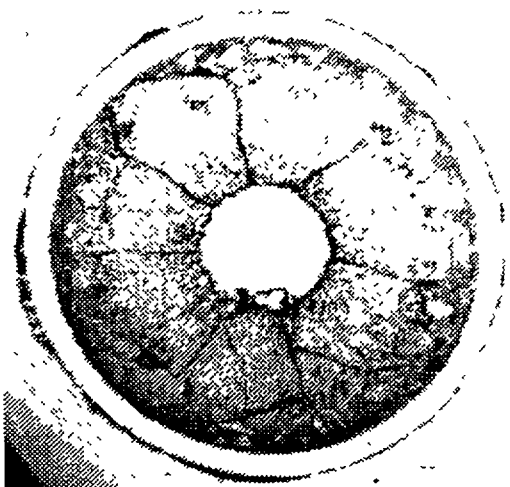
The post-irradiation examination of the BOR-60 reactor fuel pin claddings with 21.0; 24.4 and 26.0% burnup fully confirmed the technical solutions of the design and promising estimations of their serviceability, carried out by "VICOND" program. In none of the investigated cross-sections there were found any indications of the fuel-cladding chemical interaction. Typical macrostructures of the irradiated vibropacked fuel column at



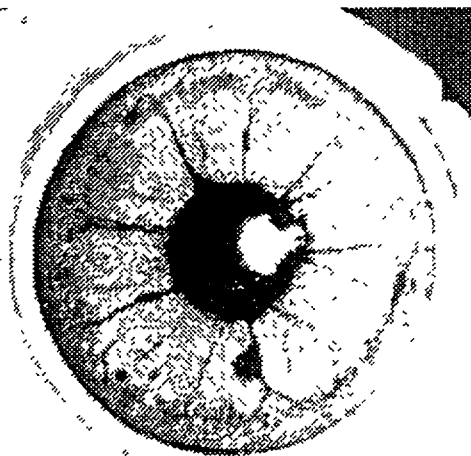
a



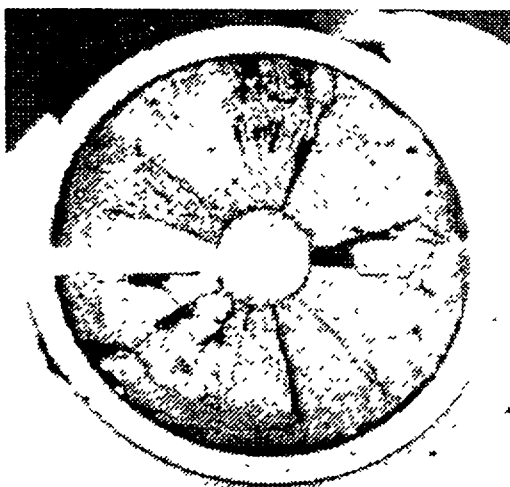
e



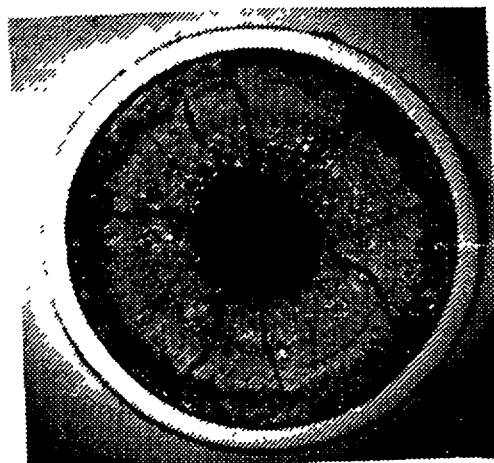
b



d



c



f

FIG. 3.7. Macrostructure of the vibropac fuel column

a) initial

c) 21% burnup

e) 24% burnup, upper A.C.

b) 12% burnup

d) 24% burnup, center A.C.

f) 26% burnup, center A.C.

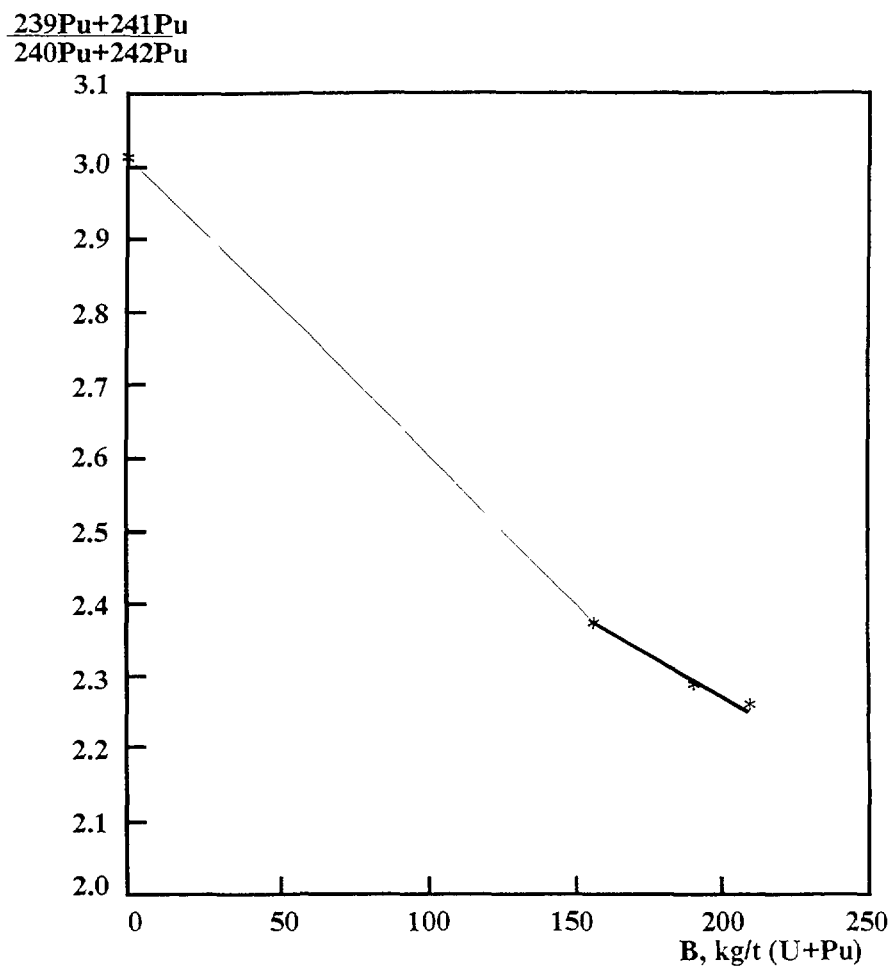


FIG. 3.8. Dependence of ratio even and odd Pu isotopes change vs burnup.

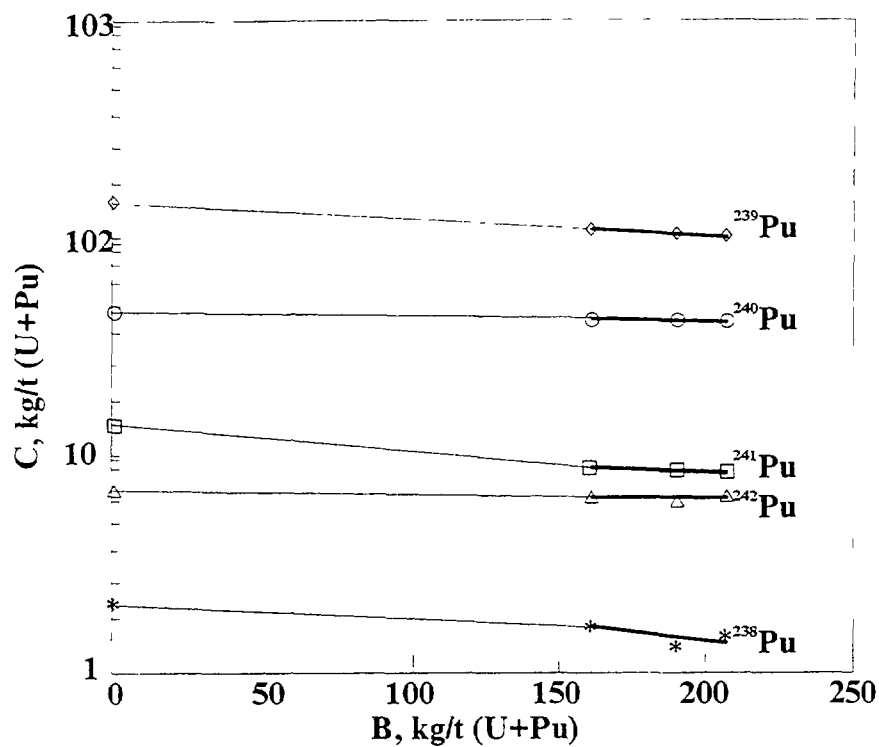


FIG. 3.9. Content of the Pu isotopes as a function of burnup.

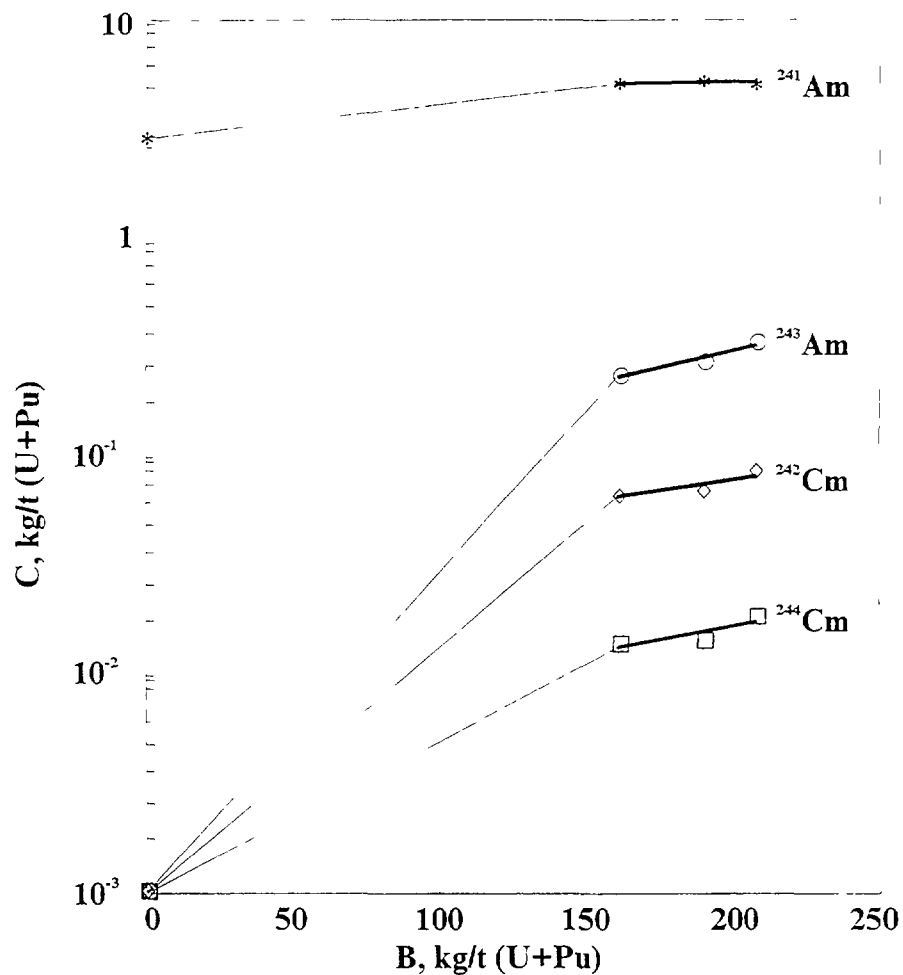


FIG. 3.10. Content of MA as a function of burnup.

different burnup are shown in Fig.3.6. The analysis of stressed-strained state of the fuel pin claddings of fuel assemblies with more than 20% burnup, estimation of their mechanical characteristics have given possibility to plan further experiments on fuel pins of this very design for achieving more high burnups. The radiochemical analysis of the UPuO_2 fuel isotope composition, irradiated up to 21.0% h.a. burnup allowed not only to precise the calculated values of the fuel burnup, but to estimate kinetics of content changes of the main isotopes presented in Fig. 3.7 - 3.9. In Fig.3.7 there is seen a clear tendency for decreasing even and odd Pu isotopes correlation due to burnup in the BOR-60 reactor spectrum and for increasing curium isotopes concentration. All these data in combination with the next radiochemical investigations of fuel isotope content with 26% burnup, which are carried out now will allow to precise

the programs for calculation the minor-actinides transmutation in the BOR-60 reactor spectrum.

CONCLUSION

Large-scale testing of the BOR-60 reactor fuel pins with vibropac uranium-plutonium oxide fuel confirmed high operation characteristics of these fuel pins in standard and transient conditions, as well as in experiments with cladding overheating. The addition of a getter - metallic uranium powder to the fuel composition allowed to suppress completely physical-chemical fuel-cladding interaction and eliminate the burnup due to this factor.

Considering the shown advantages and successful tests of fuel pins with vibropac MOX fuel and Cr13Mo2NbVB steel claddings in the BOR-60 reactor up to 28% burnup there are planned tests of similar fuel pins with $UPuO_2 + U$ fuel in the BN-600 reactor.

REFERENCES

1. R.D.Legget, L.C.Walters "Status of LMR fuel development in the United States of America" J.Nucl.Mat., 204(1993) 23-32.
2. M.Katsuragawa, H.Kashihara, M.Akebi "Status of liquid metal fast breeder reactor fuel development in Japan" J.Nucl.Mat., 204(1993) 14-22.
3. R.B.Baker et al "Status of fuel blanket and absorber testing in the fast flux test facility" J.Nucl.Mat., 204(1993) 109-118.
4. C.Brown, A.Languille, G.Muchling "Status of LMR fuel development in Europe" J.Nucl.Mat., 204(1993) 33-38.
5. O.V.Skiba, A.A.Mayorshin et al "Development and Operation Experience of the Pilot Plant for Fuel Pin and Subassembly Production Based on Vibropac Uranium-Plutonium Fuel"
/Proc.Int.Conference on Fast Reactors and Related Fuel Cycles,
October 28-November 1, 1991, Kyoto, Japan, N2, R15-4.

6. O.V.Skiba, Yu.P.Savochkin et al "Technology of Pyroelectrochemical Reprocessing and Production of Nuclear fuel"/ Proc.Int.Confermce on Future Nuclear Systems: Emerging Fuel Cycles and Waste Disposal Options Global - 93, September 12-17, 1993, Seattle, WA. ANS 1993, r.z.p. 1344-1350.
7. R.Herbig, O.V.Skiba, A.A.Mayorshin et al "Vibrocompacted Fuel for the Siquid Metal Reactor BOR-60" J.Nucl.Mat. 204(1993) 93-104.
8. A.A.Mayorshin, A.A.Petukhov et al "Development af Vibropac Oxide Fuel Element for Fast Reactor"/ Int.Conference Global-93. Seattle, USA, September 12-17, 1993.
9. A.A.Mayorschin, V.A.Tzykanov et al. "The Features of Radiation Behavior of Fuel Elements with Vibropac MOX Fuel", Proc.Int. Conference, Alushta, May 22-25, 1990, v.4, pp. 90-97.
10. V.K.Shamardin, F.N.Kryukov at al. "Effect of Tellur on Corrosion of Fuel Pin Clads for Fast Breeder Reactor" Preprint, RIAR-8(791), Dimitrovgrad, 1990.
11. A.A.Mayorshin, O.V.Skiba et al "Production and irradiation of $UPuO_2$ fuel with 40% of Pu in BOR-60. Vibrotechnology application for utilization of Plutonium and Minor Actinides"/ Int. CAPRA Seminar, Karlsruhe, September 21-22, 1994.



ASSEMBLIES AND FUEL PIN BEHAVIOUR UNDER IRRADIATION IN FBR BN-350

V.N. KARAULOV, A.P. BLYNSKI,
I.L. YAKOVLEV, E.V. KONONOVA
Mangyshlak Atomic Energy Complex, Aktau,
Kazakhstan

Abstract

The efficiency of all types of assemblies and fuel pins of the reactor BN-350 is in detail considered. The factors limiting the efficiency are indicated. The behaviour of assemblies with stainless steels ducts is studied. It is shown that the efficiency is restricted in this case by shape and dimensional changes of hexagonal ducts due to radiation swelling and radiation creep of structural materials. The problem of dimensional changes of ducts was solved for cores of reactors BN-350 and BN-600 after testing in BN-350 of experimental assemblies with ducts made of ferritic-martensitic steel 12Cr13Mo2NbVB.

For fuel pins of the second type of loading with clad made of stainless steel 0Cr16Ni15Mo3Nb the efficiency is limited by burnup of 13% h.a. and damage dose of 90 dpa.

To increase the burnup the core of the BN-350 is supplied by assemblies of modernized type with pins having a large gas plenum and clad made of the stainless steel 0Cr16Ni15Mo2Mn2TiVB that has a good resistance to irradiation.

The efficiency of fuel pins of modernized assemblies in the reactor BN-350 core conditions is provided up to 15% h.a. and damage dose 105 dpa.

1. INTRODUCTION

The liquid metal cooled reactor BN-350 is located on West of Kazakstan and more than 20 years is successfully operated since 1973. The reliable and safe operation of reactor is in many respects obliged not only to knowledge of behaviour of elements of the core (assemblies, fuel pins, control rods, guided tubes), development of criteria of their serviceability in the core, but also to development and introduction in practice of appropriate methods and means of the control and researches. Under serviceability in this case is understood:

- Absence of melting of fuel;
- Existing of assemblies, pins, control rods and guided tubes deformations, not interfering to normal heat release by work in the core and not leading to some problems at realization of handling operations;
- Preservation of integrity and continuity of structural elements.

A circle of the phenomena, responsible for serviceability of elements of the core of fast reactor is rather well established at present:

- Radiation change of shape of elements because of radiation swelling and radiation creep of materials;
- Swelling and gas release in fuel and absorbing compositions;

- Hardening and brittleness of structure materials under irradiation;
- Corrosion affection of pins cladding by fission products on the part of nuclear fuel.

Study of these phenomena in conditions of reactor BN-350, the establishment of criteria of serviceability is urgent and has practical and scientific interest. The characteristics of fuel assemblies of reactor BN-350 is submitted in Table 1.

2. METHODS AND MEANS OF RESEARCH OF SERVICEABILITY

On reactor a complex of hot cells equipped for dismantling techniques and devices for research of serviceability of assemblies, control rods and guiding tubes by non-destructive and destructive methods is introduced. The application was found by the following methods:

- Visual and measuring control (profilometry and wall thickness measurement);
- Radiography of spent elements of the core with the help of betatron;
- Gamma-spectrometry of pins;
- Control of electroresistance of cladding;
- Control of tightness of pins cladding on availability of gaseous fission products, for example Kr-85;
- Definition of a location of defects in cladding;
- Measurement of density of steel on samples by a hydrostatic method.

The destructive tests are carried out on samples, cut out of irradiated elements, by universal test machine with maximum load up to 10 tons in temperature range (20-1000)° C. The machine does the following kinds of tests: tensile - compression, bend, low cycle fatigue and short-term creep.

At service life tests of assemblies in reactor are used in-pile systems, enabling to receive the primary information on condition of assemblies: failed fuel detection system, including gaseous fission products monitoring system and delayed neutrons monitoring system. Measurement of elongation of assemblies depended on radiation swelling is carried out with the help of the charge gear, enabling to conduct readout with accuracy $\pm 1,5$ mm. After discharge from the reactor elongation of assemblies is measured in the hot cell with accuracy $\pm 0,1$ mm. Measurement of a force extraction of assemblies is carried out by system, mounted on the charge machine.

3. FUEL ASSEMBLIES BEHAVIOUR

As already was marked the primary information on behaviour of assemblies has been received directly in reactor on data of location of the charge machine during load-discharge works (relative to registration point). Hereinafter this information was specified and supplemented by measurements of elongation of assemblies in the hot cell. Such data for assemblies with wrappers made of steels 12-18Cr-10Ni-Ti annealed, 08-16Cr-11Ni-

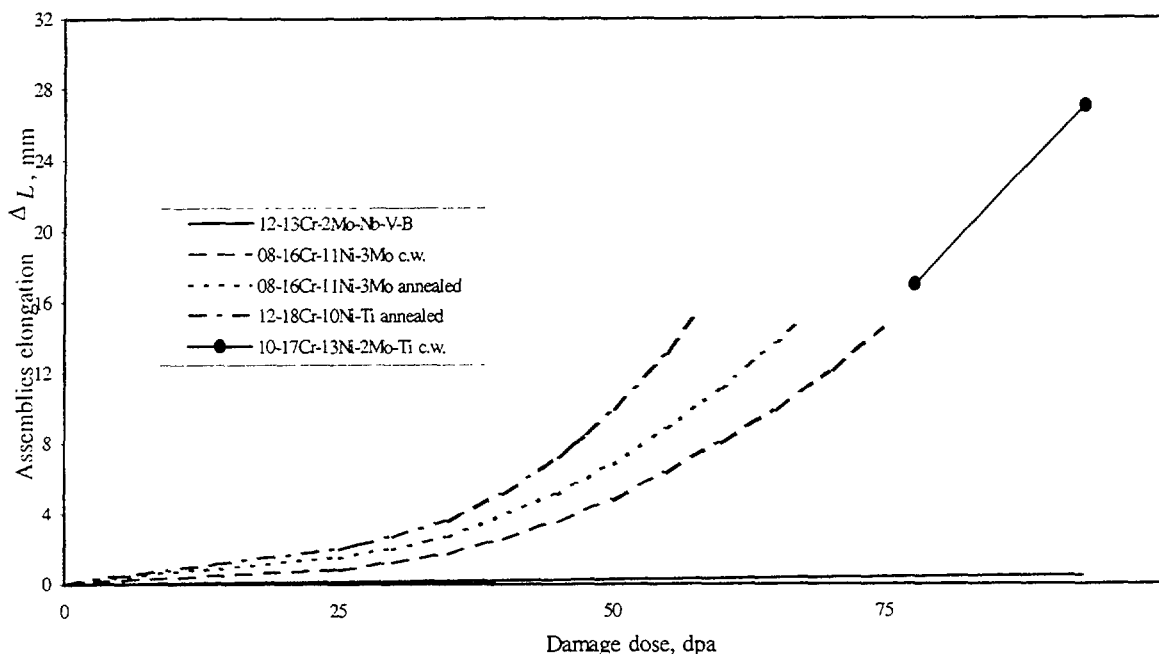


Fig.1. BN-350 assemblies elongation due to swelling of hexagonal ducts

3Mo annealed, 08-16Cr-11Ni-3Mo c.w., 10-17Cr-13Ni-2Mo-Ti c.w., 12-13Cr-2Mo-Nb-V-B and 05-12Cr-2Ni-Mo are submitted in Fig. 1.

From submitted data increase of resistance of ducts of assemblies to radiation is well visible for ferritic-martensitic steels in comparison with austenitic steels. Serviceability of assemblies on elongation is determined by an ability of loading gears of reactor BN-350 and is limited by size of 25 mm. Practical application of knowledge on elongation of assemblies has been found on reactor by work with swelling ducts, when elongation of assemblies is perceived by the operator of reactor by its installation in cell of the core as a non-placing. And if "non-placing" of assembly is in consent with swelling, was accepted, that the assembly in cell of the core is normal installed, that excluded operation of jacking down force applying. The researches on radiation deformation of ducts of assemblies on reactor are carried out since December 1974, when on ducts made of stainless steel 12-18Cr-10Ni-Ti annealed was for the first time found out ovalization of sides because of radiation creep of material. In accordance with increase of capacity of reactor the contribution in radiation deformation of assemblies ducts has become greater due to radiation swelling. Non-uniform swelling of sides resulted in bends and twisting of ducts. For 08-16Cr-11Ni-3Mo steel ducts a sag achieved $\sim (15 \pm 1)$ mm, and twist $\sim 1^\circ$. The most important phenomenon which has determined a serviceability of austenitic steels ducts has become dimensions changing. Typical character of such changing is submitted in Fig. 2. The danger of size changing and bends resides in a jam of assemblies in the core after taking up a technological gap and because of occurrence of contact forces. The exception of jam was conducted on criterion of allowable shape changing. In this case for the core of BN-350 it is recommended to organize the program of charging so that total change of the size of next assemblies do not exceed size, equal to two technological gaps, i.e.:

$$\Delta S + \Delta S' \leq 2\Delta \quad (1)$$

where

$\Delta = 2 \text{ mm}$ is the size of a technological gap for the core of BN-350.

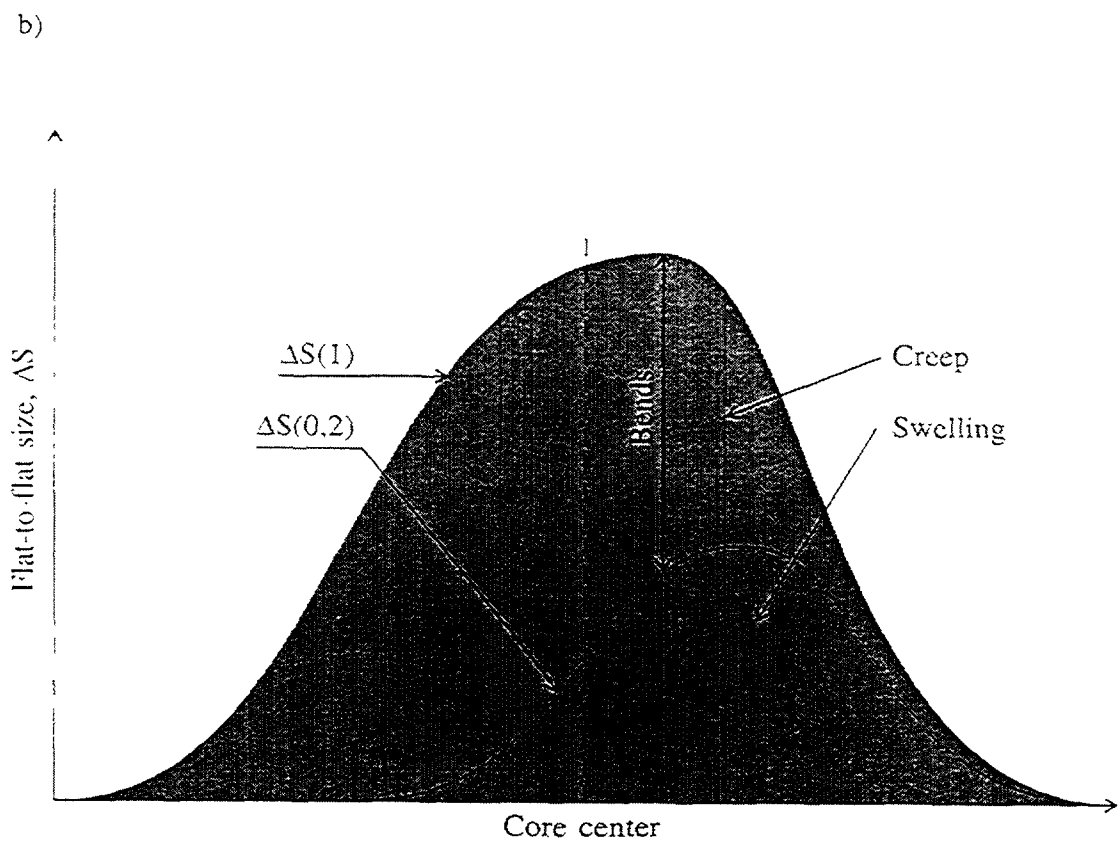
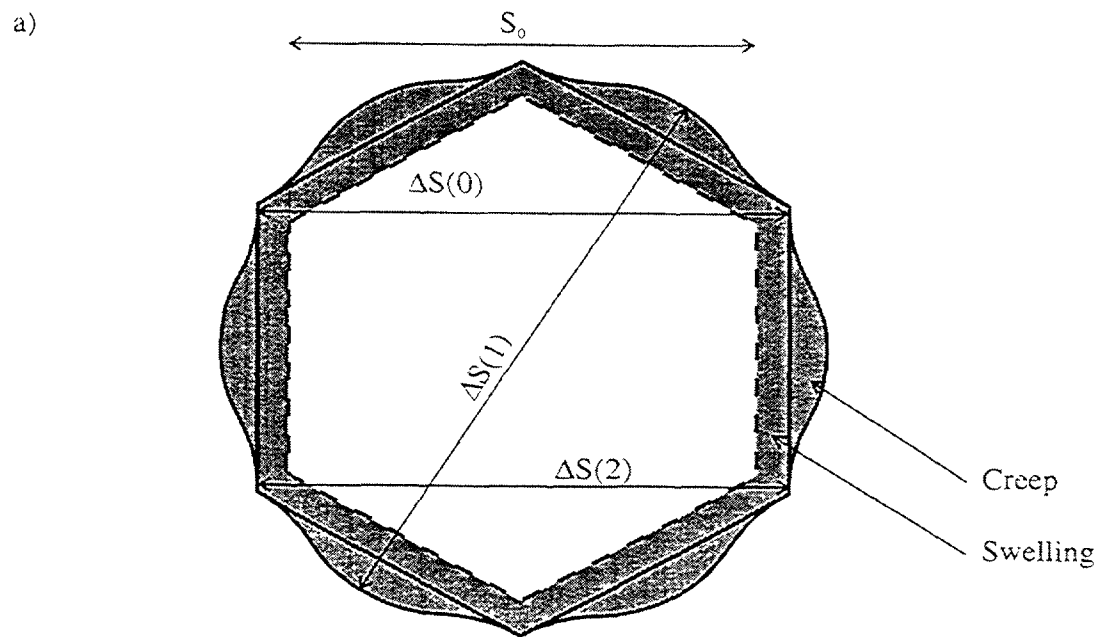


Fig.2. Ducts size changes:
a - transversal; b - longitudinal

TABLE 1. THE CHARACTERISTICS OF FUEL ASSEMBLIES OF REACTOR BN-350

Characteristic	Assembly type		
	First type	Second type	Modernized type
1	2	3	4
Duct material; flat-to-flat size × wall thickness, mm	12-18Cr-10Ni-Ti annealed 96×2	08-16Cr-11Ni-3Mo annealed 96×2	12-13Cr-2Mo-Nb- V-B 96×2
Pins number in one assembly, pcs	169	127	127
Pin length, mm	1140	1790	2440
Cladding diameter × wall thickness, mm	6.1×0.4	6.9×0.4	6.9×0.4
Cladding material	0-16Cr-15Ni-3Mo- Nb annealed	0-16Cr-15Ni-3Mo-Nb cold-worked	0-16Cr-15Ni-2Mo- 2Mn-Ti-V-B cold-worked
Core fuel length, mm	1060	1060	1000
Gas plenum length, mm	25	250	720
Fuel	UO ₂ : 17 and 26 % of U ²³⁵	UO ₂ : 17 and 26 % of U ²³⁵	UO ₂ : 17,21,26 % of U ²³⁵
Burnup achieved, %h.a./dose, dpa	(5.6÷5.8)/50÷60	13/85	≤ 13/90

On condition of strength the forces of extraction of assemblies should not exceed 800 kgf. The problem was resolved after test on reactor BN-350 of six experimental assemblies of a series "ОП" with ferritic-martensitic steel 12-13Cr-2Mo-Nb-V-B ducts. Results of tests have shown, that shape changing was caused only by radiation creep. The maximum change of the transversal size was of 0,35 mm at the damage dose of 47,5 dpa and temperature ~ 370°C.

The extrapolation of received results to the damage dose of 100 dpa gives the change of the size of 0,9 mm for ducts with the size of 96 mm with thickness of a wall of 2 mm. Thus, use of steel 12-13Cr-2Mo-Nb-V-B for assemblies ducts removes a problem of shape changing of the ducts in power fast reactors to the field of high damage doses. It is necessary to note, that successful completion of tests of assemblies of a series "ОП" in reactor BN-350 has allowed to take the decision on convert of the core of reactors BN-350 and BN-600 to assemblies with ducts made of steel 12-13Cr-2Mo-Nb-V-B. Besides practical application the study of behaviour of assemblies has resulted us

together with IPPE (Obninsk, Russia) in development of methods and means of investigation of radiation creep and swelling of steels depending on data of shape change of ducts of assemblies. It was shown, that the general change of the size is equal to change of the cross size on account of radiation swelling and bends of opposite sides on account of radiation creep under pressure of the coolant. Was proved, that the bends of sides are proportional to a damage dose and load from pressure of the coolant. It has allowed with use of the decision of a task of creep of a side of the duct, to do an estimation of the module of radiation creep for number of steels. Such data are shown in Table 2. Weak dependence of the radiation creep module from temperature in investigated temperature intervals is marked.

TABLE 2. THE MODULE OF RADIATION CREEP FOR SOME STEELS

Duct material	$B \cdot 10^6$, [MPa-dpa] ⁻¹	Temperature, °C	kt^{\max} , dpa
1	2	3	4
12-18Cr-10Ni-Ti, annealed	1÷7	290÷530	56
08-16Cr-11Ni-3Mo, annealed	1.2÷3.5	290÷570	60
08-16Cr-11Ni-3Mo, cold-worked	1.2÷2.5	290÷510	60
12-13Cr-2Mo-Nb-V-B	0.4±0.06	290÷540	90
05-12Cr-2Ni-Mo	0.8÷1.2	290÷540	70
10-17Cr-13Ni-2Mo-Mn, cold-worked	2.3÷4.0	290÷550	81

Is shown, that swelling of austenitic stainless steels can be rather reliably described by dependence of a kind:

$$\frac{\Delta V}{V} = A(kt - \tau)^m \text{ch}^{-1} \left[B \left(\frac{1}{T} - \frac{1}{T_m} \right) \right] \quad (2)$$

Where

$\frac{\Delta V}{V}$ is the volumetric swelling of a material (%),

kt is the neutron damage dose (dpa),

τ is the incubation dose (dpa),

A, B are the constants,

T is the irradiation temperature (K),

T_m is the maximum temperature of peak swelling (K),

m is the power index.

In particular, for the steels 12-18Cr-10Ni-Ti annealed and 08-16Cr-11Ni3Mo annealed are ascertained the exponent laws of dependence of swelling from irradiation dose with power indexes of $2,0 \pm 0,2$ and $2,4 \pm 0,4$ accordingly. For these steels is found out one peak of swelling with temperature maximum of 743 K for steel 12-18Cr-10Ni-Ti and 723 K for steel 08-16Cr-11Ni3Mo. For cold worked steels is found, that in dependence (2) m is equal to 1.

4. The pins behaviour

The linear thermal rate in fuel pins of the reactor BN-350, as a rule, did not exceed 450 W/cm, temperature of cladding did not exceed 700°C.

Under these conditions the nuclear fuel UO_2 behaves by an usual image:

- In fuel three-zoned structure is formed;
- Swelling of fuel makes $(1,0 \div 1,5)$ % on 1 % burnup;
- At density of fission $\sim 10^{13} \text{ cm}^{-3} \cdot \text{s}$, typical for BN-350, the fuel is subjected to radiation creep.

The radiography of pins reached burnup of ~ 13 % h.a. (assembly II-8) has confirmed preservation of the form of fuel pellets and absence of melting. As have shown estimations, a tense condition of cladding is defined by the following factors:

- pressure of gas fission products (GFP);
- fuel-cladding interaction (FCI);
- bundle-duct interaction (BDI);
- thinning of cladding because of corrosion affection by fission products.

For pins of the first and second types a determining stress is a stress by pressure of GFP.

For pins of a modernized type the account of a pressure from BDI and FCI is necessary. Experimental data on GFP pressure for pins of the reactor BN-350 are submitted in Fig. 3. The drop of GFP pressure at transition from pins of the first type with a small gas plenum to pins with a large gas plenum is well noticeable.

Typical character of radiation shape change of the pins of BN-350 (assembly II-17 with pins of the second type) is submitted in Figs. 4 and 5. The ovalization of cladding reaches $(0,4-0,5)$ mm and is the result of mechanical interaction between bundle and duct due to radiation creep of cladding (austenitic stainless steel (0-16Cr-15Ni-3Mo-Nb cold worked) under action of contact forces. The degree of ovalization from the acting factors can be calculated under formula:

$$D^+ - D^- = \frac{P_k}{b} B(T) \cdot (kt - \tau) \left(\frac{D}{\delta} \right)^3 \quad (3)$$

Where

$D^+ - D^-$ is the ovalization,

P_k is the contact force (MPa),

$B(T)$ is the radiation creep module $(\text{MPa} \times \text{dpa})^{-1}$,

$(kt - \tau)$ is the dose (dpa),

D is the diameter (m),

δ is the cladding thickness (m),

$b = 1$.

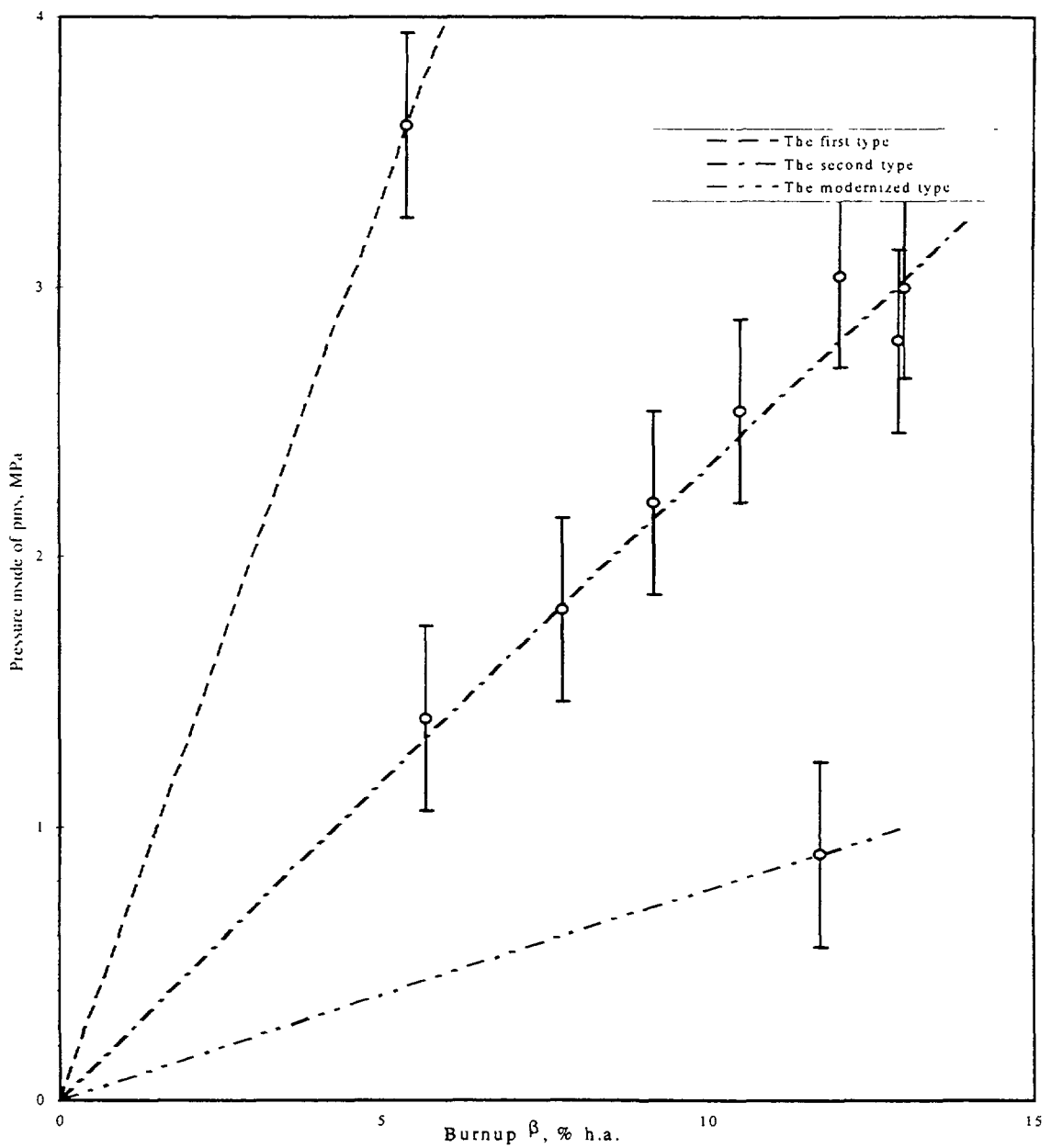


Fig.3. Gas fission products pressure under cladding for different types of pins of BN-350

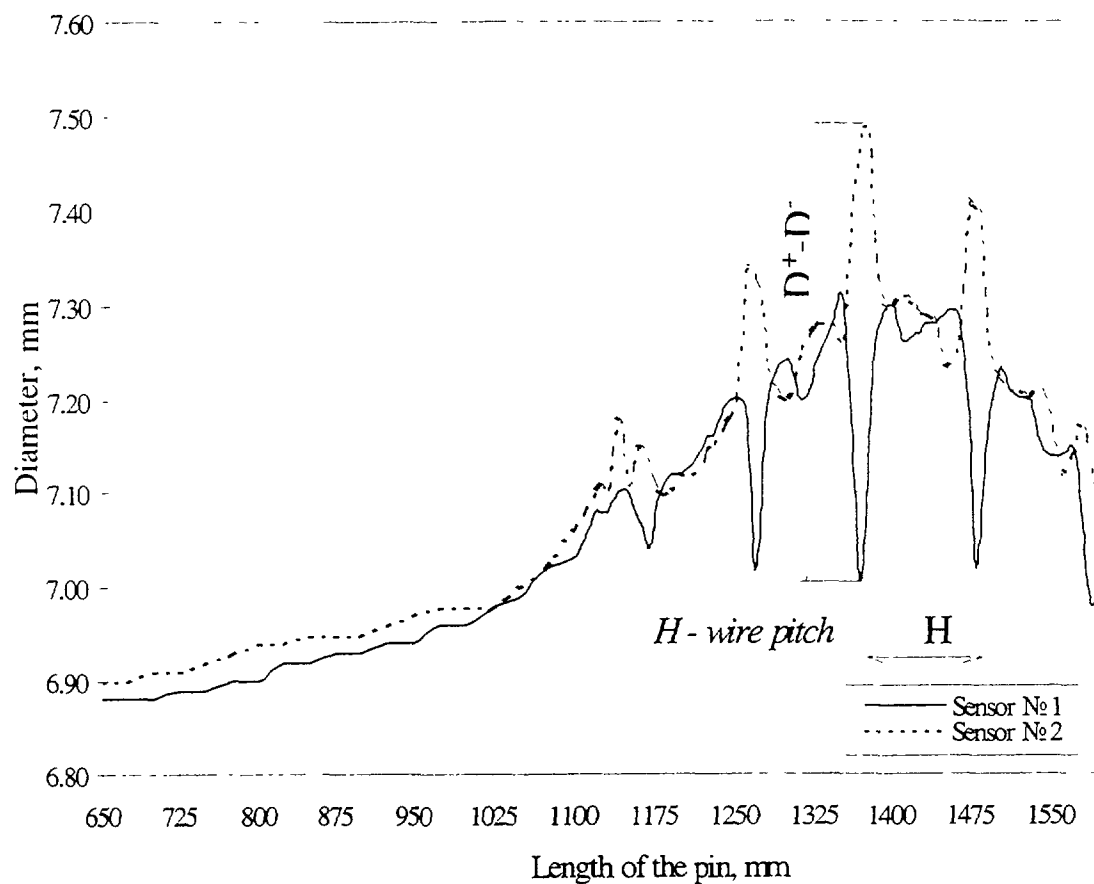


Fig. 4. Pin No1 profilgram (peripheral), assembly II-17

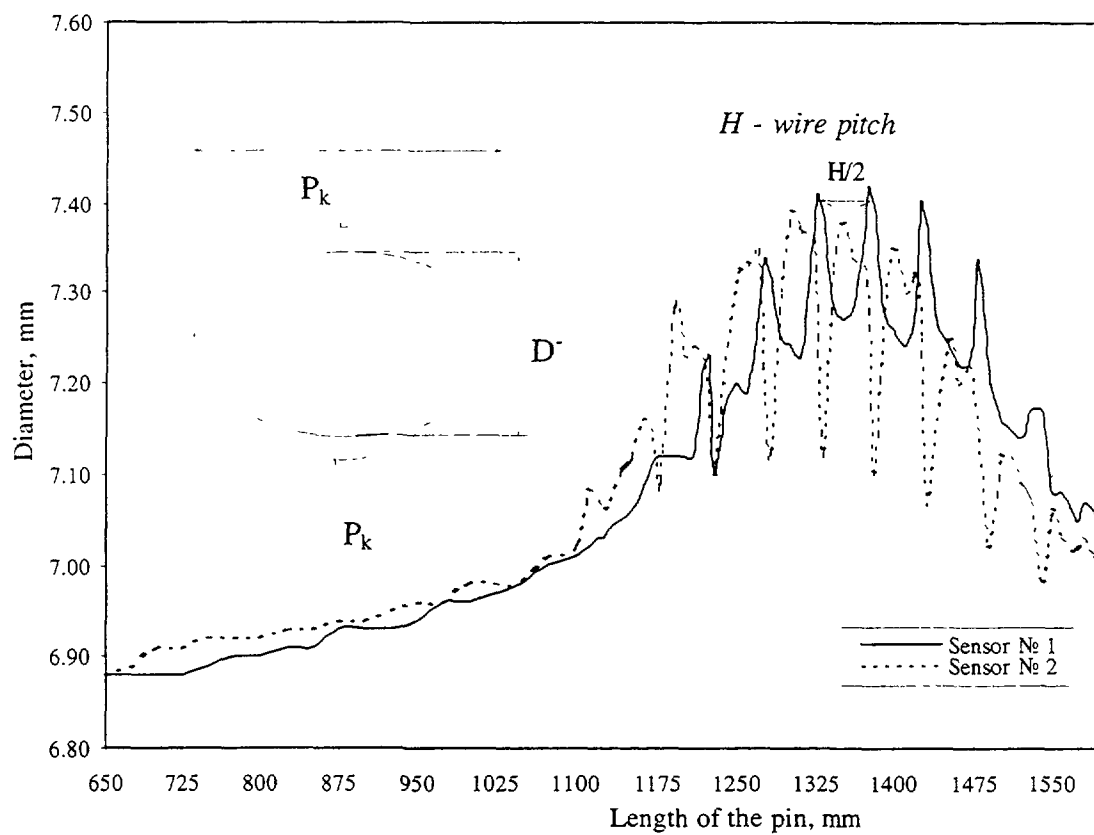


Fig.5. Pin № 64 profilgram (central), assembly II-17

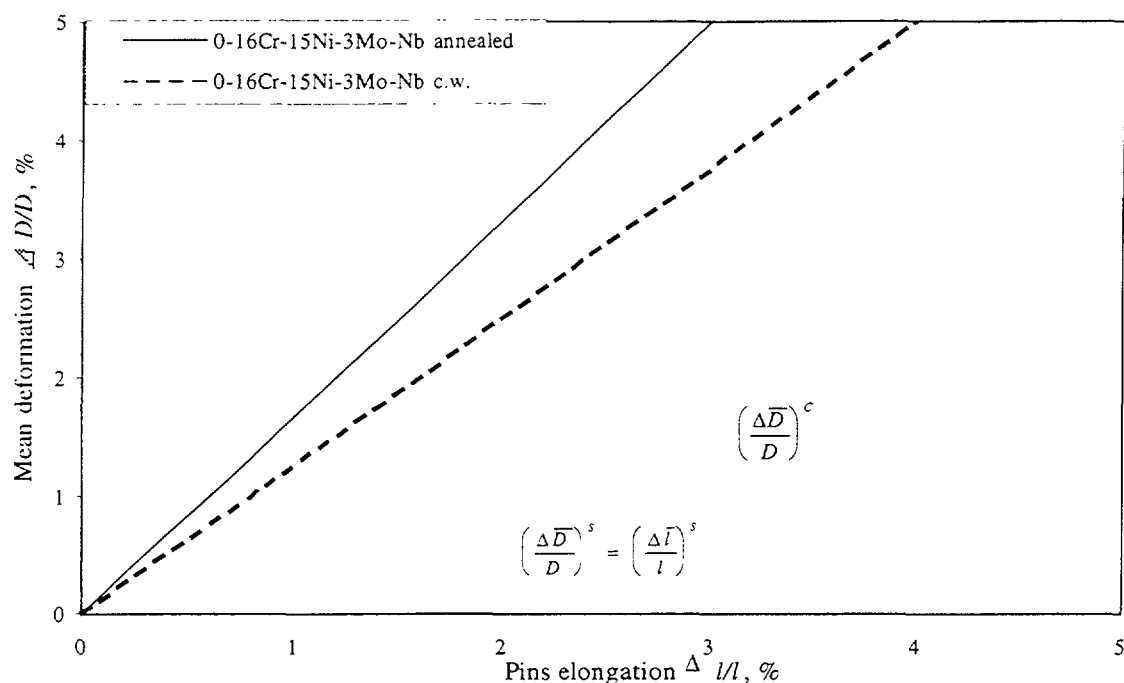


Fig.6. Dependence of mean deformation of cladding (steel 0-16Cr-15Ni-3Mo-Nb) on elongation due to swelling

Fig. 6 illustrates the analysis of components of general deformation of steel 0-16Cr-15Ni-3Mo-Nb cladding in assumption, that the contribution of swelling in elongation of cladding and in diametrical deformation is identical. Then the plastic deformation of cladding is defined as a difference:

$$\left(\frac{\Delta \bar{D}}{D}\right)^c = \left(\frac{\Delta \bar{D}}{D}\right) - \frac{\Delta L}{L} \quad (4)$$

Assuming, that $\left(\frac{\Delta \bar{D}}{D}\right)^c$ is stipulated mainly by radiation creep it is possible to evaluate the module of radiation creep of the steel 0-16Cr-15Ni-3Mo-Nb. The contribution of radiation creep to general deformation of cladding for pins of the first and second type is rather great and reaches 40 - 50 % for cladding in austenitic condition and 10 - 20 % for cold-worked cladding. The estimation of the module of radiation creep for steel 0-16Cr-15Ni-3Mo-Nb is shown in the Table 3.

TABLE 3. THE ESTIMATION OF THE MODULE OF RADIATION CREEP FOR STEEL 0-16CR-15NI-3MO-NB

Cladding material	$B \cdot 10^6, [MPa \cdot dpa]^{-1}$	Temperature range, °C
1	2	3
0-16Cr-15Ni-3Mo-Nb, annealed	7÷12	300÷550
0-16Cr-15Ni-3Mo-Nb, cold-worked	2.5÷4.0	300÷550

As already was specified above, for cladding of pins of the first and second types made of 0-16Cr-15Ni-3Mo-Nb the principal stress is the stress of GFP pressure.

Level of stress reaches in pins at the end of work the value of (100 - 120) MPa. As show experimental data of profilometry of the cladding of pins of the second type deformation reaches values of ~ 6 - 14 % (assembly ОП-4) for cladding of steel 0-16Cr-15Ni-3Mo-Nb annealed and 7 % for cladding of steel 0-16Cr-15Ni-3Mo-Nb c.w. (assembly И-17). Thus in indicated assemblies a destruction of cladding was not observed. In too time as have shown mechanical tests of a material of cladding a plasticity of steel is close to zero in places with maximum of shape and dimensions changes. It testifies to exhaustion of life time of pins of the second type with cladding made of steel 0-16Cr-15Ni-3Mo-Nb c.w. by reaching them of 13 % h.a of burnup and damage dose ~ 90 dpa. The analysis of serviceability of pins of the second type on criterion of creep rupture strength also confirms exhaustion of serviceability of cladding of steel 0-16Cr-15Ni-3Mo-Nb c.w. by dose 90 dpa and burnup ~13 % h.a.

Now the core of the reactor is converted to assemblies of a modernized type with increased gas plenum and low pressure of GFP. Moreover for cladding of pins the steel 0-16Cr-15Ni-2Mo-2Mn-Ti-V-B c.w. with higher resistance to irradiation is applied. All this permits to hope to have in reactor BN-350 burnup~ 15 % h.a. (dose ~ 105 dpa).

For the assembly of the reactor BN-350 with 0-16Cr-15Ni-3Mo-Nb steel cladding took place cases of reaching by fuel pins of a limiting condition on serviceability: 5,8 % h.a. for cladding of fuel pins of the first type and by 13 % h.a. for cladding of fuel pins of the second type.

As show settlement estimations of stress in cladding, basic contribution to an intense condition of cladding of fuel pins both first, and second type gives a pressure from gas fission products and consequently it is possible to assume, that the law of change of pressure from a burnup will be close to linear since pressure of fission gas release under cladding accrues under the linear law.

In this case the stress divided by burnup during work of fuel pins will be practically at the same level. Then if to put, that the time of work of fuel pins in a reactor coincides with time of reaching by them of a limiting condition, construction of parametrical dependence of creep rupture strength of cladding of fuel pins is possible, namely:

$$\lg\left(\frac{\sigma}{\beta}\right) - \text{LMP} \quad (5)$$

Where

(σ/β) is the stress normalized on a burnup (MPa/% h.a.),

LMP is the Larson-Miller parameter $\equiv T (13,5 + \lg t_r)$,

T is the maximum temperature of cladding (K),

T_r is the time before destruction (hours).

Such dependence for cladding of fuel pins for steel 0-16Cr-15Ni-3Mo-Nb is submitted in fig. 7. The time before destruction can be designed under the formula:

$$t_r = \frac{4,24 - \left[\lg\left(\frac{\sigma}{\beta}\right) + 0,1 \right]}{2,03 \cdot 10^{-4} T} - 13,5 \quad (6)$$

Presence of the given dependence for cladding of fuel pins of a reactor BN-350 testifies that a major factor of going out of fuel pins BN-350 is exhaustion of creep rupture strength of cladding (steel 0-16Cr-15Ni-3Mo-Nb) under irradiation.

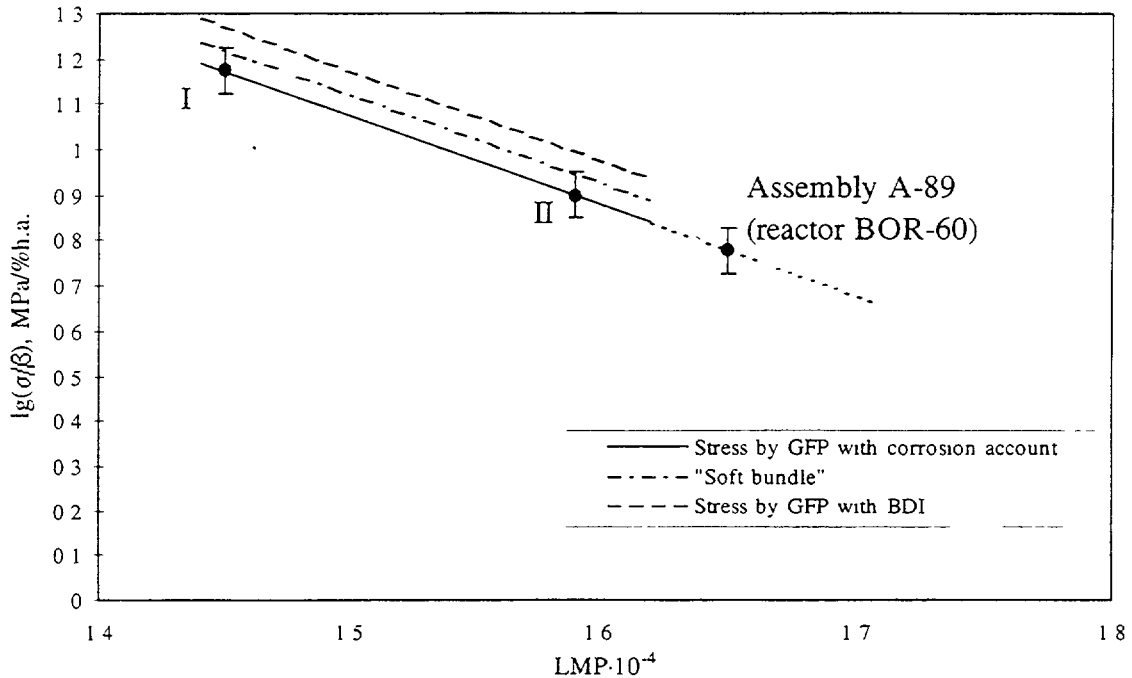


Fig.7. Creep rupture strength of BN-350 pins cladding (steel 0-16Cr-15Ni-3Mo-Nb)

The received dependence allows to estimate time before destruction of cladding of fuel pins in reactor and is used at an estimation of serviceability of fuel pins of the second type (steel 0-16Cr-15Ni-3Mo-Nb).

5. Conclusion

5.1. The reliable and safe work of reactor BN-350 was provided on extent more than 20 years by study of behaviour of assemblies and pins under irradiation. For that at the reactor has been built a complex of hot cells with appropriate methods and means of research of serviceability of assemblies.

5.2. Behaviour of assemblies with cladding made of number of austenitic steels is investigated. Is shown, that in this case serviceability of assemblies is limited by radiation changes of shape and dimensions of hexagonal ducts because of swelling and radiation creep of constructional materials. The problem of radiation changes of shape and dimensions was resolved for cores of reactors BN-350 and BN-600 after testing on reactor BN-350 of experimental assemblies with cladding of ferritic-martensitic steel 12-13Cr-2Mo-Nb-V-B.

5.3. Serviceability of pins of reactor is limited by:

- Pressure of GFP of fuel,
- Interaction of fuel with cladding,
- Mechanical interaction of bundle with duct,
- Corrosion affecting by GFP of fuel.

For pins of the second type with steel 0-16Cr-15Ni-3Mo-Nb c.w. cladding of the serviceability is exhausted by burnup 13 % h.a. and damage dose 90 dpa.

5.4. For increasing of burnup the reactor BN-350 is converted to assemblies of modernized type with large gas plenum and cladding made of a new steel 0-16Cr-15Ni-2Mo-2Mn-Ti-V-B c.w. with higher resistance to irradiation.

It is expected that the serviceability of pins of modernized type will be provided up to 15% h.a (dose 105 dpa).

5.5. Analysis of serviceability of fuel pins of a reactor BN-350 allows to make a conclusion that the main cause of going out of fuel pins is reaching of cladding (steel 0-16Cr-15Ni-3Mo-Nb) creep rupture strength under irradiation.

REFERENCES

[1]. V.N.KARAULOV, T.G.SHKOL'NIK. "Study of swelling and radiation creep of constructional materials of ducts of the reactor BN -350 by results of their deformation." Radiation material study. V.8, (Transactions of International conference on radiation material study, Alushta, on May 22-25, 1990) Har'kov (1991) 132-143.

[2]. V.N.KARAULOV et al. "Development of radiation stable corrosion-proof steels for ducts of subassemblies of fast reactors." Radiation material study. (Transactions of International conference on radiation material study, Alushta, on May 22-25, 1990) V.3, Har'kov (1990) 43-48.

[3]. V.N.KARAULOV. "Behaviour of cladding of fuel pins of fast reactor BN -350 in conditions of mechanical interaction of fuel pins bundle with duct of subassembly." Researches of constructional materials of elements of cores of fast sodium reactors: [Transactions of scientific works]. Ekaterinburg. (1994) 177-188.

[4]. L.M.ZABUD'KO, JU.I.LIHACHEV, A.A.PROSHKIN. "Serviceability of a subassembly of fast reactors." M., Energoatomizdat, (1988) 168 pp.

[5]. I.S.GOLOVNIN, L.M.ZABUD'KO, V.N.KARAULOV et al. "The analysis of data on deformation of subassemblies of a reactor BN-600." Safety and reliability of operation of atomic power stations with fast reactors. Part II, Sverdlovsk, (1986) 25-80.

[6]. V.S.NEUSTROEV, V.N.GOLOVANOV, V.K.SHAMARDIN. "Radiation embrittlement of materials of subassemblies in a temperature interval of a maximum of a swelling." Atomic energy, V.69, Ser.4, October 1990, p.223-226.

[7]. A.A.PROSHKIN et al. "The analysis of experimental data about change of the form of subassemblies of fast reactors." Atomic energy, V.50, Ser.1, January 1981, p.13-17.

IN-PILE TESTS AND POST-REACTOR INVESTIGATIONS OF FUEL PINS WITH U-Pu FUEL



XA9848044

L.I. MOSEEV, A.N. VOROBYEV, L.M. ZABUDKO,
B.S. KIRYANOV, S.I. POROLLO, S.V. SHULEPIN
State Scientific Center, Institute of Physics and Power Engineering,
Obninsk

S.A. ANTIPOV, T.S. MENSHIKOVA
Institute of Inorganic Materials, Moscow

Russian Federation

Abstract

Resulting of testing experimental fuel subassemblies with oxide uranium-plutonium fuel and data of fuel pin investigations at the IPPE hot laboratory have been presented. MOX and UOX fuels behaviour under irradiation are compared.

1. INTRODUCTION

The present-day concepts of fast neutron power reactors include the use of U-Pu oxide fuel as a fissile material. Radiation stability of MOX fuel widely used in the Western countries with up to 20% content of plutonium has been studied well enough, including the fuel compatibility with cladding materials, problems of reprocessing, etc. The use of fast reactors as facilities for utilization of weapons-grade plutonium suggests a changeover to fuel with a higher content of Pu (40% and more) and requires an additional information on radiation behavior of fuel of this kind. Obviously, post-radiation investigations of MOX fuel still remain actual. Reactors BN-600 and BN-350 operated in Russia and Kazakhstan are fueled with UO₂ pellets as a standard fuel. However, to substantiate the serviceability of subassemblies of BN-800 supposed to be fueled with MOX, a series of experimental subassemblies with U-Pu oxide pellet fuel fabricated by various technologies was irradiated in reactors BOR-60, BN-350, and BN-600. The subassemblies were subjected to non-destructive analysis (NDA) in hot cells of reactors BN-350 and BN-600 and at the hot laboratory of NIIAR¹ after irradiation to various burn-up levels and damaging doses. Some of the fuel pins were sent to the IPPE hot laboratory for detailed material studies.

The following issues were studied at the IPPE hot cell laboratory:

- release of gas and volatile fission products from the nuclear fuel under the fuel pin claddings, and effect of factors such as fuel fabrication technology (U_nPu_m)O_x, burn-up, temperature, and the O/M ratio on this release;
- redistribution of plutonium, fission products, and oxygen along the fuel column radius and height, as dependent on the burn-up and initial structure of pellets;
- interaction of chemically active fission products and nuclear fuel with the fuel pin cladding materials, and effect of various factors on the interaction: temperature, oxygen coefficient, steel composition and its state;
- change of homogeneity of solid solution of (U_nPu_m)O_x in the course of irradiation;

The report presents principle results of these investigations.

¹ R&D Institute of Nuclear Reactors, Dimitrovgrad

TABLE 1 DESIGN AND IRRADIATION PARAMETERS OF FUEL PINS

S/A parameters			Technological parameters			Irradiation parameters			
Reactor, S/A №	U/Pu ratio	Cladding material	Technology of fuel	Density g/cm ³	O/M	Burnup %h a	Q _i kW/m	T _{max} /T _{min} (°C) for cladding	Dose dpa
BN-350 2	0 79/ 0 21 0 69/ 0 31	Cr15Ni16Mo3Nb Austenization	Mix	10 2	2 00	4 95	37	479/360	28
			Chem co precip	10 2	2 00	4 95	35-42	579/447	28
BN-350 4	0 79/ 0 21	Cr15Ni16Mo3Nb Austenization	Mix	10 4	1 98	4 90	42	450/380	28
				10 5	1 99	4 90	42	560/380	28
				10 6	1 98	4 90	42	600/380	28
BN-350 9	0 8/0 2	Cr15Ni16Mo3Nb Austenization	Mix	10 4	1 97	4 95	45	580/350	65
				10 4	1 97	4 95	45	490/350	65
BN-350 C-11	0 8/0 2	Cr15Ni16Mo3NbB Cold Work	Mix	10 2	1 97	9 70	49	580/340	62
BOR-60 NIM-1	0 8/0 2	PE-16	Mix	10 2	2 01	12 10	42	640/360	58
BOR-60 NIM 2	0 85/ 0 15	PE-16	Mix	10 2	2 01	12 10	44	708/360	58
BOR-60 PG	0 8/0 2	Cr15Ni16Mo3Nb Austenization	Mix Plazmo-chem	10 4	1 97	12 60	49	470/370	43
				10 4	2 00	12 60	49	590/370	43
BOR-60 PKG	0 8/0 2	Cr15Ni16Mo3Nb Cold Work	Mix	10 1	1 99	7 40	50	565/340	31
BOR-60 PKK	0 8/0 2	Cr15Ni16Mo3NbB Cold Work	Mix	10 3	1 99	10 80	44	648/380	65
			zol-gel	10 3	1 99	10 80	44	470/380	65
BOR-60 PKG	0 69/ 0 31	Cr15Ni16Mo3Nb Austenization	Mix	10 0-10 25	1 99-2 01	7 4	49	697/565	31

TABLE 2 DEPTH OF CORROSION IN FUEL PIN CLADDINGS

Reactor, pin s materials	Burn-up % h a	Temperature of cladding °C	O/M	Q _i kW/m	Peak depth of corrosion μm
BN-350 (U _{0.79} Pu _{0.21})O _{1.9720} Cr16Ni15Mo3Nb Austenization	4 95	479	2 0	37	1-2
	4 95	579	2 0	42	42
	13 2	440	1 97	43	0
	13 2	570	1 97	43	62
	4 90	450	1 98	42	0
	4 90	560	1 99	42	29
BN-350, (U _{0.8} Pu _{0.2})O _{1.97} Cr16Ni15Mo3NbB Cold Work	9 70	490	1 97	49	32
	9 70	580	1 97	49	69
BOR-60 (U _{0.8} Pu _{0.2})O _{1.9720} Cr16Ni15Mo3Nb Austenization	12 6	470	1 97	49	12
	12 6	590	2 0	49	69
BOR-60, (U _{0.8} Pu _{0.2})O _{1.99} Cr16Ni15Mo3NbB Cold Work 20%	10 8	470	1 99	44	2-3
	10 8	648	1 99	44	28
BN-600 UO ₂ Cr16Ni15Mo3NbB Cold Work 20%	8 93	560	2 0	36 1	30
BN-600 UO ₂ Cr16Ni15Mo3NbB Cold Work 20%	10 7	530	2 0	40 5	65

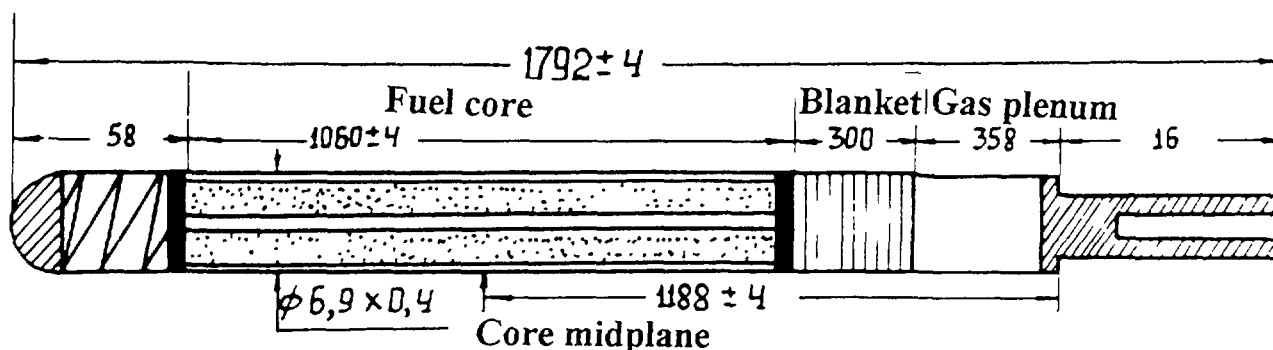
2 IN-PILE TESTS OF FUEL SUBASSEMBLIES WITH MIXED OXIDE FUEL IN BN-350 AND BN-600 REACTORS

The tests of 14 full-scale fuel subassemblies with MOX fuel in BN-350 have been completed. All fuel pins in experimental subassemblies prove to retain their tightness after irradiation to various burn-up levels. The maximum burn-up and damage dose for the first 10 subassemblies (N N1-10) loaded into the BN-350 core in 1982 appeared to be limited by a high shape change of hexagonal wrappers fabricated from steel 0X16H11M3 (MTO). Maximum burn-up of various different subassemblies amounted to 4.5 - 5.0% h a, damage dose - 30-35 dpa. In the next set of four subassemblies, more radiation-resistant steels were used as cladding materials of fuel pins.

12 subassemblies with uranium-plutonium fuel have been irradiated in reactor BN-600. The first eight subassemblies were tested during the three micro-runs up to the burn-up level of 10.0-10.5% h a (maximum damage dose - 70-71 dpa). The other four subassemblies have been irradiated during four micro-runs up to the burn-up level of 11.0-11.8% h a (maximum damaging dose - 80.7 dpa). Three subassemblies were investigated at Beloyarsk NPP hot cells using NDA. Preliminary post-reactor investigations have shown that the subassemblies are in a good condition. 12 subassemblies with pelleted uranium-plutonium oxide fuel are being under irradiation in the BN-600 core.

3 INITIAL CHARACTERISTICS OF FUEL PINS AND TEST CONDITIONS

A mixed oxide fuel was used for the fabrication of fuel pellets (U_nP_m)O_x produced by various technologies: from mechanical mixture of uranium and plutonium oxides, chemical co-precipitation, plasmochemical method, sol-gel process, etc. The various compositions of fuel tested are 15, 20, 21, and 31% Pu mass. Oxygen coefficient in the nuclear fuel varied from 1.97 to 2.01. The fuel pellets were used with external diameter of 5.9 mm, internal channel diameter - 1.7 mm, density of 10.0-10.6 g/cm³. The nuclear fuel pellets were inserted into cladding tubes made from the high nickel alloy PE-16 (43% Ni) stainless steel 0X16H15M3B (EI-847) in solution-treated condition and austenitic stainless steel 0X16H15M3BP (EP-172), 20% cold-worked. The fuel pin cladding diameter is 6.9 mm, the wall thickness is 0.4 mm. The data on fuel pins fabrication and operation conditions are shown in Table 1. Fig. 1 shows the structure



Type of fuel: ($U_{0.8}Pu_{0.2}$)O₂ (pellets)

Cladding material: Cr16Ni15Mo3NbB (20% c.w.)

Fig. 1. BN-350 reactor fuel pin design

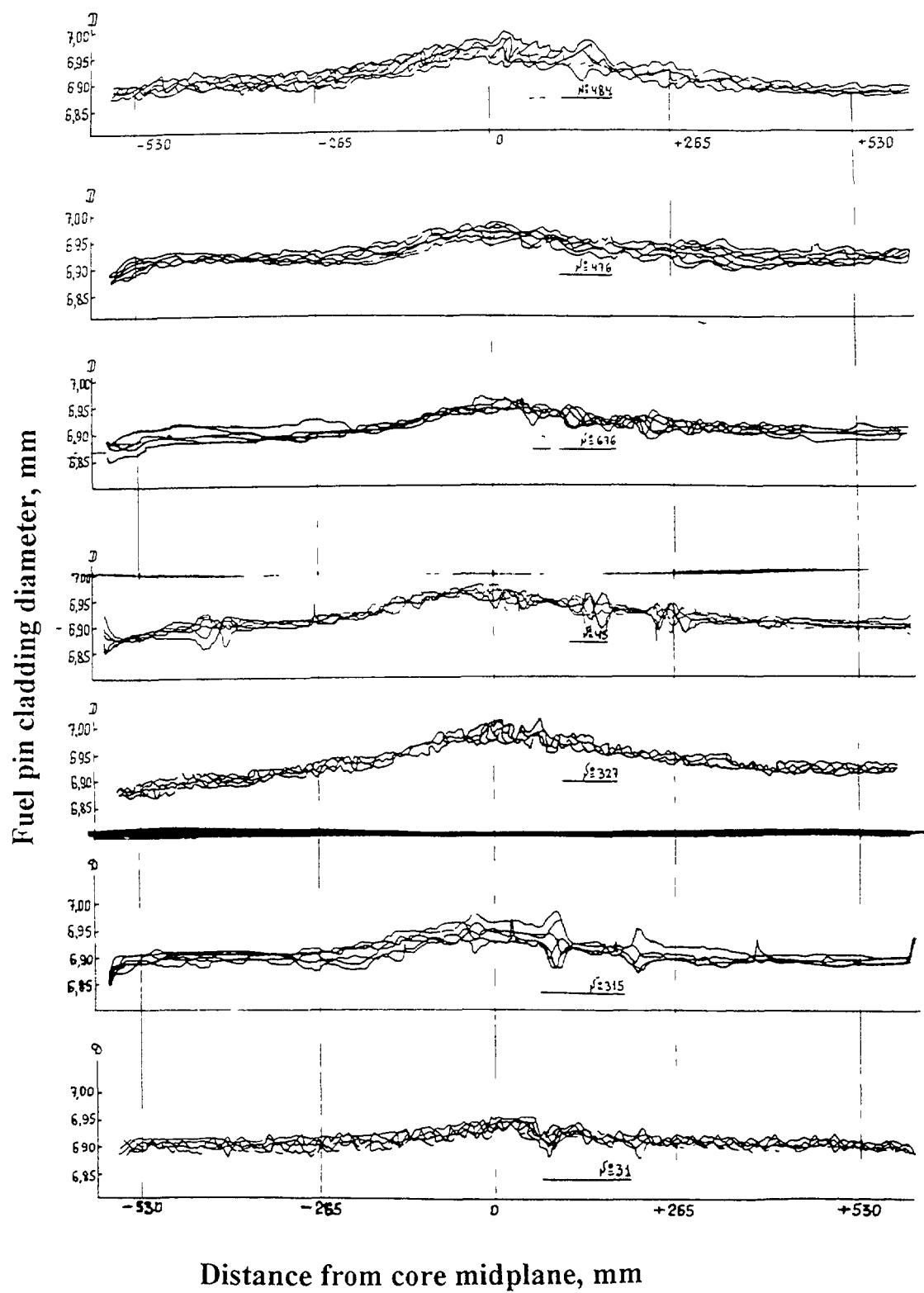


Fig. 2. Fuel pin cladding profiles (BN-350 reactor, Type EI-847 SS, burn up of 11.6% h.a)

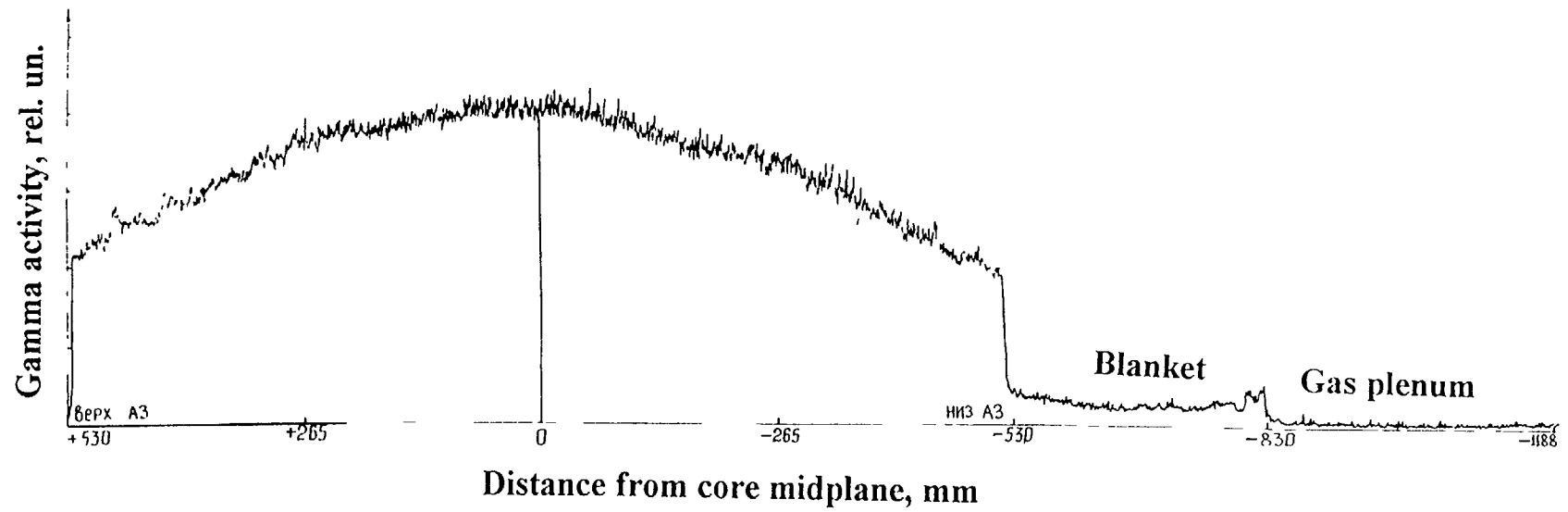


Fig. 3. Total gamma activity profile for fuel pin (S/A C-11, BN-350 reactor).

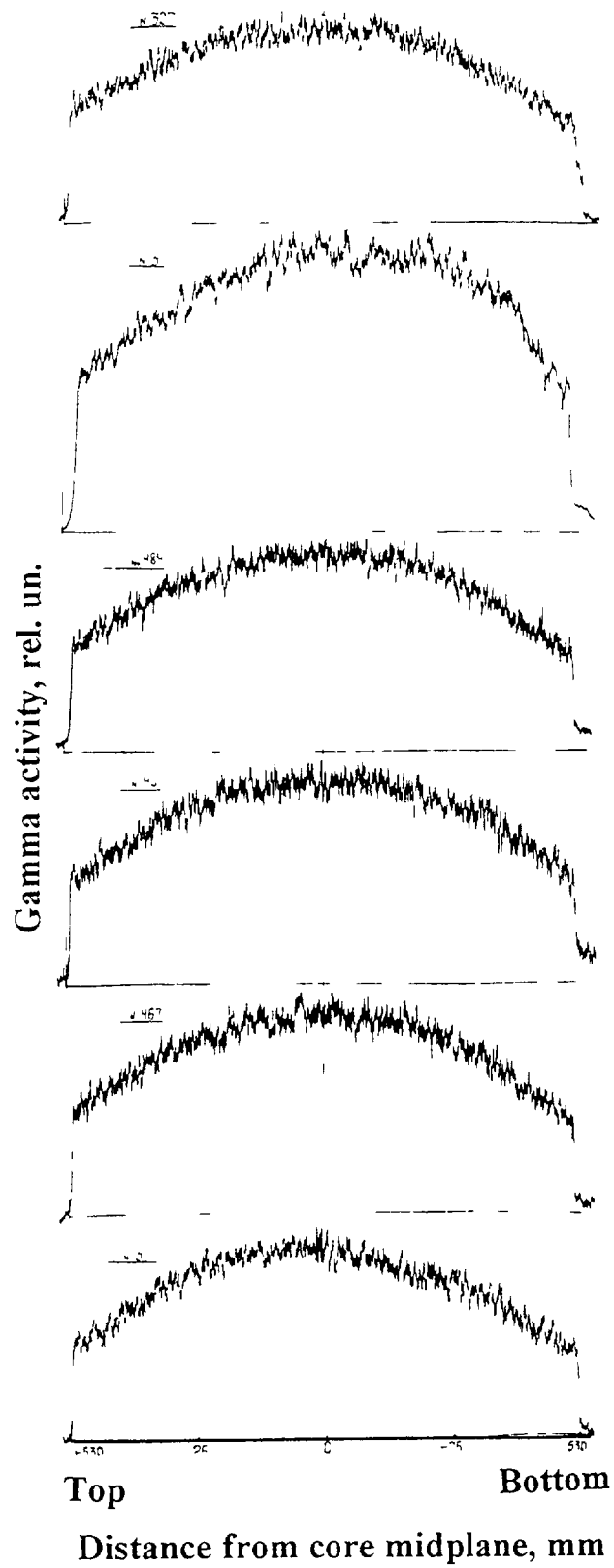


Fig. 4. Cs-137 gamma-activity profile for fuel pins (S/A C-11, BN-350 reactor).

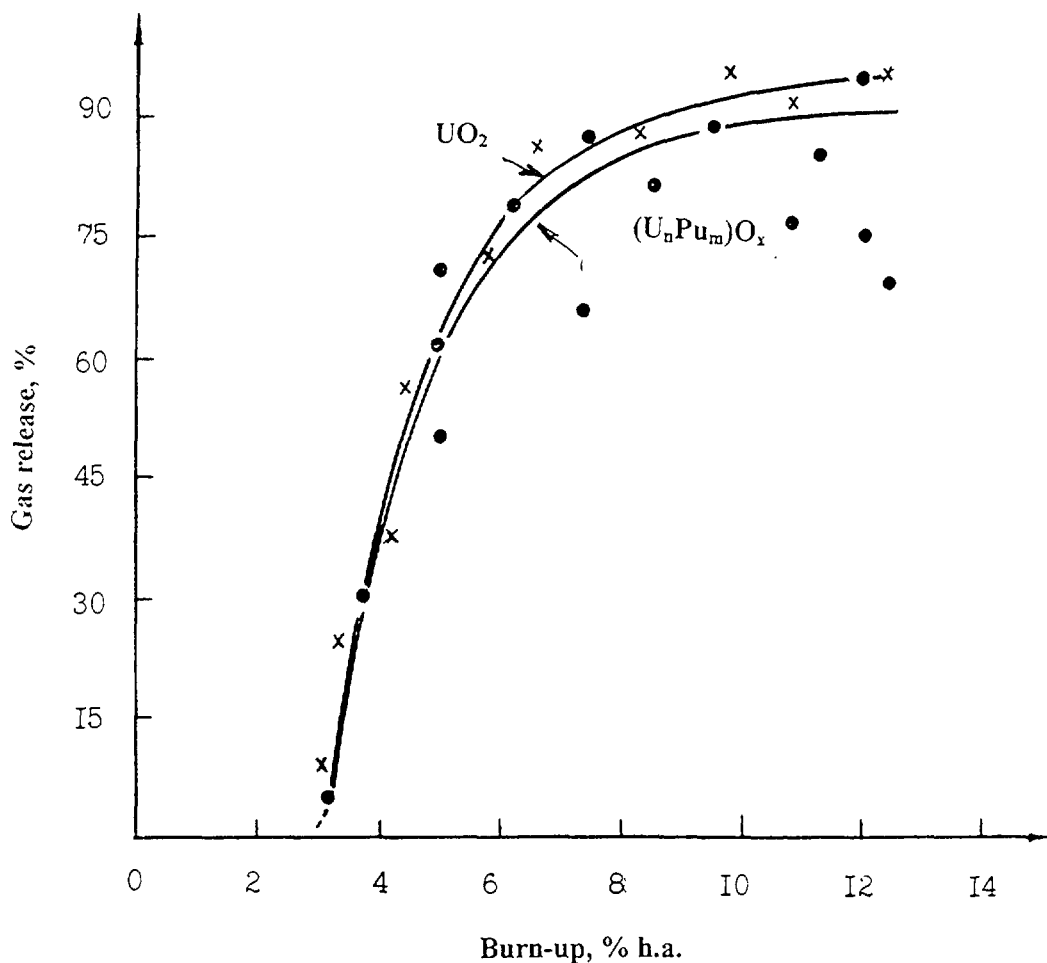


Fig. 5. Gas release from UO_2 and $(\text{U}_n\text{Pu}_m)\text{O}_x$ fuel as a function of burn-up (\times - UO_2 , \bullet - UPuO_2 , \square - PuO_2).

of fuel pins with uranium-plutonium nuclear fuel tested in BN-350 reactor. The fuel pins have been assembled in a hexagonal wrapper tube of 96 mm in flat-to-flat size. Each subassembly contains 127 fuel pins. The fuel pins were spaced using a wire of 1.5 mm in diameter for the central bundle and 1.3 x 0.6 mm - for the peripheral fuel pins. To lower a non-uniformity of fuel pins temperature in a peripheral areas, displacers of 2 mm in diameter were installed along the facets of a wrapper tube.

4. RESULTS FOR FUEL PINS

4.1. Appearance of fuel pins

An inspection of fuel pins in a hot cell using a binocular did not reveal visible defects on cladding outer surfaces. The spacing wire was closely adjacent to the pin surface. After the removal of oxidized coolant residues, the fuel pin surfaces were of frosted-silvery color.

4.2. Fuel pin diameter measurements

Outer diameters of fuel pins were measured using a distant profile meter, six profilograms being taken for each fuel pin rotated clock-wise, at every 30 degrees.

Figure 2 shows the results of fuel pin diameter measurements for the subassembly C-11 irradiated in reactor BN-350. A maximum diameter increase was observed for central parts of reactor core (cladding temperature of 440-470 °C) in the region where the neutron flux is maximal. Diameter of fuel pins with claddings made from steel 0X16H15M3B (SA) near the core midplane increased from 3.6% to 4.3% as compared with the initial one. Diameter of fuel pins with claddings of type 0X16H15M3BR (20% CW) stainless steel changed by approximately 1.8%. From a comparison of fuel pin diameters in case of oxide uranium-plutonium fuel and oxide uranium one after irradiation in the reactor BN-350 it follows that the increase of fuel pin diameter is determined by the type (different types of steel, high nickel alloy) and condition (solution-treated, cold worked) of cladding tubes, and does not depend on the type of fuel used. As it has been shown by electron microscopy and density measurements of cladding swelling, the increase of cladding diameters is due to void swelling.

4.3. Axial profile of radionuclides

The axial profile of fission product distribution was obtained by the registration of γ -radiation intensity by continuous pulling the fuel pins in front of a collimated detector. Figures 3 and 4 show typical scannograms of total γ -activity and that of one of fission products (Cs-137) in fuel pins with the oxide uranium-plutonium fuel. Solid fission products, such as Zr-95, are distributed proportionally to the linear power of the fuel pin, that is similar to an oxide uranium nuclear fuel, i.e., no migration of fission products along the fuel pin height is observed.

4.4. Release of gas fission products (GFP) from nuclear fuel

Figure 5 shows the GFP release into the fuel pin internal space versus the fuel burn-up after irradiation in the reactors BN-350 and BOR-60. It is evident from the figure that with the increase of burn-up exceeding 3% h a, GFP release increases sharply. The same figure shows for comparison the relationship of GFP release from uranium dioxide irradiated in the BN-350. Evidently, the release levels from both types of nuclear fuel are approximately similar, and reach ~95% of GFPs accumulated in fuel at burn-up levels above 10% h a.

Major components of a gas in fuel pins are krypton, xenon, and helium ($\Sigma \sim 90\%$). A release of GFP from nuclear fuel along with a burn-up level depends on the fuel fabrication technology, on fuel composition, and its oxygen coefficient. At similar other conditions, less GFP is released from nuclear fuel subjected to a chemical co-precipitation. Release of GFP from nuclear fuel with $O/M > 2$ is smaller than that from fuel with $O/M < 2$. Also, more GFP is retained in nuclear fuel of a smaller density, evidently due to the relationship between closed and open porosities. With the increase of linear porosity value, GFP release from nuclear fuel increases by 15-20%.

4.5. Fuel microstructure

According to data of a metallographic analysis, the mixed uranium-plutonium pellet fuel has a specific three-zone structure consisting of an area of columnar grains, equiaxial grains, and a peripheral area of the initial microstructure. The relationship between sizes of these zones is determined mainly by the value of linear power in fuel pin cross-sections studied. The irradiated fuel had numerous fractures, mainly radially oriented. The outer diameter of fuel pellets in the region of the core midplane increased to 0.6-1.2% at maximum burn-up due to fuel swelling. Diameter of the central pellet hole increased by 15-10% (core center). The central hole

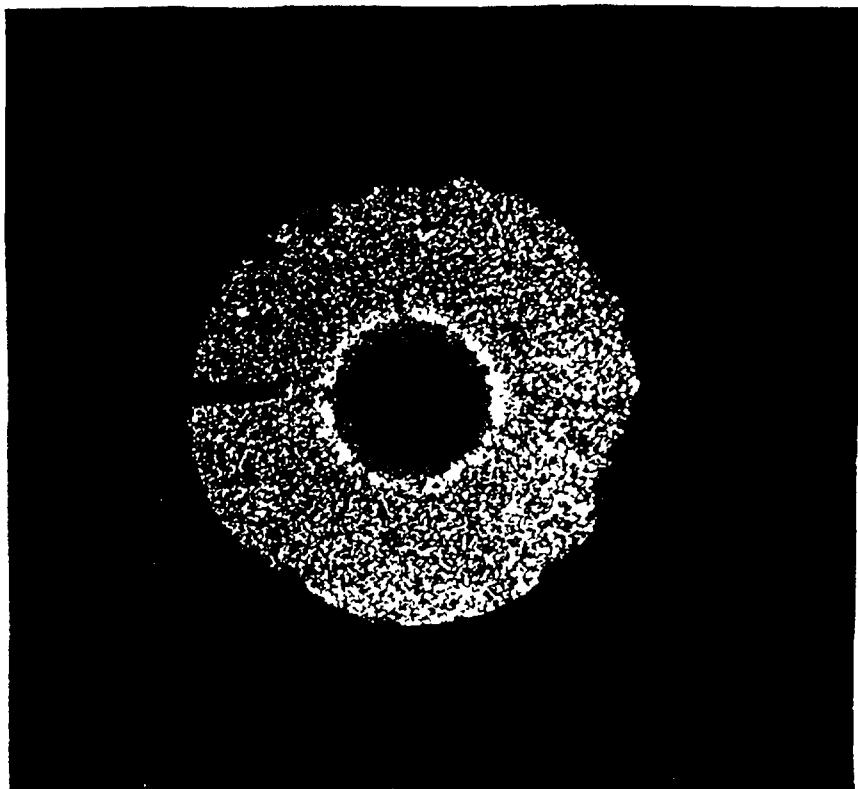


Fig. 6. Alpha radiography of MOX-pellet cross-section after irradiation in BN-350 reactor.

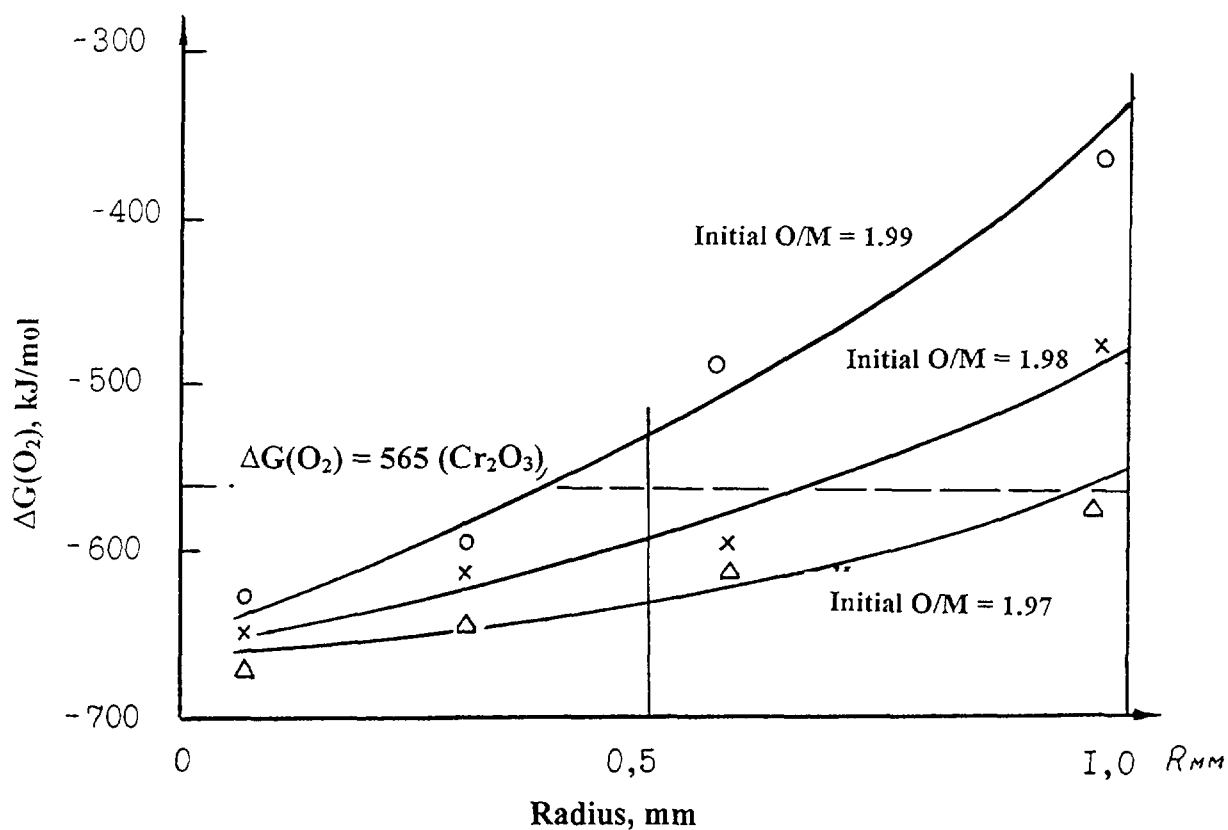


Fig. 7. Radial distribution of O/M in MOX-fuel pellet after irradiation in the BN-350 reactor.

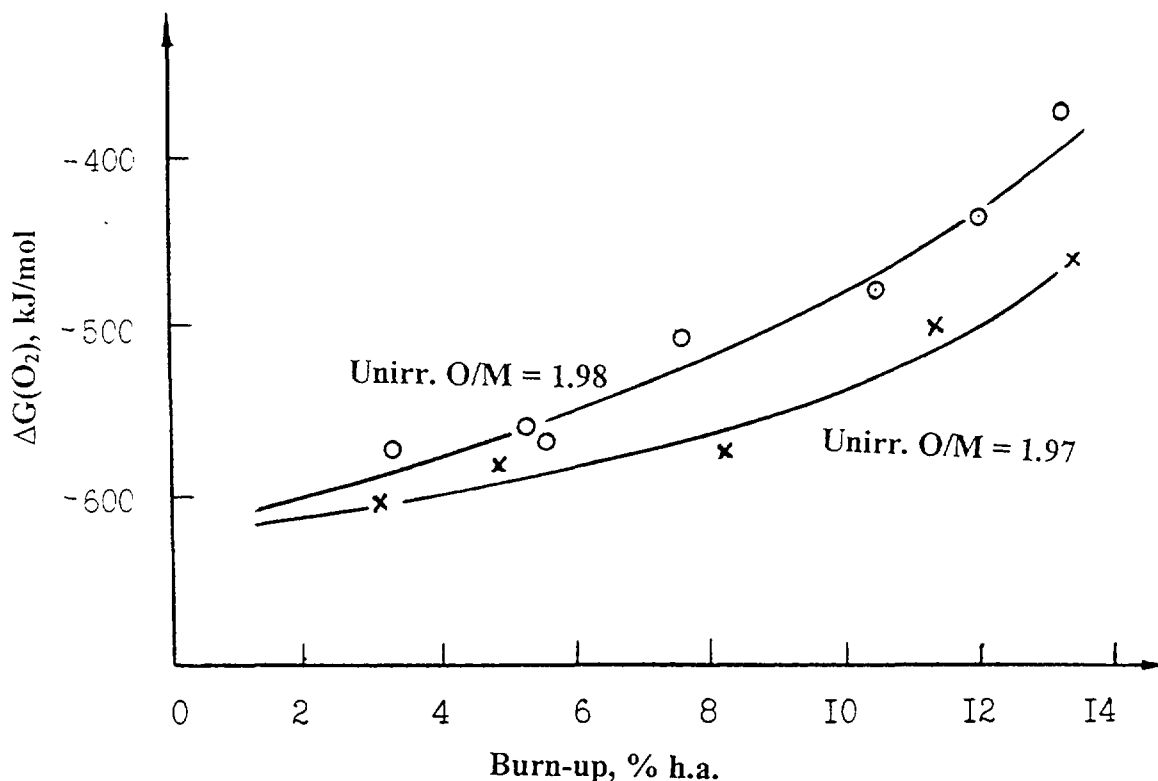


Fig. 8. MOX-fuel O/M as a function of burn-up.

shape in different cross-sections varies from a circle to ellipse, which, evidently, may be due to the temperature non-uniformity. In most cases the gap between fuel and fuel pin cladding is filled with fission products. In the peripheral zone of pellets fabricated from a mechanical mixture of oxides phases of UO_2 and PuO_2 remaining from the primary fuel are observed. In the columnar zone such phases are absent. A fuel fabricated by the sol-gel technology appears to be more homogenous after irradiation. Only phases consisting of fission products are present in the material structure.

4.6. Radial plutonium distribution

An enrichment of Pu in the zone of columnar grains near the central pellet hole (15-20% compared to the initial value, see Fig. 6) is observed in the fuel made from mechanical mixture of U and Pu oxides with O/M ratio of 2.001. In a more homogenous fuel, the enrichment in Pu approaches 2-7%. The extent of Pu re-distribution depends on O/M ratio. The smaller is O/M for the fuel, the less significant is the enrichment in Pu for the central part of pellets. No distribution of Pu is observed along the fuel axis.

4.7 Chemical potential of oxygen in the fuel

The depth of chemical interaction between fuel and fuel pin cladding, as well as the radiation stability of the fuel itself depend on the chemical potential of oxygen as a function of O/M ratio. A radial re-distribution of oxygen takes place during of irradiation of U-Pu oxide fuel as depending on the initial O/M value. The relationships found are shown in Figures 7-8.

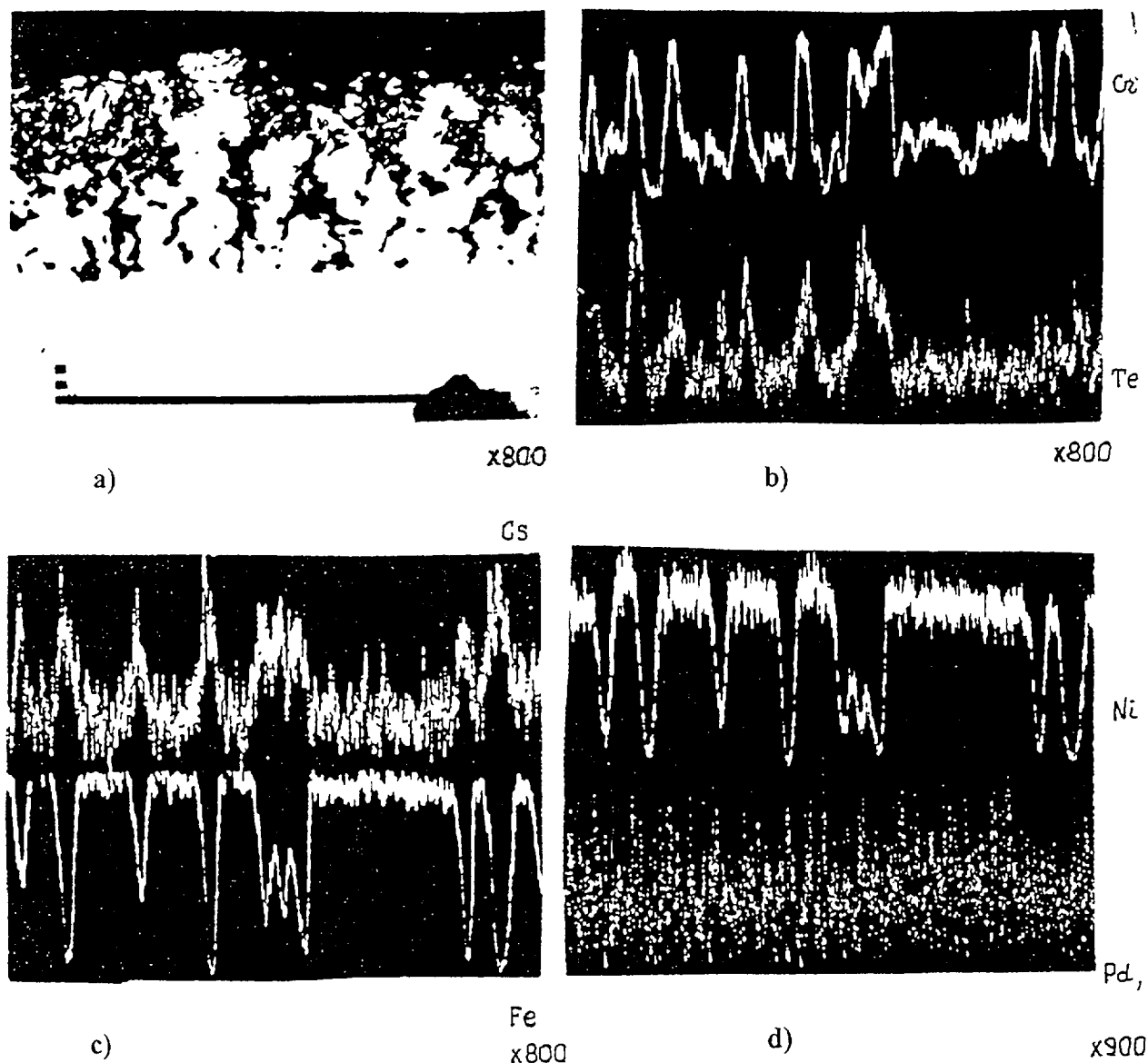


Fig. 9. Back-scattering electron image of corrosion in fuel pin cladding near cross-section +215 mm from core midplane (inner surface) (a), Cr and Te content distributions (b), Cs and Fe content distributions (c), Ni, Pd and I content distributions (d), x 800.

With the increase of both the O/M ratio and burn-up in the fuel, $-\Delta G_{O_2}$ increases in the nuclear fuel, especially in outer parts of fuel pellets with holes. In nuclear fuel with the initial ratio of $O/M > 1.97$ at burn-ups more than 5% h a in the peripheral zones of pellets $-\Delta G_{O_2}$ exceeds $-\Delta G_{O_2}$ for Cr_2O_3 , which corresponds to an enhanced corrosion of fuel pin claddings.

No re-distribution of oxygen along the active part of fuel pin was observed. Radial re-distribution of oxygen in a nuclear fuel occurs mainly in central parts of fuel pins with maximum linear rate.

4.8. Chemical interaction of cladding with fuel and fission products

Table 2 shows data on the corrosion depth in fuel pin claddings made from austenitic steels. For the same type of steel, depth of the chemical interaction with fission products

increases with increasing of burn-up level, temperature, linear power, and initial O/M ratio. In the case when the fuel pin cladding temperature is below 500°C, burn-up is less than 3% h.a., $O/M < 1.97$, the corrosion is insignificant (1-3 μm). A fuel pin damage character is matrix and intergranular, with microcracks formed. Figure 9 shows a typical character of corrosion in fuel pin cladding with mixed uranium-plutonium fuel and also the distribution of some fission products in the corrosion layer. Under similar conditions, oxide uranium-plutonium fuel in the form of pellets with holes is in fact similar to the uranium dioxide in its compatibility with cladding manufactured from the type OX16H15M3BR (20% CW) stainless steel.

4.9. Microstructure and mechanical properties of fuel pin cladding material

Microstructure and mechanical properties of cladding materials in fuel pins with mixed oxide fuel were similar to those in pins with uranium fuel for close irradiation conditions.

5. CONCLUSION

On the whole, results of the complex study carried out lead to a conclusion that fuel pins with oxide uranium-plutonium fuel in pellets with holes after irradiation to maximum burn-up of ~12% h.a. have a satisfactory performance. In many aspects, the behavior of uranium-plutonium fuel under irradiation is similar to uranium dioxide fuel. It is necessary only to upgrade the technology of solid solution fabrication $(\text{U}_n\text{P}_m)\text{O}_x$, making it more homogenous.

INNER WALL ATTACK AND ITS INHIBITION METHOD FOR FBR FUEL PIN CLADDING AT HIGH BURNUP



XA9848045

XU YONGLI, LONG BIN, LI JINGANG, WAN JIAYING
China Institute of Atomic Energy,
Beijing, China

Abstract

The inner wall attack of the modified 316-Ti S S cladding tubes manufactured in China used FBR at 10at % burnup was investigated by means of the out of pile simulation tests. The inner surface morphologies of the cladding tubes attacked by fission products Cs,Te,I and Se at 700°C under lower and high oxygen potentials were observed respectively, and the depth of attack was also measured. The burst strength, maximum circum expansion and the appearances of fracture were measured and observed respectively for the cladding tubes attacked by fission products. Based on the mechanism of FBR fuel cladding chemical interaction (FCCI), Cr,Zr and Nb were used as the oxygen absorbers respectively, in order to inhibit the inner wall attack of the cladding tubes. The corrosion morphologies and depth, the penetration depth of the fission products in the inner surface of the cladding tubes were detected. The inhibition effectiveness of the oxygen absorbers for the inner wall attack of the cladding tubes was evaluated.

1.INTRODUCTION

A number of the in pile irradiation tests of the oxide fuel pins have indicated that the attack depth of the cladding inner wall caused by fuel cladding chemical interaction (FCCI) at high burnup will exceed greatly the corrosion margin for fuel pin cladding design, the maximum attack depth is nearly 150 μ m, and there are three kinds of essential attack morphologies on the inner surface of cladding^[1-5]. As all know, both decreasing in the thickness and local intergranular attack will degrade the mechanical properties and limit the life time of the cladding tube. Therefore, the inner wall attack and its inhibition method should be given more attention for the FBR fuel pin design used at high burnup.

The purpose of this paper is to describe primarily the inner wall attack characteristics caused by fission products for the modified 316-Ti S.S. cladding tubes manufactured in China, in order to provide the information for in pile irradiation tests of the domestic cladding in the near future and to investigate the possibility of the inhibition of inner wall attack for the fuel pin cladding tubes used at high burnup.

2.EXPERIMENTAL

Three kinds of 316-Ti S.S. tubes $\Phi 6 \times 0.4$ mm manufactured in China were used as the specimens in this investigation.

Their composition are listed in table 1. The Cr/Cr₂O₃ and Ni/NiO were used as oxygen buffer respectively, to establish the different oxygen potential.

Cs,I,Te and Se mixture was used as the simulation fission products, and their quantities correspond to those generated when the burnup reaches 10at.%^[1].

The buffer and Te, I, Se mixture were loaded into the cladding tubes through a Kovar tube, and degased under vacuum. For the specimens used to investigate the inhibition effectiveness of the

TABLE 1 CHEMICAL COMPOSITION OF 316-TI S.S. TUBES (wt.%)

Specimens	Elements											C W (%)
	C	Cr	Ni	Mo	Mn	Si	Ti	P	S	B	Fe	
I	0.07	14.97	15.23	1.20	0.73	0.68	0.45	—	—	0.06	balance	15
II	0.04	16.8	12.5	3.17	1.67	0.73	0.63	0.016	0.0078	—	balance	30
III	0.066	17.08	12.75	2.25	1.37	0.67	0.68	0.028	0.016	—	balance	15

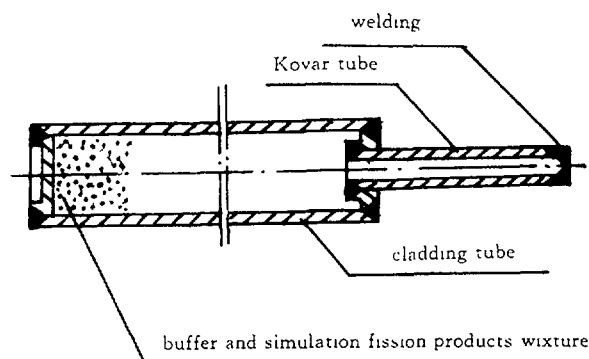


FIG.1 Profile of the prepared cladding tube specimen

inner wall attack, Cr, Zr and Nb powder were loaded respectively into the cladding tubes together with the Ni/NiO buffer and the fission products. Their quantity corresponds to the oxygen absorber coating $25\text{ }\mu\text{m}$ thick on the surface of the fuel pellet ($\Phi 5.1 \times \text{high } 100\text{mm}$). Then Cs was injected quantitatively into the cladding tubes by a microinjector in a glove box with high purity inert gas ($\text{H}_2\text{O} < 10\text{ppm}$, $\text{O}_2 < 5\text{ppm}$), the tubes were welded first and afterwards by a cold welding pliers and argon arc for sealing. The prepared specimens (Fig.1) were installed into a capsule with Ar and annealed in a furnace at 700°C for 120h. The specimens attacked by fission products at lower and high oxygen potentials were connected respectively with a burst machine to measure their burst strength and maximum circum expansion.

3.RESULTS AND DISCUSSION

3.1 Attack characteristics

3.1.1 The attack under lower oxygen potential

The equilibrium oxygen potential established by $\text{Cr/Cr}_2\text{O}_3$ at 700°C is near the level of the oxydation threshold of Cr in stainless steel. Most of the inner surface of 316-Ti cladding tubes have not been attacked by the fission products under this oxygen potential. The shallow intergranular attack (IGA) is observed only at local surface of the specimens (Fig.2). Their maximum IGA depth is less than $28\text{ }\mu\text{m}$. EDAX demonstrates that there are no Cs and Te penetration on the inner surface of the cladding tubes.

Thermodynamics investigations of fission products[1,6,7] indicate that the reactive fission products Cs, I, Te and Se react with each other to some extent and form the stable Cs_2Te , Cs_2Se and CsI at lower oxygen potential. The formation of these cesium compounds makes the attack of single fission products to stainless steel reduce. A little or no reaction occurs between Cr_2O_3 and Cs under this oxygen potential[7].

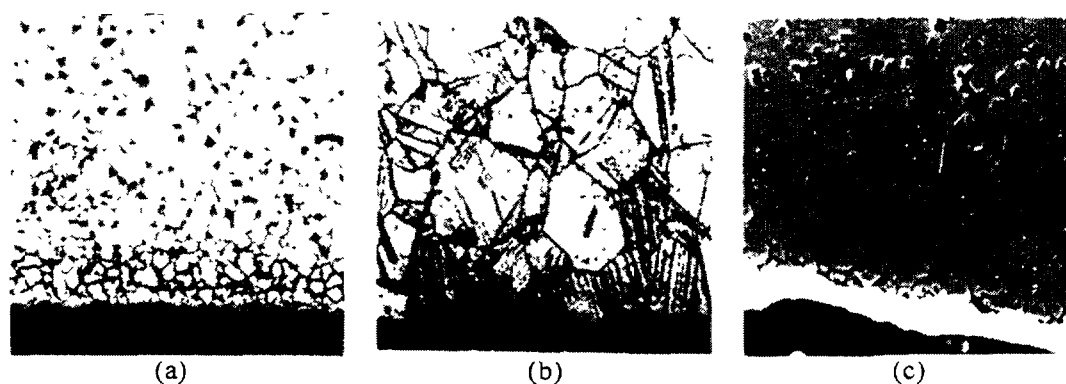


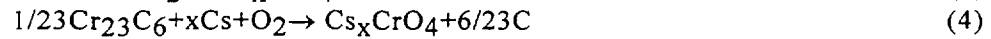
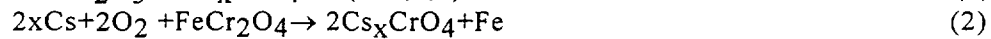
FIG.2 Shallow intergranular attack under lower oxygen potential with $\text{Cr/Cr}_2\text{O}_3$
 (a)cladding tube I (b)cladding tube II (c)cladding tube III

3.1.2 The attack under high oxygen potential

The matrix erosive attack and IGA occur simultaneously under high oxygen potential established by Ni/NiO buffer. The cladding inner surface appears to be dissolved by fission products, and the grains of matrix are stripped due to IGA and oxidative attack. The attacked zone on local inner surface appears to be "Ulcer" (Fig.3). In this case, the maximum attack depth is about 100 μ m.

Face-scanning indicates that the erosion zone consists of rich Cr/depleted Ni and rich Ni/depleted Cr layers alternatively (Fig.4). EDAX demonstrates that rich Cr is always accompanied by Te and Cs. It can be seen from Fig.5 that the attack depth is approximately proportional to depletion of Cr, Ni and the penetration depth of Cs and Te in the inner surface of the cladding.

Under high oxygen potential, CsI and the cesium chalcogenides are no longer stable thermodynamically, but cesium chromate become stable[1,6-8]. Therefore, the "Ulcer" erosion may result from the reactions of Cs and Te with cladding. The reactions can be expressed respectively as following[6,7,9]:



Due to the reaction of Cs with cladding, the partial potential of Cs is reduced and Te activity is increased, the reaction of Te with cladding occurs as[8,10]: $2\text{Cr} + 3\text{Te} \rightarrow \text{Cr}_2\text{Te}_3$ (6)

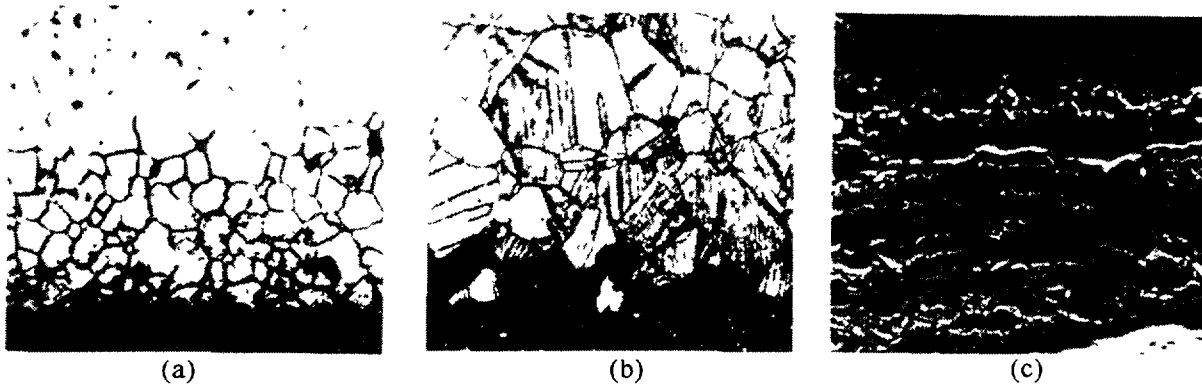


FIG.3 Erosive attack under high oxygen potential with Ni/NiO
(a)cladding tube I (b)cladding tube II (c)cladding tube III

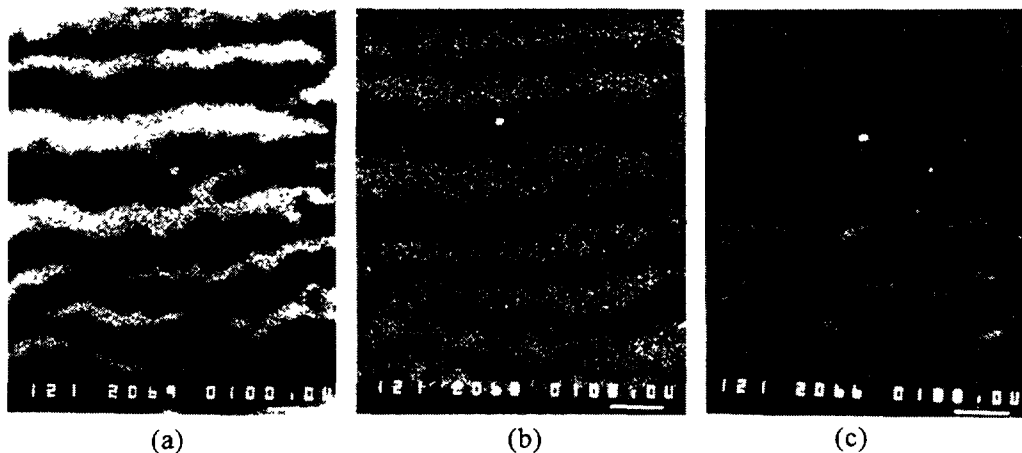


FIG.4 Distribution of Fe,Ni and Cr in attacked zone
(a)Fe (b)Cr (c)Ni

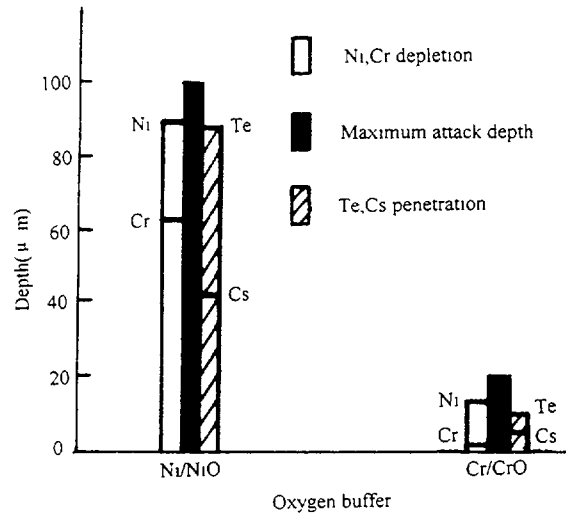
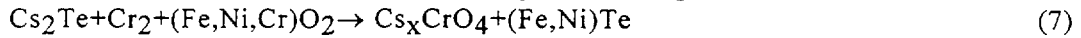


FIG.5 Maximum attack, Te,Cs penetration and Ni,Cr depletion depth

On the other hand, Te and Se penetrate along the grain boundary of cladding, and induce the embrittlement of the grain boundary. When oxygen potential is high enough, cesium chalcogenides react also with the composition elements of cladding as following[8]:



In this case, the stripping of matrix grain becomes severe.

3.2 Burst strength and circum expansion

Fuel pin cladding suffers the stress due to the internal pressure increasing and the mechanical interaction between cladding and pellets at high burnup. On the other hand, the cladding is also weakened by internal fission products attack. Therefore, it is necessary to understand the mechanical properties change of the cladding after fission products attack. Many tests about this topic have been performed in other countries[11-17]. In this paper, the burst strength and maximum circum expansion of the cladding tubes I and II were measured, the results are shown in table 2 、 Fig.6 and Fig.7.

It can be seen from table 2 that the strength of cladding tube II is degraded and his circum expansion is improved at lower oxygen potential as compared with those of cold work tubes. It may result mainly from annealing effect. Comparing with those of annealing tubes, the burst strength of attacked cladding tubes seems to be no many change, and their circum expansion are slightly low. For cladding tube I attacked under lower oxygen potential, the strength and circum expansion are degraded slightly. The burst strength and circum expansion have not been obtained for the cladding tubes attacked under high oxygen potential, because they breacked down before the measurements were completed.

The appearances of fracture for the cladding tubes I and II attacked under lower and high oxygen potentials are shown in Fig.6. It can be seen that the appearance of fracture is intergranular brittle for the attacked cladding tubes under high oxygen potential, while the tenacious is for those of the annealing and lower oxygen potential.

The axial sections of the bursted cladding tubes are shown in Fig.7. The bursted cladding tubes are shown in Fig.8.

The inner surface is nearly no change for the cladding tubes attacked under lower oxygen potential, the stripping of matrix grain caused by IGA is for those attacked under high oxygen potential. It is clear that the grain boundaries embrittlement is resulted from the fission products attack under high oxygen potential. The Cs and Te penetration in the broken grain boundaries which is shown in Fig.5 is another evidence for this. This phenomenon may be the liquid metal embrittlement which has been described in many papers[10,13,14,18,19].

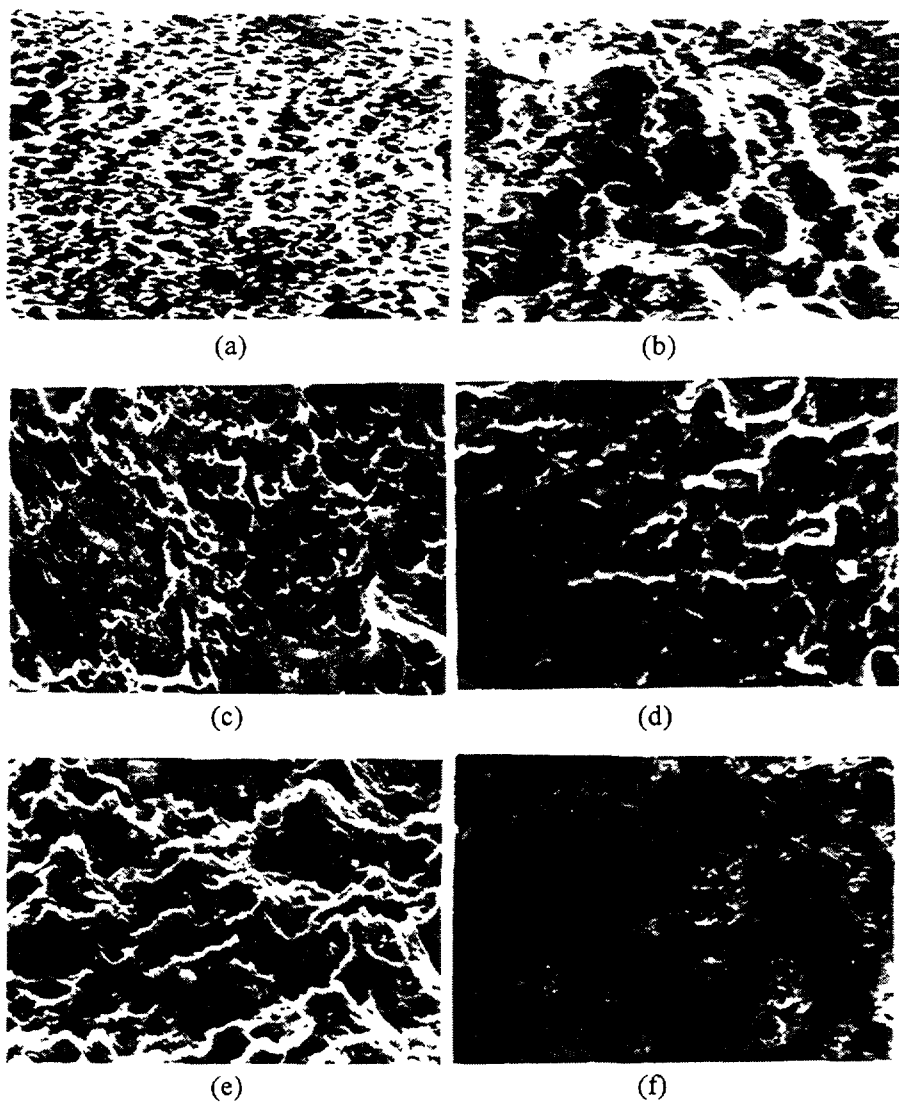


FIG.6 Appearances of fracture for the cladding tube
 (a)original cladding tube I
 (b)attacked cladding tube I under lower oxygen potential
 (c)original cladding tube II
 (d)annealed cladding tube II
 (e)attacked cladding tube II under lower oxygen potential
 (f)attacked cladding tube II under high oxygen potential

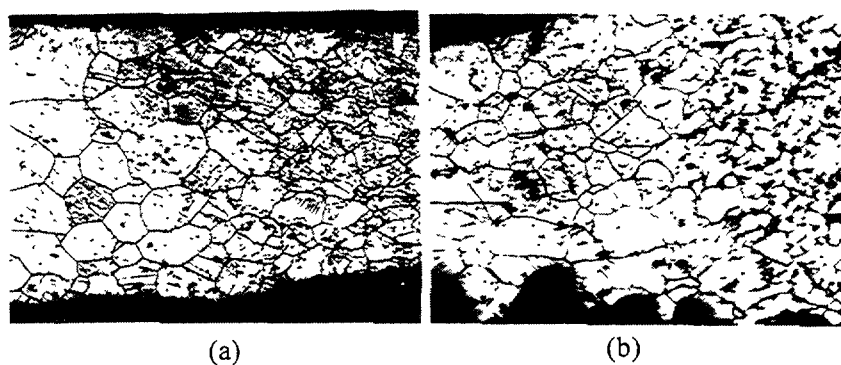


FIG.7 Axial section of the bursted cladding tube II
 (a)attacked under lower oxygen potential
 (b)attacked under high oxygen potential

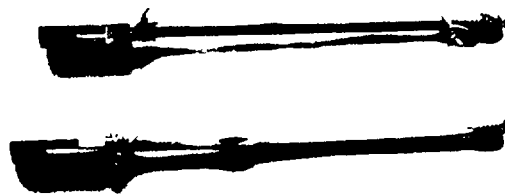


FIG.8 Burstcd cladding tubes

TABLE 2 BURST STRENGTH AND CIRCULAR EXPANSION OF 316-TI CLADDING TUBES(1)

Specimens class		Burst strength(MPa)		Circular expansion(%)	
		single	average	single	average
cladding tube I	15%c.w.	685.1		24.67	
		684.8	684.9	29.87	28.14
		684.7		29.89	
	attacked under tested conditions with Cr/Cr ₂ O ₃	—		—	
		673.9	65.17	24.15	25.64
		629.4		27.12	
	attacked under tested conditions with Ni/NiO	breack down before the burst test completion			
		975.0		6.42	
	30%c.w.	975.0	975.0	6.16	6.33
		975.0		6.42	
cladding tube II	above conditions +700℃ annealing 120h	637.0		—	
		715.0	684.7	14.12	16.78
		702.0		19.43	
	attacked nder tested conditions with Cr/Cr ₂ O ₃	669.5		12.26	
		682.5	697.7	16.77	14.52
		741.0		—	
	attacked under tested conditions with Ni/NiO	breack down before the burst test completion			

(1)At room temperature

3.3 Inhibition effectiveness of the oxygen absorbers in the inner wall attack of the cladding tubes

It is well known that the oxygen activity in the gap between cladding and fuel pellet is a very important factor for inner wall attack of the cladding tube at high burnup. With increasing of oxygen potential, the attack on cladding tube inner wall becomes severe. There are two ways to reduce the oxygen activity[20], one is to reduce the initial O/M ratio of the fuel, another is adding of the oxygen absorber in the pin. Lower O/M ratio may lead to decreasing of the thermoconductivity of fuel pellets and increasing the melting probability of the pellets, so adding of the oxygen absorber should be an effective method.

Based on the mechanism of FCCI, Cr, Zr and Nb were selected as the inhibitor respectively in this investigation. The attack morphologies and depth, the penetration depth of the fission products in the inner surface of the cladding tubes were detected.

3.3.1 Attack morphologies and depth

The attack morphologies of the cladding tubes containing Cr, Zr and Nb are respectively shown in Fig.9(a)–(c). There is severe erosion on the inner surface of the cladding tubes without

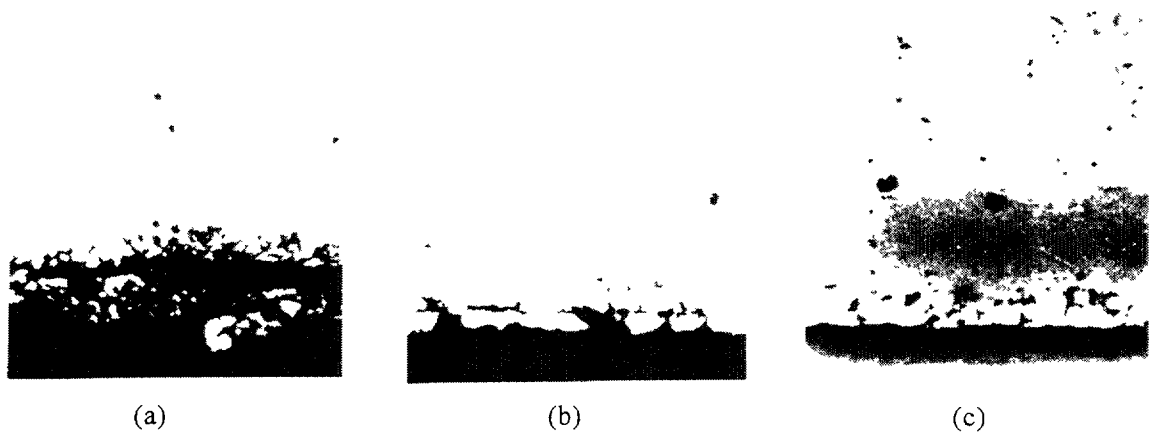


FIG.9 Inner wall morphologies of the cladding tube II attacked under high oxygen potential
(a)with inhibitor Cr (b)with inhibitor Zr (c)with inhibitor Nb

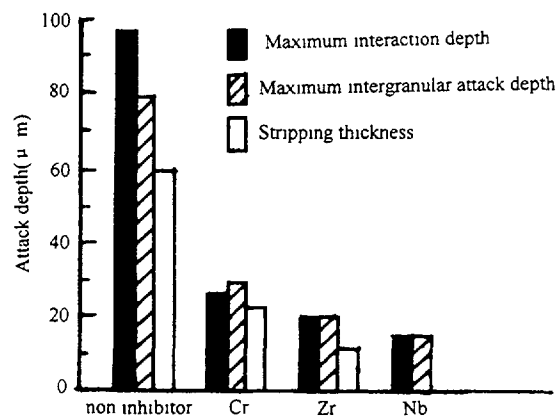


FIG.10 Inner wall attack depth of cladding tube II with and without inhibitor

inhibitor (see Fig.3 (b)). For the cladding tubes with Cr inhibitor, there is also IGA and erosion (Fig.9 (a)), but the depth is more less than that without inhibitor. For the cladding tubes containing inhibitor Zr, a little erosion was observed, the attack depth is less than that with inhibitor Cr (Fig.9 (b)). Neither erosion nor grain stripping (Fig.9 (c)) was observed, but a little IGA was only observed for the cladding tubes with inhibitor Nb. The inner wall attack depth of the cladding tubes with and without inhibitor is shown in Fig.10.

3.3.2 Fission products penetration

The tellurium penetration along the grain boundary of the cladding inner wall was detected by EPMA and EDAX, and the results are shown in Fig.11 and Fig.12. It is clear that the Te penetration depth and its content reduce orderly with adding of Cr, Zr, Nb inhibitor respectively (Fig.11). EDAX diagram (Fig.12) shows that the peaks of Cr and Te are reduced orderly with adding of Cr, Zr, Nb respectively, and almost no tellurium was detected in the attack area of the cladding inner surface containing inhibitor Nb. A little cesium was detected by EDAX in the grain boundaries of the attacked area for the cladding tubes which containing Cr, Zr and Nb respectively. On the other hand, in the presence of inhibitor Cr, the Cr content in attacked area increases obviously, and in the presence of the inhibitor of Zr and Nb, Zr and Nb were found by EPMA separately in attacked grain boundaries (table 3). It can be inferred from table 3 and table 4[21,22] that the oxygen reacts with inhibitor in the cladding tubes at first, to form the Cr_2O_3 , ZrO_2 and Nb_2O_5 respectively, at the meantime, Cs_xCrO_4 and some Cs-Zr-O and Cs-Nb-O compounds may formed in the attacked grain boundaries, then the surplus oxygen participats the attack of fission products to cladding tubes.

Mereover, with oxygen absorber is loaded into cladding tubes, oxygen activity is decreased. and the stability of cesium compounds (such as Cs_2Te) increased. In this case, the activity of tellurium is dropped, and the attack of Te to the grain boundaries of cladding is decreased.

TABLE 3 THE CONTENTS OF Cr,Zr AND Nb IN ATTACK GRAIN BOUNDARIES

Oxygen absorber	Content(%)		
	Cr	Zr	Nb
Cr	23.2111	0.0000	—
Zr	19.5908	0.6623	—
Nb	18.2353	0.0000	0.1695

TABLE 4 THE STANDARD FREE ENTHALPY FOR FORMATION OF Cr_2O_3 , Zr_2O_3 and Nb_2O_5

Oxide	$\Delta G_{298\text{K}}(\text{kJ} \cdot \text{mol}^{-1})$	$\Delta G_{973\text{K}}(\text{kJ} \cdot \text{mol}^{-1})$
$\text{Cr}_2\text{O}_3^{(1)}$	-695.18	-578.26
$\text{ZrO}_2^{(2)}$	-1016.12	-891.87
$\text{Nb}_2\text{O}_5^{(3)}$	-1751.95	-1475.33
Cs_2O		-310 ^④

① $\Delta G_T^O = -746800 + 173.2 \cdot T(\text{J} \cdot \text{mol}^{-1})$ [21]

② $\Delta G_T^O = -1071000 + 184.1 \cdot T(\text{J} \cdot \text{mol}^{-1})$ [21]

③ $\Delta G_T^O = -446200 + 97.56 \cdot T(\text{cal} \cdot \text{mol}^{-1})$ [22]

④ at 1000K[9]

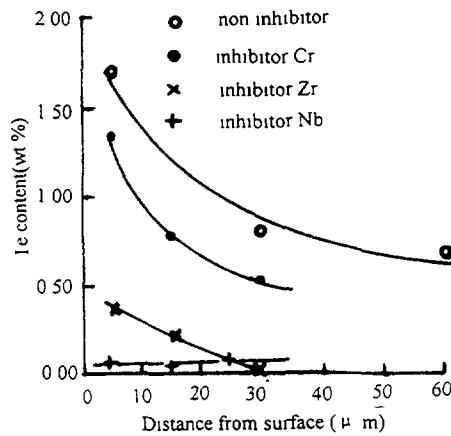


FIG.11 Te penetration in attacked grain boundaries of cladding II

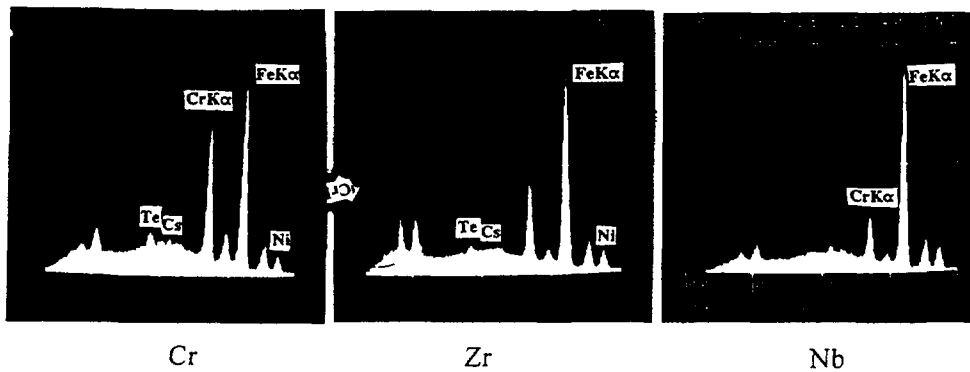


FIG.12 EDAX diagram in attacked area of cladding tube II

4.CONCLUSION

(1) For the 316-Ti S.S. cladding tubes attacked by fission products Cs, Te, I and Se at 10at.% burnup and 700°C, the shallow intergranular attack or a negligible corrosion under lower oxygen potential with Cr/Cr₂O₃ buffer and the serious erosive attack under high oxygen potential with Ni/NiO buffer were observed. The attack depth for the former is less than 28 μm, but about 100 μm is for the later.

(2) The degradations of strength and toughness for attacked tubes under high oxygen potential are considerably larger than that under lower oxygen potential. The appearance of fracture is intergranular brittle for the attacked cladding tubes under high oxygen potential, while the tenacious under lower oxygen potential.

(3) The oxygen absorbers inhibit significantly the inner wall attack of 316-Ti S.S. cladding tubes with the order of the inhibition effectiveness Nb>Zr>Cr. The niobium may become an effective inhibitor for the erosive and intergranular attack of fission products to FBR fuel pin cladding at high burnup.

REFERENCES

- [1] O.Götzman, P.Hofman and F.thummler
J.Nucl.Mater.52(1974)33
- [2] L.A.Lawrence and J.W.Jost
Trans. Am. Nucl. Soc. 36(1981)211
- [3] L.A.Lawrence
Trans. Am. Nucl. Soc. 32,(1979)249
- [4] M.G.Adamson, E.A.Aitken, S.K.Evans, W.Mccarthy
US GEAP-14075 (Dec.1976)
- [5] M.G.Adamson
Technical Committee Meeting On Fule And Cladding Interaction
IWGFR-16, Tokyo, Japan. 1977. p180
- [6] M.G.Adamson
Technical Committee Meeting On Fule And Cladding Interaction
IWGFR-16, Tokyo, Japan. 1977. p108
- [7] M.G.Bradury, S.Pickering, W.H.Whitiow
Technical Committee Meeting On Fule And Cladding Interaction
IWGFR-16, Tokyo, Japan. 1977. p51
- [8] O.Götzmann
Report of Int. Conf. On Fast Reactor core And Fuel Structural Behaviour
(BNES, London, 1990)
- [9] C.T.Walker, S.Pickering
Nucl. Technol. 42-43(1979)207
- [10] M.G.Adamson, E.A.Aitken
J.Nucl.Mater. 132(1985)160
- [11] O.Götzmann
Technical Committee Meeting On Fule And Cladding Interaction
IWGFR-16, Tokyo, Japan. 1977. p37
- [12] L.Schafer, P.Hofmann
J.Nucl.Mater. 115(1983)169
- [13] O.Götzmann, O.Hofmann
J.Nucl.Mater. 59—60(1976)194
- [14] M.Koizumi, H.Furuya, S.Nagai, H.Kawamata
Technical Committee Meeting On Fule And Cladding Interaction
IWGFR-16, Tokyo, Japan. 1977. p73
- [15] D.R.Duncan, N.F.Panayotou, E.L.Wood
Trans. Am. Nucl. Soc. 38(1981)265.

- [16] C.W.Hunten,G.D.Johnson
Int. Conf.On Fast Breeder Reactor Fuel Performance ANS.Monterey, California,
1979. p478
- [17] S.Vaidyanathan,M.G.Admson
Trans.Am.Nucl.Soc.38(1981)262
- [18] M.G.Adamson
Metal Trans.17A(1986)2090
- [19] J.A.Hemsworth,M.G.Nicholas, R.M.Crispin
J.Mater.Sci.25(1990)5248
- [20] E.T.Weber,L.A.Lawrenc and C.N.Wilson(HEDL),M.G.Adamson(GE)
Proc.Int.Conf. Fast Breeder Reactor,Monterey California,1979.p445
- [21] Cheng Lanzheng,Zhang Yanhao
《Physics and Chemistry》 by Shanghai Science Technology Press,Appendix III,1988
- [22] Yei Tianlun
《Metallurgy Thermodynamical》 Zhongnan Engineering College press,Appendix9, 1987



MATERIAL PROPERTIES OF A HIGH-DOSE IRRADIATED MARTENSITIC WRAPPER: STEEL 1.4914

E. MATERNA-MORRIS, K. EHRLICH

Forschungszentrum Karlsruhe,
Institut für Materialforschung,
Karlsruhe, Germany

Abstract

The post-irradiation examinations of a wrapper made of martensitic X18CrMoVNb12.1 steel were performed after a two years operation in the French fast breeder reactor PHENIX. A maximum dose of 105 dpa_{NRT} was accumulated. Particular attention was paid to the welds connecting the martensitic wrapper material with the austenitic (AISI 316) top and bottom sleeves. Another area of importance was that of the highest dose in the center of the wrapper. The irradiation temperature varied from 380 °C entry temperature of the sodium at the foot of the wrapper up to the top of the wrapper with about 630 °C.

The unirradiated reference material showed a typical increase in ductility with higher temperature. During welding, the material lost plasticity. The structure of the material was investigated and the irradiation induced microstructure exhibited characteristic features dependent on irradiation temperature and doses. In the lower part of the wrapper the formation of fine coherent α' -precipitates with a high concentration was detected. The material received an increase in strength. In the centre of the wrapper voids and bubbles could be observed, but they did hardly influence the mechanical behaviour. The measured swelling attained a value of max. 0.05%. Towards higher temperatures the voids disappeared and the density of bubbles increased. The effects of sodium corrosion showed a minimum influence to the tensile strength in the lower welded seam.

1 INTRODUCTION

Within the EFR (European Fast Breeder Reactor) project in collaboration with the Centre d'Etudes Nucleaires de Cadarache and members of the German-Belgian AGT 1 working group, a program of irradiation and post-irradiation examinations was performed. A martensitic wrapper was inserted into the French PHENIX reactor. The examinations were aimed to check the wrapper for impacts of irradiation on the service life and integrity. Complex mechanical tests and structural analyses were carried out in order to determine the material behaviour following two years of irradiation at the PHENIX reactor. During 719 EFPD (Equivalent Full Power Days) a maximum dose of 105 dpa_{NRT} (Displacements per atom) was accumulated in the centre of the wrapper. The irradiation temperature varied from 380 °C entry temperature of the sodium at the foot of the wrapper up to the top of the wrapper with about 630 °C [1]. The investigations of the wrapper showed the material behaviour after non-destructive tests, including tensile, creep and Charpy-V-notched impact tests and the microstructure, corrosion and fracture behaviour. All these tests were performed with base material as well as with welds, at room temperature and at the different reactor temperatures.

2 EXPERIMENTAL PROCEDURE

2.1. Wrapper Material

The wrapper material was a delta-ferrite free melt based on the 1.4914 steel specification, see table 1. The carbon content was low and the nitrogen was strongly reduced to achieve a low transition temperature to brittle fracture (DBTT) [2-4]. A wrapper tube, a hexagonal pipe of 2.50 m length having an inner gap width of 116.9 and a wall thickness of 3.4 mm was manufactured. The wrapper was produced by means of hot extrusion, cold pilger rolling, cold

TABLE 1 CHEMICAL COMPOSITION OF THE ALLOYS [wt %]

Elements	1 4914, Wrapper Material	AISI 316	INCONEL 82	SNR- Specification
C	0 17	0 040	0 046	0 16-0 18
Si	0 31	0 32	0 21	0 25-0 35
Mn	0 64	1 30	3 03	0 60-0 80
P	0 005	0 024	0 003	max 0 008
S	0 005	0 009	0 008	max 0 008
Cr	10 45	16 30	19 13	10 2-10 7
Ni	0 87	12 17	70 92	0 75-0 95
Mo	0 56	2 64		0 45-0 65
V	0 25			0 20-0 30
Nb	0 20			0 10-0 25
Al	0 046	<0 01		0 03-0 10
N ₂ ppm	30	420		max 100
Cu	0 010	0 32	0 01	max 100
B ppm	20	10		max 15
Fe	balance	balance	balance	balance

drawing with intermediate annealing and a final heat treatment of 0 5 h at 1075°C and 2 h at 700°C. The wrapper sleeves were made of AISI 316 and connect the massive parts on the top and bottom of the wrapper. Both sleeves are welded to the wrapper by TIG (Tungsten-inert gas) welding. INCONEL 82 wire was applied as filler material. After the welding of the sleeves, the welded joint was subjected to stress free annealing of 30 min at 700°C. A survey of the chemical composition of the alloys used is given in Table 1.

2.2. Reactor Irradiation

The 1 4914 wrapper was inserted into the PHENIX reactor core in France. The irradiation period corresponds to a total of 719 full power days of operation under irradiation and temperature. Over this period, a dose of about 105 dpa_{NRT} was attained. During the irradiation, the wrapper was exposed to a temperature gradient between the sodium coolant inlet temperature into the wrapper of about 380°C and the outlet temperature of about 630°C at the top of the wrapper [5].

2.3. Sample Preparation, Methods of Inspection and Mechanical Tests

From the hexagonal wrapper six segments were removed according to the sectioning plan for the post-irradiation examinations, Figure 1. They were taken from the most important areas of the wrapper and contained the welds and interesting fluence and temperature positions of the base material.

The segments were investigated by means of non-destructive methods to detect surface cracks by colour penetration tests or cavities in the welds by radioscopy. Tensile, creep and Charpy-V-notched impact samples were prepared and tested. The samples were cut parallel to the rolling direction of the wrapper and the thickness was reduced to 2 5 mm depending on the convex buckling of the welding seam. The tests were performed on a static mechanical tensile testing machine with a strain rate of 1% min⁻¹. Some tensile tests were repeated with the original wall thickness of the wrapper. The tensile samples taken from the foot or the top of the wrapper had the welded joint in the centre of the gauge length.

The notches of the welded impact specimens were cut in the HAZ (Heat affected zone) of the martensitic steel. All impact samples were designed as a quarter ISO-V-sample and

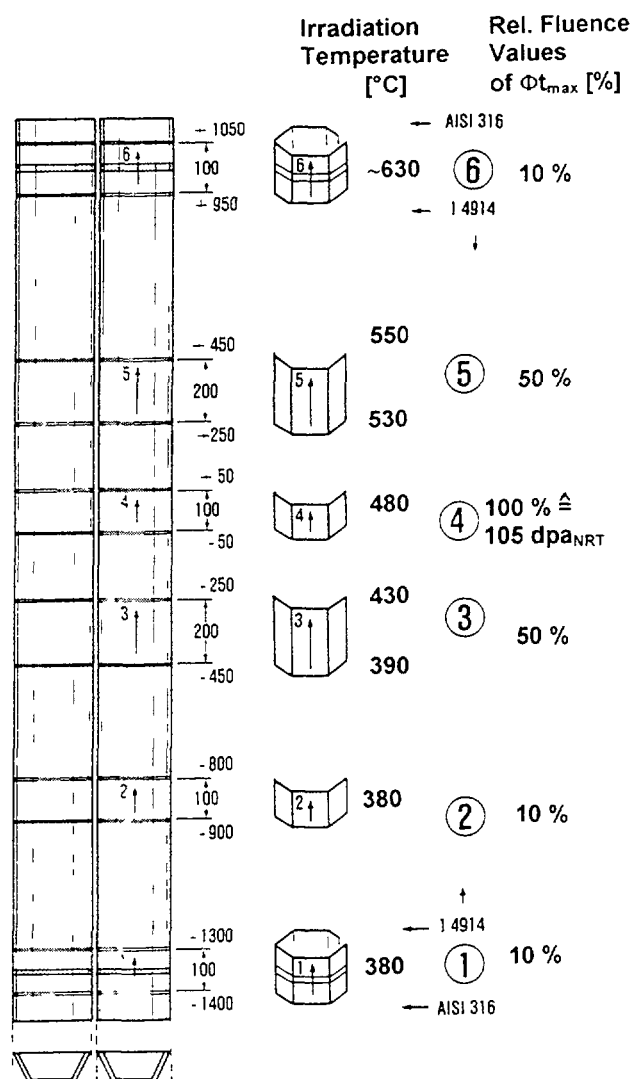


FIG 1 Sectioning plan of the wrapper

tested with a 15 J pendulum impact hammer. The impact tests were conducted in the instrumented mode, i.e. a force versus bending curve of the respective specimen was recorded with each test.

Creep tests were also carried out with the flat specimens which had been fitted to inductive displacement transducer pairs to detect creep development. Creep development was recorded continuously by a tension-time-recorder. Three thermocouples distributed over the length of the specimens measured the test temperature and controlled the 3-zone furnace. The test stress was applied by means of a lever system employing weight plates.

All these examinations were performed with the unirradiated and irradiated as well as with welded unirradiated and irradiated welded wrapper material at RT (Room temperature) and at different reactor temperatures.

2.4. Investigations of Fractures, Corrosion and Microstructure

The fracture behaviour of the wrapper material was investigated by analysing the fracture surfaces and the microstructure of the material. The wrapper surfaces were checked on material excavation or sodium corrosion. The structures and surfaces were investigated by light-, scanning- and transmission electron microscopy methods. EDX (Energy dispersive x-rays analysis) or WDX (Wave length dispersive analysis) were used to analyse the chemical composition of the material and particles. The irradiation induced swelling of the material was

determined by means of immersion density measurement. A further method was to count the voids in the material by transmission electron microscopy.

3. EXPERIMENTAL RESULTS

3.1. Non-destructive Investigations

Compared to the unirradiated wrapper, no macroscopic changes in dimension could be found, a deformation of the component was not observed. The wall thickness was found to be within the tolerance range of 3.4 ± 0.35 mm. The inner and the outer surfaces were investigated in particular for sodium corrosion. Schlieren arrangements were encountered on the inner surfaces, especially in segment 5. This is a sign of desoxidation of the metal surface by sodium

3.2. Impact Tests

The impact tests were carried out in a test temperature range between -180°C and $+450^{\circ}\text{C}$. The impact energy was measured and plotted in impact energy curves to determine the DBTT and the USE (Upper shelf energy), as represented in figure 2 and Table 2.

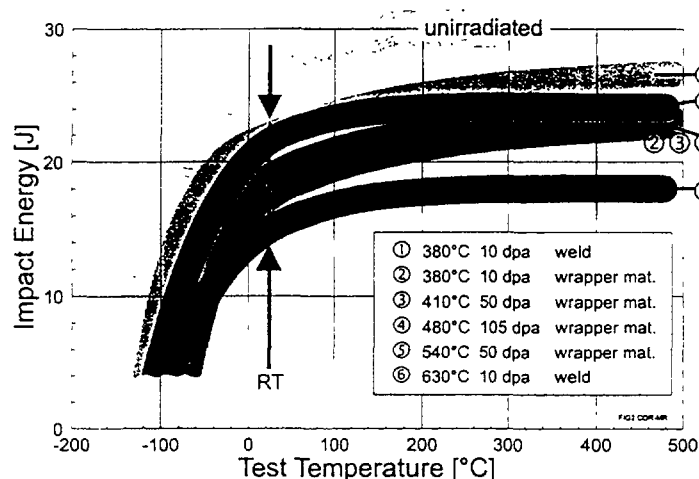


FIG. 2. Impact energy curves as a function of test temperature.

TABLE 2. IMPACT DATA OF THE WRAPPER MATERIAL

Wrapper Material Conditions	Aging [°C]	Dose [dpa]	Irradiation Temperature [°C]	DBTT [°C]	USE at 300 °C [J]	Energy at RT [J]
Steel 1.4914	-	-	-	100 ± 20	30 ± 2.5	26
Steel 1.4914	400°C/719 d	-	-	-80	27	33
Steel 1.4914	500°C/719 d	-	-	-80	32	31
Steel 1.4914	600°C/719 d	-	-	-80	28	28
Weld	-	-	-	-80 ± 20	35 ± 2	32
Weld	-	10	380	-65 ± 15	24	22
Steel 1.4914	-	10	380	-60 ± 5	23	19
Steel 1.4914	-	50	410	-35 ± 10	23	19
Steel 1.4914	-	105	480	-40 ± 10	22	19
Steel 1.4914	-	50	540	-80 ± 5	26	22
Weld	-	10	630	-55 ± 20	18	16

For the irradiated material a decrease of upper shelf was generally observed and the reduction of upper shelf energy is temperature and fluence dependent. The welded samples from the top of the wrapper had a reduction of approximately 50%. It is the weakest part of the wrapper. The DBTT was hardly influenced. The highest DBTT was found at -35°C [6].

3.3. Tensile Tests

In figures 3-5 the yield and ultimate tensile strength data of the reference heat are plotted and show a nearly linear decrease with increasing test temperature. For wrapper samples irradiated between $380 - 430^{\circ}\text{C}$ and tested at 400°C a moderate increase in both properties is

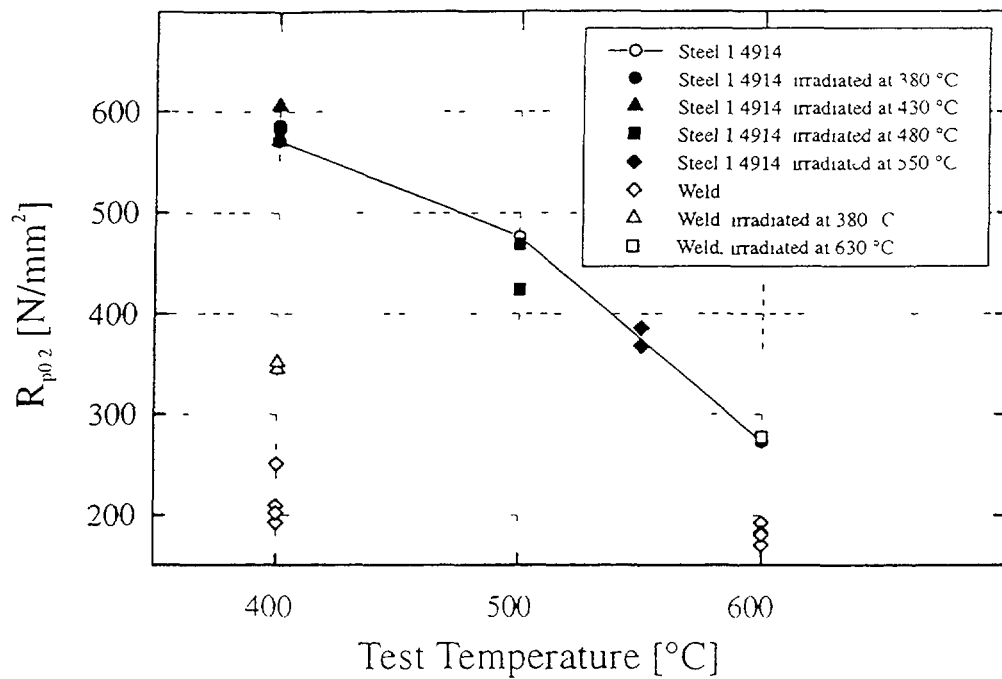


FIG 3 The yield strenght, $R_{p0.2}$

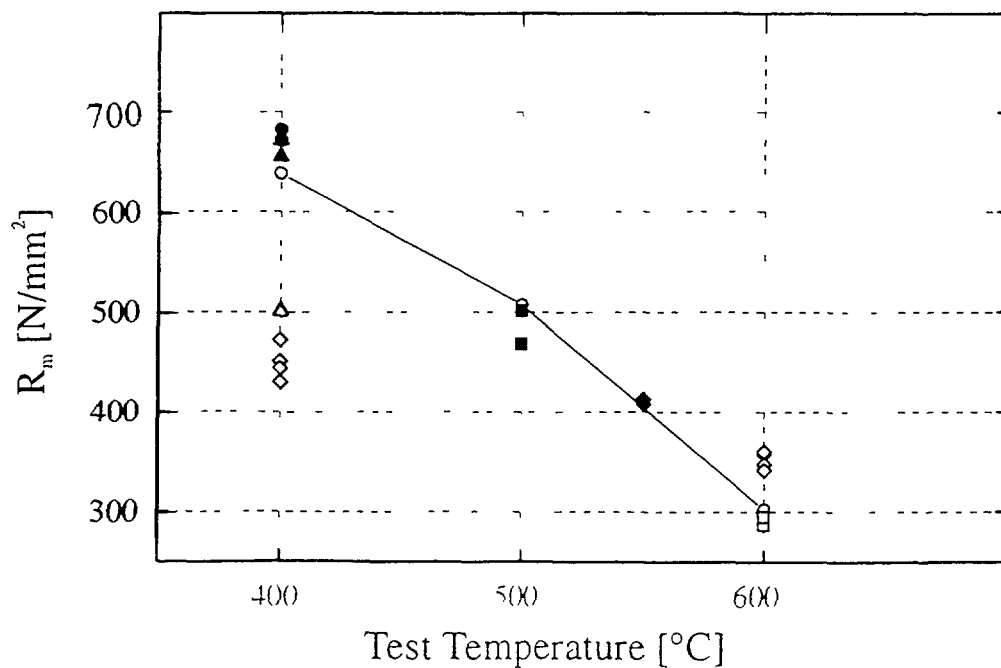


FIG 4 The tensile strenght, R_m

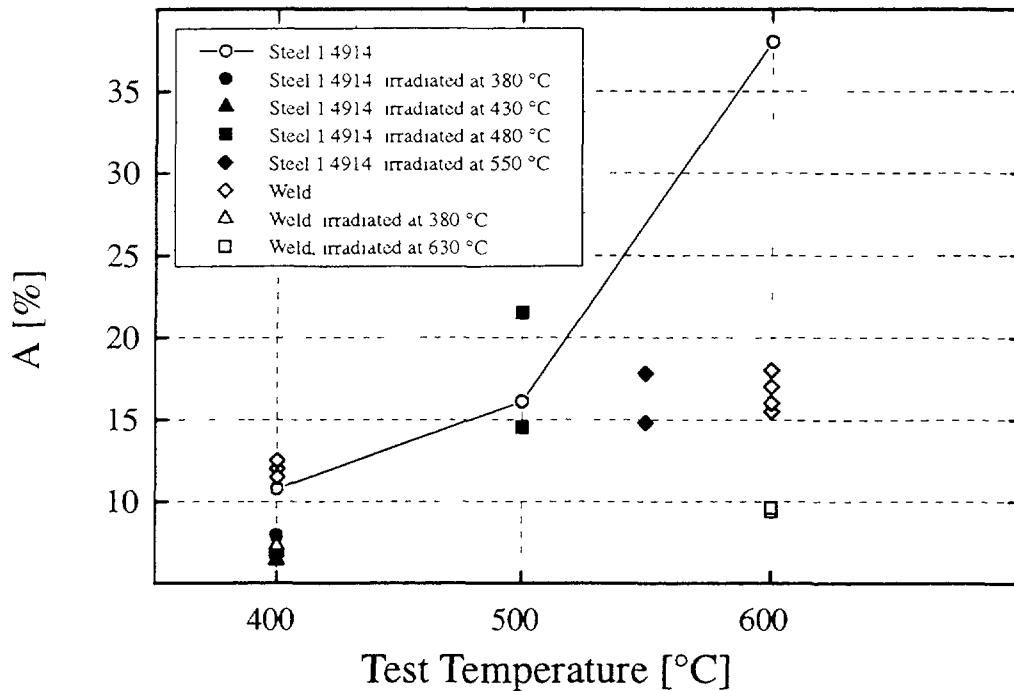


FIG 5 The total elongation

observed. From the accumulated neutron fluence varying between 10 and 105 dpa_{NRT} it can be concluded that the temperature and fluence dependence of radiation hardening is small, well in accordance with previous results [7]. Correspondingly, the total elongation is reduced. For wrapper samples irradiated at 480°C and above and tested at about the same temperature no influence on strength properties, but a stronger reduction of total elongation was observed.

The unirradiated tensile properties of the welds show a much lower strength level and a small temperature dependence indicating different material composition. Also the effect of irradiation is different compared to the martensitic wrapper material.

The most results of the tensile tests with the original wrapper thickness were found in the same scatter band as the samples with the reduced wall thickness. But the tests of the lower welded seam showed a reduction yield strength (about 30%) compared with the reduced sample thickness.

3.4. Creep Rupture Tests

Creep tests of the base and welded materials were performed at 600°C. The results of the base material, of welds and irradiated wrapper material are in the same scatter band, figure 6.

3.5. Microstructure, Fracture and Corrosion

The fracture behaviour of the base metal during tensile tests was not strongly influenced by the irradiation. The fracture mode was ductile. In the welded samples, the material separation took place in the melting zone at 380°C, and at 600°C between the martensitic base material and the martensitic HAZ, figure 7. The same fracture behaviour could be found in the broken creep samples.

The crack propagation of the impact samples were investigated in all welded samples. Unirradiated and irradiated samples in the region of DBTT and lower test temperatures were separated in the HAZ of the steel 14914. At higher test temperatures or in the region of USE the samples were broken in the melting zone. The fracture started behind the notch in the HAZ, then the cracks proceeded into the melting zone.

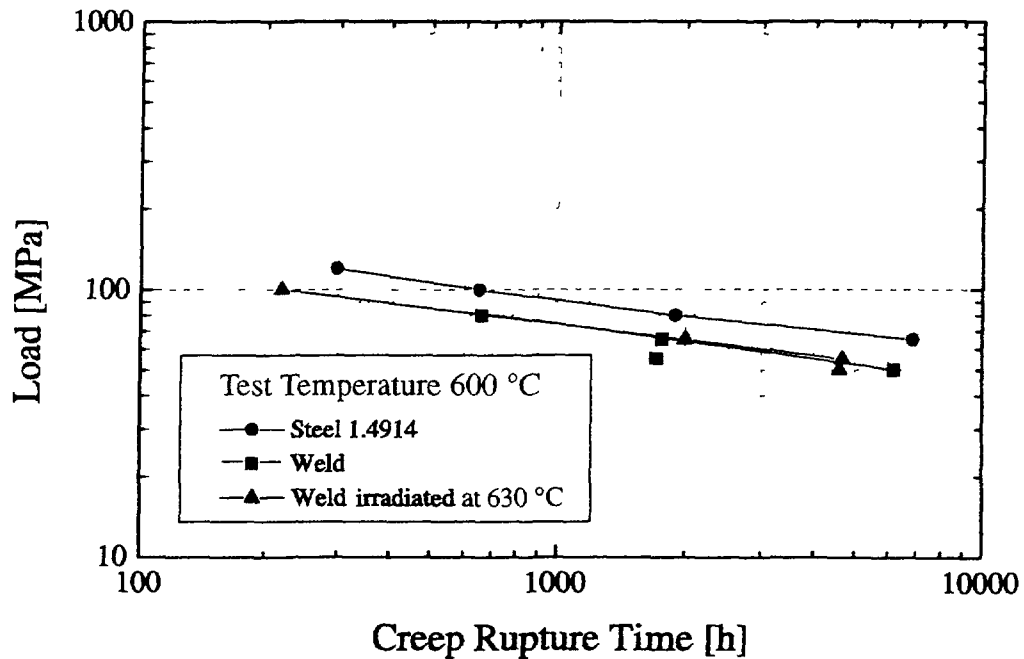


FIG 6 Creep strength depending on time, tested at 600 °C

The welds of the wrapper material were a connection of different materials. Martensitic and austenitic steel were welded. Between the steels the melting zone occurred. The melting zone was a two-phase (fcc/bcc) dendritic structure of austenite and ferrite in a fine distribution. The HAZ was developed with coarse grains and coarse precipitates; a further formation of ferrite grains was found in the HAZ of the martensitic steel, near the transition to the melting zone. In the upper weld, more ferrite was found than in the lower.

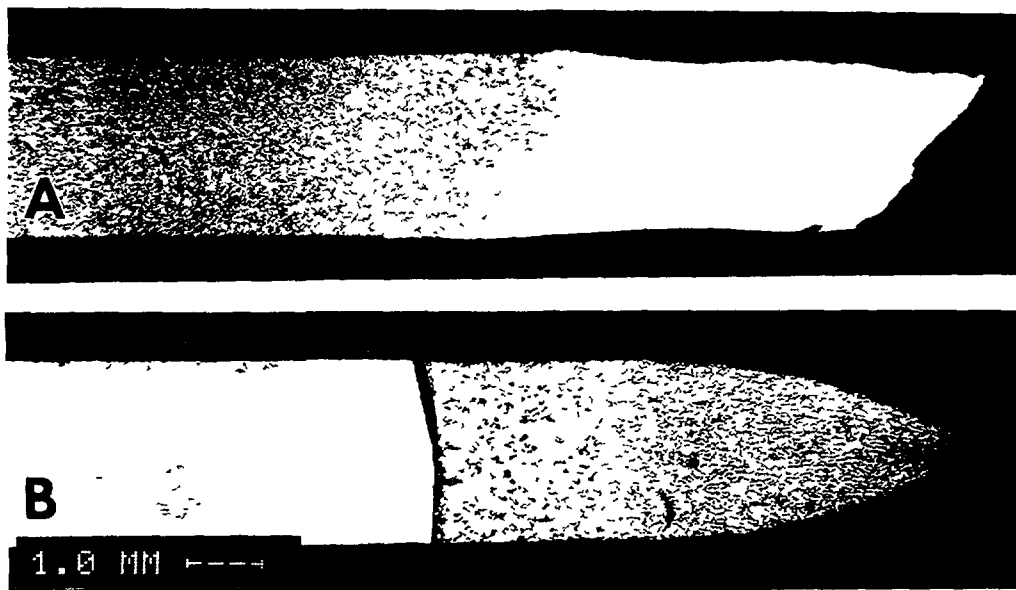


FIG 7 Metallographic cut through the ruptured tensile sample
 A) Lower weld (380°C) fracture in the melting zone and
 B) upper weld (630°C) fracture in the HAZ of martensite

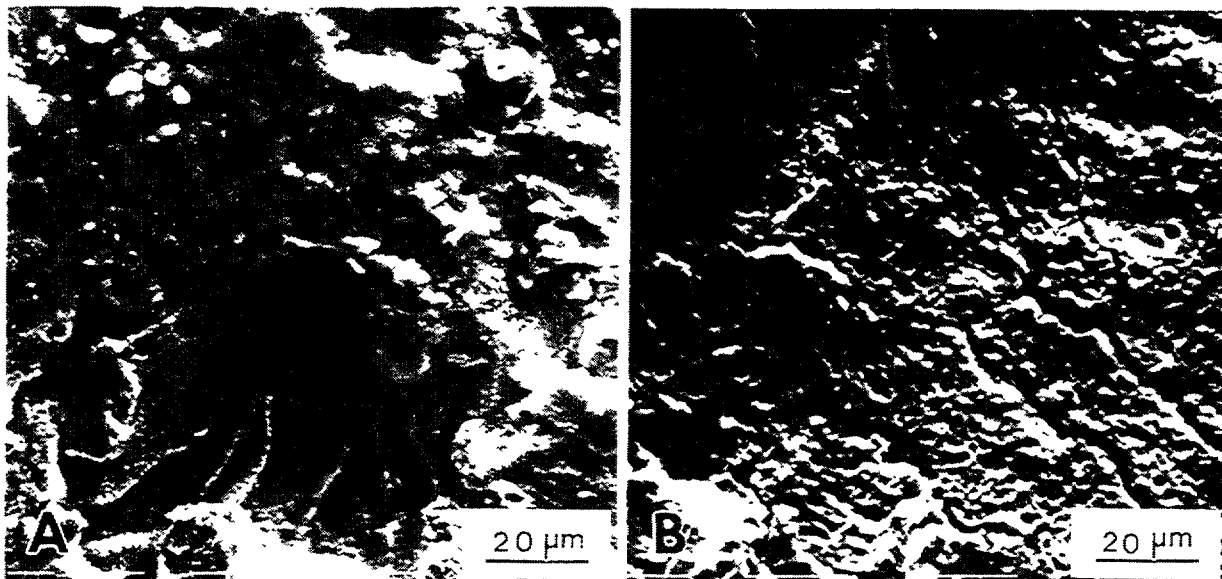


FIG. 8. Lower weld: A) Caverns in the melted zone.
B) grain structure in the HAZ of the martensite.

On the surfaces of the welded seams some influences of the sodium could be detected. Ni-rich regions were washed out and small caverns occurred with a diameter up to 25 μm , figure 8. In the HAZ of the martensite the grain boundaries have been exposed.

By means of transmission electron microscopy, the effects of neutron irradiation on the material could be made visible; figure 9. In the temperature range of 380°C up to about 410°C, irradiation-induced coherent α' -precipitates with a density of $2 \times 10^{15} \text{ cm}^{-3}$ were formed in the martensitic laths. Void formation took place in the range of the highest dose at temperatures from 400°C up to 480°C. Counting of the voids yielded a maximum swelling of 0.05% in the high-dose range. This low value could be confirmed by immersion density measurements, too. At higher temperatures (>430°C) He bubbles were observed at dislocations and subgrain boundaries. In the upper heat-affected zone the He bubbles were distributed homogeneously in the matrix, but with considerably increased concentration of about $3.5 \times 10^{17} \text{ cm}^{-3}$ towards the regions of lower temperature, where the He bubbles were mainly found in subgrain boundaries or dislocations.

4. MATERIAL BEHAVIOUR

4.1. Wrapper Material

Radiation hardening by coherent α' -precipitates was observed in the temperature range of 380 to 430°C. Strengthening of the material occurred in connection with the reduction of tensile ductility as observed in the total elongation. In the central position of the wrapper at 105 dpa_{NRT} no influence of irradiation could be observed. The void formation and the He bubbles are negligible. A remarkable excavation by sodium was not found. Comparable tests with the same steel were carried out in a sodium loop at 570°C and an excavation was measured of about 1 $\mu\text{m/a}$ [8].

The impact tests showed a small reduction of USE without any influence on ΔDBTT after the reactor irradiation.

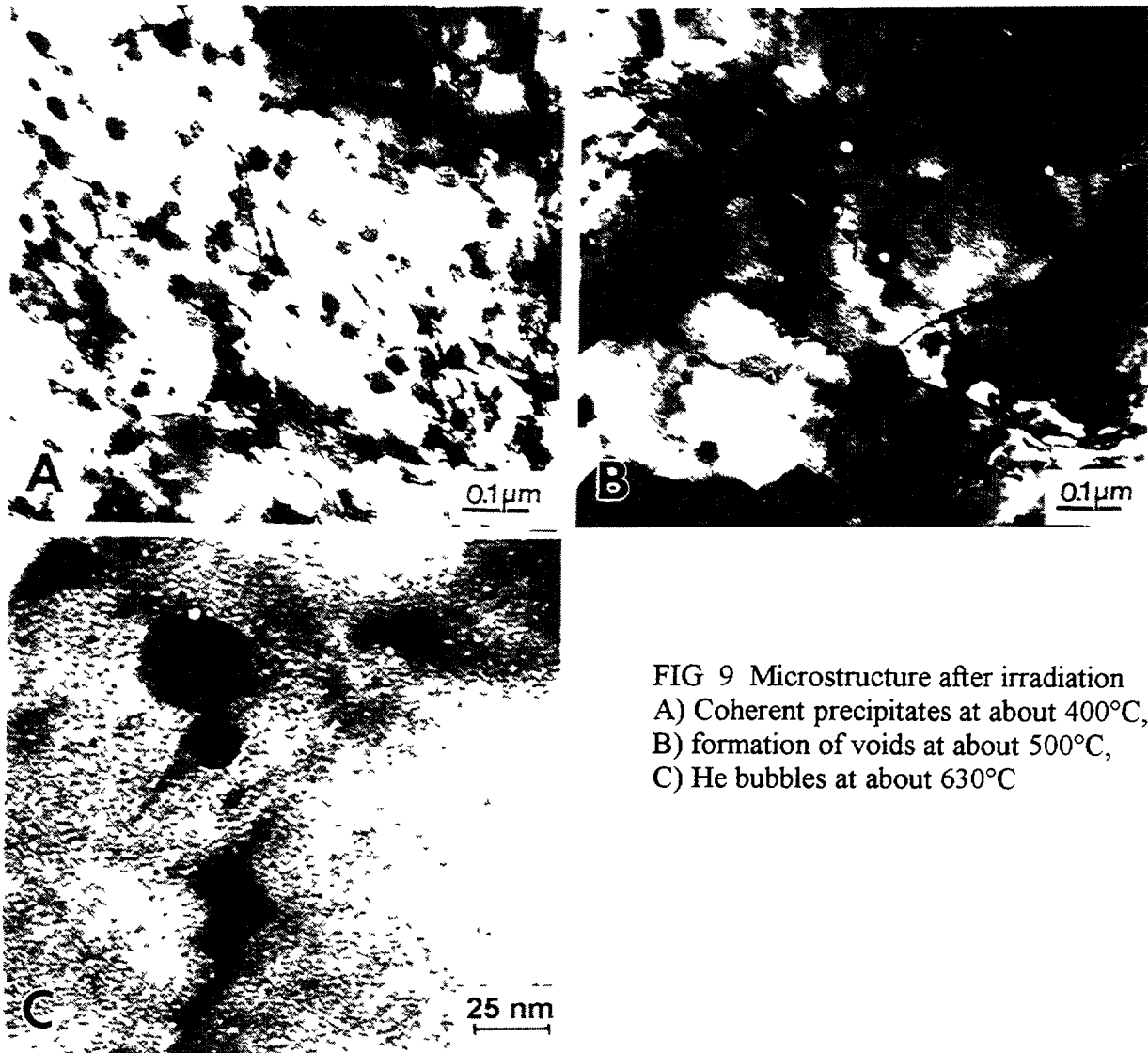


FIG 9 Microstructure after irradiation
 A) Coherent precipitates at about 400°C,
 B) formation of voids at about 500°C,
 C) He bubbles at about 630°C

4.2. Welded Material

During the mechanical tests the samples failed in the weakest material. In the lower weld, irradiated at 380°C, the separation during tensile tests took place in the melting zone, near the transition to the martensite, as in the unirradiated material.

Nearly the same tensile values were attained at the higher irradiation temperature, at 630°C, but, the fracture appeared in the martensitic material. The separation took place in the transition between HAZ and unaffected wrapper material. In the HAZ of the martensite a high concentration of He bubbles was observed. It led to a small strengthening.

The crack formation during impact test was different, too. In the region of DBTT the crack was observed in the HAZ of the martensitic steel near the transition to the melting zone and through the ferrite grains. At higher test temperatures in the upper shelf the fracture progressed through the melting zone.

Creep tests of the base wrapper material were performed at 550°C and 600°C. The long term behaviour of martensitic material or welds is not influenced by irradiation. All values are in the same scatter band. The separation of the welds took place in the HAZ at 600°C test temperature.

The sodium washed out the Ni-rich regions in the welded seams and exposed the grain structure in the HAZ of the martensite in the lower as well as in the upper weld. The small tendency to a lower strength of tensile tests with the original wall thickness can be influenced by the caverns which are like micro notches on the material surface.

5 SUMMARY

The martensitic 10% Cr-steel showed good mechanical properties as wrapper material after an irradiation period of about two years reactor operation, especially in the regions of high neutron fluence. Down to the handling temperature the material always had a ductile fracture behaviour [6, 9].

REFERENCES

- [1] MATERNA-MORRIS E, PETERSEN C, RIETH M, ROMER O, SCHIRRA M, EHRLICH K, Proc of EUROMAT 96 Top Conf on Materials and Nuclear Power, Bournemouth, UK (1996) 273
- [2] ANDERKO K, DAVID K, OHLY W, SCHIRRA M, WASSILEW C, Proc Top Conf on Ferritic Alloys for Use in Nuclear Energy Technologies, Snowbird, USA (1983) 229
- [3] SCHIRRA M, KfK 3640, August 1984, Kernforschungszentrum Karlsruhe, Germany
- [4] MATERNA-MORRIS E, SCHIRRA M, EHRLICH K, Proc Int Conf Materials for Nuclear Reactor Core Applications, Bristol, UK (1987) 263
- [5] BERGMANN H-J, Abschlußbericht EA 22 121 06, Bericht Nr KWU S541/92/0023, Oktober 1992, Bergisch Gladbach 1, Germany
- [6] RIETH M, DAFFENER B, RIES H, ROMER O, KfK 5264, August 1994, Kernforschungszentrum Karlsruhe, Germany
- [7] WASSILEW C, HERSCHBACH K, MATERNA-MORRIS E, EHRLICH K, Proc Top Conf on Ferritic Alloys for Use in Nuclear Energy Technologies, Snowbird, USA (1983) 607
- [8] GARCIA A M, ESPIGARES M M, ARROYO J, BORGSTEDT U H, Liquid Metal Engineering and Technology, Vol 1, Brit Nucl Energy Soc, London, 1984, 223-227
- [9] MATERNA-MORRIS E, et al Will be published in FZKA 5660, Forschungszentrum Karlsruhe, Germany

THE PERFORMANCE OF TYPE EP-450 FERRITIC-MARTENSITIC STEEL UNDER NEUTRON IRRADIATION AT LOW TEMPERATURES

V S KHABAROV, A M DVORIASHIN, S.I POROLLO
Institute of Physics and Power Engineering, State Scientific Center,
Obninsk, Russian Federation



XA9848047

Abstract

Up-to-date structural materials for fast breeder reactor core applications must have a high irradiation performance at large displacement doses (up to 100 dpa and more) achieved at high burn-up (12-15%) in the fuel. Type 13Cr2MoNbVB (EP-450) ferritic-martensitic steel used as the material of hexagonal wrappers in the BN-600 and BN-350 fast reactors exhibits a high resistance to swelling. It is known, however, that the steel is prone to an embrittlement at low irradiation temperatures. Eight hexagonal wrappers irradiated in the BN-600 and BN-350 reactors up to 85-90 dpa have been investigated, and data on tensile and impact properties have been obtained. Central parts of the wrappers irradiated up to higher damage doses than others exhibited satisfactory tensile properties, i.e. at high neutron dose, at temperatures in the range from 450 to 500°C, there is no severe degradation of tensile and impact properties. For these irradiation temperatures, mechanical properties of ferritic-martensitic steels depend only slightly on damage dose as compared to a low temperature neutron irradiation (<350°C). The highest levels of strengthening and embrittlement in the steel were observed after irradiation at 320°C. At high doses the performance of the ferritic-martensitic steel EP-450 in a fast reactor will be limited at low temperatures. TEM-study data on the microstructure of irradiated wrapper material are presented.

1 INTRODUCTION

An achievement of a high burn-up levels in nuclear fuel in fast reactors is considered as an important commercial objective. However, an increase of burn-up is restricted to irradiation performance of structural and fuel materials. In particular, various dimensional and structural changes can occur as a result of swelling, creep or embrittlement of structural materials at high damage doses of neutron irradiation. To minimize the dimensional changes in hexagonal wrappers at high dpa, ferritic-martensitic steels Type HT-9 (in USA) and EP-450 (in Russia) have been chosen as a wrapper material. However, a successful application of ferritic-martensitic steels in fast reactor cores at high burn-up levels (12-15%) is limited by irradiation embrittlement at temperatures lower than 400°C [1, 2].

In this paper experimental data on tensile and impact properties of the wrapper material (ferritic-martensitic steel EP-450) irradiated in the BN-600 and BN-350 reactors are presented.

2 EXPERIMENTAL PROCEDURES

The chemical composition and final heat treatment of Type EP-450 steel used as a wrapper material in the BN-600 and BN-350 fast reactors are given in Table 1.

TABLE 1 CHEMICAL COMPOSITION AND HEAT TREATMENT OF TYPE EP-450 STEEL (wt %)

C	Si	Mn	S	P	Cr	Ni	Nb	Mo
0.10-0.15	<0.5	<0.8	<0.015	<0.025	11.0-13.5	0.05-0.30	0.3-0.6	1.2-1.8
V	B	Fe						
0.1-0.3	0.004	Balance						
Normalization (1050-1100°C), tempering (720°C) 45-60 min								

After the heat treatment the microstructure consists of ferrite and tempered martensite grains with 1:1 ratio. Tensile and impact specimens machined from eight wrappers irradiated in the BN-600 and BN-350 reactors have been tested. Wrappers are hexagonal tubes with flat-to-flat size of 96 mm and

width of wall of 2 mm. Specimens with gauge sizes of 12 x 2 x 2 mm were cut in longitudinal and transversal directions. Irradiation parameters for the wrappers are given in Table 2. In addition, irradiation parameters for every set of specimens are shown in figures together with test results.

Tensile specimens were tested at strain rate of $1.4 \times 10^{-3} \text{ s}^{-1}$ at several test temperatures in the range from room to irradiation temperature using remote tensile machine.

U-notch (2 mm depth, 1 mm radius) impact specimens with sizes of 50 x 8 x 2 mm were tested at temperatures from 25 to 300°C, using a pendulum machine. The ductile-to-brittle transition temperature (DBTT) was determined as the temperature corresponding to the average energy in DBT range.

A part of specimens was TEM-analyzed in a JEM-100CX electron microscope.

TABLE 2 IRRADIATION PARAMETERS

Wrappers	Reactor	Peak damage dose, dpa	Irradiation temperature range, °C
OP-3	BN-350	47	280-520
OP-4	BN-350	47	280-520
C-6	BN-350	91	280-455
C-11	BN-600	61	345-545
C-63	BN-600	87.5	355-535
S-109	BN-600	86	360-560
S-112	BN-600	86	350-560
0841	BN-600	86.5	360-590

2 RESULTS

2.1. Tensile tests

The tensile properties of specimens machined from the S-112 subassembly's wrapper irradiated in the BN-600 reactor are shown in Figs. 1 and 2 as ultimate strength and total elongation profiles along the wrapper. These profiles are similar to ones for other seven wrappers investigated. It is seen that maximal strength and minimal ductility were measured for specimens cut from the lower parts of the wrapper (close to the core bottom). For specimens cut from the upper parts of the wrapper, changes of strength and ductility were smaller in spite of much higher damage doses. It seems that the irradiation temperature is the most significant irradiation parameter affecting the irradiation strengthening and embrittlement.

The largest effect of dose on the tensile properties was observed for low temperatures (<400°C). For specimens cut from lower (BN-600) and middle (BN-350) parts of wrappers and irradiated at 340-360 dpa, the dose dependence of ultimate strength is shown in Fig. 3. It is seen that the increment of ultimate strength reaches a maximum at 30-40 dpa and then begins to decrease. Data on yield stress increment at room test temperature in the dose range from 2 to 20-25 dpa can be fitted by the following equation:

$$\Delta \sigma_y, \text{ MPa} = 300 \times (\text{dpa})^{0.2}.$$

The transversal specimens have demonstrated more severe embrittlement as compared with the longitudinal specimens because grains in the steel were stretched along the wrapper axis. Therefore, data for transversal specimens were used for a conservative evaluation of the steel irradiation performance. It were transversal specimens cut from lower part of S-112 wrapper ($T_{\text{irr}} = 350\text{-}370^\circ\text{C}$, $D = 35\text{-}40 \text{ dpa}$, $T_{\text{test}} = 300\text{-}400^\circ\text{C}$) which demonstrated nil ductility at tensile tests. Severe embrittlement in the C-6 wrapper material irradiated in the BN-350 reactor at 280-345°C to damage doses in range

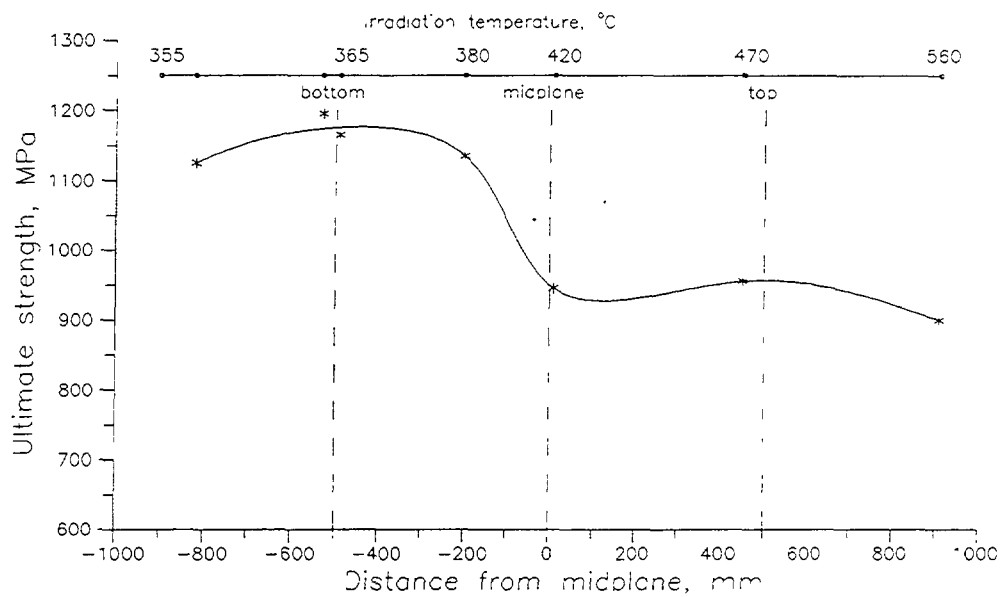


Fig. 1. Ultimate strength profile for the S-112 SA wrapper material tested at room temperature

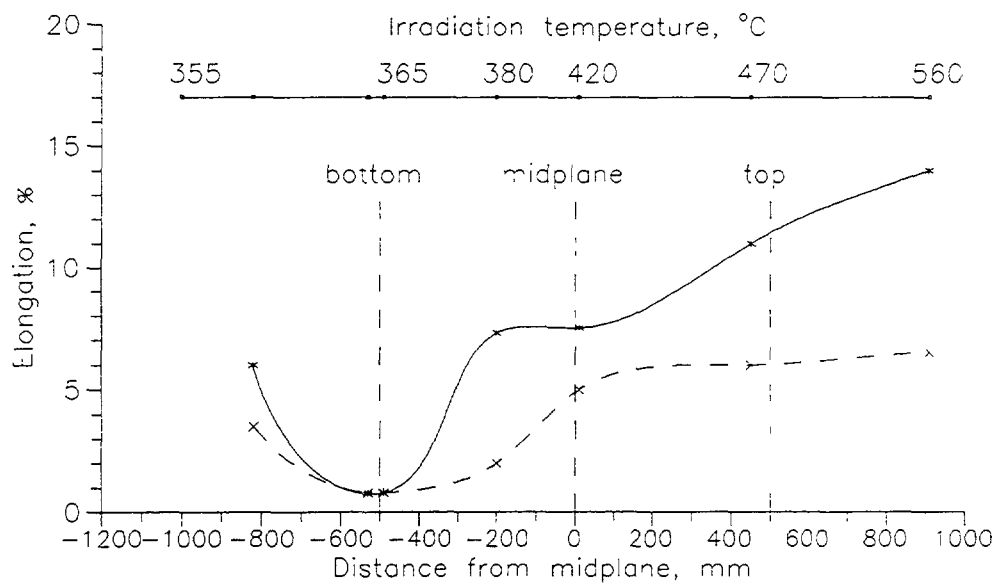


Fig. 2. Total (*) and uniform (x) elongation profile for the S-112 SA wrapper material tested at room temperature

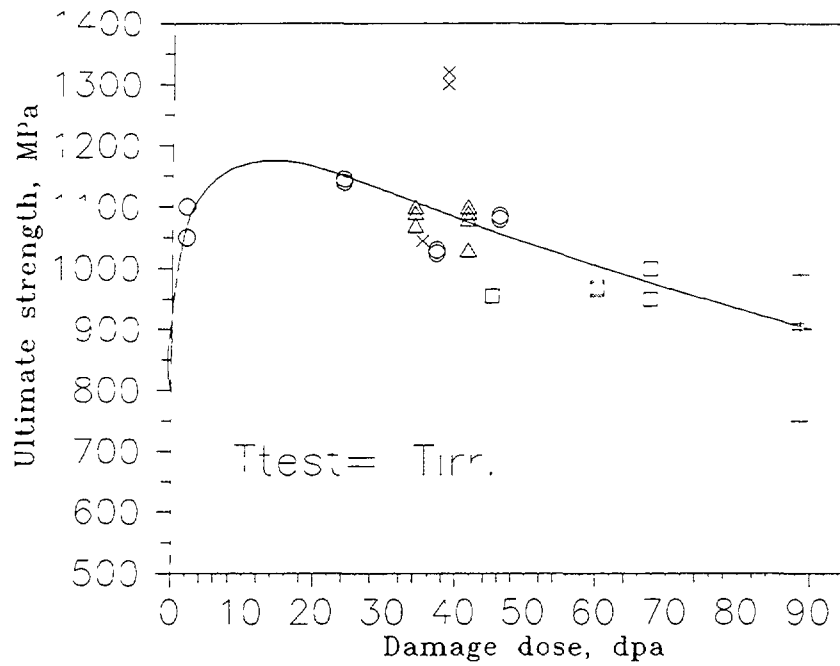


Fig. 3. Effect of damage dose on ultimate strength of the EP-450 steel used as a wrapper material and neutron-irradiated at 350-365°C.

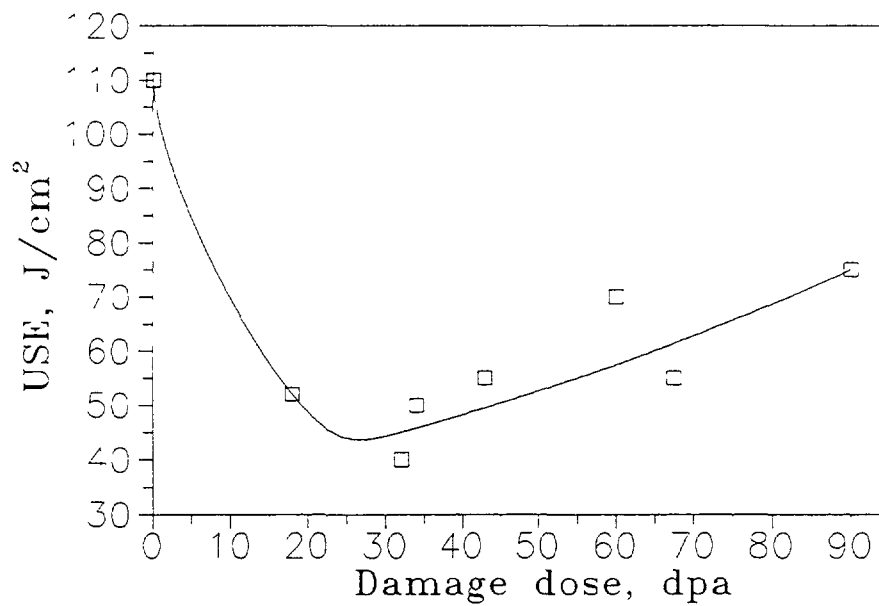


Fig. 4. Effect of damage dose on USE of the EP-450 steel used as wrapper material in subassemblies and irradiated at 350-365°C.

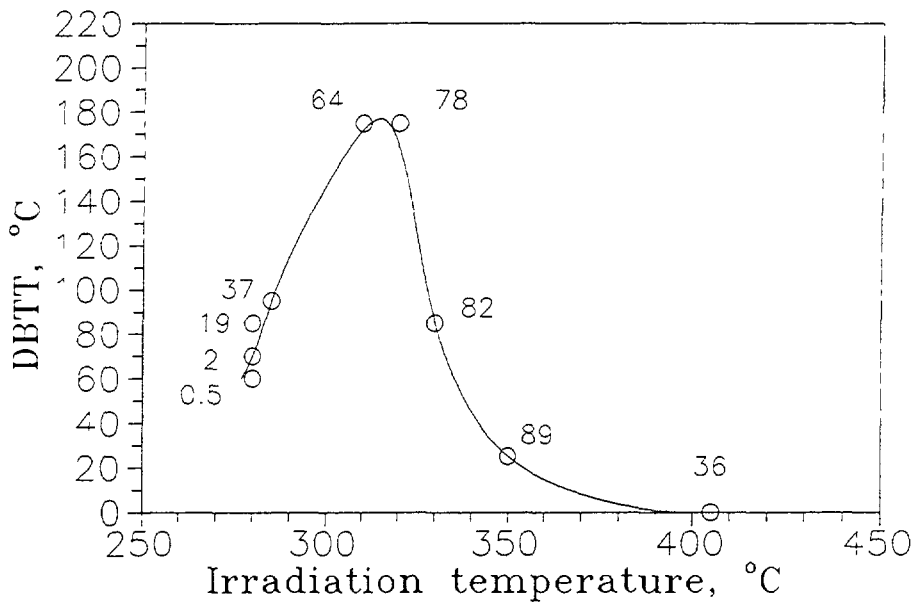


Fig. 5. Effect of irradiation on DBTT of the EP-450 steel used as a material in the C-6 subassembly wrapper in the BN-350 reactor. Numbers near points stand for dpa.

from 1.5 to 68 dpa was also observed in low temperature tests ($T_{\text{test}} = 25, 100, 150^\circ\text{C}$). But, brittle strength values for this material are rather high ($US = 800\text{--}1215\text{ MPa}$).

One-hour annealing experiments showed that low ductility began to recover at 450°C . A complete recovery of the ductility to a level corresponding to aged steel condition was observed after annealing at 550°C .

2.2. Impact tests

Low temperature neutron irradiation resulted in an increase of the DBTT and decrease of the upper shelf energy (USE) both of which are dependent on irradiation temperature and damage dose. A maximum of DBTT ($+180^\circ\text{C}$) and a minimum of USE ($30\text{--}40\text{ J/cm}^2$) values have been observed for specimens irradiated at $310\text{--}320^\circ\text{C}$ to $60\text{--}80\text{ dpa}$ (Fig. 4, 5). At higher irradiation temperatures, the DBTT was lower despite of high doses of $82\text{--}89\text{ dpa}$.

In one-hour annealing experiments the impact energy recovered to $USE > 120 \times 10^4\text{ J/m}^2$.

2.3. Microstructure

Main features of the irradiation-induced microstructure in EP-450 steel are voids, dislocation loops, dislocations, precipitates of α' - and M_2X phases [3]. The irradiation temperature ranges of their formation are shown in Table 3.

TABLE 3. IRRADIATION-INDUCED MICROSTRUCTURAL FEATURES AND IRRADIATION TEMPERATURE RANGES OF THEIR EXISTENCE IN THE EP-450 STEEL.

Feature	Irradiation temperature, $^\circ\text{C}$
Dislocation loops	285-520
α' -phase	285-510
Voids	285-520
χ -phase precipitates	460-590
M_2X precipitates	460-690

It is known that ferritic-martensitic steel are high resistant to void swelling. The maximum of swelling in the EP-450 steel was observed at the irradiation temperature of 420°C. The largest swelling (0.4%) was measured for the wrapper material irradiated to 90 dpa at 350°C in the BN-350 reactor.

Using data on microstructure and tensile properties measured the barrier strength constants were determined as $\alpha_{\text{loop}} = 1.38$ for dislocation loops, $\alpha_{\text{void}} = 0.3-2.0$ for voids and $\alpha_p = 0.1-0.3$ for precipitates. One can conclude, that the strengthening is mainly caused by dislocation loops.

At damage doses higher than 40 dpa a transformation of dislocation loops into a high density dislocation network are likely to be a main reason of irradiation softening and irradiation-induced recovery of embrittlement [4].

3 SUMMARY

Post-irradiation tensile tests and TEM-examinations showed that the ferritic-martensitic steel EP-450 has a high swelling resistance and has a high strength at irradiation to high doses (90 dpa). The most favorable temperature range for their applications seems to be 400-550°C. No restrictions for the performance of the steel as a wrapper or cladding material have been met at such temperatures so far.

However, ferritic-martensitic steels have a tendency to a low temperature irradiation embrittlement of both the ductility and upper shelf energy decrease and DBTT increases. These phenomena occur in the materials at lower irradiation temperatures ($T_{\text{irr}} < 380-400^\circ\text{C}$) e.g. in lower parts of a fuel core where damage dose didn't exceed a half of the peak dose. From test results it follows that at low temperatures the irradiation embrittlement occurs mostly at damage doses of 10-40 dpa. So, a performance of ferritic-martensitic steels at high neutron doses can be mainly restricted by the degradation of tensile and impact properties at low temperatures ($<400^\circ\text{C}$) and low damage doses (10-40 dpa) irradiation. At higher damage doses a problem of embrittlement in the lower part of fuel core becomes to be less severe. As for the central and the upper parts of wrapper, the irradiation hardening and embrittlement are not significant.

Thus, the 12%Cr-steels widely used in fast reactors as a structural material of hexagonal wrappers demonstrate a high dimension stability and acceptable performance at high irradiation doses in the irradiation temperature range of 400-550°C.

REFERENCES

- [1] KHABAROV, V S, et al, "Mechanical properties and microstructure of neutron-irradiated ferritic martensitic steel used as wrapper material for the BN-350 and BN-600 fast reactors", Fast Reactor Core and Fuel Structural Behaviour (Proc. of Int. Conf. BNES, Inverness, UK, 4-6 June 1990), BNES, London (1990) 263-267.
- [2] POVSTYANKO, A V, et al, "The results of post-reactor examinations of steels and alloys irradiated to high damage doses" (Proc. of Int. Conf. on Radiation Material Science, Alushta, May 22-25), Vol. 3, Kharkov (1990) 94-107.
- [3] DVORIASHIN, A M, et al, "The effect of neutron irradiation on the microstructure and tensile properties of 1Cr13Mo2NbVB steel", Effects of Radiation in Materials (Proc. 15th International Symposium), ASTM STP 1125 (R. E. Stoller, A. S. Kumar, and D. S. Gelles, Eds.), ASTM Philadelphia (1992) 1180-1189.
- [4] KHABAROV, V S, et al, "Microstructure, irradiation hardening and embrittlement of 13Cr2MoNbVB ferritic-martensitic steel after neutron irradiation at low temperatures", Journ. of Nucl. Mater. v 233-237 (1996) 236-239.

POST-IRRADIATION EXAMINATION OF Ti OR Nb STABILIZED AUSTENITIC STEELS IRRADIATED AS BN-600 REACTOR FUEL PIN CLADDINGS UP TO 87 dpa

S.I. POROLLO, A.N. VOROBYEV, S.V. SHULEPIN
Institute of Physics and Power Engineering, State Scientific Center,
Obninsk, Russian Federation



XA9848048

Abstract

The results of postirradiation study of fuel pins with claddings fabricated from the 16Cr-15Ni-3Mo-Nb (EI-847), 16Cr-15Ni-3Mo-Nb-B (EP-172) and 16Cr-15Ni-2Mo-Ti-V-B (ChS-68) austenitic stainless steels in 20% cold-work condition are given. All fuel pins after irradiation in the BN-600 reactor to peak burn up of 11.6 % (displacement dose of 83 dpa) and remained its tightness. At the same time, a number of fuel pins have failed during low-load handling in hot cells. Tensile mechanical tests revealed a drastic decrease in strength and a severe embrittlement of the cladding material taken from some parts of fuel pins. For these parts numerous deep microcracks at the inner surface of pin cladding have been observed. Locations of the maximum cladding property degradation coincides with locations of the peak diameter increase and peak swelling. The effects of high swelling and radiation-induced segregation on mechanical properties and corrosion resistance of the fuel pin cladding are discussed.

1. INTRODUCTION

For improving the economy of LMRs one needs in structural materials, which can withstand in the reactor core environment for neutron irradiation to peak burn up of 15-20 % h.a. and displacement doses of 180-200 dpa. The use of the Type EP-450 ferritic-martensitic steel as a wrapper material in the BN-600 fast reactor guarantees a high performance of subassemblies. In contrast, the problem with the fuel pin cladding materials is not so favorable. The Ti or Nb stabilized austenitic stainless steels (ChS-68 and EP-172), which are now used as the reference fuel pin cladding material in the BN-600 reactor retain its performance at burn up level less than 10-12 % h.a. and displacement dose of 90 dpa. Some alternative materials such as ferritic-martensitic steels or high-nickel alloys are being not used as a cladding material for different reasons. At the same time, the operation experience for Western LMR shows that fuel pins with the claddings fabricated from austenitic stainless steels may be in service to a damage level of ~ 150 dpa. The development of new advanced stainless steels for clad applications in the BN-600 and BN-800 reactors requires the determination of main factors which responsible for the irradiation-induced degradation of steel properties. This goal may be reached only if the detailed post-irradiation study of high irradiated pins is to be continued.

2. FAILURE MODE OF BN-600 REACTOR FUEL PINS UNDER HIGH DOSE IRRADIATION

The former concepts on the operation conditions of fuel pins in the LMR suggest that the main properties which limit life-time of fuel pins are long-term mechanical properties of cladding materials at temperatures above 500°C and fuel fission products attack resulting in thinning of clad in the top parts of fuel pins. On these assumptions some requirements are being imposed on high temperature mechanical strength and corrosion resistance of cladding material.

The post-irradiation experience for BN-350 and BN-600 reactors pins (the total number of pins investigated in IPPI hot lab exceeds 100) showed that the character of pin failure is different. The region of severe degradation of cladding properties is located in lower parts of pins that corresponds to irradiation temperatures around 450°C. The observed character of failure is irrespective of the austenitic steel type. Fig. 1 shows an example of the mechanical property degradation in the pin cladding made from ChS-68 type steel for three subassemblies irradiated to different fuel burn-up levels.

The decrease of strength characteristics of claddings results in the fuel pin failure during low-load handling of the pins in hot cells. It should be noted that initially all pins irradiated were tight. A metallographic examination

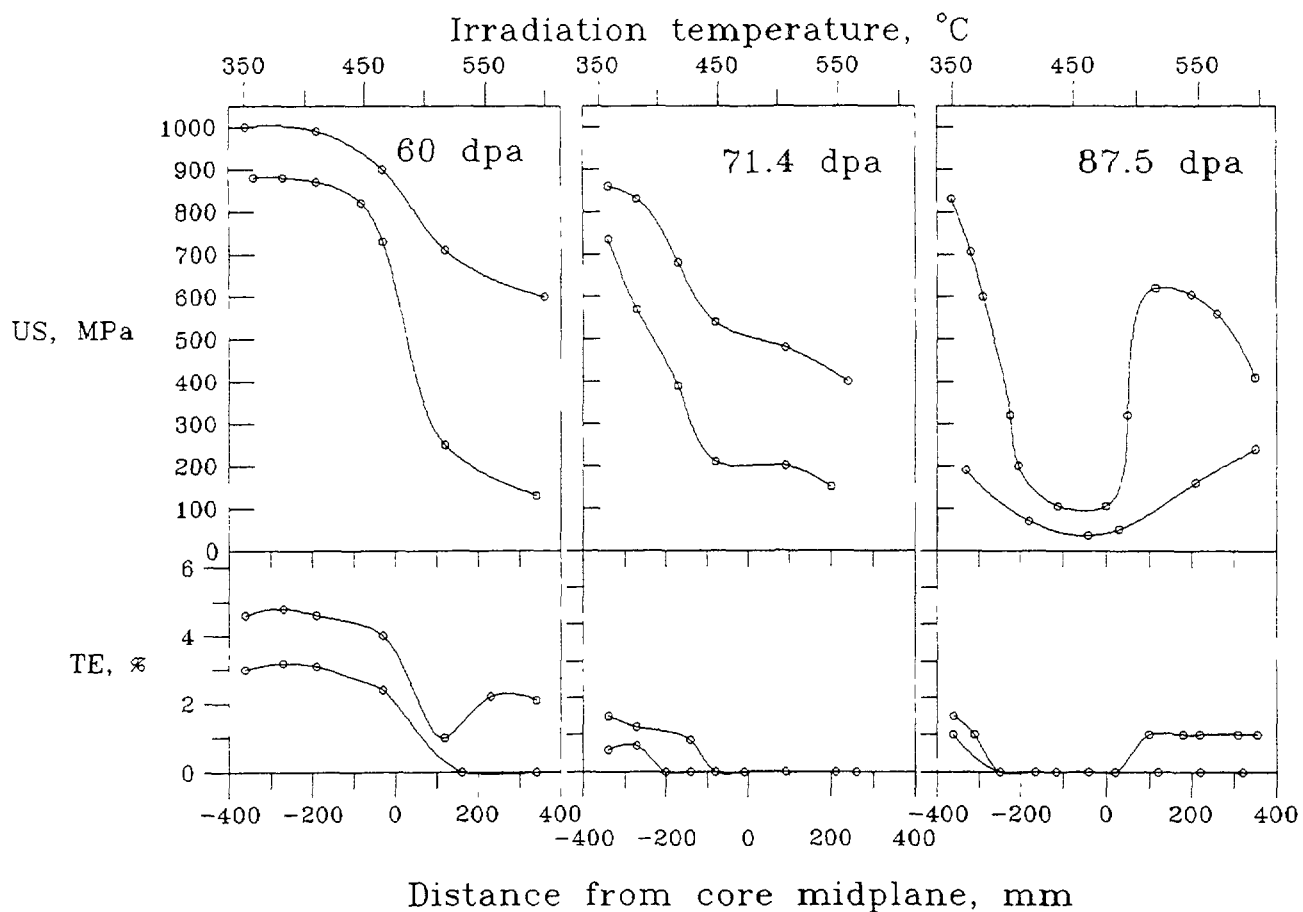


Fig. 1 Axial profiles of the ultimate strength (US) and total elongation (TE) for BN-600 reactor pin claddings (ChS-68 20% c.w.)

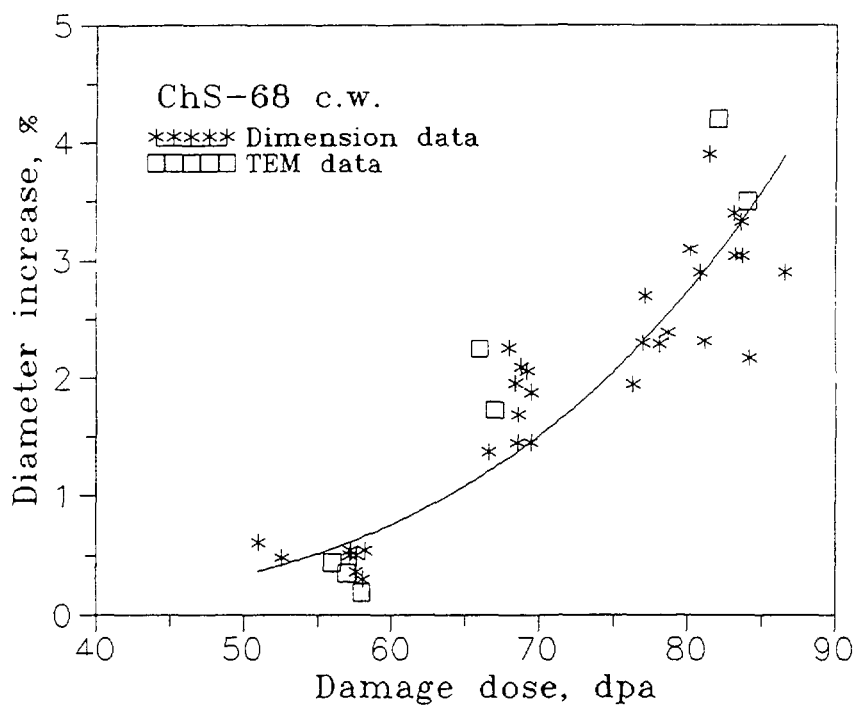


Fig. 2 The peak diameter increase of 20 c.w. ChS-68 SS cladding versus displacement dose.

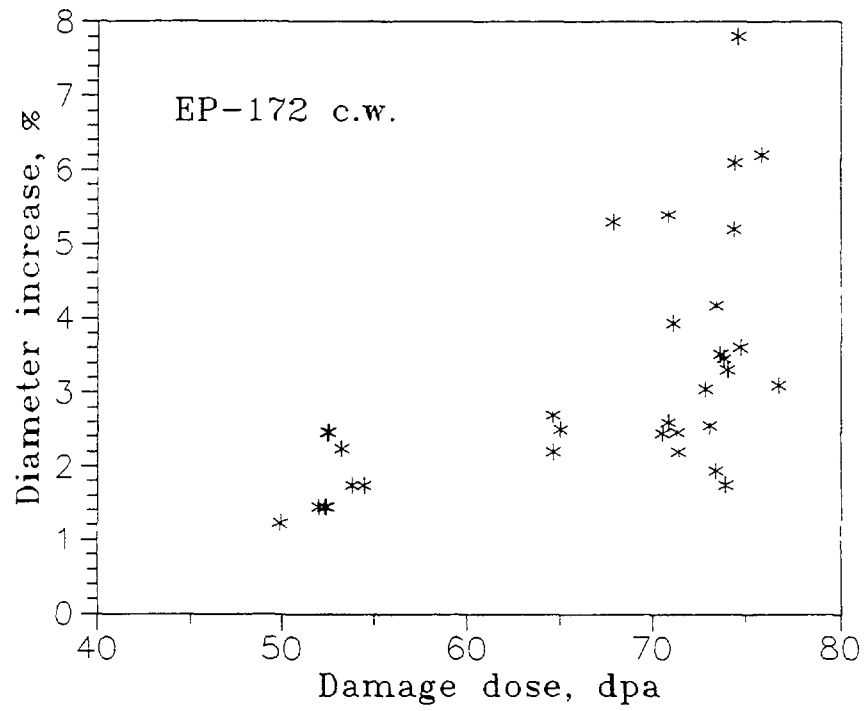


Fig 3 The peak diameter increase of 20 c w EP-172 SS cladding versus displacement dose

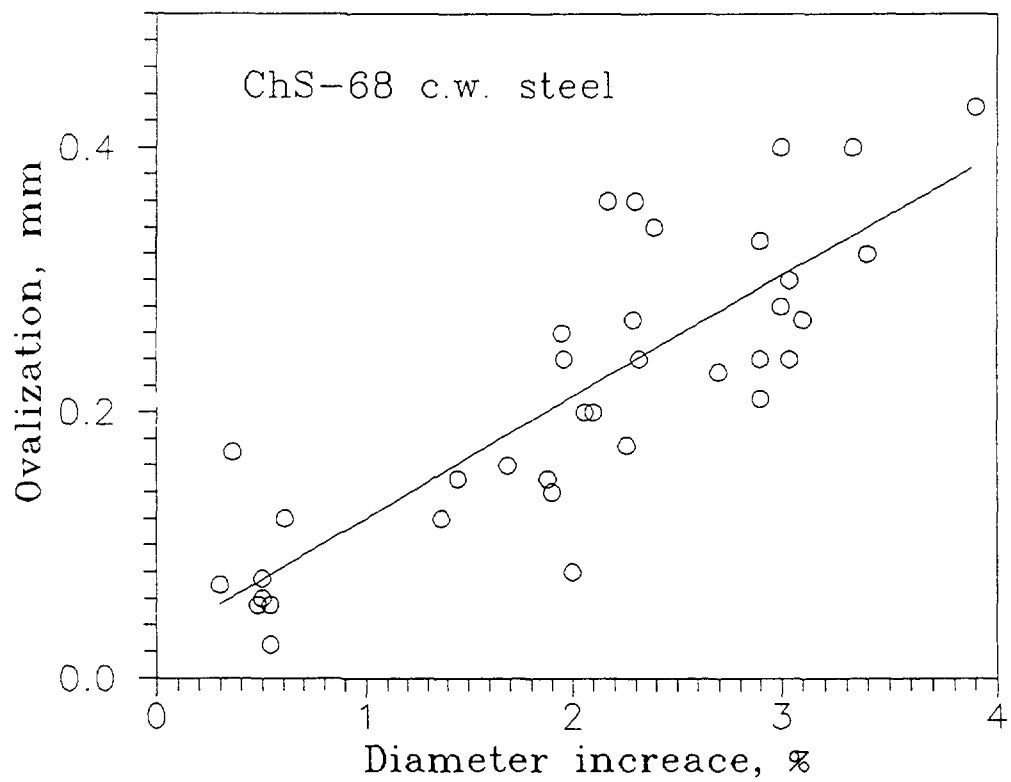


Fig 4 The peak ovalization of 20% c w ChS-68 SS claddings versus peak diameter increase

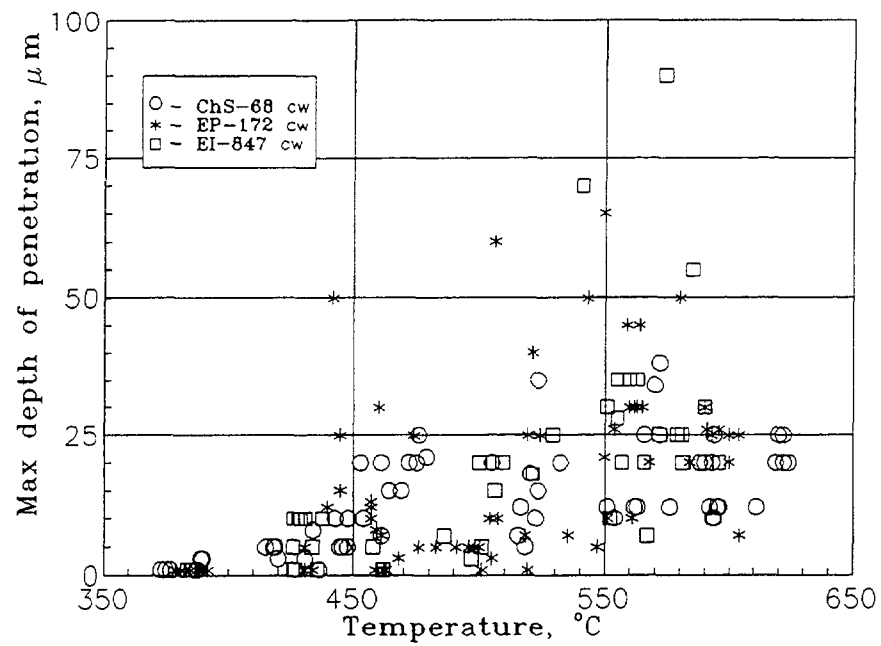


Fig 5 Temperature dependence of the depth of corrosion in BN-600 fuel pin claddings

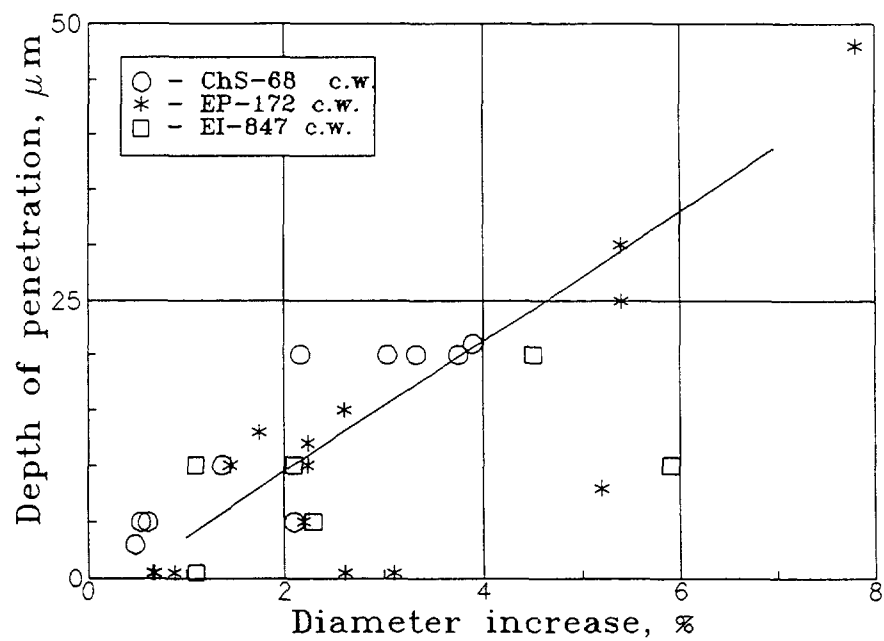


Fig 6 Depth of corrosion as a function of pin diameter increase for BN-600 fuel pin claddings

and study of cladding inner surfaces by SEM method has revealed numerous microcracks in fuel pin cross-sections where the severe degradation of cladding mechanical properties occurred. In most cases the microcracks had axial orientation and intergranular propagation mode.

An analysis of experimental data has showed that the pins failed when the diameter increase of the cladding exceeded some value (~3%). At the same time for pins having the peak diameter increase less than 3% the degradation of both the ultimate strength and ductility have not been observed. Besides, the location of the maximum cladding property degradation coincides with the peak diameter increase region. The dose dependence of the peak diameter increase in fuel pin claddings made from ChS-68 (20% c w) and EP-172 (20% c w) steels are shown in Figs 2 and 3, respectively. It is seen from the figures that the diameter increase up to ~50 dpa is negligible. The rate of the diameter change increases with damage dose increasing and for some pins the peak diameter increment exceeds 7%. The pins diameter increase result in the cladding ovalization caused by the mechanical interaction between pins. The ovalization increases with dose increasing and reaches the peak values of 0.4 mm and more (Fig 4). Immersion density and TEM measurements have showed that the largest contribution to pin diameter change was made by the void swelling in cladding materials, but not by the creep deformation process.

Thus, there is a clear interrelation between swelling and degradation of properties in fuel pin claddings.

3 EFFECT OF SWELLING ON FUEL PIN PERFORMANCE

3.1. Fuel pin cladding embrittlement

Measurements of mechanical properties for irradiated pin claddings have revealed that a severe embrittlement of steels is observed when the level of swelling in cladding exceeds 10-15%. A similar phenomenon was also observed for hexagonal wrappers and test specimens. In this case an intergranular fracture mode with the high number density of voids on the fracture surface were found. The reason of embrittlement in stainless steels has not been understood so far, but most of the results indicate that this embrittlement is to be related to the radiation-induced segregation of steel components at point defect sinks. A TEM-examination of fuel pin cladding with large swelling (>10%) showed that in addition to irradiation defects (voids, dislocations) and phase precipitates the planar spread defects have been observed. The defects give some extra reflections in the microdiffraction pattern. From a preliminary analysis of dark field micrographs and corresponding selected areas diffraction patterns it follows that most probably these defects are the martensite phase. It should be noted that the martensite has not been found in unfailed parts of TEM-specimens. So, if a deformation at room temperature is absent, the martensite phase did not form. It is well known that the martensite phase is a very brittle and its formation in the vicinity of a crack may explain the nil ductility of heavily swelled stainless steels. The martensite formation in its turn can be related to the Ni segregation at void surfaces, to a lower Ni content in the intervoid space and hence to a low matrix resistance to γ - α transformation.

3.2. Deterioration of pin cladding corrosion resistance

The inner cladding attack at lower part of fuel pins ($T_{irr} < 500^\circ\text{C}$) reveals itself as an intergranular corrosion up to depth of 40 μm and the formation of microcracks having lengths more than 100 μm . The temperature dependence of corrosion depth is shown in Fig 5. One can see, that a noticeable cladding attack begins even at irradiation temperature of 400°C . The corrosion depths in the temperature range from 440 to 480°C are 20 μm and higher. Besides, there is some interrelation between the depth of corrosion attack and the pin diameter increase (Fig 6). In corrosion zones, at grain boundaries the ratio of the most aggressive fission products, Cs and Te, changes in favor of Te.

Since the character of both the microcrack propagation and corrosion are intergranular, one could expect that one of the factors which lower the corrosion resistance of steels is a change of grain boundary state. It is known that the corrosion resistance of stainless steels depends on Cr content and in the cases when the Cr content drops below a certain value the rate of corrosion increases sharply. The TEM-study of irradiated steels revealed void denuded zones up to 2000-3000 Å in width at grain boundaries. Along with microstructural changes a change of steel chemical composition occurs in void denuded zones as a result of the radiation-induced segregation. As for the corrosion resistance of steels, a decrease of Cr content is of primary importance [3]. By appearance the microcrack surfaces containing no voids one can conclude that the microcracks propagate through the void denuded zones, where the Cr content is less than in matrix.

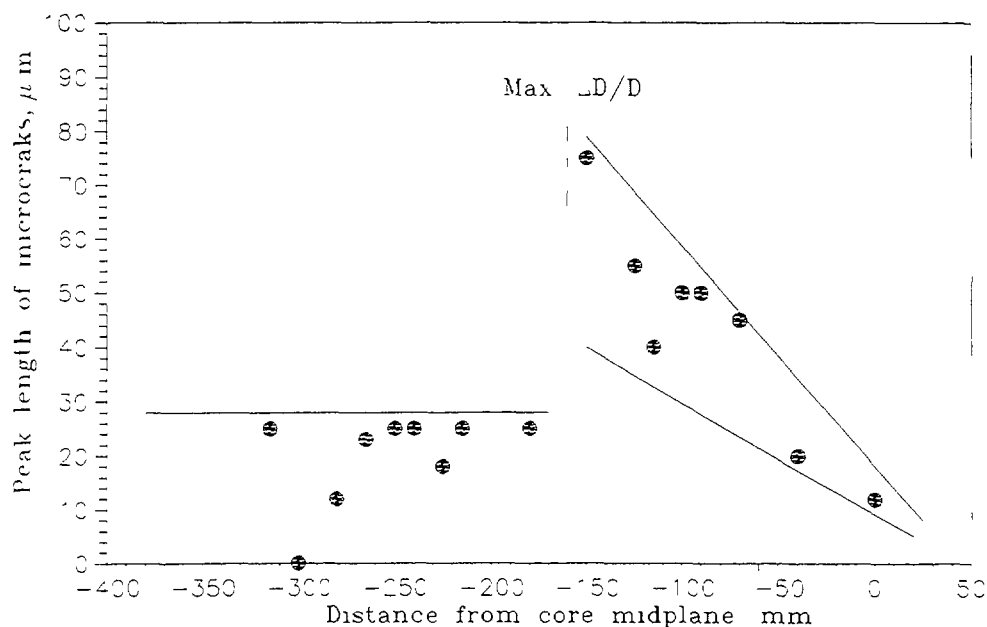


Fig 7 Axial distribution of the maximal length of microcracks for fuel pin irradiated to burn-up of 11.6% ha (ChS-68 20% c w)

Another significant circumstance which enhances the cladding corrosion rate is increase of Te content in the gap between the cladding and fuel pellets. A larger content of Te can result from a higher fuel pellet temperature, when the gap between cladding and fuel becomes to be larger. An elevation of fuel temperature in pin cross-sections with maximal diameter increase is confirmed by an observation of zones of long columnar grains the width of which is comparable or exceeds the width of columnar grain zones in the core midplane cross-section.

3.3. New sources of stress in pin cross-sections of high cladding swelling

From an analysis of possible sources of stress in fuel pin claddings it follows that some additional stresses can arise in the pin cross-sections where the clad material swelled significantly. These stresses result from swelling gradient through cladding wall and from a pin-to-pin mechanical interaction. Both the level and sign of the stresses vary along the pin length and depend on the cladding wall thickness. The mechanical interaction between fuel pins results in an ovalization of pin claddings. The ovality of central pins oscillated, the distance between the neighbour maxima being 17 mm. For cross-sections of maximal ovalization one can expect the peak stresses resulting from pin mechanical interaction as well as a non-uniform microcracks distribution along cladding perimeter. Microcracks of a maximal length should be observed on two opposite sides of the perimeter.

Stresses resulting from a swelling gradient through the cladding wall vary along the pin in other way. For the fuel pin cross-sections, in which the irradiation temperature of middle cladding layer is lower than the peak swelling temperature (below the pin cross-section of the peak diameter increase) such stresses at inner surface of cladding are compressive. And on the contrary, in a cladding cross-section of more high temperature, inner layers of cladding are to be tensile. Microcracks distribution along cladding perimeter and along pin axis have been investigated for a pin from the B-163 subassembly. The measured peak diameter increase for this pin is 5.4% and corresponds to the cross-section located at 160 mm below the core midplane. The axial distribution of maximal microcrack lengths for the fuel pin is shown in Fig 7. This figure shows that the maximal length of microcracks in the region extending from -300 mm to -160 mm from core midplane is about 30 μm. A sharp rise of length up to 80 μm was observed in the region above the pin cross-section of highest diameter increase and then decreased smoothly to upper parts of the pin. A substantial non-uniformity in microcracks lengths along cladding perimeter has not been found. This means that Fig 7 proves the existence of a certain interrelation between the corrosion process and swelling phenomenon in claddings.

Coming back to the question of the pin failure during post-irradiation handling, two important points should be noted. Firstly, the martensite formation during the clad deformation occurs more easily when the temperature drops from irradiation one to the room temperature, and hence, a brittle fracture of cladding at room temperature becomes to be more probable. Secondly, during the reactor shut down, thermal stresses in pin claddings arise. The level of thermal stresses are similar to the those in cladding during the reactor start up. But in contrast to the initial period of irradiation, when the thermal stresses can be reduced due to irradiation creep, the thermal stresses arising during the reactor shut down have no possibility to relax. These stresses are added to existing ones and may result in the pin failure in the course of pin handling in hot cells. The experience obtained for specimens cut from pin cladding having a large diametral swelling indicates that the cladding begin to fail in the regions near core midplane and below it. Specimens from upper parts of irradiated pin claddings were cut without any failure.

4 CONCLUSIONS

- 1 From the results of the post-irradiation study of BN-600 reactor fuel pins follows that the largest degradation of pin cladding properties took place in cross-sections of maximal fuel pin diameter increase. In these cross-sections the nil ductility and numerous microcracks at inner cladding surface were observed.
- 2 The factors which lead to a degradation of pin cladding properties (the cladding embrittlement, deterioration of corrosion resistance, the additional stresses formation) are to be related to void swelling in cladding materials as well as to radiation-induced segregation.
- 3 The pin failure during low-load handling in hot cells is caused by internal stresses formed in the pin cladding during irradiation and at a reactor shut-down.

REFERENCES

- [1] BROWN, C, et al, "Cladding and wrapper development for fast breeder reactor high performance" (Proc. of Inter. Conf. on Fast Reactor and Related Fuel Cycles, Kyoto, Japan), (1991), p. 75-1
- [2] GUDREMON, E. Special Steels Moscow, "Metallurgy", (1966)
- [3] KENIK, E. A, et al, "Radiation-induced grain boundary segregation and sensitization of a neutron irradiated austenitic stainless steel" - J. Nucl. Mater., 183 (1991) 145-153

**NEXT PAGE(S)
left BLANK**

P. PUTHIYAVINAYAGAM, S. GOPAL, S.J. WINSTON,
S. GOVINDARAJAN, S.C. CHETAL, S.B. BHOJE

Reactor Group, Indira Gandhi Centre for Atomic Research,
Kalpakkam, India

Abstract

For the 500 MWe Prototype Fast Breeder Reactor (PFBR), 20% CW D9 has been chosen as the material for fuel clad and wrapper. A peak burnup of 100,000 MWd/t is targeted for the fuel. While experimental data on irradiation behaviour of this material will be generated by irradiation in the test reactor FBTR, presently in operation, correlations have been derived from data available in literature for neutron induced void swelling and creep. The derived data has been used in assessing the deformation in hexagonal wrapper and clad and for optimising core restraint system design. This paper presents results of sensitivity studies carried out in respect of the above data. The parameters considered are hexcan dilation, differential deformation between hexcan and pin bundle and core deformation parameters. It is observed that the fluence parameter has the highest influence on the design parameters.

1. INTRODUCTION

The choice of structural materials for the core components of a fast reactor is very important from the point of view of fuel performance and economics. As the core materials work in a hostile environment of high temperature and high neutron irradiation, they should possess good mechanical and radiation resistant properties apart from good physical properties. The choice of suitable materials for clad and wrapper hold the key for high burnup potential of the fuel. Austenitic stainless steels of various grades have been the universal choice for fast reactor core components. Primarily, their moderate to good resistance to fast neutron radiation induced deformation was responsible for its selection. Various grades of austenitic SS have evolved over the past three decades to meet the increasing design demands. The evolution originated from the conventional solution annealed 304/316 to cold worked Ti stabilized/modified varieties to satisfy the ever increasing fuel burnup target. Of late, more attention is being paid to the use of ferritic steel for hexagonal wrapper tubes while it has some limitations for use as fuel clad tubes.

For the 500 MWe, mixed oxide fuelled Indian Prototype Fast Breeder Reactor (PFBR), presently at an advanced stage of design, 20 % CW D9 has been chosen for both fuel clad and wrapper. A peak burnup of 100,000 MWd/t is targeted for the fuel. Analysis of core and fuel subassembly (SA) require data on the behaviour of core materials under the influence of high temperature and high irradiation. Further, detailed fuel pin modelling studies have to be carried out to assess the performance of fuel pin which require data on fuel material apart from the data on structural material. It is planned to get experimental data on irradiation behaviour of the 20 % CW D9 material through in-pile tests in FBTR, a test reactor presently in operation. However, in order to proceed with the design studies and analyses, correlations have been derived for 20 % CW D9 from the data available in open literature for the most important properties such as void swelling and irradiation creep.

In this paper, the attention is focussed only on the core behaviour, fuel SA behaviour and implications of core structural material properties on them. The data derived for 20 % CW D9 have been used in assessing the deformation in hexagonal wrapper and optimising core restraint

system design. Since the data is derived from open literature, some variations are bound to be there and hence studies were conducted to assess the influence of swelling and creep data on some of the important core design parameters. The parameters considered are wrapper dilation, differential deformation between wrapper and pin bundle, core SA deformation due to bowing, and extraction force required for unloading the spent fuel SA. For these studies, computer codes developed in-house are used. This paper presents the results of the studies carried out.

2. DATA FOR STRUCTURAL MATERIAL

The swelling and creep data for 20 % CW D9, either derived/adopted from literature, are presented in this section.

2.1. Void Swelling Data

The general swelling behaviour of austenitic steel is shown in Fig.1. The swelling rate attains a steady state value beyond a point called the incubation fluence and there is a minimum threshold fluence upto which swelling of the material does not occur. This threshold value is dependent on the temperature. Published papers report that the steady state swelling occurs approximately at 2% swelling for D9 material [1]. The steady state swelling rate beyond incubation dose is reported to be approximately 1% per dpa for all austenitic SS materials in several papers [2, 3, 4, 5]. However, French data obtained from Phenix irradiation suggest that this rate is found to be much smaller.

For the D9 material, the correlation for swelling is derived by approximating the swelling curve as forming three linear regions. Between F_{th} (*threshold fluence*) and F_{cu} (*curvature fluence*) it is called the threshold region, between F_{cu} and F_{in} (*incubation fluence*) it is called the curvature region and beyond F_{in} it is called the steady state region. The swelling rate in the respective regions are called *threshold rate* (R_{th}), *curvature rate* (R_{cu}) and *steady state rate* (R_s). The swelling value corresponding to the beginning of curvature region is called *curvature swelling* (S_{cu}). All the parameters are dependent on the temperature of operation. For this study, the parameters assumed at various temperature points are given in Table - I. Swelling of the material at any fluence and temperature is obtained by interpolating these parameters. Swelling at start of steady state region is assumed as 2 %. From table -I, the swelling of D9 material is calculated using the following form of correlation.

$$\% \Delta V/V = A^* + R^* \cdot [F - F^*]$$

where A^* , R^* , F^* are constants denoting the % swelling, rate of swelling and the fluence at the respective regions. 'F' is the actual fluence seen by the material. The above constants are as follows for the different swelling regions.

Region	Threshold region	Curvature region	Steady state region
Parameter			
F^*	F_{th}	F_{cu}	F_{in}
R^*	R_{th}	R_{cu}	R_s
A^*	0.0	S_{cu}	2.0

TABLE I. SWELLING DATA

TEMP °C	F_{th} dpa	F_{cu} dpa	F_n dpa	S_{cu} dpa	R_i %/ dpa	R_{th} %/ dpa	R_{cu} %/ dpa
380	28.20	28.20	28.20	1.070	0.0	0.0	0.0
460	48.75	55.00	64.35	0.660	0.2128	0.1056	0.1433
500	58.80	71.75	81.96	0.451	0.3937	0.0348	0.1517
540	68.78	81.22	90.87	0.482	0.1889	0.0387	0.1574
600	82.40	86.25	93.50	0.530	0.0	0.1218	0.2178

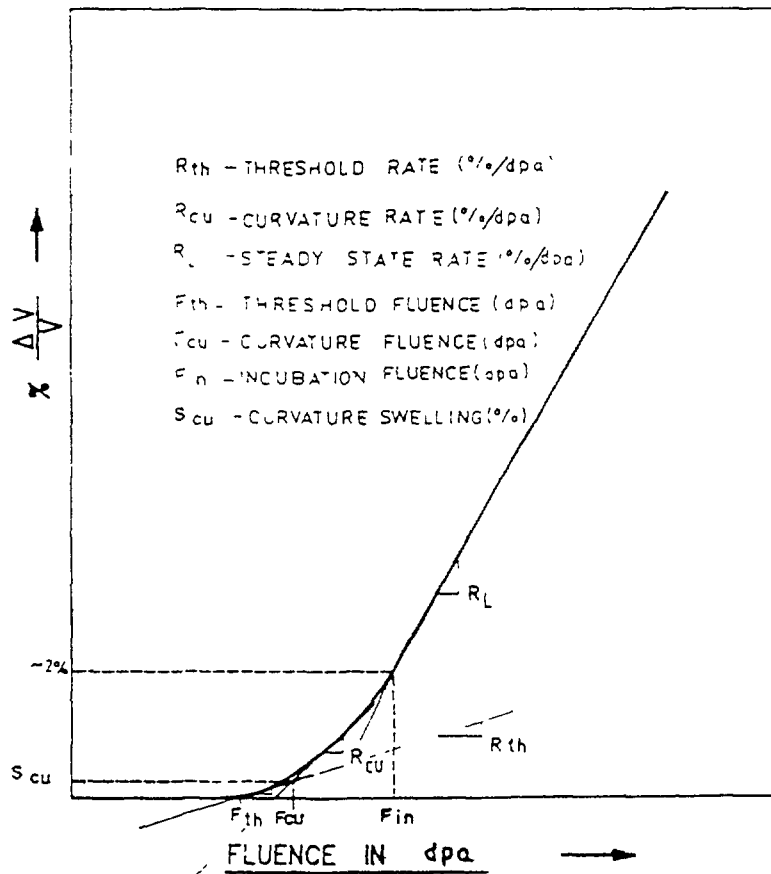
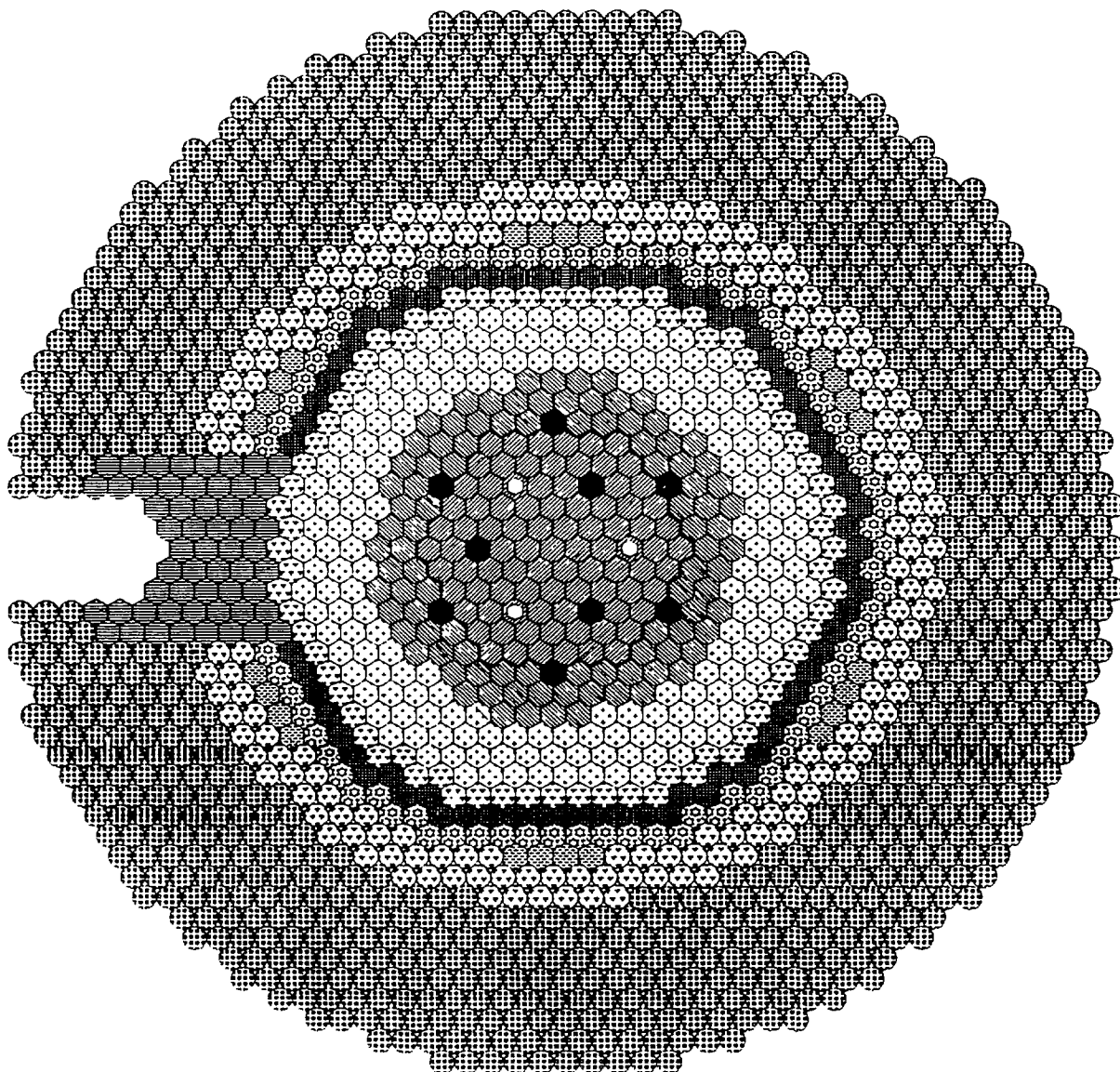


Fig. 1. GENERAL SWELLING BEHAVIOUR OF AUSTENITIC -SS















SYMBOL	TYPE OF SUBASSEMBLY	No.	MASS PER SUBASSY. IN Kg
	FUEL (INNER)	85	245
	FUEL (OUTER)	96	245
	CONTROL & SAFETY ROD	09	200
	DIVERSE SAFETY ROD	03	200
	BLANKET	186	320
	STEEL REFLECTOR (INNER)	72	355
	B ₄ C SHIELDING (INNER)	69	185
	STORAGE LOCATION	75	245
	RESERVE STORAGE LOCATION	24	355
	ENRICHED BORON SHIELDING	56	185
	STEEL SHIELDING (OUTER)	180	330
	B ₄ C SHIELDING (OUTER)	903	265
TOTAL		1758	

Fig. 2. PFBR CORE CONFIGURATION

2.2. Creep Data

French data suggests the following correlation [1] for use in estimating the creep strain of D9 material. While many different correlations are found in literature, the French correlation is found to be simple to use and on comparison with other correlations and reported experimental values, it is found to be conservative. The correlation used for creep strain is as follows.

$$\epsilon = A \sigma^3 \phi t$$

$$\text{where, } A = 3.0 \times 10^{-6}$$

3. DETAILS OF STUDY

The correlations used for swelling and creep are given in the previous section. Since they are derived from literature, there could be variations in their predictions. Any variation in the property alters the core and SA behaviour. A variation of $\pm 20\%$ is imposed on these properties and their component parameters and the analysis is carried out for all possible combinations of them. *The parameters subjected to $\pm 20\%$ variation are creep rate, steady-state swelling rate, threshold fluence and incubation fluence.* No variation is imposed on the other swelling parameters such as curvature swelling, threshold and curvature swelling rates as they are not very important in determining the material swelling. The results of the study are presented in the following sections.

For PFBR core restraint system, naturally restrained core concept is chosen. The core configuration is shown in Fig.2. The fuel SA is of 4500 mm length. Hexagonal outer width across flats of wrapper tube is 131.3 mm. The wrapper thickness is 3.2 mm. The grid plate pitch is 135.0 mm. Fuel SA has one restraint pad at 150 mm above the active core top level. This above core load pad (ACLP) is at an axial level 2450 mm above the top of the grid plate. Inter SA gap at ACLP is 0.3 mm and it is 3.7 mm at the top of SA. The coolant pressure at entry and exit points of pin bundle are 0.6 MPa and 0.2 MPa respectively. The core inlet and outlet temperatures are 670 K and 820 K respectively. The maximum linear power rating of fuel pin is 450 W/cm.

3.1. Wrapper Dilation

The wrapper dilation is calculated using a simple expression derived from an approximate theory [6]. This method is considered adequate for the present purpose. The mathematical expression for the increase in width across flats of wrapper due to swelling and creep dilation is as follows.

$$\Delta W = W_i \chi / (W_i + 5 \chi) + (W_i + 2t) V / 300$$

Here, W_i is the inside width across flats of the wrapper, t is the wrapper thickness and V is the percentage volumetric swelling. χ is given by

$$\chi = 0.00695 \cdot K \cdot P \cdot W_i^4 / t^3$$

where P is the coolant pressure and K is the irradiation induced creep strain for unit stress for given neutron fluence. For all the combinations of swelling and creep parameters as mentioned earlier, the % change in SA maximum dilation from the reference dilation value, corresponding to nominal properties, are given in Table - II. The percentage variation in SA dilation as a function of fluence factor and creep factor are plotted in Fig. 3 and 4 respectively. From the figures it can be seen that, for the same creep rate factor, the threshold fluence and incubation fluence are very sensitive parameters while the steady state swelling rate parameter is less sensitive. For $\pm 20\%$ variation in the fluence parameters, the average range of variation in the maximum dilation is about 50 % whereas it is only about 10 % for the swelling rate parameter. For the same swelling rate parameter, again the fluence parameter is highly sensitive with 48 % variation in dilation whereas the creep rate parameter is moderately sensitive with about 22 % variation.

3.2. Differential Swelling of Clad and Wrapper

The fuel clad and wrapper operate at different temperatures leading to differential swelling in wrapper and pin bundle. As a consequence of differential swelling, the coolant flow through a SA varies for a given pressure drop across the pin bundle over the in-pile residence time of the SA. In case the bundle swells more, another problem of concern will be bundle-wrapper mechanical interaction. In this paper, only the problem of flow variation in the maximum rated fuel SA due to differential swelling between clad and wrapper is considered. In this analysis, the temperature of the coolant is assumed to be uniform across the subassembly. The linear power rating of fuel pin is assumed constant throughout its life. Deformation in clad and wrapper due to thermal expansion, thermal creep and irradiation creep are not accounted for in this study. The general design features of fuel SA are given below.

power from max. rated SA	8.2	MWt
nominal flow through max. rated SA	36.0	kg
pin bundle pressure drop	50	m of Na
max. fast neutron flux	5.33×10^{15}	n/cm ² -s
coolant ΔT through max. rated SA	170	K

The results are presented in Table - III. The variation in coolant flow through the SA is plotted as a function of fluence parameter in Fig.5. The wrapper swelling as a function of fluence factor is plotted in Fig.6. From the results, it is observed that the flow is increasing as a result of differential swelling. With regard to influence of properties, again fluence parameter is seen to be more influential and the swelling rate parameter is marginally less sensitive. For $\pm 20\%$ variation in fluence parameter, the flow variation is about 1 %. The clad swelling varies in the range from 0.7 % to 6 % and wrapper swelling varies in the range from 2.7 % to 8.5 %. Due to swelling rate parameter variation, the flow variation is about 0.3 to 0.5 % and the range of clad swelling is 0.8 - 1.2 % and wrapper swelling is 0.5 - 1.3 %.

3.3. Core deformation

Bowing analysis was performed with the use of 3-D bowing analysis computer code 'MABOW'. This code has been verified and validated against international computer codes under a Co-ordinated Research Program (CRP) of IAEA-IWGFR [7]. The performance parameters considered for the study are maximum SA bowing deflection, deflection at control rod SA position and maximum extraction force required to unload a spent fuel SA. All these values are computed for the target burnup of 100,000 MWd/t. The dose corresponding to this burnup works

TABLE II. % CHANGE IN MAX. SA DILATION

Creep rate factor	Sw. rate factor	Fluence factor	% change in dilation
1.0	1.2	1.2	-21.0
		1.0	4.1
		0.8	37.4
	1.0	1.2	-21.0
		1.0	0.0
		0.8	27.6
	0.8	1.2	-21.0
		1.0	-3.9
		0.8	17.8
0.8	1.0	1.2	-32.2
		1.0	-11.3
		0.8	16.5
1.2	1.0	1.2	-10.5
		1.0	10.6
		0.8	38.1

TABLE III. FLOW VARIATION DUE TO DIFFERENTIAL SWELLING

Sw. rate factor	Fluence factor	% flow variation	wrapper swelling	clad swelling
1.0	0.8	-1.81	8.5	6.04
	1.0	-1.49	4.79	2.22
	1.2	-0.88	2.71	0.766
0.8	0.8	-1.54	7.2	5.23
	1.0	-1.33	4.24	2.18
	1.2	-0.86	2.57	0.766
1.2	0.8	-2.07	9.8	6.85
	1.0	-1.65	5.35	2.26
	1.2	-0.91	2.85	0.766

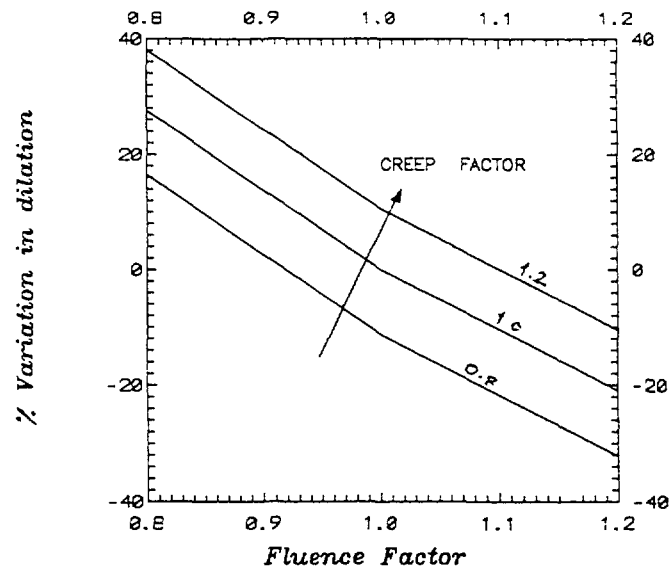


Fig.3: WRAPPER DILATION
(Sw.rate Factor Constant)

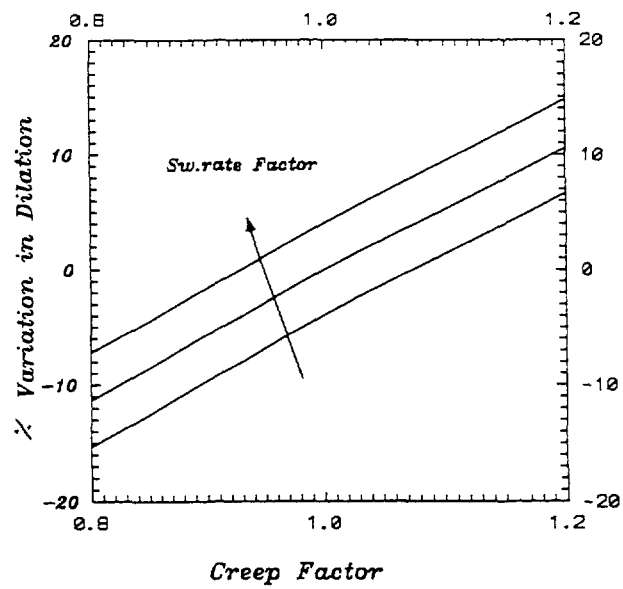


Fig.4 WRAPPER DILATION
(Fluence Factor Constant)

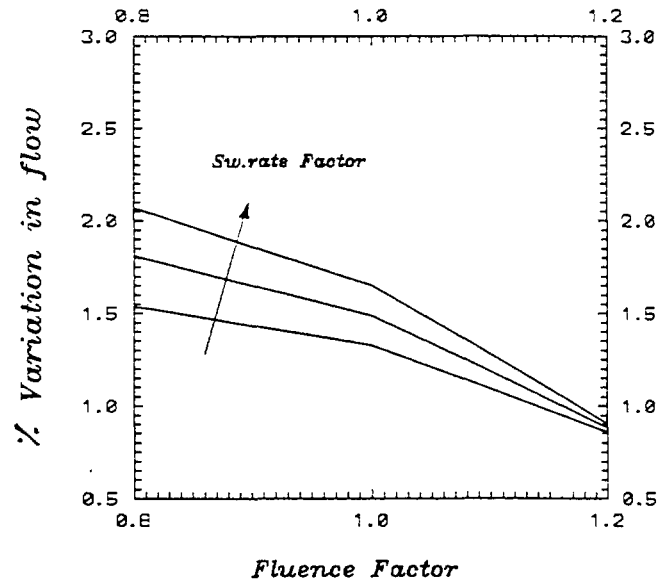


Fig. 5. FLOW VARIATION

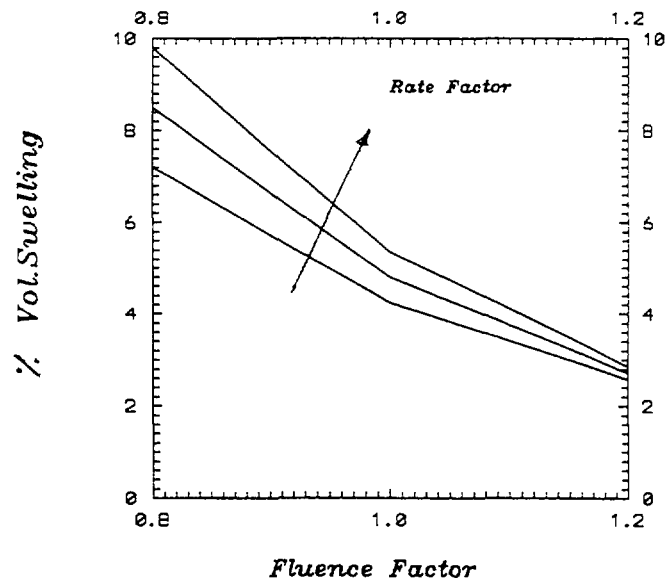


Fig:6 WRAPPER SWELLING

TABLE IV. CORE DEFORMATION

A) *CREEP RATE PARAMETER* = 1.0
SWELLING RATE PARAMETER = 1.0

PARAMETER	FLUENCE PARAMETER			% VARIATION
	0.8	1.0	1.2	
Max.SA defln, mm	21.497	18.115	13.048	18.6 to -28.0
CR defln, mm	15.265	11.199	8.858	36.0 to -21.0
Extrac. force, N	2735	1146	825	139 to -28.0

B) *CREEP RATE PARAMETER* = 1.0
SWELLING RATE PARAMETER = 0.8

PARAMETER	FLUENCE PARAMETER			% VARIATION
	0.8	1.0	1.2	
Max.SA defln, mm	21.082	18.071	13.048	16.7 to -27.8
CR defln, mm	13.733	10.737	8.858	27.9 to -17.5
Extrac. force, N	2602	1137	807	129 to -29.0

C) *CREEP RATE PARAMETER* = 1.0
SWELLING RATE PARAMETER = 1.2

PARAMETER	FLUENCE PARAMETER			% VARIATION
	0.8	1.0	1.2	
Max.SA defln, mm	21.887	18.16	13.048	20.5 to -28.1
CR defln, mm	16.665	11.647	8.858	43.1 to -23.9
Extrac. force, N	2871	1154	836	148 to -27.6

TABLE V. CORE DEFORMATION

A) *CREEP RATE PARAMETER* = 1.0
FLUENCE PARAMETER = 1.0

PARAMETER		SWELLING RATE PARAMETER			AVERAGE % VARIATION
		0.8	1.0	1.2	
Max.SA defln,	mm	18.071	18.115	18.16	0.24
CR defln,	mm	10.737	11.199	11.647	4.0
Extrac. force,	N	1137	1146	1154	0.7

B) *CREEP RATE PARAMETER* = 1.0
FLUENCE PARAMETER = 0.8

PARAMETER		SWELLING RATE PARAMETER			AVERAGE % VARIATION
		0.8	1.0	1.2	
Max.SA defln,	mm	21.082	21.497	21.887	1.8
CR defln,	mm	13.733	15.265	16.665	9.6
Extrac. force,	N	2602	2735	2871	5.0

C) *CREEP RATE PARAMETER* = 1.0
FLUENCE PARAMETER = 1.2

PARAMETER		SWELLING RATE PARAMETER			AVERAGE % VARIATION
		0.8	1.0	1.2	
Max.SA defln,	mm	13.048	13.048	13.048	0.0
CR defln,	mm	8.858	8.858	8.858	0.0
Extrac. force,	N	836	825	836	1.5

TABLE VI. CORE DEFORMATION

A) *SWELLING RATE PARAMETER* = 1.0
FLUENCE PARAMETER = 1.0

PARAMETER		CREEP RATE PARAMETER			AVERAGE % VARIATION
		0.8	1.0	1.2	
Max.SA defln,	mm	18.401	18.115	17.840	1.57
CR defln,	mm	11.384	11.199	11.033	1.65
Extrac. force,	N	1168	1146	1128	1.92

B) *SWELLING RATE PARAMETER* = 1.0
FLUENCE PARAMETER = 0.8

PARAMETER		CREEP RATE PARAMETER			AVERAGE % VARIATION
		0.8	1.0	1.2	
Max.SA defln,	mm	21.994	21.497	20.997	2.3
CR defln,	mm	15.647	15.265	14.953	2.3
Extrac. force,	N	2913	2735	2580	6.15

C) *SWELLING RATE PARAMETER* = 1.0
FLUENCE PARAMETER = 1.2

PARAMETER		CREEP RATE PARAMETER			AVERAGE % VARIATION
		0.8	1.0	1.2	
Max.SA defln,	mm	13.227	13.048	12.911	1.21
CR defln,	mm	8.945	8.858	8.777	0.95
Extrac. force,	N	830	825	810	1.20

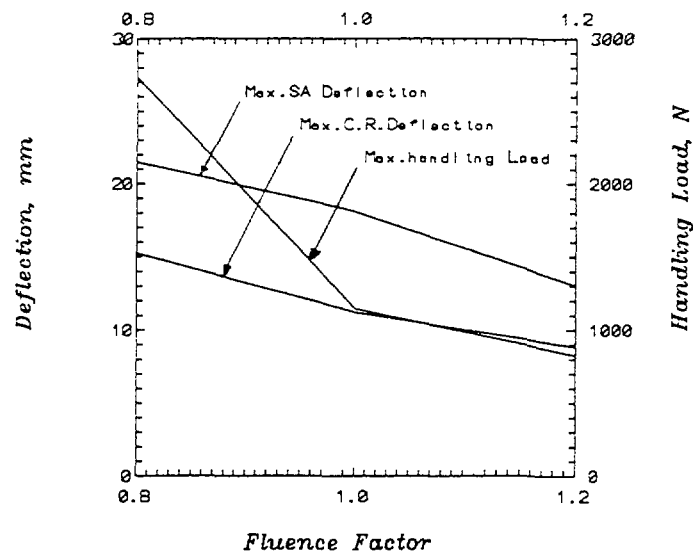


Fig. 7. BOWING PARAMETERS
 (Sw. rate Factor Constant)
 (Creep Factor Constant)

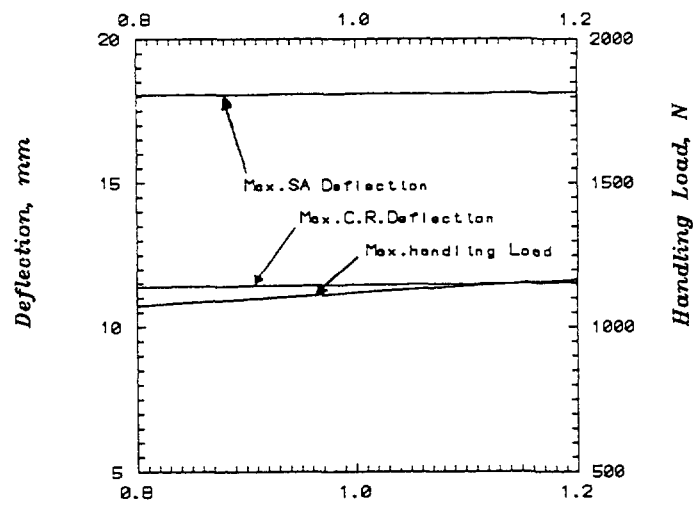


Fig. 8 BOWING PARAMETERS
 (Fluence Factor constant)
 (Creep Factor constant)

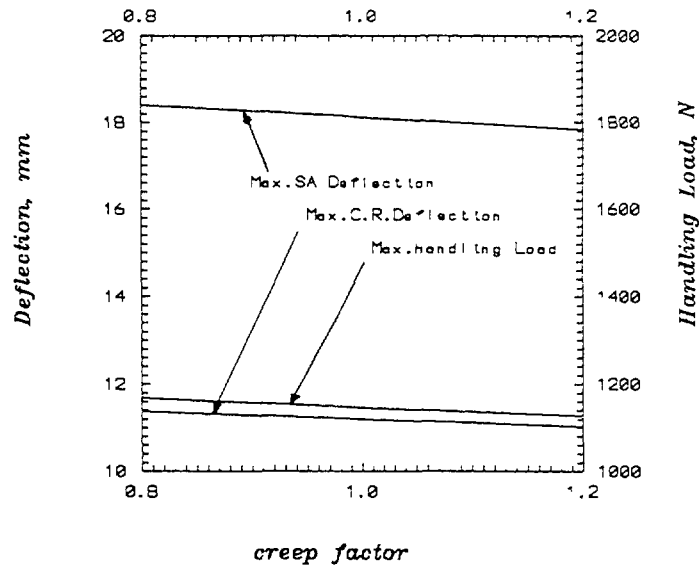


Fig.9 BOWING PARAMETERS
(Rate Factor constant)
(Fluence Factor constant)

out to 80 dpa and the residence time of the maximum rated SA works out to 515 days (EFPD). For this analysis, 60° sector of the core was considered. The results are presented here for various combinations of creep rate, fluence and swelling rate parameters.

For the same nominal creep rate, the performance parameters as a function of fluence parameter are given in Table - IV for various swelling rate parameters. The results for the nominal swelling rate alone are plotted in Fig.7. In this figure, all the bowing performance parameters as a function of fluence parameter are graphically represented.

For the same nominal creep rate, the performance parameters as a function of swelling rate parameter are given in Table - V for various fluence parameters. The results for the nominal fluence parameter alone are plotted in Fig.8.

For the same swelling rate parameter, the performance parameters as a function of creep rate parameter are given in Table - VI for various fluence parameters. The results for the nominal fluence parameter alone are plotted in Fig.9.

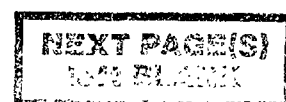
From the results presented it is observed that the fluence parameter has the largest influence compared to swelling rate and creep rate.

4. CONCLUSION

It is observed from the results presented that threshold fluence and incubation fluence are the most important parameters in the structural material swelling behaviour. Steady-state swelling rate parameter and creep rate are found to be comparatively less effective. Analysis of the results with respect to wrapper dilation, differential deformation between clad and wrapper and bowing performance conform to the above mentioned observation. In the in-pile experiments to measure swelling data, more attention should be directed towards fluence parameters. Similarly material development should be in the direction of delaying the onset of swelling.

REFERENCES

- [1] SERAN, et al., Behaviour under neutron irradiation of the 15-15 Ti and EM10 steels used as standard material of the Phenix fuel subassembly, ASTM STP 1125.
- [2] GARNER, BRAGER, The influence of Mo, Si, P, C, Ti, Cr, Zr and various trace elements on the neutron induced swelling of AISI SS 316, JNM 155-157.
- [3] GARNER, BRAGER, Swelling of austenitic Fe-Cr-Ni ternary alloys during fast neutrons irradiation, ASTM-STP-870.
- [4] MAKENAS, Swelling of 20% CW SS 316 fuel pin cladding and ducts, ASTM-STP-870.
- [5] GARNER, et al., Recent insights on the swelling and creep of irradiated austenitic alloys, JNM - 122.
- [6] CHARAK, I. et al., The effect of coolant temperature on estimates of fast reactor inter subassembly spacing, 21 st meeting of AN, New Orleans, Louisiana, June 1975.
- [7] IAEA-IWGFR Co-ordinated Research Program on "Inter comparison of LMFBR Core Mechanics Codes", 1986-1989.





DEVELOPMENT OF MARTENSITIC STEELS FOR HIGH NEUTRON DAMAGE APPLICATIONS

D.S. GELLES*

Battelle Pacific Northwest National Laboratory,
Richland, WA, USA

Presented by F.A. Garner

Abstract

Martensitic stainless steels have been developed for both in-core applications in advanced liquid metal fast breeder reactors (LMFBR) and for first wall and structural materials applications for commercial fusion reactors. It can now be shown that these steels can be expected to maintain properties to levels as high as 175 or 200 dpa, respectively. The 12Cr-1Mo-0.5W-0.2C alloy HT-9 has been extensively tested for LMFBR applications and shown to resist radiation damage, providing a creep and swelling resistant alternative to austenitic steels. Degradation of fracture toughness and Charpy impact properties have been observed, but properties are sufficient to provide reliable service. In comparison, alloys with lower chromium contents are found to decarburize in contact with liquid sodium and are therefore not recommended. Tungsten stabilized martensitic stainless steels have appropriate properties for fusion applications. Radioactivity levels are benign less than 500 years after service, radiation damage resistance is excellent, including impact properties, and swelling is modest. This report describes the history of the development effort.

1. INTRODUCTION

A nuclear energy option has only been available to mankind for one generation; therefore, materials development for nuclear energy applications has been a modern effort. Nuclear energy involves large investments of resources for individual plants and is politically controlled for nuclear non-proliferation reasons, thereby assuring major government involvement, so that sufficient funding has been available to optimize the materials used in these systems within large research and development programs. Many programs have been operated to develop new or improve materials for nuclear reactor systems. The objective of this paper is to describe two of those programs that have been concerned with ferrous metallurgy. The author has been directly involved with both liquid metal fast breeder reactor cladding and duct materials development, and fusion reactor structural materials development. The progress made in both programs is directly pertinent to materials selection for an advanced fast reactor core structure.

* Staff Engineer, Battelle Pacific Northwest National Laboratory, Richland, WA 99352, USA. Battelle Pacific Northwest National Laboratory is operated for the U.S. Department of Energy by Battelle Memorial Institute under Contract DE-AC06-76RLO 1830.

2. REACTOR SYSTEMS

The nuclear reactor systems that have been developed based on fission technology can be classified as a function of cooling system parameters. Coolants have included water, liquid metal, and gas as heat transfer media so that restrictions on operating temperatures were 100 to 250°C, 350 to 700°C, and up to 900°C, respectively. Consequently, ferrous metals were often the materials of choice for water and liquid metal technology, but nickel-based metals and high temperature materials were often required for high temperature gas-cooled reactors. Fusion reactor systems cannot be classified so straightforwardly. System designs are not yet well defined, but several design studies have recommended ferrous metals for structural components based on either water or liquid metal coolant systems, so ferrous metals are also being developed for fusion applications. To provide the basis for discussion of the ferrous alloy development programs associated with the nuclear reactor systems, the reactor systems will first be described with particular emphasis on application of ferrous metallurgy.

2.1 Liquid metal-cooled systems

Several liquid metal-cooled reactors (LMRs) have been built primarily as breeder reactor prototypes, but no commercial design is yet in full-scale production. Reactor systems are generally sodium cooled and use stainless steel fuel cladding, piping, and welded reactor pressure vessels. Some components are fabricated from high nickel alloys for neutronic considerations. However, early operation showed that austenitic stainless steels were susceptible to a form of radiation damage called swelling that resulted in gross dimensional instability in in-core structural components that could limit the life of those components.

2.2 Fusion Reactors

Control of a fusion reaction for power generation is not yet possible. Several design concepts have been proposed, but the physics of controlled fusion power have yet to be demonstrated. Most systems involve control of a high temperature plasma using magnetic fields, so that designs have generally required a structural barrier or first wall to contain the plasma under high vacuum conditions. Most designs have considered either austenitic or martensitic steels for first wall applications, although alternate materials such as vanadium alloys and silicon carbide composites are also under consideration. Materials development for fusion systems has been a world-wide effort. It has been noted that one inherent advantage of fusion in comparison with fission is the relatively short radioactive lifetimes of the reaction products, and the effort has shifted to develop low activation structural materials so that, after reactor decommissioning, waste storage is minimized, and the reactor and its site can be returned to other uses.

3. VOID SWELLING RESISTANCE

Prior to 1974, the undisputed materials choice for LMR structural components was AISI 316, an austenitic stainless steel in the 17% Cr range with 13% Ni and 2% Mo. The choice was based on good high temperature properties, excellent corrosion resistance and ease of fabrication and welding. That choice was first challenged following the observation that AISI 316 developed cavities during neutron irradiation, indicating a volumetric expansion of the material, now called swelling [1]. Swelling and its associated phenomenon, irradiation creep, proved to be the life-limiting factors in the application of AISI 316 for LMR fuel cladding. The discovery that cold working to the level of about 20% delayed the development of swelling [2] allowed interim use of AISI 316. In about 1974, efforts began around the world to find a replacement alloy in order to permit optimization of fast breeder reactor systems [3].

These programs took as their missions the testing of alternative alloys for fast breeder reactor structural applications. The major goal was to reduce the tendency for irradiation induced swelling, but, at the same time, other materials properties such as creep, rupture strength, and postirradiation tensile strength were measured. A wide range of alloys was investigated including austenitic, ferritic and martensitic steels, nickel-based superalloys, and molybdenum- and niobium-based alloys. The primary candidates were titanium-stabilized austenitic steels and precipitation-strengthened superalloys. Martensitic steels were included initially as a low priority option based on observations of swelling inhibition in the ferrite phase of a ferritic/austenitic dual phase steel [4]. The original observation is reproduced in Figure 1. As it became apparent that titanium stabilization only delayed the onset of swelling [5-7] and precipitation strengthening led to severe postirradiation embrittlement [8-9], the suitability of ferritic/martensitic alloys became more apparent.

Ferritic/martensitic alloys are now finding expanded application in fast breeder reactor systems as substitutes for austenitic steels. Two martensitic alloys are of greatest interest in the United States. Sandvik HT-9 is a 12% Cr, 1% Mo, 0.2% C alloy containing intentional additions of W and V. ASTM designation T91 is a modified 9% Cr alloy with 1% Mo, 0.1% C, 0.25% V, 0.1% Nb, 0.05% N. More complete compositional information is given in Table 1. Both alloys were developed for high temperature applications where the corrosion resistance inherent in austenitic stainless steels was not required. The high temperature mechanical properties of these alloys are similar, with the higher carbon and chromium additions of HT-9 balanced by careful control of vanadium, niobium, and carbon additions in T91. However, T91 has inherently better resistance to irradiation embrittlement at about 350°C [10], whereas HT-9 has better corrosion and swelling resistance and provides better resistance to irradiation embrittlement at 60°C [11].

The most significant consequence of these alloy development programs has been the application of HT-9 to most of the internal components in the U.S. experimental liquid metal-cooled test reactor, Fast Flux Test Facility (FFTF) located in Richland, WA [14], and the expected application of similar steels in European plants [15]. For FFTF, both fuel cladding and duct work which contains

the clad fuel have been manufactured from HT-9 by cold tube drawing operations. As the duct geometry requires a hexagonal cross section, manufacture required development of hexagonal drawing operations for a martensitic steel with a ductile-brittle transition temperature (DBTT) at about room temperature. The transition from austenitic to martensitic stainless steel has dictated reduced operating temperatures in FFTF and consequential lowering of the power of the reactor from 400 to 300 MW in return for more efficient fuel cycle performance.

More recently, independent design efforts for the Power Reactor Inherently Safe Module (PRISM) and Sodium Advanced Fast Reactor (SAFR) systems have also recommended the use of HT-9 for in-core structural components [16,17]. In both cases, HT-9 was chosen for in-core structural applications to improve fuel cycle economy. Fuel recycling is anticipated only every 4 years to doses as high as $3.4 \times 10^{23} \text{ n/cm}^2$ ($E > 0.1 \text{ MeV}$) or 170 dpa for PRISM and $3.5 \times 10^{23} \text{ n/cm}^2$ or 175 dpa for SAFR. Austenitic steels are not expected to remain serviceable to such high doses.



Figure 1. Voids in IN-744, a duplex austenite/ferrite alloy showing that void swelling is limited to face centered cubic (F) grains, as originally published by Harkness, Kestel and Okamoto in Reference 4.

Table 1. Chemical Analysis of Martensitic Steels Used for Nuclear Systems in the United States.

Element	Content, wt%	
	HT-9 [12]	T91 [13]
Carbon	0.20	0.08-0.12
Chromium	11.5	8.00-9.50
Molybdenum	1.0	0.85-1.05
Manganese	0.6	0.30-0.60
Silicon	0.4	0.20-0.50
Nickel	0.5	0.40 max
Tungsten	0.5	not spec.
Vanadium	0.3	0.18-0.25
Niobium	not spec.	0.06-0.10
Phosphorus	0.030 max	0.020 max
Sulfur	0.020 max	0.010 max
Aluminum	not spec.	0.04 max
Nitrogen	not spec.	0.030-0.070

4. MATERIALS DEVELOPMENT FOR FUSION

Concurrent with LMR materials development, an effort has evolved to develop materials for fusion reactor applications. There are similarities between the irradiation environments of a fusion first wall and fast reactor in-core components. As a result, development of fusion first wall materials has closely paralleled the LMR effort. Materials development for fusion was initiated in the U.S. in 1978, with similar efforts in Europe and Japan. As originally defined for the U.S. program, materials development concentrated on four classes of materials: austenitic alloys, higher strength Fe-Ni-Cr alloys, refractory/reactive alloys, and innovative concepts [18]. However, in part based on the encouraging results being obtained by the fast reactor effort, a fifth class of ferritic steels was added by late 1979 [19].

Over the last fifteen years, the attractiveness of ferritic steels for first wall applications has steadily increased. A major concern, the effect of extremely high electromagnetic fields on a ferromagnetic structure, was alleviated when it was realized that a ferromagnetic material would behave paramagnetically in an extremely strong electromagnetic field [20-21]. The status of martensitic steels for fusion applications can best be measured based on the recommendations of fusion design studies. The five most recent design studies all seriously consider HT-9 [22-26], ranking it second in comparison either with an austenitic steel or with a vanadium alloy for water-cooled Tokamak designs and, in the case of Tandem Mirror designs, ranking HT-9 first [24] or on a par with a vanadium alloy [25]. These design studies are particularly notable because, for the water-cooled designs (a very inefficient concept), martensitic steels must be operated at temperatures where very little data is available and where the material is not expected to behave well, whereas higher temperature designs will be more efficient and operate in a regime where martensitic steels can be expected to out-perform austenitic steels.

Therefore, martensitic steels have become or are becoming the materials of choice for high neutron damage irradiation environments. In order to reach this status, it has been necessary to compile materials property data bases, including irradiation response. This has been done both for LMRs [27] and for fusion systems [28] applications.

4.1 Low Activation Structural Materials

Laboratories in Japan, Europe, the USSR, and the U.S. are each designing, fabricating, and testing low activation alloys for fusion reactor structural materials that would satisfy regulations for near surface disposal of radioactive waste. A call for development of such alloys in the U.S. originated with the U.S. Department of Energy (DOE) Panel on Low Activation Materials for Fusion Applications [29]. The panel noted that "lower activation materials for fusion reactors are technically possible, may be important to the public acceptance of fusion energy, and should be a main goal of the fusion program." The element additions that must be carefully controlled are Cu, Ni, Mo, Nb, and N, with Nb representing the most severe restriction [30-34]. For near surface disposal of ferritic or martensitic steels, only minor changes in composition appear to be

required, whereas for austenitic steels, a substitute for nickel must be found. Alternately, isotopic tailoring could provide equivalent performance. For example, HT-9, a 12Cr martensitic steel under study for fusion applications, could be made acceptable if Mo additions were isotopically tailored to remove the unwanted isotope ^{92}Mo [35].

The alloy compositions being considered for low activation ferritic or martensitic steels are based on two commercially important alloy classes: 2-1/4Cr steels and the super 9 to 12Cr steels. The former is in fact a bainitic class and the latter a martensitic class. Both of these steels contain Mo at levels of about 1%. Therefore, design of low activation alternatives requires substitution for Mo. Leading candidates are W and V, with consideration given for using Ta as a substitute for Nb. In order to obtain a fully martensitic 12Cr steel without additions of Ni, austenite stabilizing additions must be included. Thus far, Mn and C have been considered. Therefore, three classes of low activation ferritic/martensitic alloys are possible: low chromium bainitic alloys, 7 to 9Cr martensitic alloys, and 12Cr stabilized martensitic alloys. The alloy compositions which have been considered have been published elsewhere [36]. The 7 to 9Cr alloy class and the 12Cr alloy class are about equal in size and the smallest group is the 2Cr range. In each class, each of the alloying approaches have been tried: W substituted for Mo, V substituted for Mo, and small additions of Ta substituted for Nb (except for Ta additions to 2Cr alloys). However, in many cases, the higher Cr alloys were found to be duplex martensitic/delta ferritic and therefore further changes in compositional specification were needed.

Therefore, a broad range of low activation ferritic alloys are possible. Low activation bainitic alloys in the Fe-2Cr composition range, martensitic alloys in the Fe-7 to 9Cr range and stabilized martensitic alloys in the Fe-12Cr range have been successfully fabricated and are undergoing testing on an international level. However, it is found that irradiation significantly degrades the properties of bainitic and stabilized martensitic alloys [36]. Bainitic alloys develop severe hardening due to irradiation-induced precipitation at temperatures below 450°C [36-38] and extreme softening due to carbide coarsening at temperatures above 500°C [36]. Stabilized martensitic alloys which rely on manganese additions to provide a fully martensitic microstructure are embrittled at grain boundaries following irradiation, leading to severe degradation of impact properties. Furthermore, in a fusion environment, transmutation of manganese from iron will occur, producing about 1%Mn following irradiation to 200 dpa [39]. The most promising composition regime appears to be the 7 to 9Cr range with tungsten additions in the 2% range, where high temperature mechanical properties and microstructural stability are retained [36] and impact properties are relatively unaffected by irradiation [36,40,41]. The higher void swelling behavior observed in these alloys is not expected to be a major problem, as demonstrated by recent results to doses of 200 dpa [42-44].

4.2 Issues remaining

Issues remaining before martensitic steel is acceptable for fusion applications are 1) an engineering data base is needed and 2) it must be determined if the consequences of helium generation will be significant.

An international effort has been instituted under International Energy Agency (IEA) auspices to develop an engineering data base for low activation martensitic steels [45]. The IEA Working Group on Ferritic/Martensitic Steels has held a series of meetings to collaborate on testing two 5 ton heats of F82H, a 1 ton heat of JLF-1 and smaller experimental heats similar in composition to JLF-1. The steels were manufactured in Japan and have been made available for international testing. Testing will include material characterization, base property mechanical testing, weld property mechanical testing and the effect of irradiation on mechanical properties. The working group includes representatives from Japan, the European Community, Switzerland and the United States.

Helium will be generated in a fusion machine at a rate which is difficult to simulate with presently available irradiation techniques. A data base has been generated using alloys HT-9 and T91 with intentional nickel additions in order to provide suitable helium levels using a mixed spectrum reactor [46]. The data are presented in Figure 2 showing behavior following irradiation at 50, 300 and 400°C. When interpreted from the point of view of a helium effect, this data base demonstrates, for irradiation at 400°C, that a shift in ductile to brittle transition temperature (DBTT) using Charpy impact testing is on the order of 350°C at helium levels of 400 appm and indicates for levels expected in a fusion device (on the order of 1000 appm He), that the shift in DBTT will be greater than 500°C [47]. If helium has such a strong effect, ferritic alloys cannot be used for fusion applications. However, it is possible to interpret the available data base from a different point of view, that of precipitation hardening due to the presence of nickel [47]. Experiments are in progress intended to provide more understanding on this problem and recent results confirm precipitation hardening due to the presence of nickel [48,49]. However, the effect of helium on mechanical properties is a difficult problem to verify because no facility now exists providing fusion neutrons to adequate doses. The answer to this question may have to await the availability of a 14 MeV neutron source.

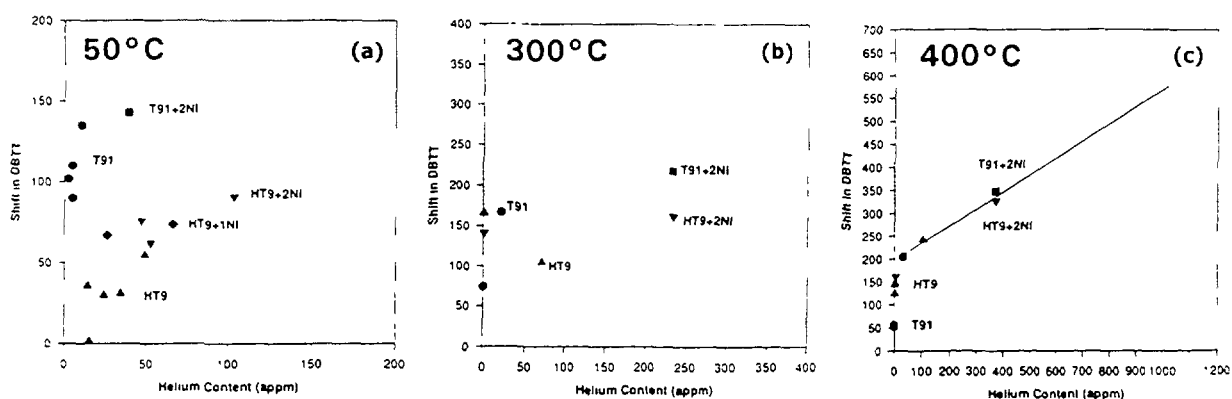


Figure 2. Interpretation of the Ductile-to-Brittle-Transition-Temperature results as a helium effect, for Martensitic steels containing nickel irradiated in HFIR, from reference 47, for irradiation at a) 50°C, b) 300°C and c) 390-400°C.

5. CONCLUSIONS

Martensitic stainless steels have been developed for both in-core applications in advanced liquid metal fast breeder reactors and for first wall and structural materials applications for commercial fusion reactors.

HT-9 has been extensively tested for LMFBR applications and shown to resist radiation damage, providing a creep and swelling resistant alternative to austenitic steels. Degradation of fracture toughness and Charpy impact properties have been observed, but properties are sufficient to provide reliable service. In comparison, alloys with lower chromium contents are found to decarburize in contact with liquid sodium and are therefore not recommended.

Tungsten stabilized martensitic stainless steels have appropriate properties for fusion applications. Radioactivity levels are benign less than 500 years after service, radiation damage resistance is excellent, including impact properties, and swelling is modest.

It can now be shown that these steels can be expected to maintain properties to levels as high as 175 dpa for LMFBR applications or 200 dpa for fusion applications. Efforts on fusion materials development continue in order to provide an engineering data base and to resolve issues concerning helium embrittlement.

These development efforts indicate that use of a tungsten stabilized martensitic steel can be expected to provide an optimum structural material for an advanced fast reactor providing that swelling and liquid metal compatibility are satisfactory.

REFERENCES

- [1] CAWTHORNE C, FULTON EJ, Nature 216 (1967) 515.
- [2] STRAALSUND JL, BRAGER HR, HOLMES JJ, in 'Radiation-Induced Voids in Metals', CONF-710601 (1972) 142.
- [3] See Session 1 in 'Radiation Effects in Breeder Reactor Structural Materials' Metallurgical Society of AIME (New York) 1977.
- [4] HARKNESS SD, KESTEL, BJ OKAMOTO P, IBID 2, 334.
- [5] GARNER FA, BRAGER HR, PUIGH RJ, J Nucl Mater 133&4 (1985) 535.
- [6] SERAN JL, LENAOUR L, GROSJEAN P, HUGON MP, CARTERET Y, MAILLARD A, in 'Effects of Radiation on Materials: 12th International Symposium' ASTM STP 870 (Philadelphia, 1985) 233.
- [7] PUIGH RJ, GARNER FA, in 'Radiation-Induced Changes in Microstructure: 13th International Symposium' (Part 1) ASTM STP 955 (Philadelphia, 1987) 154.
- [8] BAJAJ R, et al, in 'Effects of Radiation on Materials: 10th Conference', ASTM STP 725 (Philadelphia, 1981) 326.
- [9] YANG WJS, GELLES DS, STRAALSUND JL, BAJAJ R, J Nucl Mater 132 (1985) 249.

- [10] HU WL, GELLES DS, in IBID 7, 83.
- [11] W. L. HU WL, AND D. S. GELLES DS, in 'Effects of Radiation on Materials: 14th International Symposium', V 2, ASTM STP 1046 (Philadelphia, 1990) 453.
- [12] Sandvik HT-9 data sheet S-1,720-ENG, May 1981.
- [13] SIKKA VK, in 'Proceedings of Topical Conference on Ferritic Alloys for use in Nuclear Energy Technologies', Metallurgical Society of AIME (New York, 1984) 317.
- [14] LOVELL AJ, FOX AL, SUTHERLAND WH, HECHT SL, in 'International Conference on Reliable Fuels for Liquid Metal Reactors', ANS (1987) 3-25.
- [15] BAGLEY KQ, LITTLE EA, LEVY V, ALAMO A, EHRICH K, ANDERKO K, CALZA BINI A, in 'Materials for Nuclear Reactor Core Applications', Vol. 2, BNES (London, 1988) 37.
- [16] TIPPETS FE, SALERNO LN, BOARDMAN CE, KWANT W, MURATA RE, SNYDER CR, Proc Amer Power Council, 49 (1987) 874-883 or Vaidyanathan S, Murata RE, ibid Ref. 32, 1-43.
- [17] BOST DS, FELTEN LD, ibid Ref. 32, 1-61.
- [18] 'The Fusion Reactor Materials Program Plan', Section 1, Alloy Development for Irradiation Performance, DOE/ET-0032/1, July 1978.
- [19] 'Alloy Development for Irradiation Performance Quarterly Progress Reports' beginning with the period ending December 31, 1979, DOE/ER-0045/1-16.
- [20] ROSENWASSER SN, MILLER P, DALESSANDRO JA, RAWLS JM, TOFFOLO WE, CHEN W, J Nucl Mater 85-6 (1979) 177.
- [21] ATTAYA H, KULCINSKI GL, WOLFER WG, J Nucl Mater 122-3 (1984) 96.
- [22] 'Starfire, A Commercial Tokamak Fusion Power Plant Study', ANL/FPP-80-1, V1, (1980) 10-232.
- [23] 'A Demonstration Tokamak Power Plant Study', ANL/Fpp/82-1, (1982) 2-3.
- [24] 'MARS Mirror Advanced Reactor Study Final Report', Volume 1-B, UCRL-53480, (1984) 12-9.
- [25] 'Blanket Comparison and Selection Study', Final Report, ANL/FPP-84-1 (1984) 7.3.
- [26] 'Modeling, Analysis & Experiments for Fusion Nuclear Technology', FNT Progress Report: Modeling and FINESSE (1987) 1021.
- [27] STRAALSUND JL, AND GELLES DS, oral presentation, ibid 13, HEDL-SA-2771, May 1983.
- [28] GELLES DS, J Nucl Mater 149 (1987) 192.
- [29] 'Report of the DOE Panel on Low Activation Materials for Fusion Applications', Conn RW, Panel Chairman, UCLA/PPG-728, June 1983.
- [30] DORAN DG, ROWCLIFFE AF, MANN FM, J Nucl Mater 141-3 (1986) 1074.
- [31] JARVIS ON, 'Low-Activity Materials Reuse and Disposal', AERE - R 10860, (1983).
- [32] PONTI C, Fusion Tech 13 (1988) 157.
- [33] BUTTERWORTH GJ, GIANCARLI L, J Nucl Mater 155-7 (1988) 575.
- [34] EHRICH K, CIERJACKS SW, KELZENBERG S, MÖSLANG A, in 'Effects of Radiation on Materials: 17th International Symposium', ASTM STP 1270 (W. Conshohocken, 1996) 1109.
- [35] GORDON JD, THOMSON JJ, SUCHARD SN, 'Isotopically Tailored HT-9 Steel for Radioactive Waste Management', TRW-FRE-001, (1983).
- [36] GELLES DS, in 'Reduced Activation Materials for Fusion Reactors', ASTM STP 1047, (Philadelphia, 1990) 113.

- [37] KLUEH RL, MAZIASZ PJ, in IBID 36, 140.
- [38] KOHYAMA A, in 'The Proceedings of the IEA Working Group Meeting on Ferritic/Martensitic Steels', ORNL/M-3777 (1994).
- [39] MANN FM, "Transmutation of Alloys in MFE Facilities as Calculated by REAC", HEDL-TME 81-37, August 1982.
- [40] KLUEH RL, ALEXANDER DJ, J Nucl Mater 233-237 (1996) 336.
- [41] RIETH M, "Irradiation Project MANITU, Results of first 0.8 dpa irradiation," presented at the IEA Working Group Meeting on Ferritic Steels, Baden, Switzerland, 19-20 September 1995, and in J Nucl Mater 233-237 (1996) 351.
- [42] GELLES DS, J Nucl Mater 212-5 (1994) 714.
- [43] GELLES DS, J Nucl Mater 225 (1995) 163.
- [44] GELLES DS, IBID 40.
- [45] KOHYAMA A, et al., IBID 40.
- [46] KLUEH RL, ALEXANDER DJ, J Nucl Mater 218 (1995) 151.
- [47] GELLES DS, J Nucl Mater 230 (1996) 187.
- [48] GELLES DS, to be published in the proceedings 'Effects of Radiation on Materials: 18th International Symposium' in ASTM STP 1325 and abbreviated in 'Fusion Materials DOE/ER-0313/ 20.
- [49] GELLES DS, HANKIN, GL AND HAMILTON, ML, to be published in the Proceedings of the International Workshop on Defect Production, Accumulation & Materials Performance, in J Nucl Mater.



IRRADIATION CREEP OF AUSTENITIC STEELS IRRADIATED UP TO HIGH FLUENCE IN THE BOR-60 REACTOR

V.S. NEUSTROEV, V.K. SHAMARDIN
SSC RF Research Institute of Atomic Reactors,
Dimitrovgrad, Russian Federation

Abstract

This gas-pressurized tube experiment was conducted in Row 6 of the BOR-60 reactor. The rate of damage dose was varied with the height of specimen from 3 to $6 \cdot 10^{-7}$ dpa/sec. During 11 years of irradiation the maximum neutron fluence was $21.8 \cdot 10^{26} \text{ m}^{-2}$ $E > 0.1 \text{ MeV}$ (100 dpa). Each tube was 200 mm long, 6.0 or 6.9 mm inner diameter and 0.3 or 0.4 mm thick. It was specified seven values of stress varied from 0 to 320 MPa at irradiation temperature -420°C . During reloading the tubes were taken out of the reactor to measure their deformation.

The swelling rate of nondepressurized specimens on the basis of 16Cr-15Ni-3Mo-Nb steel was decreased with increasing the carbon and boron content under irradiation up to fluence $21.8 \cdot 10^{26} \text{ m}^{-2}$ ($E > 0.1 \text{ MeV}$) at temperature 420°C .

The rate of irradiation creep on investigated steels was rather exactly defined by the equation $\varepsilon/\sigma = B(\sigma) = B_0 + D \cdot S$, at the values of B_0 and D coefficients $1 \cdot 10^{-6} (\text{MPa} \cdot \text{dpa})^{-1}$ and $(0.3-1.02) \cdot 10^{-2} \text{ MPa}^{-1}$, respectively. The coefficients are in well agreement with similar coefficients of another steels attributed to austenitic type.

1. INTRODUCTION

Most investigations of irradiation-induced creep on steels and its interrelation with swelling was studied with gas-pressurized tubes made of non-stabilized or titanium-stabilized Type AISI 316, AISI 304L, PCA austenitic steels [1-4, 8-12, 14, 15]. All efforts of our investigators were focused on the study of creep in niobium-stabilized austenitic steels [5-17, 13, 16].

The present work highlights the analysis of creep and its interrelation with swelling of 16Cr-15Ni-3Mo-Nb austenitic steels specified by carbon and boron content irradiated up to high neutron fluences in the BOR-60 reactor.

2. EXPERIMENTAL DETAILS

This gas-pressurized tube experiment was conducted in Row 6 of the BOR-60 reactor. The rate of damage dose was varied with the height of specimen from 3 to $6 \cdot 10^{-7}$ dpa/sec. During 11 years of irradiation the maximum neutron fluence was $21.8 \cdot 10^{26} \text{ m}^{-2}$ $E > 0.1 \text{ MeV}$ (100 dpa). Each tube was 200 mm long, 6.0 or 6.9 mm inner diameter and 0.3 or 0.4 mm thick. It was specified seven values of stress varied from 0 to 320 MPa at irradiation temperature -420°C . During reloading the tubes were taken out of the reactor to measure their deformation. The analysis of deformation kinetics against dose of gas-pressurized specimens was carried out on the basis of 16Cr-15Ni-3Mo-Nb-B steel (Tab.1).

Table 1

Chemical composition of annealed austenitic steel, mass %

Type	C	Cr	Ni	Mn	Mo	Si	Nb	P	S	B
0.046C-16Cr-15Ni-3Mo-Nb	0.046	15.8	15.3	0.54	2.8	0.43	0.6	0.012	0.009	-
0.06C-16Cr-15Ni-3Mo-Nb-B	0.06	15.6	15.0	0.65	2.6	0.36	0.84	0.01	0.010	0.006
0.006C-16Cr-15Ni-3Mo-Nb	0.006	15.5	15.2	0.5	2.5	0.32	0.65	0.008	0.006	-

The finale heat treatment of all steels was vacuum austenization at 1100 °C. In measurement of diameter the error was ± 0.01 mm. Some results of steel investigation at less neutron fluence were given in earlier works [13, 16].

3. RESULTS

Figure 1 and 2 shows the dependence of maximum complete deformation in 0.046C-16Cr-15Ni-3Mo-Nb and 0.006C-16Cr-15Ni-3Mo-Nb steels on fast neutron fluence and stress. In this case the maximum complete deformation is responsible for irradiation swelling and creep. As a rule, the deformation dependence of steels on neutron fluence is linear. The deformation creep of steel specimens irradiated up to neutron fluence of $21.8 \cdot 10^{26} \text{ m}^{-2}$ ($E > 0.1$ MeV) at 420 °C does not practically dependent on carbon content. Creep-stress dependence was shown to have some anomaly along with usual deformation increasing with growing of stress. There was observed some decreasing of the creep deformation with increasing stress in the intermediate range (100-150 MPa) at 140 MPa for Type 0.046C-16Cr-15Ni-3Mo-Nb and at 120 MPa for Type 0.006C-16Cr-15Ni-3Mo-Nb, respectively (Fig.2).

The creep-stress dependence on fluence for three steels different in carbon and boron content are presented in Fig.3. The deformation of boron-containing steel 0.06C-16Cr-15Ni-3Mo-Nb-B is considerably less than that of two steels (0.046C-16Cr-15Ni-3Mo-Nb and 0.006C-16Cr-15Ni-3Mo-Nb) available the different carbon content.

The swelling-fluence dependence was also obtained for three steels when studying the specimens without stress (Fig.4). The rate of swelling for specimen without stress at temperature 420 °C is follows:

0.012 %/dpa (Type 0.06C-16Cr-15Ni-3Mo-Nb-B),
 0.034 %/dpa (Type 0.046C-16Cr-15Ni-3Mo-Nb).
 0.052 %/dpa (Type 0.006C-16Cr-15Ni-3Mo-Nb).

4. DISCUSSION

In study of irradiation-induced creep in the temperature range of swelling, the pressurized deformation of specimens is usually is defined by an equation of the form

$$\varepsilon/\sigma = B(\sigma) = B_0 + D^*S, \quad (1)$$

where ε - unsteady state (current) creep,
 σ - effective stress ($\sigma = \sqrt{3}/2 \sigma_0$),
 $B(\sigma)$ - unsteady state (current) creep coefficient,
 B_0 - swelling independent creep coefficient,
 D - pair coefficient of swelling and creep correlation.
 S - current swelling rate [1-4, 8-12, 16].

The results of creep for the austenitic type of steels showed that the creep process is defined by the equation (1) available poorly changed coefficients B_0 and D in spite of complex character of variation in the current creep coefficient with fluence [8,14]. For example, for the austenitic type of steels the coefficient B_0 is equal to about $1 \cdot 10^{-6} \text{ (MPa} \cdot \text{dpa)}^{-1}$, while the coefficient D is changing in the interval $(0.6-1.0) \cdot 10^{-2} \text{ MPa}^{-1}$.

The measurement of deformation creep on steels allowed to plot the creep module as a factor of fluence (Fig.5-7). One can see that the averaged module value is equal to about $1 \cdot 10^{-6}$ (MPa*dpa)⁻¹ at zero fluence and the range of stress from 80 to 160 MPa for all three steels. However at neutron fluence $1.55 \cdot 10^{26}$ m⁻² when the swelling rate is steel equal to zero, the creep module B_0 for different steel is equal to:

0.06C-16Cr-15Ni-3Mo-Nb-B - $1.0 \cdot 10^{-6}$ (MPa*dpa)⁻¹ (at 136 MPa),
 0.046C-16Cr-15Ni-3Mo-Nb - $1.7 \cdot 10^{-6}$ (MPa*dpa)⁻¹ (at 80-160 MPa),
 0.006C-16Cr-15Ni-3Mo-Nb - $1.4 \cdot 10^{-6}$ (MPa*dpa)⁻¹ (at 80-160 MPa).

Particular emphasis should be placed upon the dependence of creep modules of 0.046C-16Cr-15Ni-3Mo-Nb and 0.006C-16Cr-15Ni-3Mo-Nb steel on neutron fluence in the beginning part (Fig.6). At the first moment of irradiation the creep module is rather high in steels of different carbon content at the high stress value 320 MPa, the steel with larger carbon content is specified by the more high module. With increasing of fluence the module decreases reaching the values specific to other stresses. The low values of initial yield limit for steel free of boron and high relative stress result in high creep module in the beginning of irradiation. At high stress there is observed a fast rebuilding of dislocation structure, sharp increase of dislocation concentration and material strengthening. After the neutron fluence $9 \cdot 10^{26} \text{ m}^{-2}$ the characteristics of strength became uniform in specimens with the different stress and for this reason the modules of creep take the closely spaced values.

The obtained results of the creep modulus allow us to determine the coefficients of pair correlation of swelling and creep D. For steels it became equal to:

0.06C-16Cr-15Ni-3Mo-Nb-B - $1.02 \cdot 10^{-2} \text{ MPa}^{-1}$ (136 MPa)
 0.046C-16Cr-15Ni-3Mo-Nb - $0.47 \cdot 10^{-2} \text{ MPa}^{-1}$ (140 MPa)
 and $0.65 \cdot 10^{-2} \text{ MPa}^{-1}$ (80-160 MPa),
 0.006C-16Cr-15Ni-3Mo-Nb - $0.33 \cdot 10^{-2} \text{ MPa}^{-1}$ (140 MPa)
 and $0.44 \cdot 10^{-2} \text{ MPa}^{-1}$ (80-160 MPa).

The values of coefficients Bo and D obtained for BOR-60 reactor irradiated steels on the basis of 16Cr-15Ni-3Mo-Nb with different carbon and boron content $(0.33-1.02) \cdot 10^{-2} \text{ MPa}^{-1}$ were seen to be in well agreement with the coefficients determined for Type AISI 316, AISI 304L, PCA austenitic steels in the various structural compositions [8-12, 14,15].

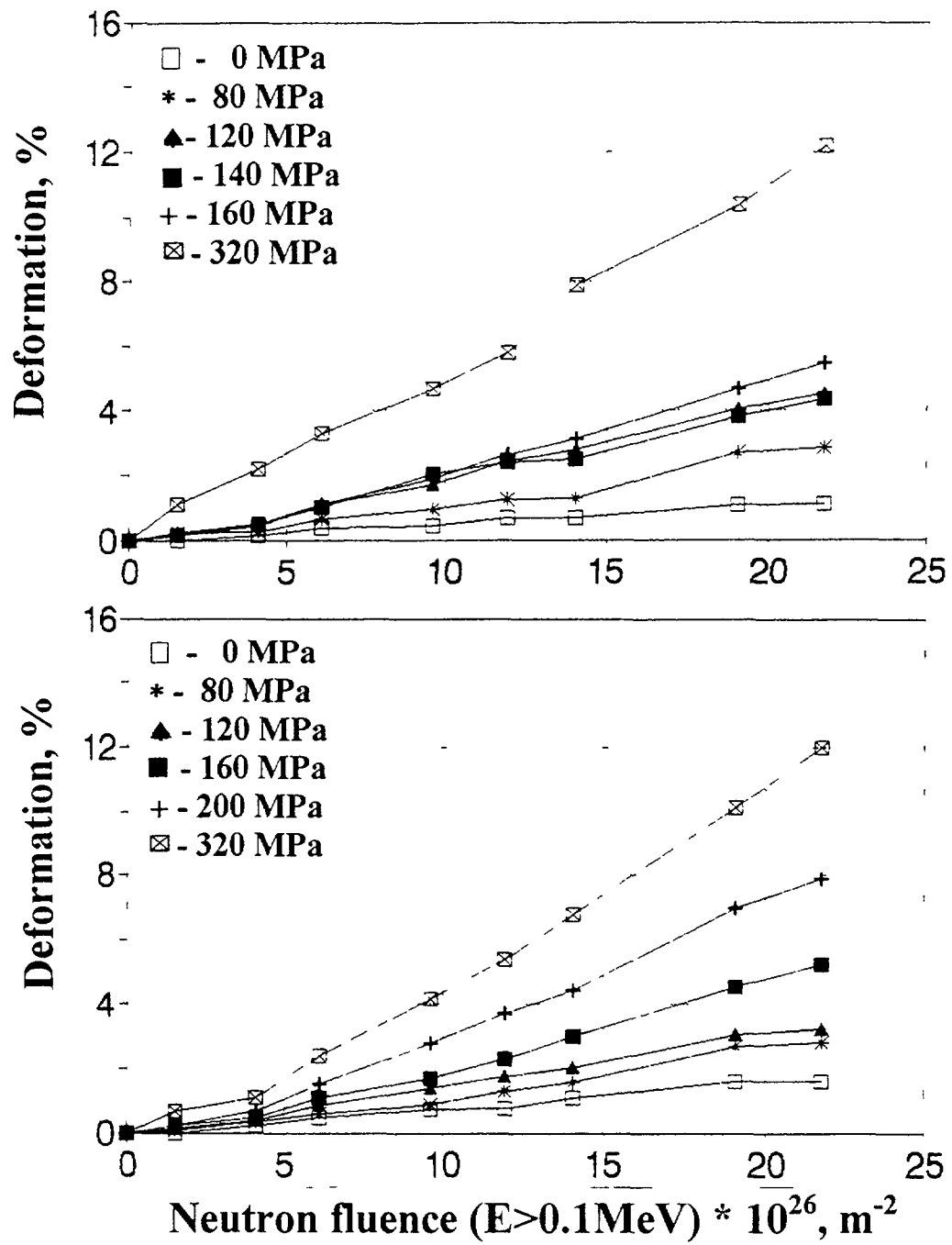


Fig 1 Creep deformation on austenized steels 0 046C-16Cr-15Ni-3Mo-Nb (a) and 0 006C-16Cr-15Ni-3Mo-Nb (b) as a function of fast neutron fluence

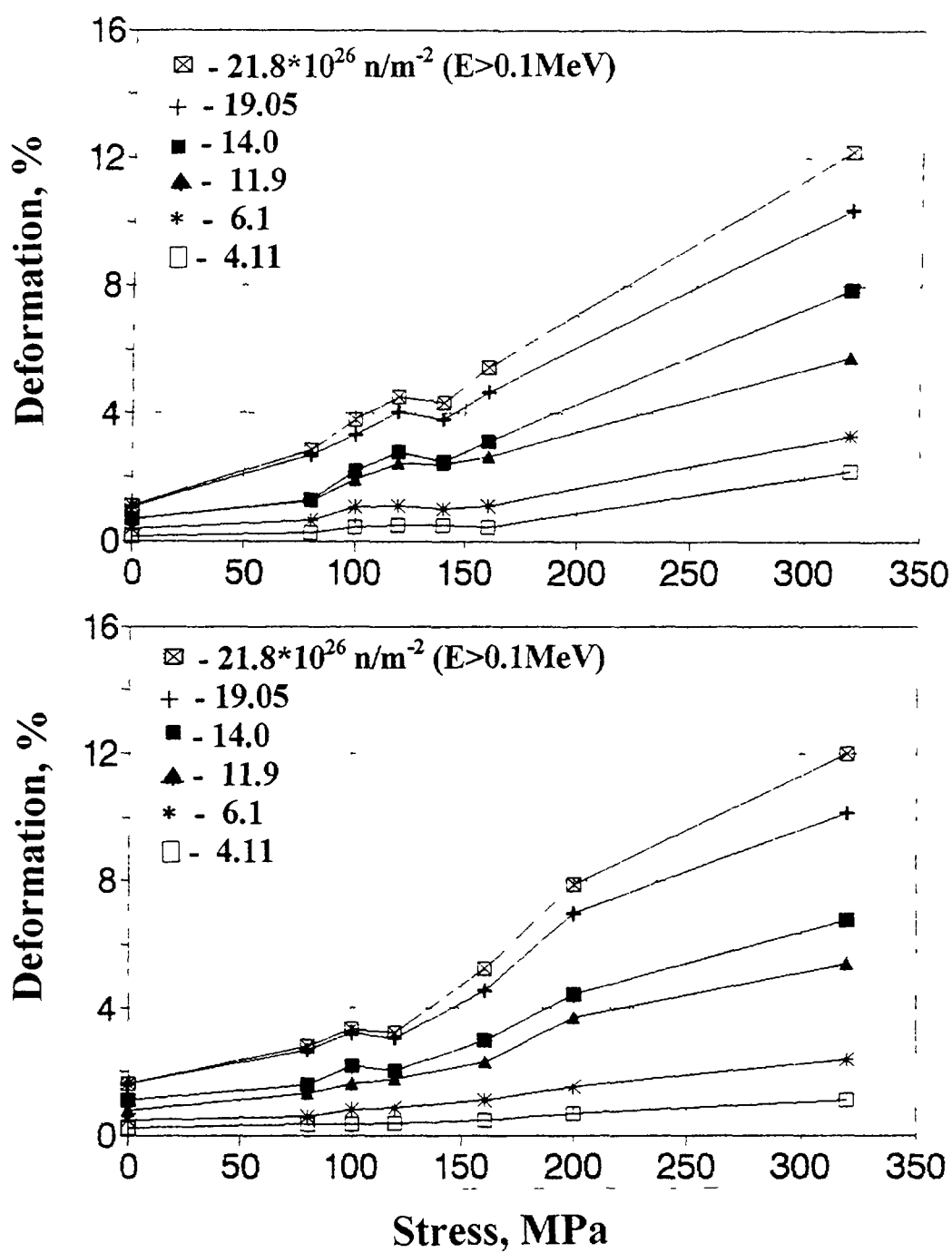


Fig.2 Creep deformation on austenized steels 0.046C-16Cr-15Ni-3Mo-Nb (a) and 0.006C-16Cr-15Ni-3Mo-Nb (b) as a function of stresses

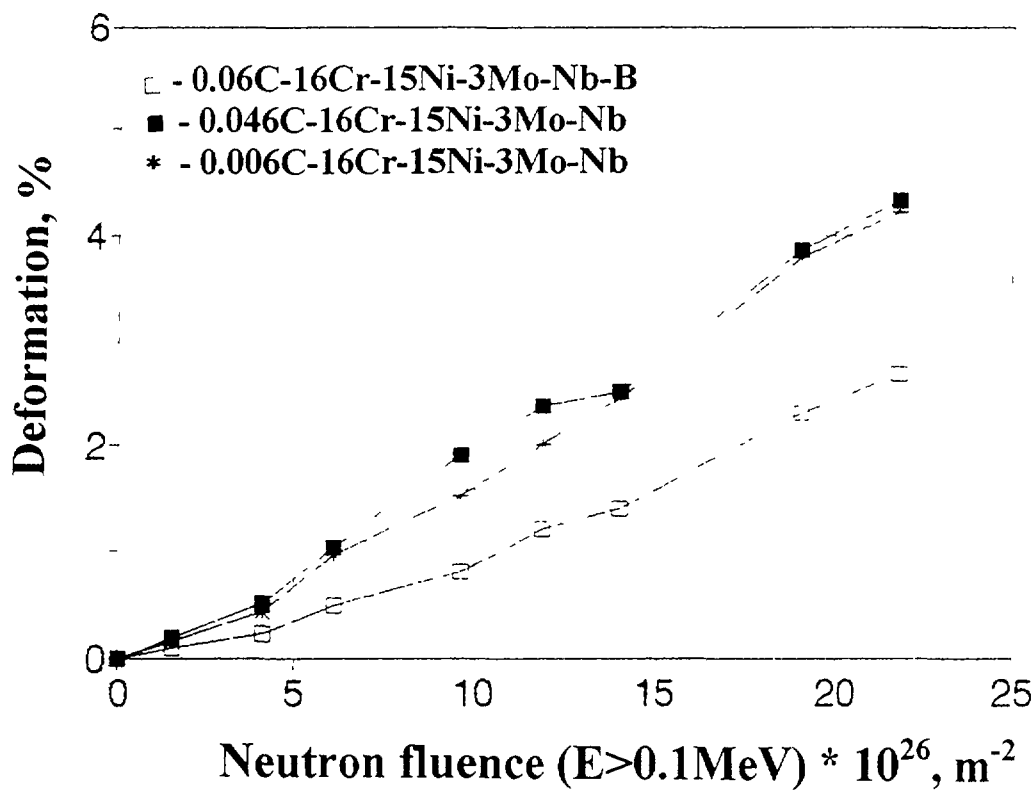


Fig.3 Creep deformation of austenized steels on the base of 16Cr-15Ni-3Mo-Nb against fast neutron fluence.

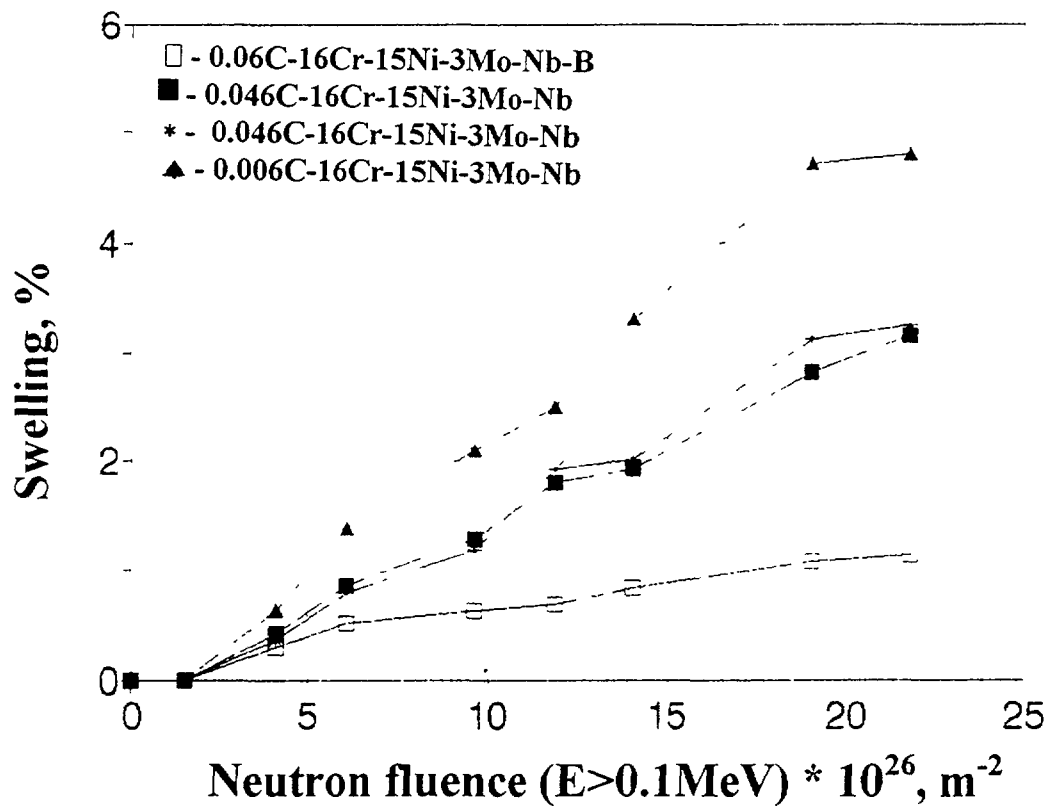


Fig.4. Swelling of austenized steels on the base of 16Cr-15Ni-3Mo-Nb against fast neutron fluence

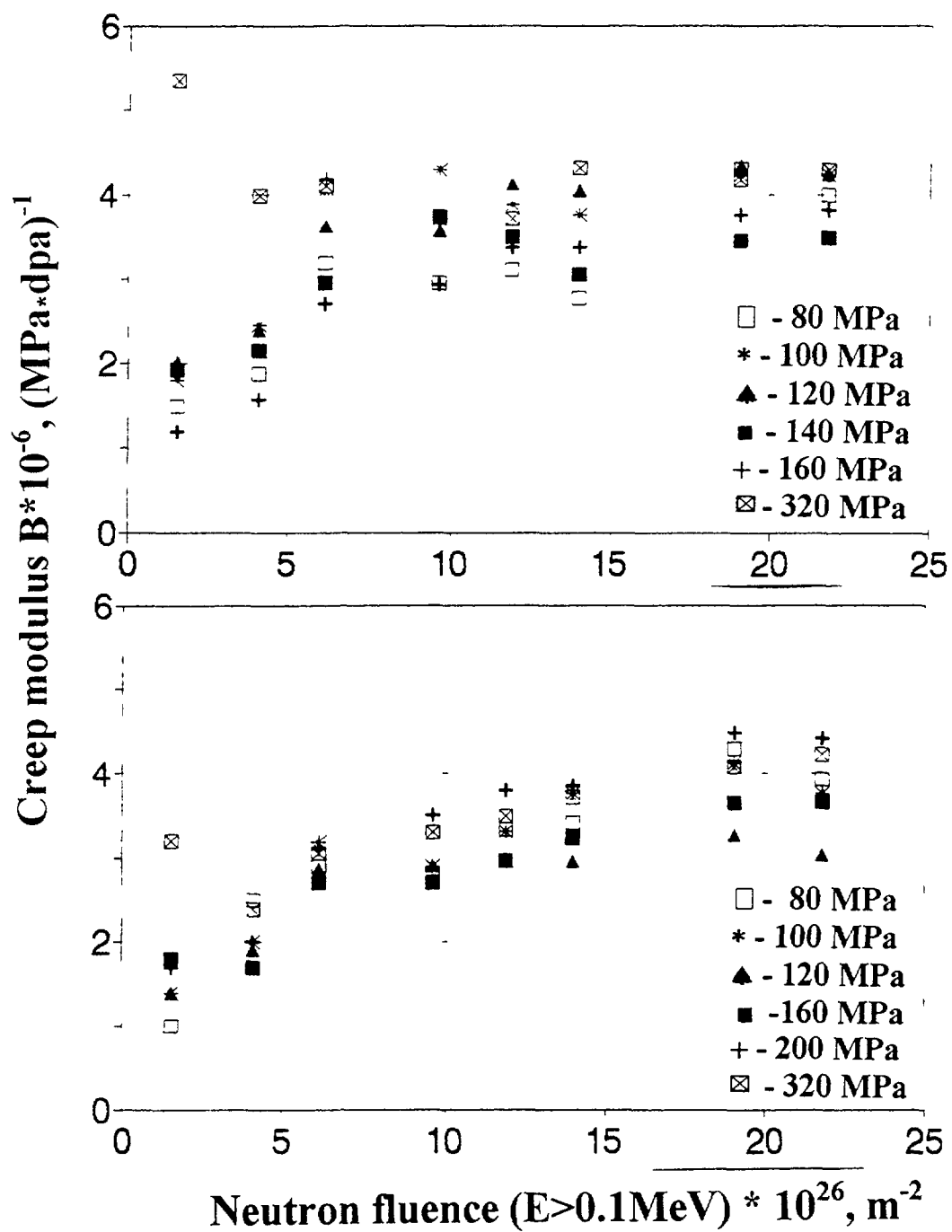


Fig 5 Creep modulus of austenized steels 0 046C-16Cr-15Ni-3Mo-Nb (a) and 0 006C-16Cr-15Ni-3Mo-Nb (b) as a function of fast neutron fluence

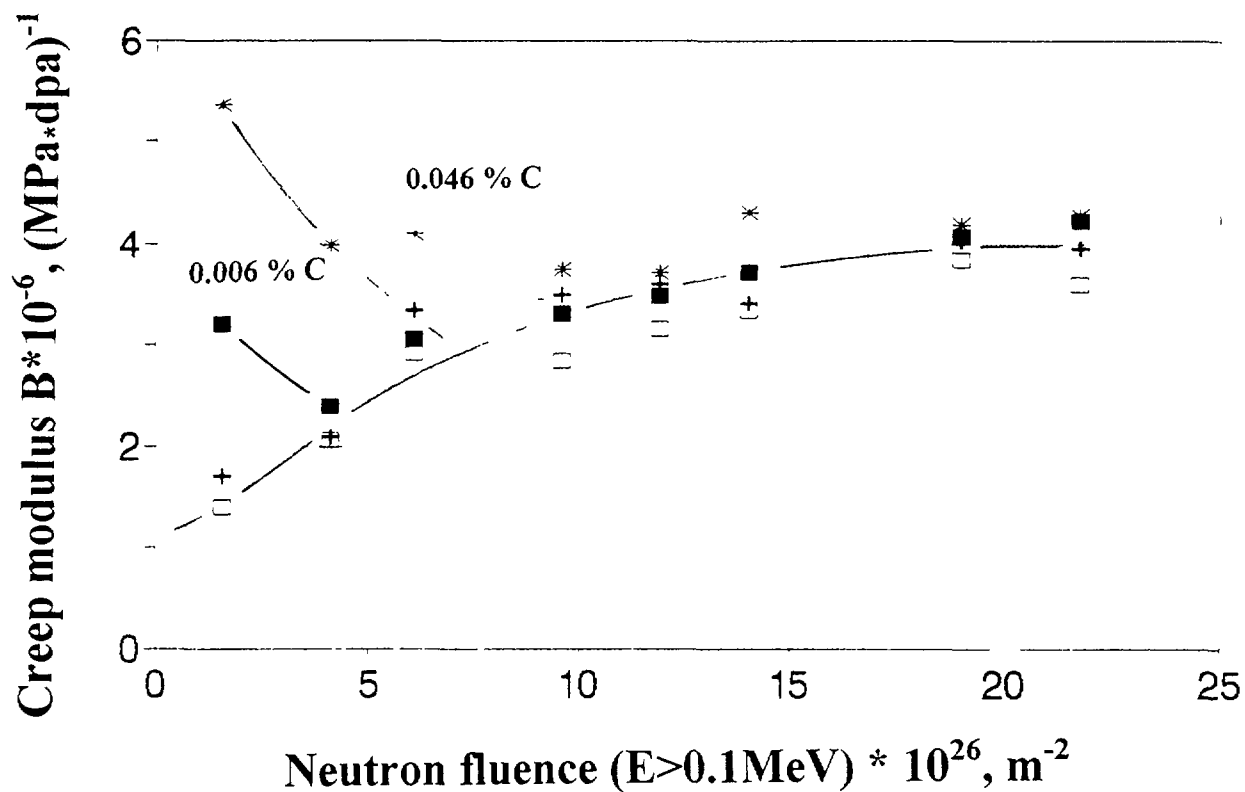


Fig 6 Creep modulus of austenized steels 0.046C-16Cr-15Ni-3Mo-Nb (+ и *) and 0.006C-16Cr-15Ni-3Mo-Nb (□ и ■) as a function of fast neutron fluence at various stresses.

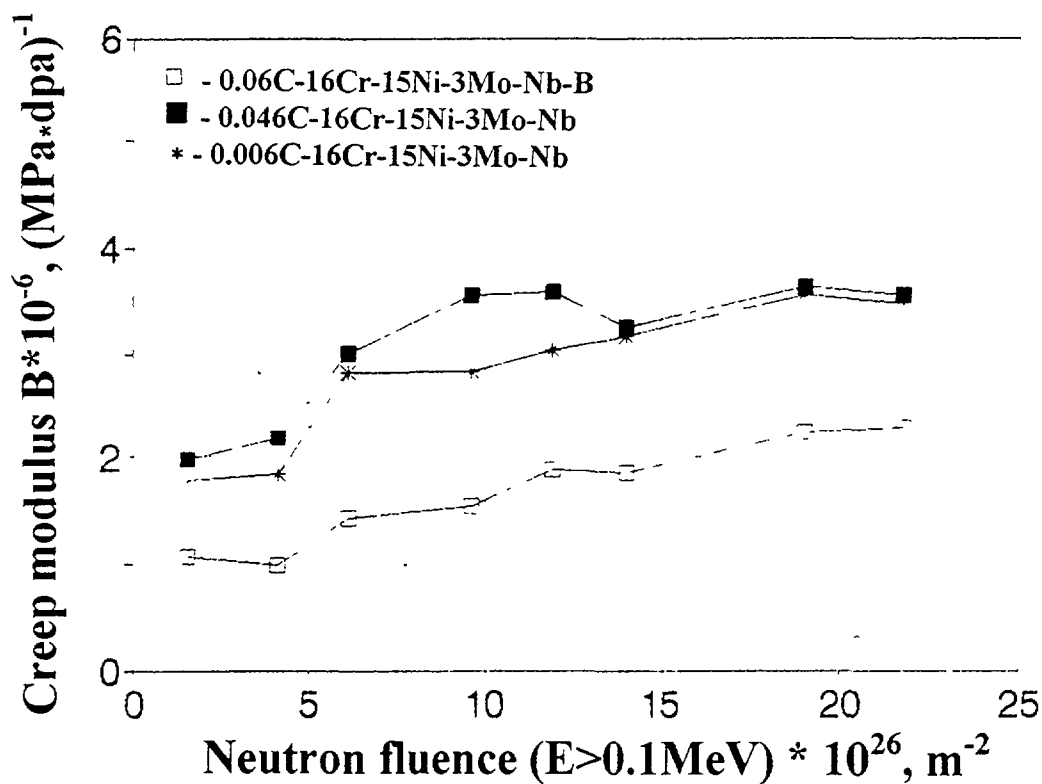


Fig.7. Creep modulus of austenized steels on the base of 16Cr-15Ni-3Mo-Nb different with carbon and boron content as a function of fast neutrons

5. CONCLUSION

On the beginning stage of specimens irradiation with high stress and low initial strength it was observed the abnormal increasing of the creep module against the content of carbon.

The swelling rate of nondepressurized specimens on the basis of 16Cr -15Ni -3Mo-Nb steel was decreased with increasing the carbon and boron content under irradiation up to fluence $21.8 \cdot 10^{26} \text{ m}^{-2}$ ($E > 0.1 \text{ MeV}$) at temperature 420°C .

The rate of irradiation creep on investigated steels was rather exactly defined by the equation (1) at the values of B_0 and D coefficients $1 \cdot 10^{-6} (\text{MPa} \cdot \text{dpa})^{-1}$ and $(0.3-1.02) \cdot 10^{-2} \text{ MPa}^{-1}$, respectively. The coefficients are in well agreement with similar coefficients of another steels attributed to austenitic type.

REFERENCES

- [1] EHRLIH K. Irradiation creep and interrelation with swelling in austenitic stainless steels. /Journal of Nuclear Materials, 1981, v.100, pp.149-153.
- [2] J.P.FOSTER, W.G.WOLFER, A.BIANCHERIA AND A.BOLTAX, in Proceedings European Conference on Irradiation Embrittlement and Creep in Fuel Cladding and Core Components, London, 1972, p.273.
- [3] H.J.BERGSMANN, D.HAAS AND K.HERSCBACH, in Proceedings International Conference on Radiation Effects in Breeder Reactor Structural Materials, Scottsdale, AZ, 1977, p.241.
- [4] J.STRAALSUND "Irradiation Creep in Breeder Reactor Materials" in Proceedings International Conference on Radiation effects in Breeder Reactor Structural Materials, Scottsdale, AZ, 1977, p.191.
- [5] KRASNOSELOV V.A., KOLESNIKOV A.N., PROKHOROV V.I., OSTROVSKY Z.E., GOLUBENKO A.V., NEUSTROEV V.S. Eksperimentlanye issledovaniya radiatsionnoy polzuchesti nerzhavayushchih staley // Preprint RIAR - 16(469)- Dimitrovgrad, 1981, 28c.
- [6] TSYKANOV V.A., RESHETNIKOV F.G., SHAMARDIN V.K. i dr. Radiatsyonnye issledovaniya konstruktsionnykh materialov, obluchehnykh v reaktore BOR-60//Voprosy atomnoy nauki i tekhniki. Ser.:Atomnoe materialovedenie, 1985, Vyp.1(18), s.45-53.
- [7] SHAMARDIN V.K., NEUSTROEV V.S., GOLOVANOV V.N. et al "Irradiation Creep and Swelling of 16Cr-15Ni-3Mo-Nb and its modification 16Cr-15Ni-3Mo-Nb-B Steel"-in effects of Radiation on Materials: 14th International Symposium (V.2), N.H.Packan, R.E.Stoller and A.S.Kumar eds., ASTM STP 1046. American Society for Testing and Materials, Philadelphia, 1990, pp.753-765.
- [8] F.A.GARNER AND D.L.PORTER, Journal of Nuclear Materials, 1987, v.148, p.279.
- [9] F.A.GARNER AND D.L.PORTER, Journal of Nuclear Materials, 1988, v.155-157, p.1006.

- [10] D.L.PORTER AND F.A.GARNER. Journal of nuclear Materials, 1988, v.155-157, p.1006.
- [11] F.A.GARNER, D.L.PORTER AND G.D.HUDMAN in Radiation Material Science (Proceedings of the International Conference on Radiation Material Science. Alushta. May 22-25, 1990), v.1, Kharkov, 1990, p.68.
- [12] F.A.GARNER AND P.J.PUIGH, in Proceedings International Conference on Radiation Effects in breeder Reactor Structural Materials, Scottsdale, AZ 1977,p.75.
- [13] NEUSTROEV V.S., SHAMARDIN V.K., OZHIGOV L.S. Vlijanie naprjahrenija na radiatsionnyu polzuchest i raspukhanie stali tipa 16Cr-15Ni-3Mo-Nb / Voprosy atomnoy nauki i tekhniki. Ser.:Fizika radiatsionnykh povrezhdeniy i reaktornoe materialovedenie. 1990.Vyp.1(52).C.20-25.
- [14] PORTER D.L., WOOD E.L., GARNER F.A. "Influence of Thermomechanical Treatment and Environmental History on Creep, Swelling and Embrittlement of AISI 316 at 400 °C and 130 dpa" in Effects of Radiation on Materials: 14th International Symposium, ASTM STP 1046, (V.2), N.H.Packan, R.E.Stoller, and A.S.Kumar, Eds., American Society for Testing and Materials, Philadelphia, 1990, pp.551-569.
- [15] K.HERSCHBACH, W.SCHNEIDER AND H.J.BERGMANN "Swelling and In-Pile Creep Behavior of Some 15Cr15NiTi Stainless Steel in the Temperature Range 400 to 600 C" in Effects of Radiation on Materials: 14th International Symposium, ASTM STP 1046, (V.2), N.H.Packan, R.E.Stoller, and A.S.Kumar, Eds., American Society for Testing and Materials, Philadelphia, 1990, pp.570-587.
- [16] NEUSTROEV V.S., SHAMARDIN V.K. "Radiation Creep and Swelling of Austenitic 16Cr-15Ni-3Mo-Nb Steel Irradiated in the Reactor BOR-60 at 350 and 420 C. effects of Radiation on Materials: 16th International Symposium, ASTM STP 1175, A.S.Kumur, R.K.Nanstad, and E.A.Little. etc.. American Society for Testing and Materials, Philadelphia, 1993, p.816-823.

INFLUENCE OF HIGH DOSE IRRADIATION ON STRUCTURE AND FRACTURE OF THE C0.1-Cr16-Ni15-Mo3-Nb STEEL

S.A. AVERIN, A.V. KOZLOV, E.N. SHCHERBAKOV
SB RDIPE, Zarechny,
Russian Federation



XA9848052

Abstract

Structure evolution of the stainless steel C0.1-Cr16-Ni15-Mo3-Nb in the austenitic state was investigated by the methods of both optics and electron microscopy and electric resistance after its irradiation up to 46 dpa in the BN-350 reactor. The influence of such structural changes on plasticity and character of steel damage at post-irradiation bending test was studied. It was shown that, radiation swelling is the most important structure factor determined physical and mechanical properties of the steel. We determined a quantitative estimate of temperature and irradiation damage dose dependence of both sizes and radiation void density. It was settled that, electric resistance of the steel is determine first of all by swelling value. Influence of other structural changes of the steel (depended on temperature) on electric resistance value was revealed. Plasticity and damage of the steel are determined by radiation void conditions at post-irradiation tests. Damage is occurred on mechanism of void growth and fusion. Estimation of critical swelling and critical void size, when sudden drop of the steel is occurred, was done.

1. INTRODUCTION

Multiple structure changes ocure in materials under neutron irradiation. Structure evolution in steels results in essential changes of their properties. Along with that, radiation embrittlement of austenitic stainless steels proceeds after high dose irradiation. However, experimental data on the interaction of radiation embrittlement with quantitative structure parameters of steel are still insufficient.

2. EXPERIMENTAL DATE

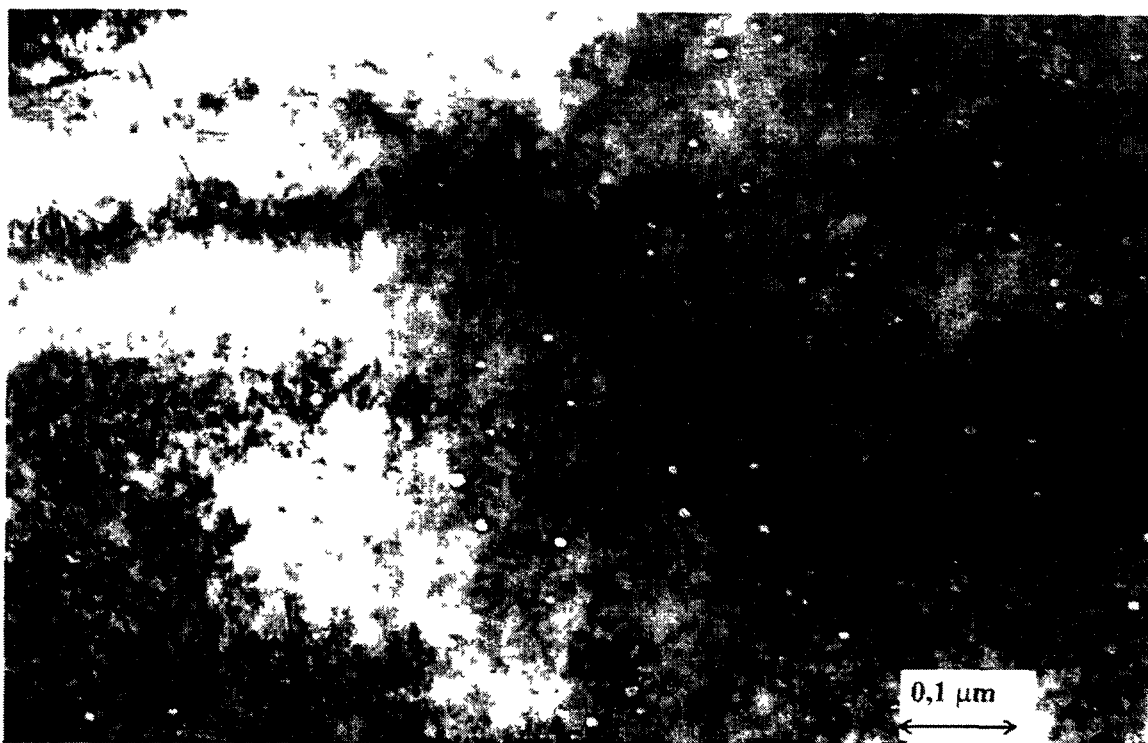
Our paper is focused on the structure evolution in C0.1-Cr16-Ni15-Mo3-Nb stainless steel in an austenitized state after irradiation to the maximum dose damage 46 dpa in the reactor BN-350. The effect of structure changes on plasticity and damage behaviour of the steel were stadied in post-reactor bend tests.

Cylinder samples of the diameter 1mm and length 20mm were made of spacing wire of fuel assemblies. The parameters of samples irradiation are shown in a table.

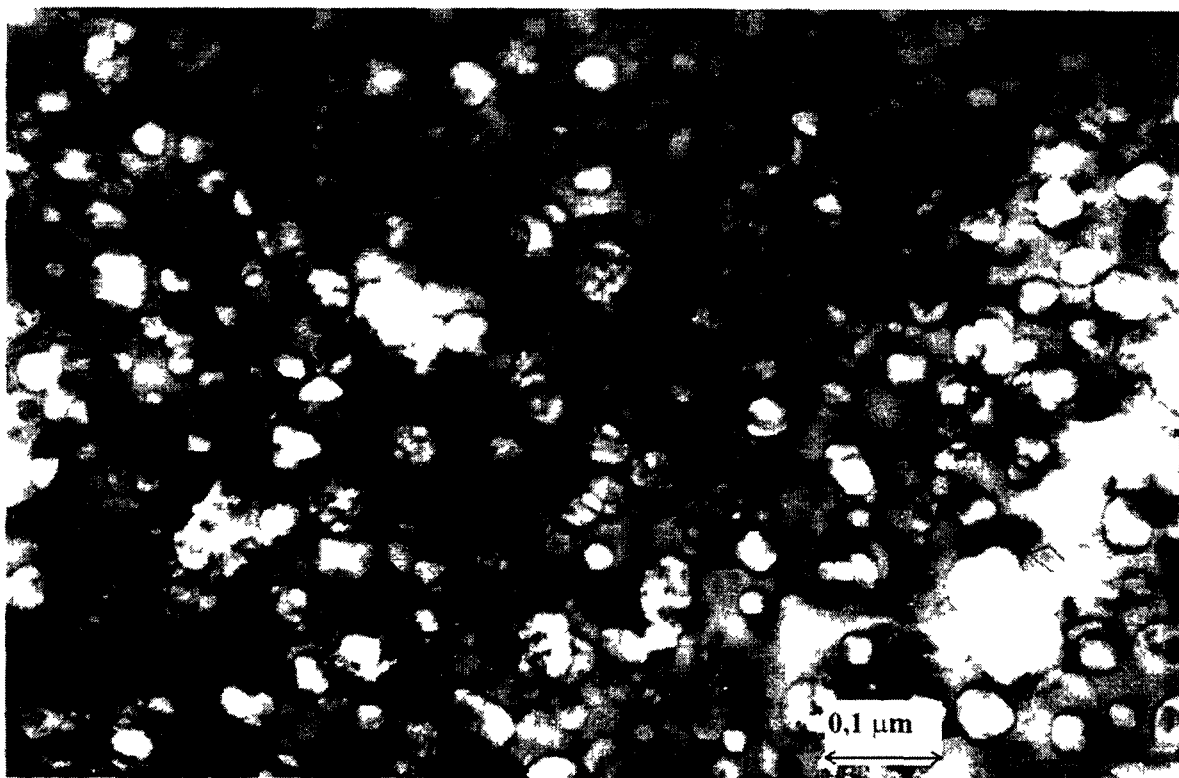
Table

№ of a sample	6	5	4	3	2	1	0
Tirr., °C	595 ±20	580 ±20	560 ±20	530 ±20	495 ±20	440 ±10	335 ±10
D, dpa	40	46	45.5	43	35	32	28

A microstructure of the samples was investigated in an transmission electron microscope (TEM). Quantitative parameters of radiation porosity were being determined based on methods described in [1,2]. Radiation swelling was revealed from the data on samples density measurement by the method of hidrostating weighing (HSW) and the results of quantitative TEM. Electrical impedance was determined by a comparison of voltage decrease in a reference sample and a measurement one. A relative error in a sample's



a



b

Fig.1. Microstructure of the C0.1-Cr16-Ni15-Mo3-Nb after its irradiation:
a - $T_{ir} = 440\text{ }^{\circ}\text{C}$, $D = 46\text{ dpa}$; б - $T_{ir} = 530\text{ }^{\circ}\text{C}$, $D = 43\text{ dpa}$.

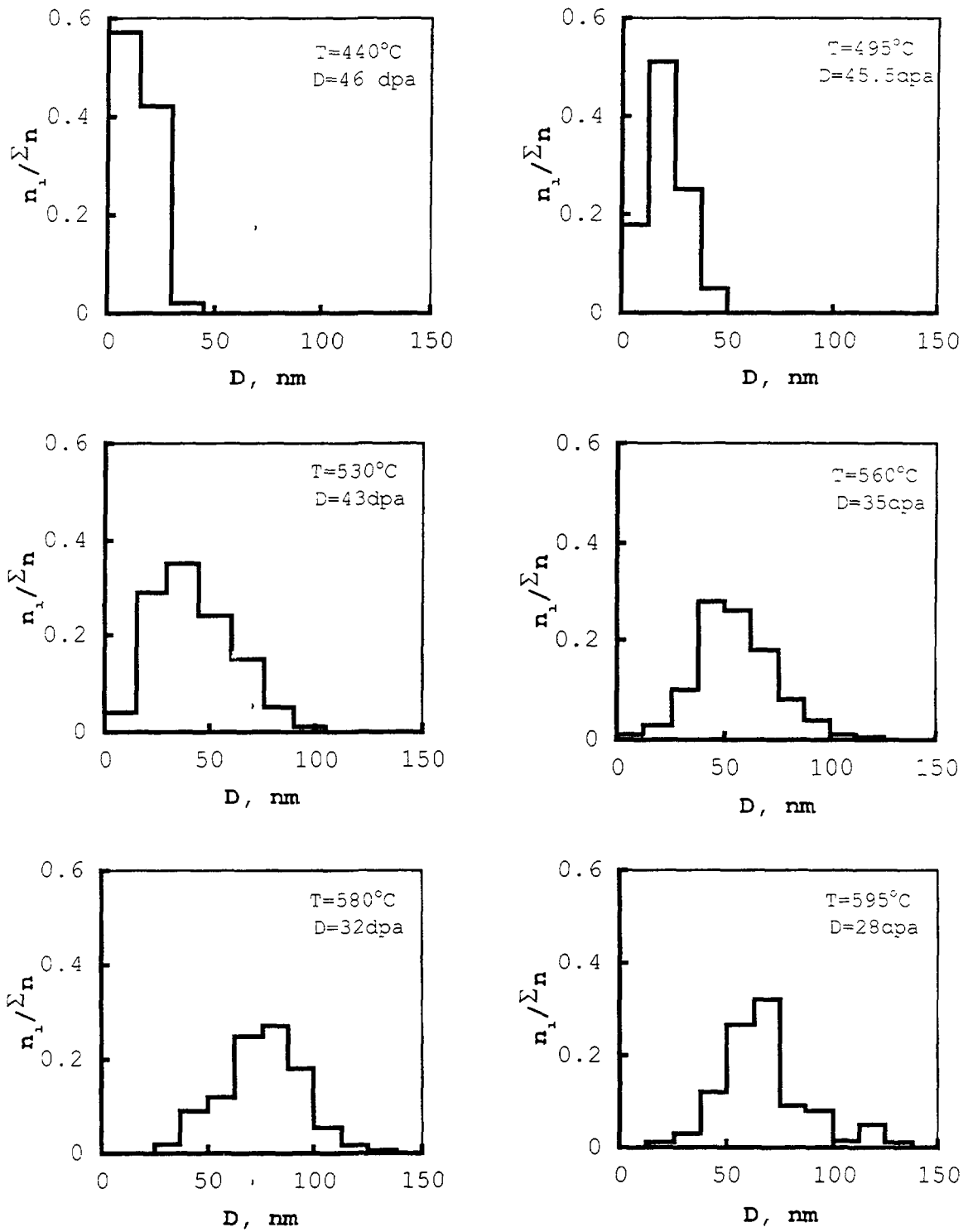


Fig.2. Hystographic patterns of radiation voids distribution in the C0.1-Cr16-Ni15-Mo3-Nb steel depending on irradiation temperature and damage dose

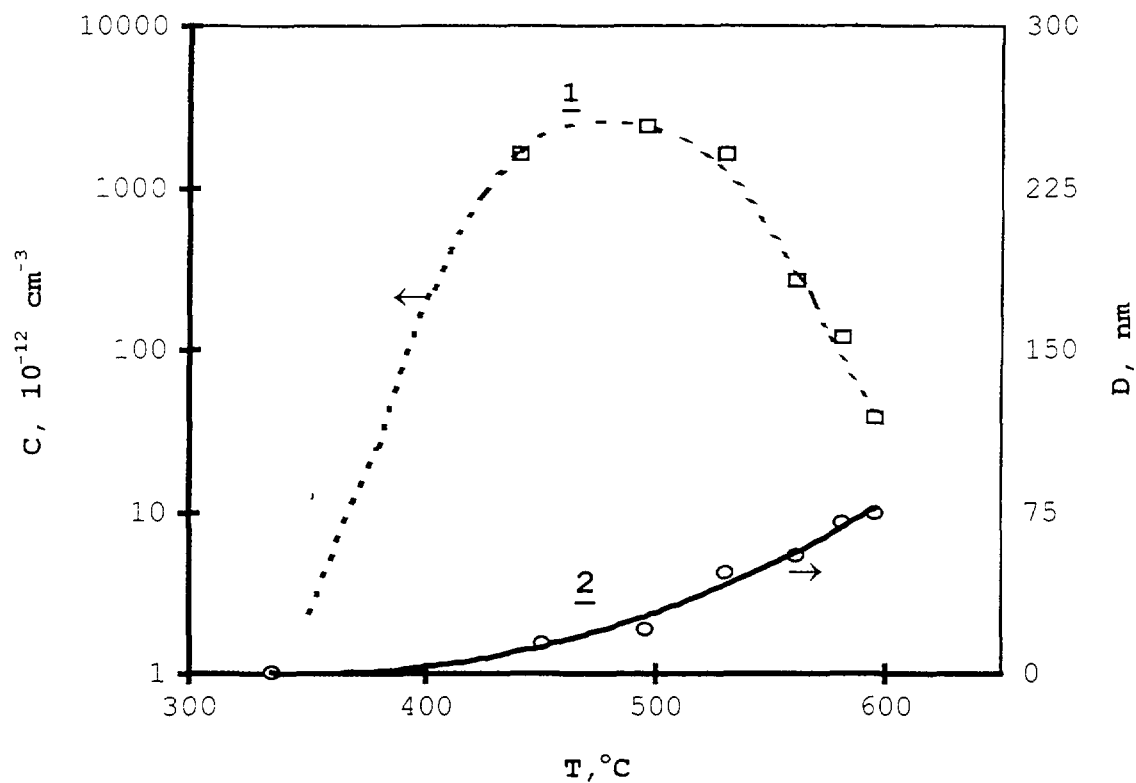


Fig.3. Variation of concentration (1) of radiation voids and their mean size (2) in the C0.1-Cr16-Ni15-Mo3-Nb steel on irradiation temperature.

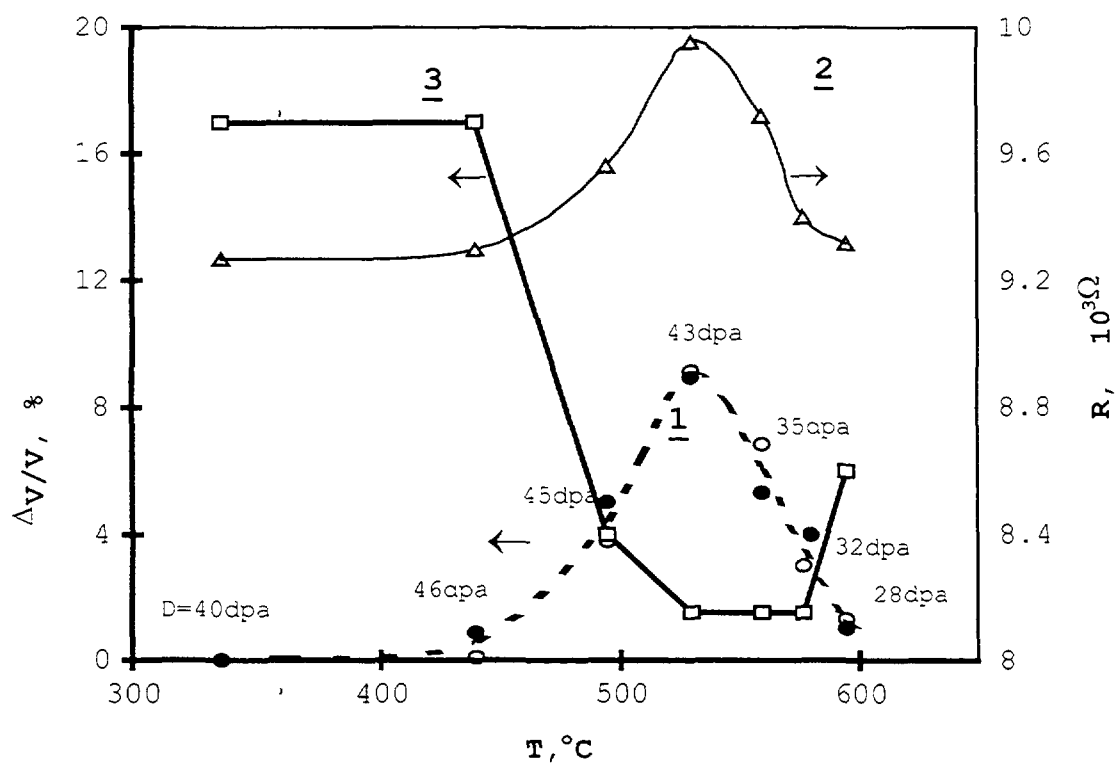


Fig.4. A dependance of radiation swelling (1), electric impedance (2), number of bendings before the fracture (3) of the samples of the C0.1-Cr16-Ni15-Mo3-Nb steel on irradiation temperature (dpa is designated by figure).

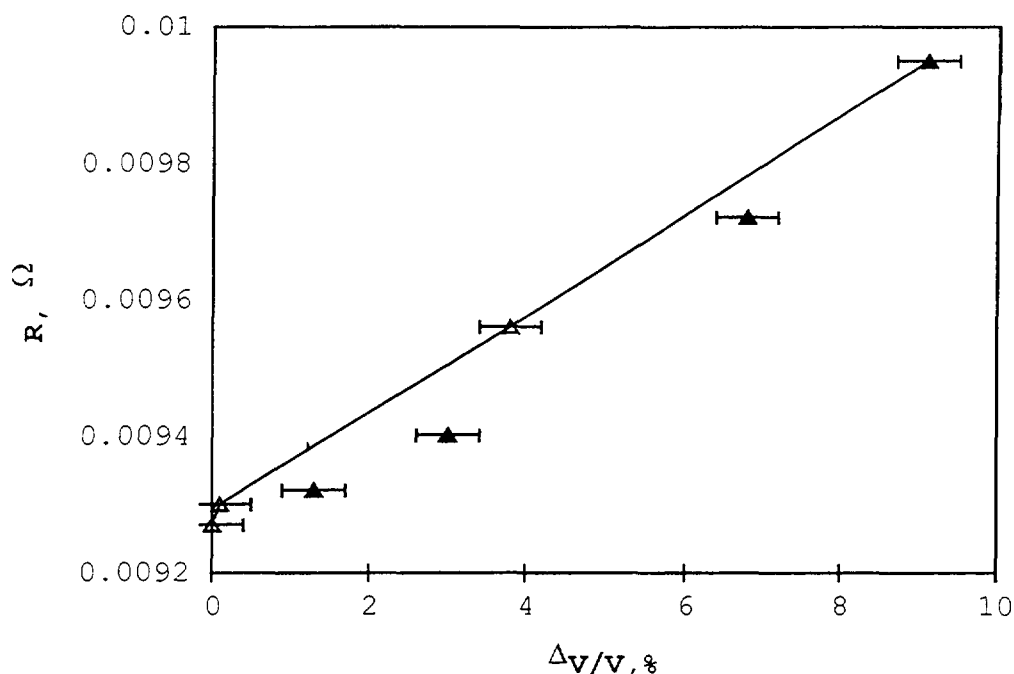


Fig.5. A dependance of electric impedance of the samples of the C0.1-Cr16-Ni15-Mo3-Nb steel on radiation swelling.

— a low temperature branch of swelling, $T_{irr} < 530^\circ C$

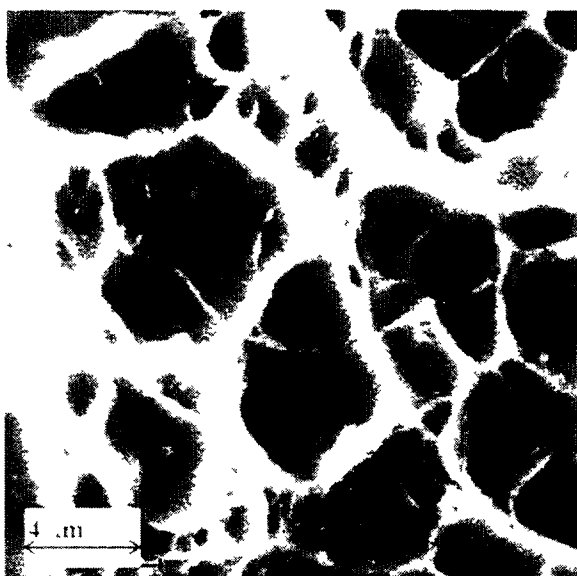
----- a high temperature branch of swelling, $T_{irr} > 530^\circ C$

impedance measurement does not exceed $\pm 0.1\%$. Plasticity was determined in bend tests when a number of bendings prior to damage were registered. The bend tests complied with the standart GOST 14019-80. Damage surface morphology was studied in a scanning electron microscope. Fracture were quantitatively analysed by the method in Ref.[3].

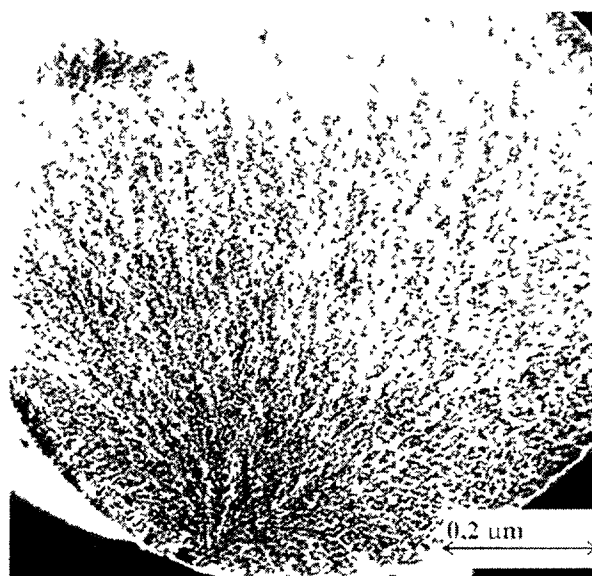
At low irradiation temperatures ($< 350^\circ C$) high density of radiation defects in the form of clusters ("black dots"), dislocation loops and lengths of dislocations are observed in the steel structure. When the radiation temperature increases radiation voids appear (fig.1.a), their sizes and concentration grow (figs 2 and 3) and their form acquires more regular cristallographic faceting (fig.1.b). Maximum concentration of voids corresponds to the temperature of about $500^\circ C$. The density of dislocation loops and clusters decrease and their sizes grow simultaneously with the temperature increase. At the temperature of $500^\circ C$ "black dots" and small dislocation loops are absent though a noticable amount of second phases emerges and their size and density grow with temperature increase. X-ray phase analysis revealed precipitation of second phases of, at least, tree types and some of them are ferromagnetic.

Materials swelling depends on irradiation temperature and damage dose. the data on steel swelling depending on temperature are shown in fig.4. These swelling values, determined by different methods, are in good agreement. The maximum swelling value corresponds to the irradiation temperature of $530^\circ C$ and damage dose of 43 dpa.

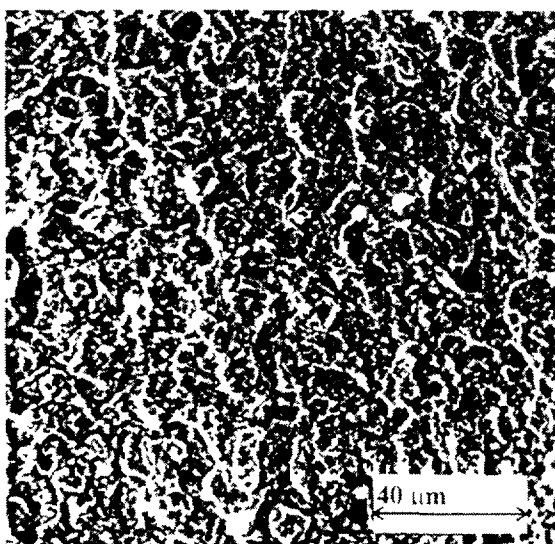
A variation of electric impedance of the tested samples after being exposed to high dose correlates with the swelling data (fig.4). At first approximation this variation can be described through swelling (fig.5). However when swelling values are the same at low and high temperature branches of the plot the electric impedance values are different. Perhaps, it can be attributed to the changes in material's matrix condition due to the changes of density and sizes of precipitations, dislocation loops and clusters.



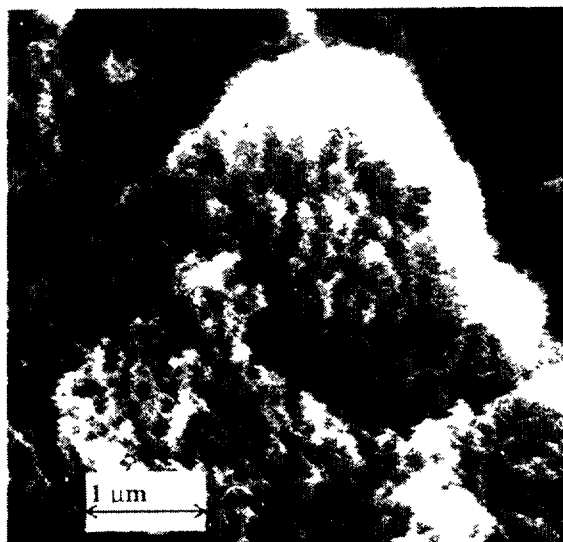
a



b



c



d

Fig.6. Fracture of the C0.1-Cr16-Ni15-Mo3-Nb after its bend tests:
a - Tir = 440 °C, D = 46 dpa;
b,c,d - Tir = 560 °C, D = 35 dpa.

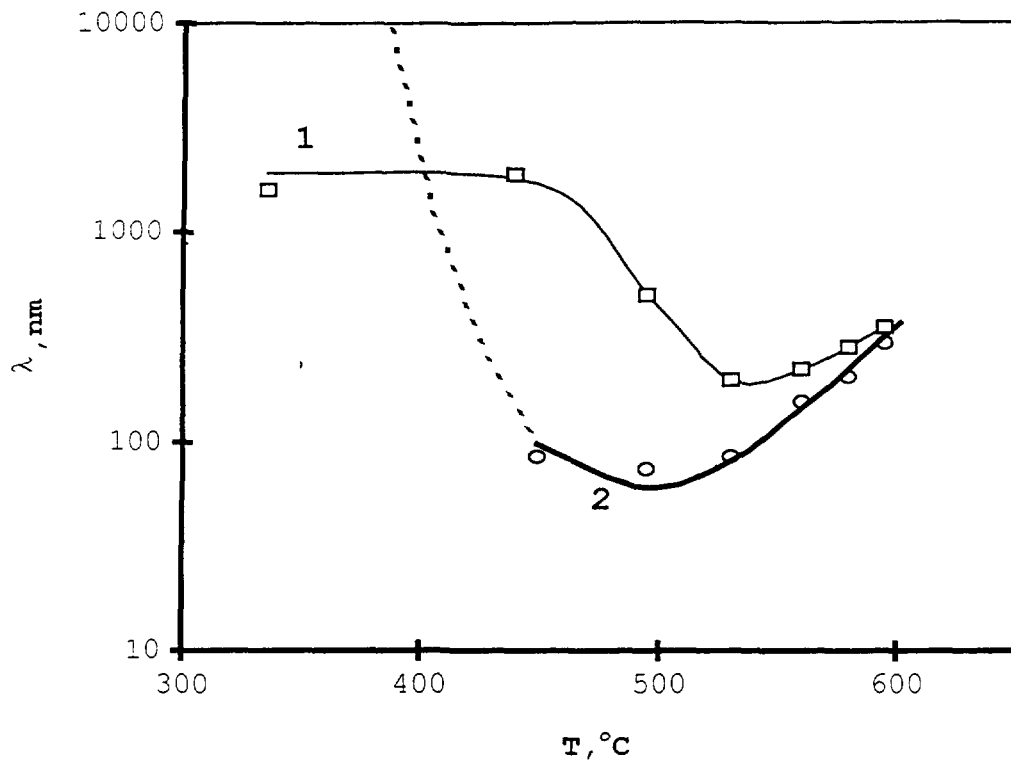


Fig.7. Variation of mean distance between the microcups on sample fracture (1) and that between the radiation voids (2) depending on irradiation temperature

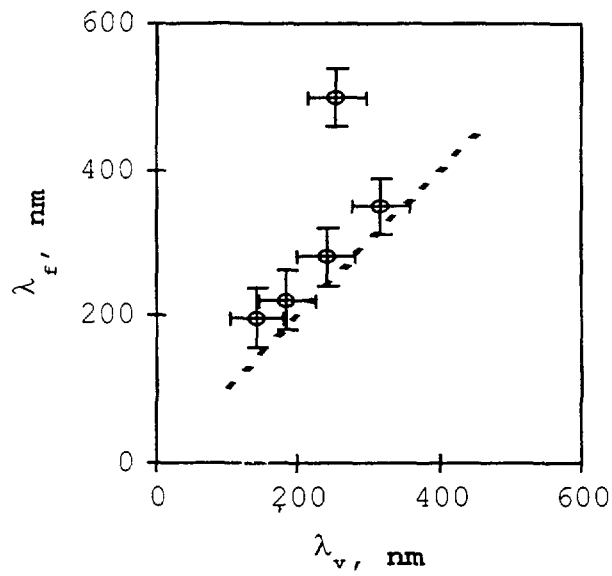


Fig.8. A dependance of mean distance between the microcups on sample fracture on that between the radiation voids of the size more than 45 nm.

A number of bendings before the damage, which characterises the plasticity, depend on swelling (fig.4). The higher swelling is lower is the steel plasticity. Minimum plasticity is observed within the irradiation temperatures of 530 °C to 580 °C. Fractographs show sufficient plasticity of the steel, which can stand 17 bendings, and a transcrystalline viscous damage with a formation of a typical cup fracture (fig.6.a) if post-irradiation steel does not contain voids or their size does not exceed 45 nm (samples # 5 and 6). The preprecipitation of the size 0.4 μm can be seen at the bottom of some cups.

The damage is brittle and transcrystalline (fig.6c and 6d) in all other samples, which have swelling more than 1% and substantial concentration of voids of the size more than 45nm. The topography of such a fracture at medium magnification (fig.6c) is characterised by flat areas, peacks of cleavage and shallow cups. This damage looks like a quasicleavage which is distinguished for such details of surface fracture [4]. The investigation with magnification of 15,000 times revealed microcups (fig.6e) covering the entire surface of the fracture. They are the traces of microvoids along which the damage proceeds. An average distance between this cups is longer than that between voids in a steel (fig.7). The analysis revealed that this distance corresponded to the distance between the voids, which had the size more than 45 nm (fig.8). Therefore nuclei of microvoids are radiation voids of the size more than 45 nm.

Thus, radiation swelling is a dominating effect in changing the properties of stainless steels. Herewith a material's plasticity will depend on both swelling amount and radiation voids concentration and size. 45 nm is the critical size for C0.1-Cr16-Ni15-Mo3-Nb steel when its plasticity decreases dramatically in the tests at room temperature.

3. CONCLUSION

A quantitative estimate of temperature and irradiation damage dose influence on both sizes and radiation void density was determined. It was shown that radiation swelling is the most important structure factor determined physical and mechanical properties of the steel. It was settled that electric resistance of the steel is determine first of all by swelling value/ Influence of other structural changes of the steel (dependent on temperatures) on electric resistance value was revealed. Plasticity and fracture of the steel are determined by radiation void conditions at post-irradiation tests. Fracture occur on mechanism of void growth and fusion. Estimation of critical swelling (>1 %) and critical void size (>45 nm), when sudden drop plasticity of the steel occur, was done.

REFERENCES

1. Saltikov S.A. Stereometric metalography. M.:Mellurgy, 1976. 272 p.
2. Chernjavsky K.S. Stereology metlloknoulige. M.: Metllurgical, 1977. 280 p.
3. Chermant J.L., Coster M. Fractographie quantitative.-"Cercle d'etudes des metaux". Bulletin , 1978, t.14, N3, p.93-146.
4. Fractography & atlas of fractogramm.: E.A.Shur; with. M.L.Bernstein. M.: Metallurgical, 1982.

VARIABILITY OF IRRADIATION CREEP AND SWELLING OF HT9 IRRADIATED TO HIGH NEUTRON FLUENCE AT 400– 600°C

M.B. TOLOCZKO, F.A. GARNER
Pacific Northwest National Laboratory,
Richland, WA,
USA



XA9848053

Abstract

Four tube-sets constructed from a combination of three lots of HT9 and two heat-treatments were examined after irradiation in FFTF-MOTA at four different temperatures between 400 and 600°C. Diametral measurements indicated that small amounts of swelling occurred at 400°C, with the magnitude of the swelling varying from tube-set to tube-set. At 495, 550, and 600°C, no indications of swelling were observed. Over a limited stress range that decreased with increasing irradiation temperature, the irradiation creep was found to be proportional to the stress level and mirrored the swelling behavior, confirming the $B_0 + D\dot{\epsilon}$ creep model. The creep compliance, B_0 , appears to be about half of that observed in austenitic steels, whereas the creep-swelling coupling coefficient, D , appears to be comparable to that of austenitics. At the highest stress levels examined, the value of the stress exponent became much greater than 1.0. Higher irradiation temperatures resulted in creep behavior with pronounced thermal creep characteristics: a primary creep transient was observed at the three higher irradiation temperatures and increased in magnitude with increasing irradiation temperature, while a stress exponent between 1.0 and 2.0 was observed at 550°C.

1. BACKGROUND

Irradiation creep data on ferritic/martensitic steels are very time-consuming and expensive to obtain for proposed fusion-relevant applications. An extensive analysis of unpublished creep data from various other reactor programs is therefore in progress to characterize the irradiation creep of ferritic/martensitic alloys as a class and also to develop a methodology for applying such data to fusion design applications.

In the current study, the deformation behavior of similar tube-sets of HT9 irradiated in the Materials Open Test Assembly in the Fast Flux Test Facility (FFTF-MOTA) are presented and analyzed. As part of the qualification process for the U.S. Liquid Metal Reactor (LMR) materials program, a series of production variants of HT9 were irradiated in FFTF-MOTA in a variety of specimen types. This paper addresses the irradiation creep and swelling behavior of four nominally similar tube-sets constructed from HT9. One of these tube-sets was the FFTF Core Demonstration Experiment (CDE) heat of HT9 which exhibited significantly lower swelling and irradiation creep than observed in austenitic steels [1-3]. Data on two of these tube-sets at 400°C were presented in an earlier paper [4]. This paper contains data derived at four irradiation temperatures between 400 and 600°C.

2. EXPERIMENTAL DETAILS

The compositions of these four steels, designated HT9-1, HT9-2, HT9-3, and HT9-5 respectively, are shown in Table 1 and are quite similar. The first two were subjected to the same heat treatment; 1038°C/5 min/air cool, followed by 760°C/30 min/air cool. The second two were subjected to a slightly different treatment; 1100°C/2 min/air cool, followed by 650°C/2 h/air cool. All tubes were helium pressurized, and except for the HT9-5 tubes, were 0.457 cm outer diameter, 0.020 cm wall thickness and 2.24 cm length. HT9-5 tubes were larger with 0.686 cm outer diameter, 0.055

cm wall thickness, and 2.82 cm length. Based on the results of earlier studies, there should be no significant influence of size differences [5].

At the end of each MOTA irradiation cycle, the tubes were discharged from the reactor, and prior to reinsertion into a new MOTA, diameter measurements were made using laser profilometry [6]. The non-creep (volumetric) component of strain was assumed to be three times the diameter strain of the stress-free tube. Outer wall creep strains were found by subtracting the diameter change of the stress-free tube, and the outer wall strain was converted to midwall strain using a multiplicative factor that is dependent on initial tube dimensions. All tubes in a given tube-set were irradiated side-by-side in each MOTA in order to minimize the influence of extraneous variables.

Depending on the individual tube-set and irradiation temperature, from three to seven successive diameter measurements (at different fluences) were acquired at various hoop stress levels, ranging from 0 MPa to an upper level determined by the irradiation temperature. The upper level ranges from 200 MPa at 400°C to only 15 MPa at 600°C. Irradiation temperatures varied somewhat (e.g. 384°C - 427°C in the 400°C irradiation series) from one MOTA to the next, but during any one irradiation interval, the temperature was actively controlled within $\pm 5^\circ\text{C}$ of the nominal temperature. Table 2 presents the nominal temperatures and accumulated displacement levels for each irradiation interval. In the case of HT9-2, there were two separate sets of irradiations carried out at 495 and 550°C. One set started early in the MOTA series and another started much later in the series. (Each separate MOTA increment spanned a 1 year period.) The two series, designated as "early" and "late", can be used to demonstrate the relative reproducibility of the creep behavior.

3 RESULTS

Only at the 400°C irradiation temperature were there any significant strains in the unpressurized tubes. It is presumed that these non-creep strains consist of contributions from both phase-related strains and void swelling strains. The non-creep strains at 400°C are shown in Fig. 1 and, assuming an isotropic distribution of strain, are calculated by multiplying the observed diameter change of a stress-free tube by a factor of three. Although the strains are not very large, there is significant variation in both magnitude and behavior between the four tube-sets. HT9-1, 2, and 3 exhibit a small amount of transient dilation followed by a plateau and then a regime of steady-state dilation. HT9-5 initially exhibits contraction, implying an increase in density, and then gradually begins to increase but never reaching a positive level of strain.

Figs. 2a and 2b present the total strains and the calculated midwall creep strains for the tubes irradiated at 400°C. The data are well behaved as is typical of the MOTA irradiation and measurement procedure. The total strain behavior mirrors the variations in the non-creep strains.

TABLE 1 Composition of alloys in weight percent

Alloy	Fe	Cr	Ni	Mo	Mn	V	W
HT9-1	Bal	11.8	0.51	1.03	0.50	0.33	0.52
HT9-2,3	Bal	11.8	0.57	0.94	0.54	0.24	0.52
HT9-5	Bal	11.8	0.60	1.06	0.62	0.33	0.52
Alloy	Si	C	Ti	Al	S	P	N
HT9-1	0.21	0.21	< 0.01	0.03	0.003	0.008	0.006
HT9-2,3	0.28	0.17	< 0.01	0.05	0.003	0.007	0.006
HT9-5	0.29	0.21	---	0.01	0.002	0.011	---

between tube-sets, and the creep strains are directly proportional to the hoop stress level up to a break-away stress, beyond which the stress exponent is much greater than 1.0. With the exception of the CDE heat, the break-away stress appears to be somewhere between 140 and 200 MPa. Table 3 presents the range of creep coefficients derived from these data, assuming that the stress normalized creep rate obeys the $B_0 + D\dot{\sigma}$ creep model often used to describe the creep behavior of austenitic steels, where B_0 and D are typically $\sim 1.0 \times 10^{-6} \text{ MPa}^{-1} \text{ dpa}^{-1}$ and $D \sim 0.6 \times 10^{-2} \text{ MPa}^{-1}$, respectively [7-9].

TABLE 2. Nominal temperatures and displacement levels for each irradiation series.

HT9-1, HT9-2	400°C Nominal	Dose, dpa	
MOTA	Temperature, °C	Incremental	Total
1A	427	30.1	30.1
1B	401	13.1	43.2
1C	396	30.8	74.0
1D	386	22.5	96.5
1E	384	29.1	125.6
1F	386	22.0	147.6
1G	384	17.4	165.0
HT9-3	400°C Nominal	Dose, dpa	
MOTA	Temperature, °C	Incremental	Total
1C	396	28.2	28.2
1D	386	22.5	50.7
1E	384	29.1	79.8
1F	386	22.0	101.8
1G	384	17.4	119.2
HT9-5	400°C Nominal	Dose, dpa	
MOTA	Temperature, °C	Incremental	Total
1D	404	28.3	28.3
1E	414	36.9	65.2
1F	405	36.8	102.0
HT9-1, HT9-2	495°C Nominal	Dose, dpa	
MOTA	Temperature, °C	Incremental	Total
1A	494	29.0	29.0
1B	490	10.6	39.6
1C	490	25.0	64.6
HT9-2 (late)	495°C Nominal	Dose, dpa	
MOTA	Temperature, °C	Incremental	Total
1E	494	20.1	20.1
1F	494	21.5	41.6
1G	495	17.0	58.6
2B	495	13.0	71.6

TABLE 2. Continued.

HT9-5	495°C Nominal	Dose, dpa	
MOTA	Temperature, °C	Incremental	Total
1E	494	26.0, 26.0	26.0, 26.0
1F	494	23.8, 26.2	49.8, 52.2
1G	495	19.0, 21.3	68.8, 73.5
HT9-2 (early)	550°C Nominal	Dose, dpa	
MOTA	Temperature, °C	Incremental	Total
1A	547	33.2	33.2
1B	548	13.9	47.1
1C	550	42.3	89.4
HT9-2 (late)	550°C Nominal	Dose, dpa	
MOTA	Temperature, °C	Incremental	Total
1E	549	43.7	43.7
1F	550	40.4	84.1
1G	550	37.1	121.2
HT9-5	550° Nominal	Dose, dpa	
MOTA	Temperature, °C	Incremental	Total
1E	549	43.4	43.4
1F	550	40.0	83.4
1G	550	35.6	119.0
HT9-1	600°C Nominal	Dose, dpa	
MOTA	Temperature, °C	Incremental	Total
1A	603	28.9	28.9
1B	600	15.6	44.5
1C	605	40.1	84.6

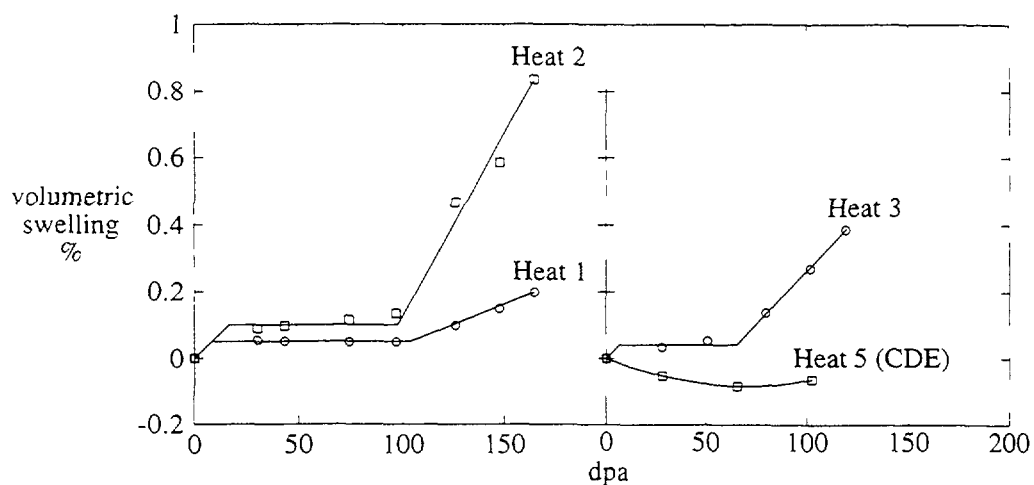


FIGURE 1. Variability observed after stress-free irradiation of four HT9 tube sets at ~400°C.

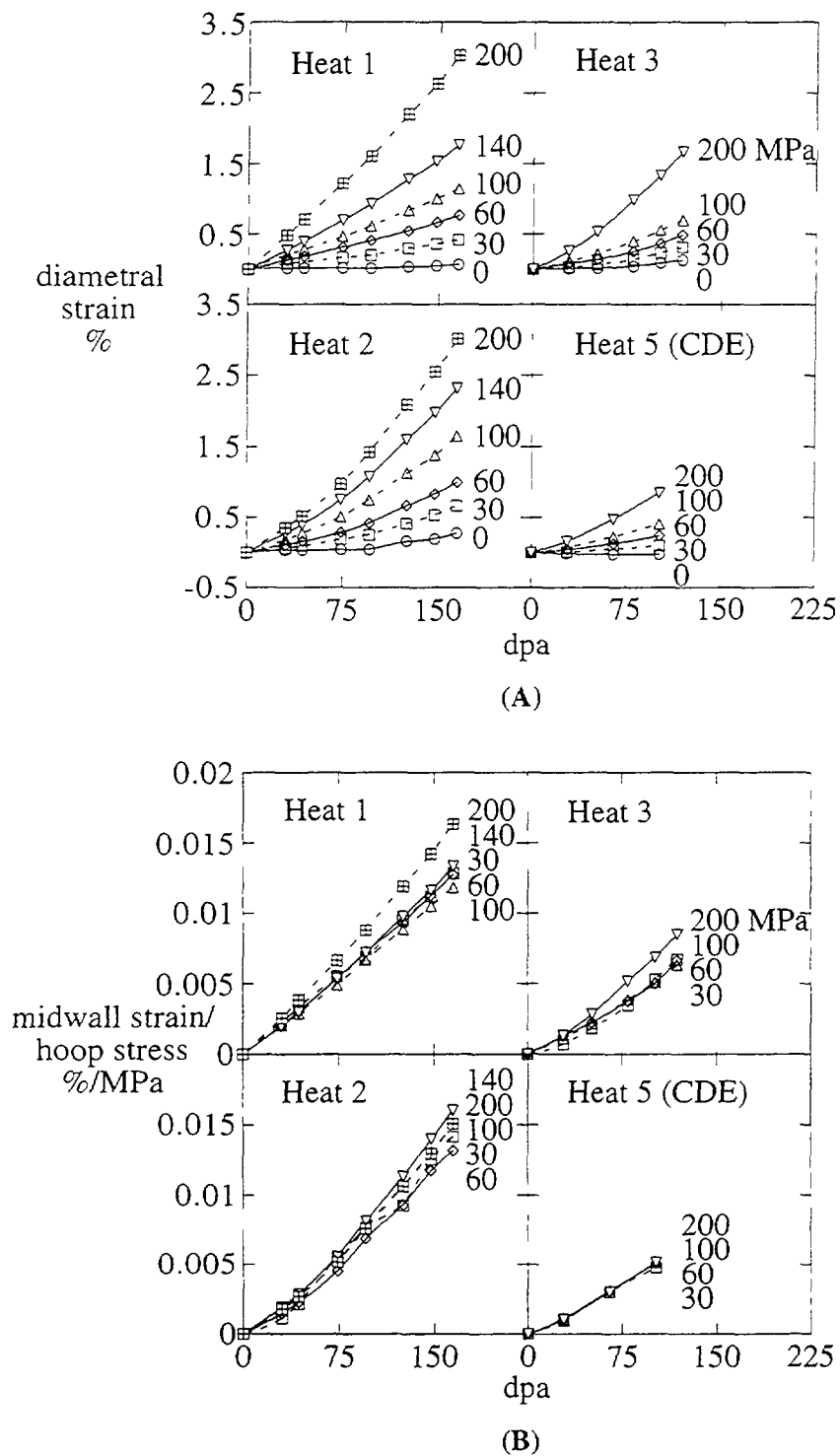


FIGURE 2. (A) Diametral strains and (B) stress-normalized midwall creep strains observed in various HT9 heats during irradiation at $\sim 400^{\circ}\text{C}$.

Figs. 3a and 3b present the data for the 495°C irradiation series. No indications of swelling were observed in the stress-free condition. There are only minor variations in creep characteristics between tube-sets where valid comparisons at identical stress levels could be made. The creep behavior of HT9-2 in the "early" and "late" series is also comparable for identical stress levels. Once

again there is an indication of a break-away stress level which varies slightly with tube-set. Unlike the behavior at 400°C, a primary creep transient was observed at 495°C. The B_0 creep coefficients shown in Table 3 are comparable to those observed at 400°C. Once again the CDE heat exhibits the best overall behavior.

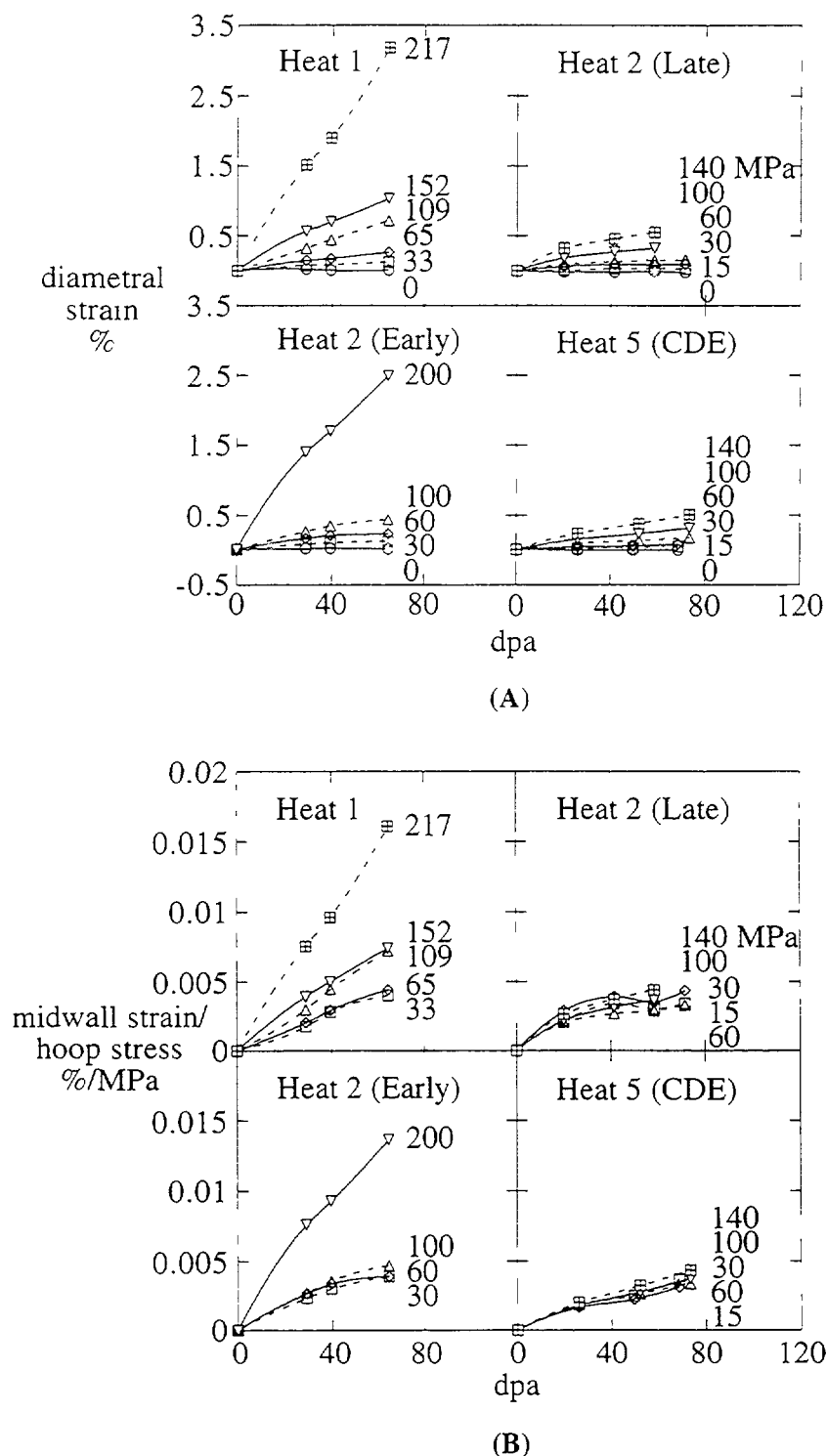


FIGURE 3. (A) Diametral strains and (B) stress-normalized midwall creep strains observed in various HT9 heats during irradiation at ~495°C.

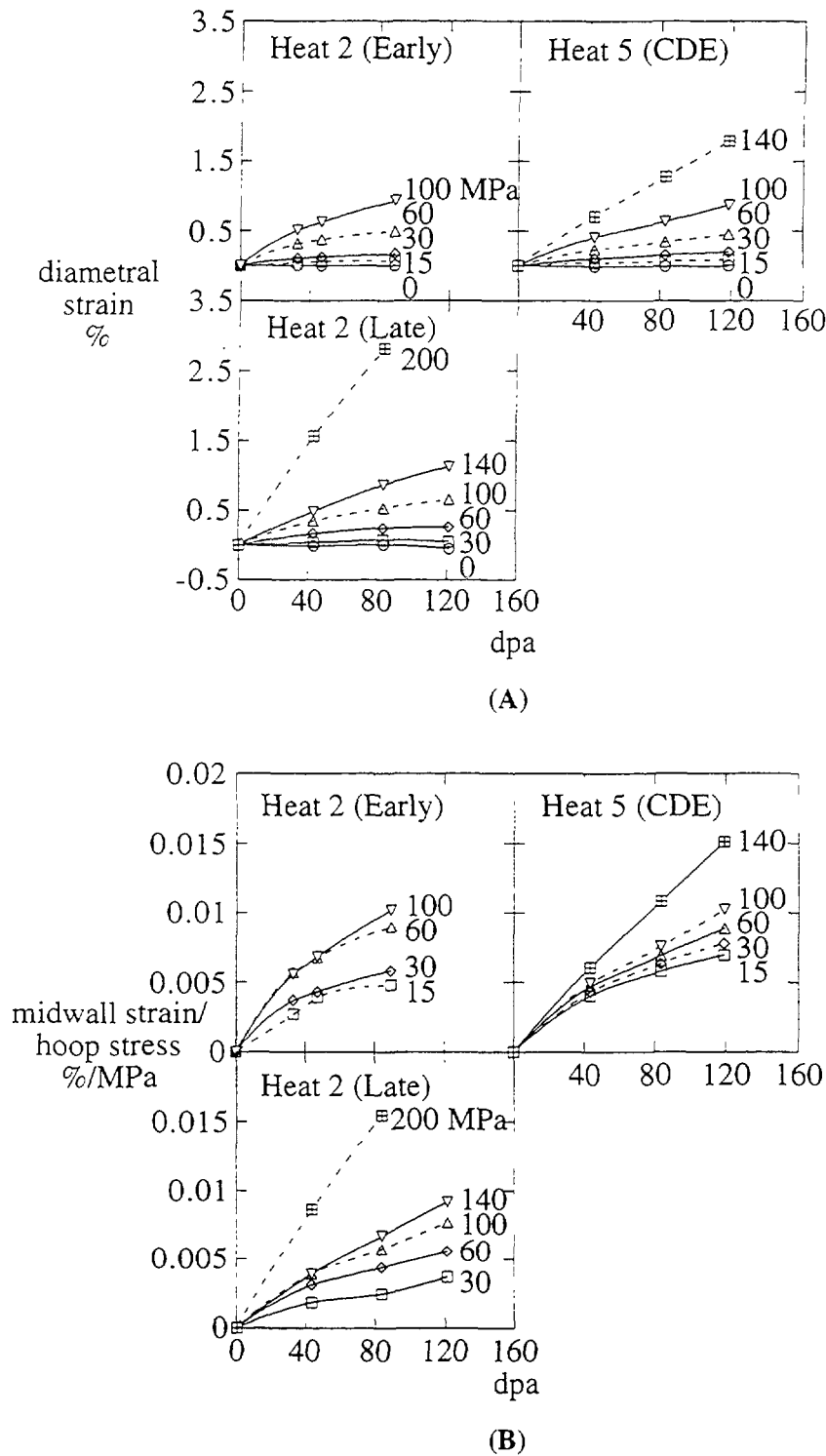


FIGURE 4. (A) Diametral strains and (B) stress-normalized midwall creep strains observed in various HT9 heats during irradiation at $\sim 550^{\circ}\text{C}$.

Figs. 4a and 4b presents the data for the 550°C irradiation series. There is no obvious stress-free swelling, the variability in creep is a little more pronounced, and there is some evidence of variation in creep between the "early" and "late" irradiation series. The primary creep transient is more pronounced, and the stress exponent is clearly above 1.0 for hoop stresses ≥ 30 MPa. For

stresses ≤ 30 MPa, the strain rate appears to be proportional to the stress, and B_0 was calculated to range from $0.3 - 0.6 \times 10^{-6} \text{ MPa}^{-1} \text{ dpa}^{-1}$ as reported in Table 3.

At 600°C only data on HT9-1 were available. As shown in Figs. 5a and 5b, even at very low stress levels of ≤ 15 MPa, the primary transient is quite pronounced. However, the post-transient creep is linear with stress in this stress range (parallel slopes in Fig. 5b), and the measured creep compliance is somewhat larger than observed at lower temperatures, ranging from 1.1 to $1.7 \times 10^{-6} \text{ MPa}^{-1} \text{ dpa}^{-1}$.

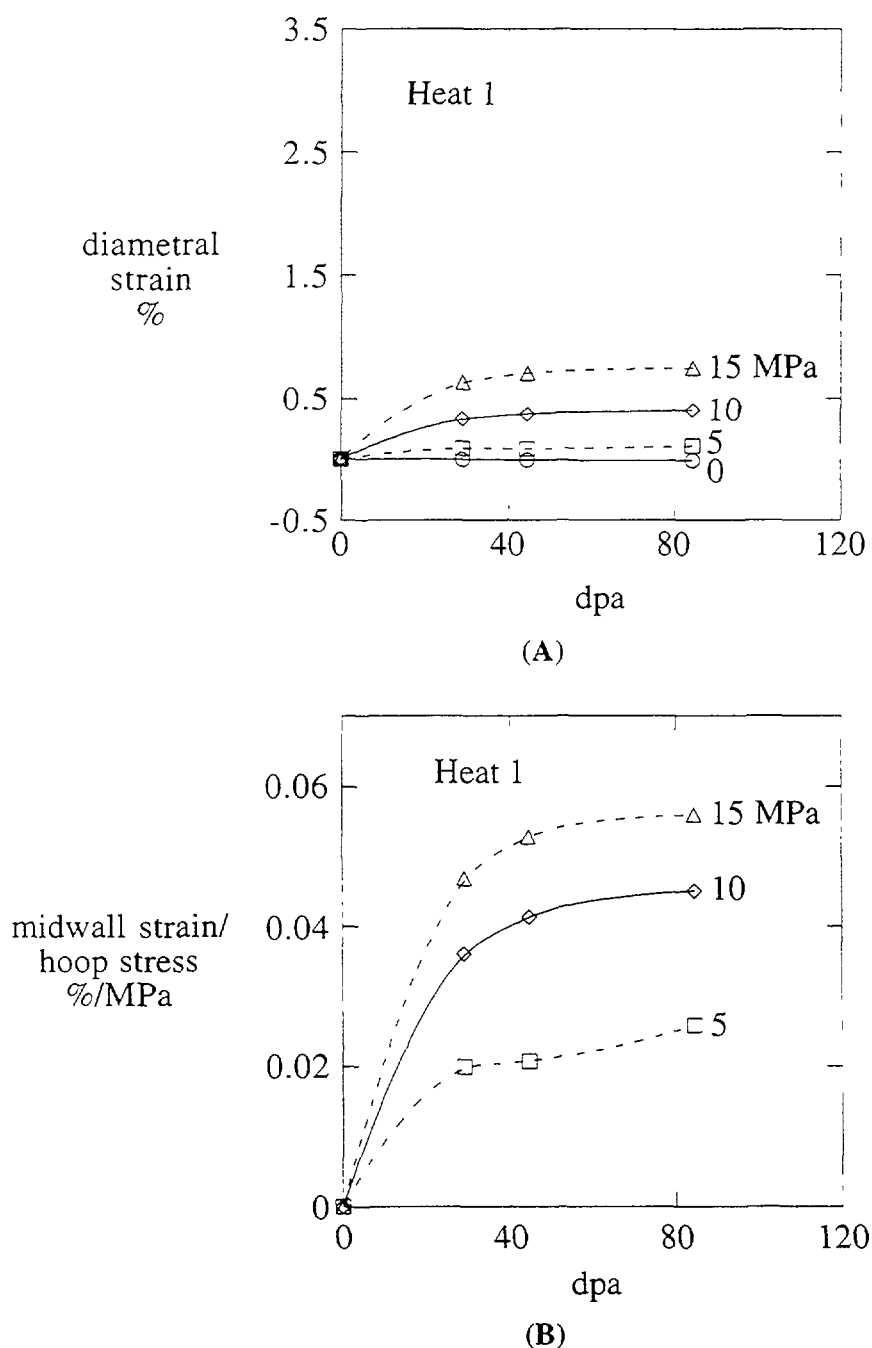


FIGURE 5. (A) Diametral strains and (B) stress-normalized midwall creep stains observed in HT9-1 during irradiation at $\sim 600^\circ\text{C}$.

TABLE 3. Creep coefficients of HT9 at 400, 495, 550 and 600°C.

$\dot{\epsilon} / \bar{\sigma} = B_0 + D\dot{S}$				
Temp. °C	Steel	B_0 MPa ⁻¹ dpa ⁻¹	D MPa ⁻¹	Stress Range MPa
400	HT9-1	0.9 - 1.0 x 10 ⁻⁶ *	0.5 - 1.1 x 10 ⁻² *	to 140
400	HT9-2	0.8 - 1.0 x 10 ⁻⁶	0.5 - 0.6 x 10 ⁻²	to 200
400	HT9-3	0.5 - 0.7 x 10 ⁻⁶	0.4 - 1.0 x 10 ⁻²	to 100
400	HT9-5	0.5 - 0.7 x 10 ⁻⁶	no swelling	to 200
495	HT9-1	0.8 - 1.5 x 10 ⁻⁶	no swelling	to 150
495	HT9-2 (early)	0.5 - 0.7 x 10 ⁻⁶	no swelling	to 100
495	HT9-2 (late)	0.3 - 0.6 x 10 ⁻⁶	no swelling	to 140
495	HT9-5	0.4 - 0.5 x 10 ⁻⁶	no swelling	to 140
550	HT9-2 (early)	0.5 x 10 ⁻⁶	no swelling	to 30
550	HT9-2 (late)	0.3 - 0.4 x 10 ⁻⁶	no swelling	to 30
550	HT9-5	0.5 - 0.6 x 10 ⁻⁶	no swelling	to 30
600	HT9-1	1.1 - 1.7 x 10 ⁻⁶	no swelling	to 15

* The variation in B_0 and D values reflects a range of values accumulated from a measurement at each stress level.

4. DISCUSSION

Void swelling of HT9 has been clearly observed by electron microscopy in a prior study of irradiation creep and swelling of the fusion heat of HT9 at ~400°C [10] and, with the exception of HT9-5, can be inferred from the diametral changes of the stress-free tubes irradiated at ~400°C in the current experiment. HT9 swells very little or not at all over the range 400-600°C in the current experiment, but measuring small amounts of swelling via diameter measurement is confounded by diameter changes induced by segregation and phase changes. In HT9-5, the diameter change of the stress-free tube was negative over the whole dose range, and for creep coefficient calculations, it was assumed that HT9-5 did not swell at this temperature. The upturn in strain in the latter portion of the HT9-5 irradiation may signal the possibility of swelling, however. The variability of swelling seen in the various tube-sets demonstrates that the onset of swelling responds to minor processing and compositional differences that are as yet undefined and uncontrolled.

Depending on irradiation temperature and stress, the measured creep possesses characteristics of both irradiation creep and thermal creep. At lower temperatures and lower stresses, classic $B_0 + D\dot{S}$ irradiation creep dominates, while at higher temperatures and stresses, thermal creep dominates. Over a limited range of stresses at 400°C, the stress exponent is 1.0, and the stress-normalized creep rate follows the well known $B_0 + D\dot{S}$ creep-swelling relationship. However, at higher stresses, the stress exponent becomes much greater than 1.0, which is thought to indicate a change in creep mechanism. As will be discussed shortly, it is believed that this latter mechanism is an irradiation controlled climb-glide mechanism. As the temperature is increased, the range of stresses decreases over which classic irradiation creep dominates. At 495°C, the first thermal creep characteristic to appear is a primary creep transient. This transient appears in all stress levels examined at this temperature. However, even in this transient regime, the stress exponent is still 1.0. As shown in

Fig 3, the transition to the high stress ($n > 1$) creep mechanism is apparent at the higher stresses. The mechanism is again thought to be an irradiation controlled climb-glide mechanism. At 550°C, thermal creep characteristics are yet more apparent. Unlike the tubes irradiated at 495°C, the creep measured at 550°C is described by a stress exponent $1 \leq n \leq 2$ over a similar range of stresses. This stress exponent is consistent with thermal creep in HT9 at this temperature and range of stresses [11]. At 550°C, the transition to high stress creep mechanism was observed, but because of the increasing dominance of thermal creep at the lower stresses, the controlling mechanism is not obvious. At 600°C, it appears that there are strong contributions from both thermal and irradiation creep over the range of stresses examined. A large primary creep transient was observed, indicative of thermal creep. The post-transient creep rate was linear with stress, consistent with a SIPA type mechanism or a thermal diffusional creep mechanism. For the stresses examined at 600°C, a transition to an $n > 1$ creep mechanism was not observed, perhaps due to the very low levels (≤ 15 MPa) of stress employed.

In an earlier report, the creep response of the fusion heats of HT9 and 9Cr-1Mo was presented after irradiation to ~ 208 dpa at temperatures ranging from 403 to 433°C in FFTF-MOTA [10]. While the fusion heat of 9Cr-1Mo was well described by the $B_0 + DS$ creep-swelling relationship over a limited stress range, the fusion heat of HT9 did not exhibit such behavior as shown in Fig 6. In particular, the apparent creep response was non-linear with stress over the whole stress range which is similar to the stress range used for pressurized tubes irradiated at $\sim 400^\circ\text{C}$ in the current experiment. The observed non-linear response to stress was thought to be due, in part, to the stress-enhanced swelling measured in the fusion heat of HT9 at this irradiation temperature as shown in Fig 7. (Minimal stress-enhanced swelling was observed in the fusion heat of 9Cr-1Mo.) Unlike the fusion heat of HT9, creep measurements of the various HT9 tube-sets in the current experiment support the $\bar{\epsilon}/\bar{\sigma} = B_0 + DS$ creep-swelling relationship over stress ranges similar to that for the fusion heat of HT9, suggesting some difference in microstructural evolution between HT9-fusion and these steels. Stress-enhanced swelling measurements were not performed on the present steels.

As the non-destructive diametral measurement technique used in both experiments cannot detect stress-enhanced swelling, any additional swelling due to stress cannot be distinguished from true creep and is therefore included as a creep contribution. This can sometimes result in misleading conclusions about the creep-swelling relationship if the stress-enhancement of swelling is large, such

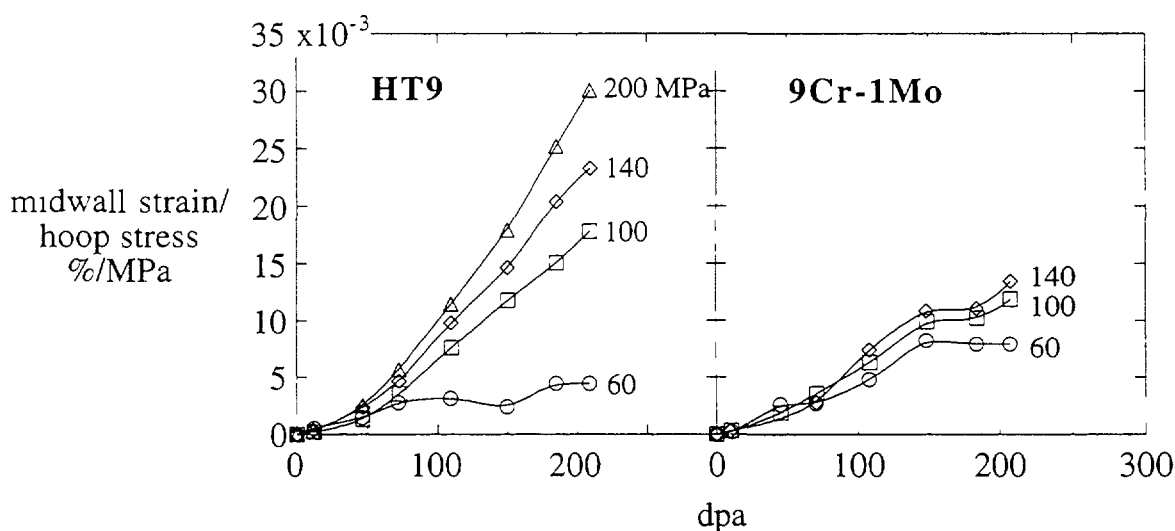


FIGURE 6 Stress-normalized midwall creep strains for the fusion heat of HT9 and 9Cr-1Mo at $\sim 400^\circ\text{C}$, ignoring stress enhancement of swelling [10]

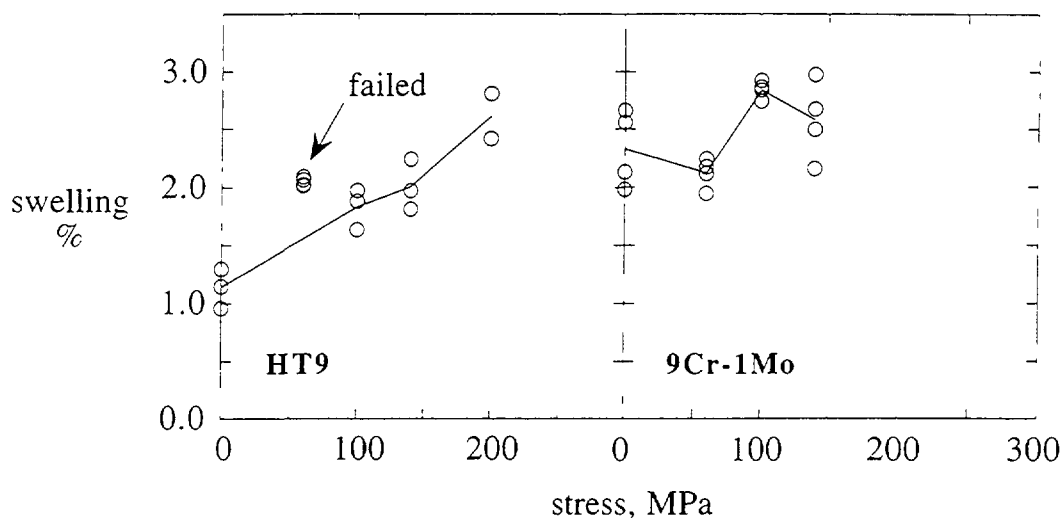


FIGURE 7. Swelling measured by density change for small segments of individual tubes at 208 dpa, showing stress enhancement of swelling [10].

as may be the cause of non-linear creep response of the fusion heat of HT9. It is also possible that the grain, precipitate, or dislocation microstructures may not be stable and thereby contribute to a non-linear response to stress.

The difference in behavior between HT9 fusion heat and the current heats may be due to the fact that the heat treatment was different in one significant aspect. The fusion heat was subjected to 1050°C/5 min/air cool followed by 760°C/2.5 hrs/air cool. The second part of the heat treatment is thus much more likely to initiate dislocation and phase changes than the 760°C/30 min and 650°C/2 hr treatments employed in the current study.

Using a stress exponent of $n = 1.0$ as the defining criterion, "classic" irradiation creep was found at all temperatures, but only over limited stress ranges that decreased with increasing temperature. The creep coefficient B_0 was on the average a little lower (~50%) than that typically observed for austenitic steel, but the creep-swelling coupling coefficient, D , appeared to be comparable to that of austenitic steels. In two earlier studies, one on 9Cr-1Mo at 400°C and another on EM10 at 400-480°C, the creep compliance was measured to be $\sim 0.5 \times 10^{-6}$ [7] and $\sim 0.4 \times 10^{-6}$ MPa⁻¹ dpa⁻¹, [12] respectively. Thus far, it appears that in general the B_0 component of creep in martensitic steels is about one half that found in austenitic steels. The creep-swelling coupling coefficient, however, appears to be independent of crystal structure, at least in iron-base steels.

The creep measurements at 400°C (and 495 and 550°C) also indicate another clear trend. At some break-away stress, the stress exponent becomes much greater than 1.0. The break-away stress appears to be between 150 and 200 MPa (effective stress). Similar irradiation creep behavior has been observed in HT9 irradiated by Grossbeck in ORR/HFIR at ~400°C where a transition to a high-stress exponent was observed in the range 150-200 MPa (effective stress) [13]. At 400°C, the flow stress of annealed low alloy ferritic steels is between 200-300 MPa [14], and the change in stress exponent is thought to be consistent with a change from a climb-only creep mechanism (SIPA-AD for instance [15,16]) to a climb-glide creep mechanism [17]. At this temperature, the climb component is thought to be an irradiation controlled mechanism rather than a thermal mechanism. This conclusion was deduced, in part, from comparison of the break-away stress under irradiation to the break-away stress under thermal aging conditions. In an experiment by Chin [10], where HT9 pressurized tubes were aged at temperatures ranging from 425 to 600°C, a transition from a low-

stress exponent to a high-stress exponent at an aging temperature $\sim 480^{\circ}\text{C}$ was near 280 MPa (effective stress). Extrapolation of his work to lower aging temperatures suggests a break-away stress greater than 300 MPa (effective stress) at $\sim 400^{\circ}\text{C}$ which is markedly greater than the break-away stress observed in this experiment at $\sim 400^{\circ}\text{C}$.

5 CONCLUSIONS

The void swelling observed in four separate tube-sets of HT9 is somewhat sensitive to production variables that are as yet unidentified and controlled. The swelling levels are low, however, compared to austenitic steels. In the temperature range of $400\text{--}600^{\circ}\text{C}$ a gradual transition in the irradiation creep mechanism appears to occur with increasing irradiation temperature, shifting from classic irradiation creep to thermal creep as the irradiation temperature increases. At high stresses, the irradiation creep mechanism appears to shift from a climb-only mechanism to a climb-glide mechanism with the climb rate driven by irradiation. Where classic irradiation creep is found, the swelling-creep coupling coefficient appears to be identical to that of austenitic steels. The creep compliance, however, appears to be approximately one-half that of austenitics.

REFERENCES

- [1] Ethridge, J. L. and Walter, A. E., 'Core Demonstration Experiment: A Liquid Metal Reactor Core Demonstration Experiment Using HT9', Transactions ANS, 60 (1989), pp. 286-287.
- [2] Bridges, A. E., Walter, A. E., Leggett, R. D., Baker, R. B., and Gneiting, B. C., 'Advanced Liquid Metal Reactor Fuel and Blanket Designs Using HT9', Proc. Int. Conf. Fast Reactor and Related Fuel Cycles, Kyoto, Japan, Vol. II, Atomic Energy Society of Japan, 1991, pp. P1-21-1 - P1-21-10.
- [3] Baker, R. B., Bard, F. E., Leggett, R. D., and Pitner, A. L., 'Status of Fuel, Blanket, and Absorber Testing in the Fast Flux Test Facility', Journal of Nuclear Materials, 204 (1993), pp. 109-118.
- [4] Toloczko, M. B., and Garner, F. A., 'Irradiation Creep and Void Swelling of Two LMR Heats of HT9 at $\sim 400^{\circ}\text{C}$ and 165 dpa', Journal of Nuclear Materials, in press.
- [5] Garner, F. A., Hamilton, M. L., Puigh, R. J., Eiholzer, C. R., Duncan, D. R., Toloczko, M. B., and Kumar, A. S., 'The Influence of Specimen Size on Measurement of Thermal or Irradiation Creep in Pressurized Tubes', Effects of Radiation on Materials: 16th International Symposium, ASTM STP 1175, American Society for Testing and Materials, Philadelphia (1993), pp. 631-645.
- [6] Gilbert, E. R., and Chin, B. A., 'Irradiated Materials Measurement Technology', Effects of Radiation on Materials, 10th Conference, ASTM STP 725, American Society for Testing and Materials, Philadelphia (1981), pp. 665-679.
- [7] Toloczko, M. B., Garner, F. A., and Eiholzer, C. R., 'Determination of the Creep Compliance and Creep-Swelling Coupling Coefficient for Neutron Irradiated Titanium-Modified Stainless Steels at $\sim 400^{\circ}\text{C}$ ', Journal of Nuclear Materials, 191-194 (1992), pp. 803-807.
- [8] Toloczko, M. B., and Garner, F. A., 'Relationship Between Swelling and Irradiation Creep in Cold-worked PCA Stainless Steel Irradiated to ~ 178 dpa at $\sim 400^{\circ}\text{C}$ ', Journal of Nuclear Materials, 212-215 (1994), pp. 509-513.
- [9] Garner, F. A., and Porter, D. L., 'Irradiation Creep and Swelling of AISI 316 Exposures of 130 dpa at $385\text{--}400^{\circ}\text{C}$ ', Journal of Nuclear Materials, 155-157 (1988), pp. 1006-1013.
- [10] Toloczko, M. B., Garner, F. A., and Eiholzer, C. R., 'Irradiation Creep and Swelling of the US Fusion heats of HT9 and 9Cr-1Mo to 208 dpa at $\sim 400^{\circ}\text{C}$ ', Journal of Nuclear Materials, 212-215 (1994), pp. 604-607.
- [11] Chin, B. A., 'An Analysis of the Creep Properties of a 12Cr-1MoWV Steel', Proceedings Topical Conference on Ferritic Alloys for Use in Nuclear Energy Technologies, The Metallurgical Society of AIME (1983), pp. 593-599.

- [12] Seran, J. L., Levy, V. Dubuisson, P., Gilbon D., Maillard, A., Fissolo, A., Tournon, H., Cauvin, R., Chalony, A., and Le Boulbin, E., "Behavior Under Neutron Irradiation of the 15-15Ti and EM10 Steels Used as Standard Materials of the Phenix Fuel Subassembly", Effects of Radiation on Materials, 15th International Symposium, ASTM STP 1125, American Society for Testing and Materials, Philadelphia (1992), pp. 1209-1233.
- [13] Grossbeck, M. L., Gibson, L. T., and Ditsukawa, S., "Irradiation Creep at Temperatures of 400°C and Below for Application to Near Term Fusion Devices", Effects of Radiation on Materials: 18th International Symposium, ASTM STP 1325, American Society for Testing and Materials. Philadelphia (1997), in press.
- [14] Metals Handbook, 10th Edition, 1, (1990), pp. 617-652.
- [15] Woo, C. H., "Irradiation Creep Due to Elastodiffusion", Journal of Nuclear Materials, 120 (1984), pp. 55-64.
- [16] Woo, C. H., "Theory of Irradiation Deformation in Non-Cubic Metals: Effects of Anisotropic Diffusion", Journal of Nuclear Materials, 159 (1988), pp. 237-256.
- [17] Matthews, J. R., and Finnis, M. W., "Irradiation Creep Models - an Overview", Journal of Nuclear Materials, 159 (1988), pp. 257-285.

**NEXT PAGE(S)
left BLANK**

A PROBLEM TO DETERMINE SHORT TERM MECHANICAL PROPERTIES CHANGES OF FERRITE-MARTENSITE AND AUSTENITIC STEELS AS MATERIALS OF FUEL ASSEMBLY OF FAST REACTORS UNDER HIGH DOSE NEUTRON IRRADIATION

A.V. KOZLOV, A.S. AVERIN, S.V. BRUSHKOVA
SB RDIPE, Zarechny, Sverdlovsk



XA9848054

G.V. KALASHNIC
ARSRIIM, Moscow

Russian Federation

Abstract

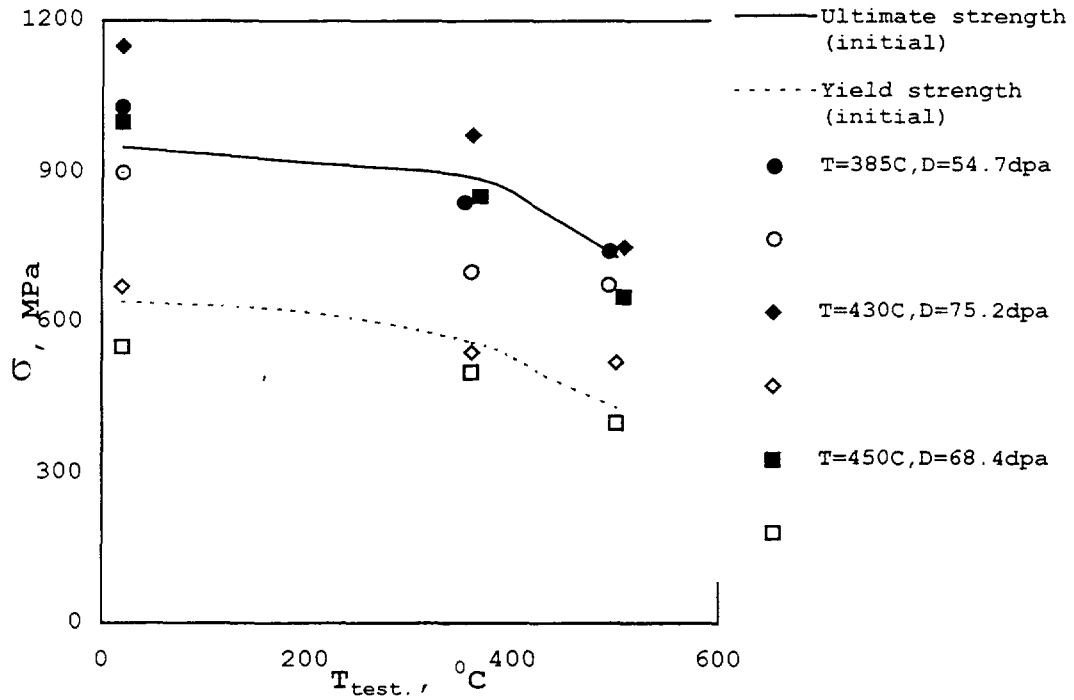
The results of mechanical tests of flat and ring-shaped samples of two ferrite-martensite steels C0.1-Cr13-Mo2-Nb-V-W and C0.1-Cr12-Mo-Nb-V-W irradiated to different damage doses (up to 100 dpa) have been performed in this work. It have been shown that values of plasticity and strength characteristics determined on this sample types are different. Specific elongation takes the values 8 - 12 % for the flat samples, at the same time, ϵ takes the values 1 - 3 % for the ring-shaped samples at room temperature. A character of fluence dependence of mechanical properties is identical. The steels show viscous damage in all tests. Samples of fuel pin cladding fabricated from the austenitic steel C0.1-Cr16-Ni15-Mo3 were also investigated after there working out in BN-600 reactor up to 76 dpa. Ring-shaped samples were tested at standard single-axle tension. Tube samples were tested by internal pressure of solid filler. All samples were fabricated from one and the same section, mechanical properties obtained are different. Specific elongation of the brittlest section of fuel pin was 0 - 0.9 % for the ring-shaped samples and 2 - 7 % for the tube samples at room temperature. Fractographic investigations were carried out on the samples after mechanical tests. Possible reasons of such difference have been discussed in the work.

INVESTIGATIONS of FLAT and RING - SHAPED SAMPLES of the C0.1-Cr13-Mo2-Nb-V-W STEEL.

Investigations of high dose irradiation influence on mechanical properties of the C0.1-Cr13-Mo2-Nb-V-W steel were carried out on samples of two material assemblies irradiated in the BN - 600 reactor [1]. Flat samples were irradiated to 54.7 - 75.2 dpa at 385 °C - 450 °C. Ring - shaped samples were fabricated from case pipe with the 22 mm dia. The gauge of the material assembly irradiated up to 94 - 108 dpa in the reactor at 425 °C - 500 °C is 1 mm. Post - irradiation short - term mechanical properties were carried out in the temperature range 20 °C - 500 °C. Both irradiated and non - irradiated samples were tested. Test temperature dependence from strength and plasticity characteristics of flat samples are shown in Fig. 1. The same dependence for the ring - shaped samples are shown in Fig. 2.

Comparison of samples properties in initial state is shown that the flat samples have yield limit slightly higher (on ~ 60 MPa) than ring - shaped samples have. It allows to expect more lower values of plasticity properties for the flat samples than for the ring - shaped samples. Really, total specific elongation has the values 15 % - 20 % , uniform specific elongation has the values 9 % - 12 %. The ring - shaped samples has the following values of such characteristics: 12 % - 15 % and 6 % - 9 % accordingly. One can see, that tests of the

Strength characteristics of the
C0.1-Cr13-Mo2-Nb-V-W (flat samples)



Plasticity characteristics of the
C0.1-Cr13-Mo3-Nb-V-W (

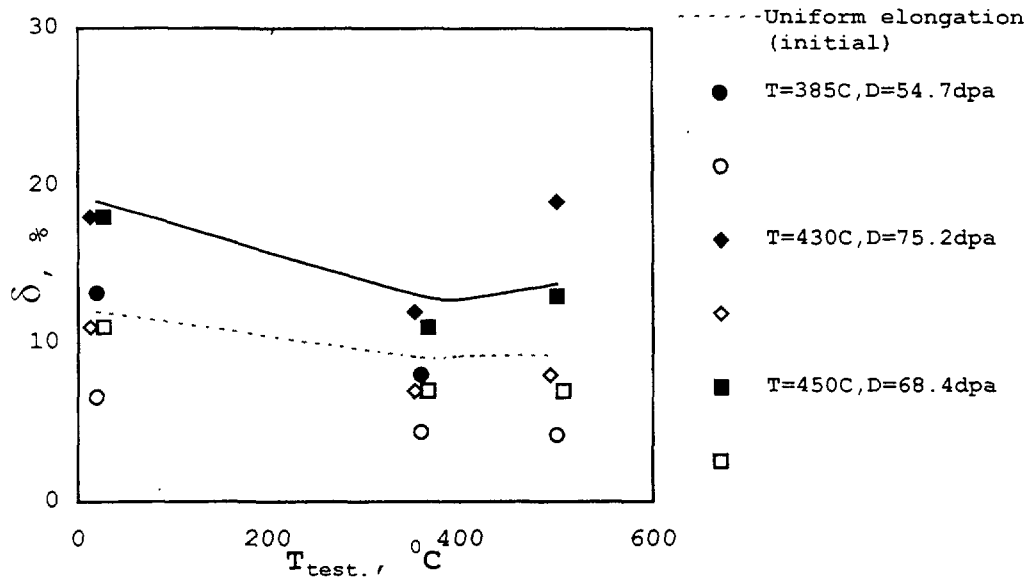
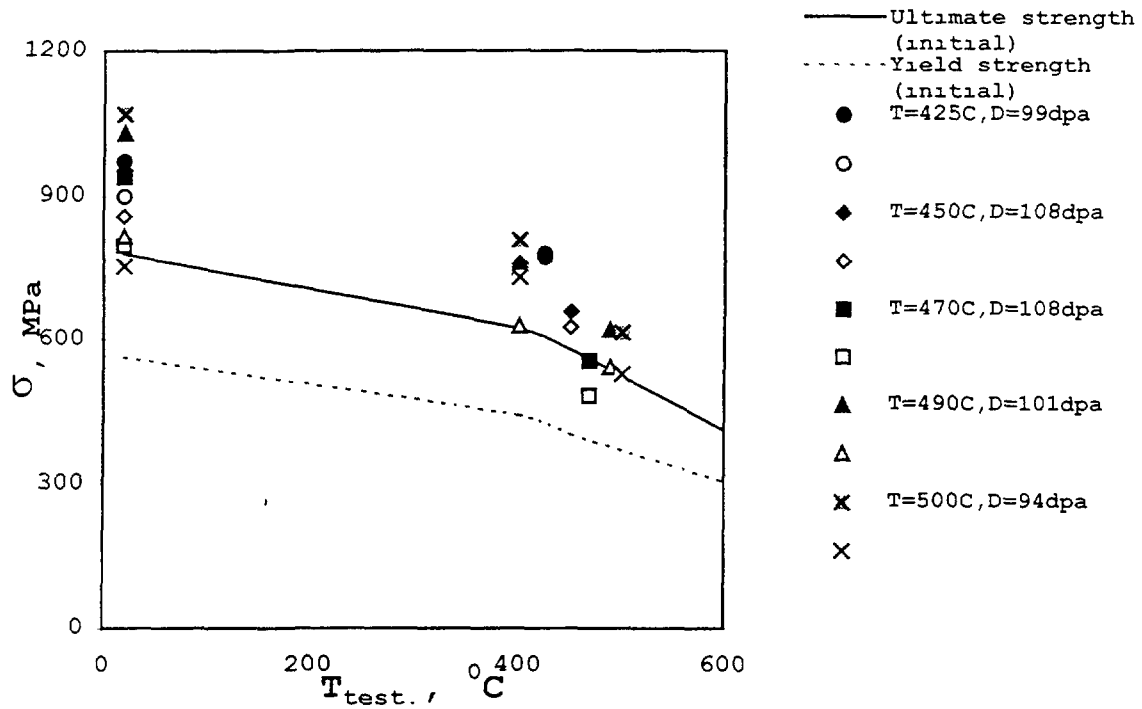


FIG.1

Plasticity characteristics of the
C0.1-Cr13-Mo2-Nb-V-W steel (ring-shaped
samples)



Plasticity characteristics of the
C0.1-Cr13-Mo2-Nb-V-W (ring-shaped samples)

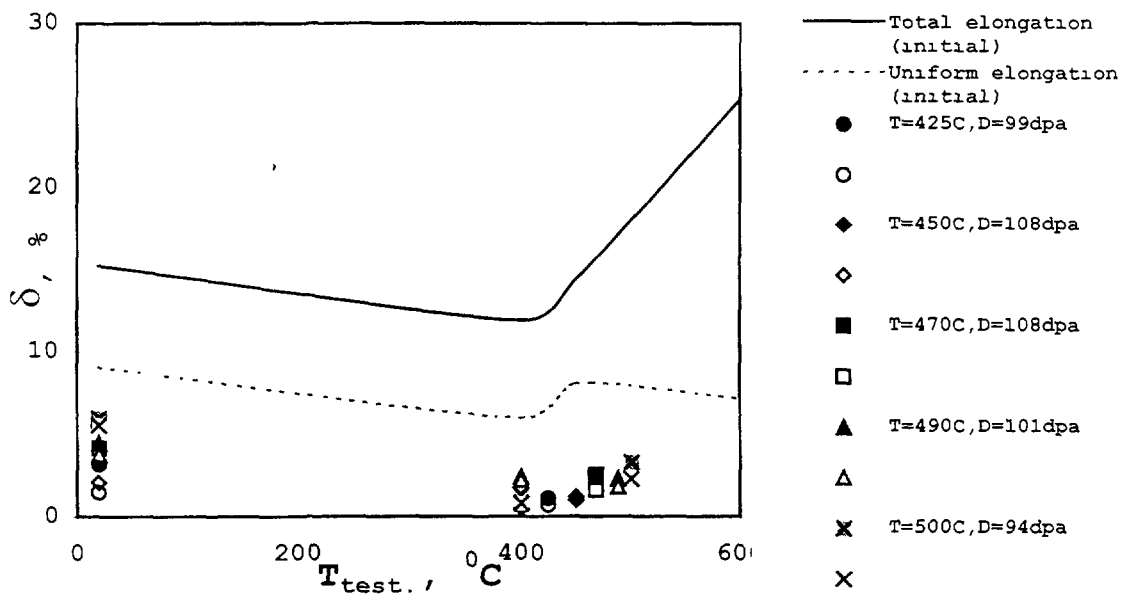


FIG. 2

ring - shaped samples have more lower values (on 3 % - 5 %) of plasticity properties than tests of the flat samples have. Ring stretching occur at first state during ring samples tests. The ring takes ellipse form and subjected by plasticity deformation on the state. The deformation isn't fixed on test diagram.

Strength characteristics of the both type samples are became practically identical. Minimum value of the plasticity properties is reached at 400 °C, at the same time specific elongation of the flat samples takes the value 9 % - 12 %, the ring - shaped samples 1% - 3 %. The difference of the plasticity characteristics between the flat and ring - shaped samples are obtained higher damage dose (on 3 times). The steel shows viscous damage in all tests.

INVESTIGATIONS of RING - SHAPED and TUBE SAMPLES of the Cr15-Ni16-Mo3 STEEL.

Considerably more extensive data are accumulated during mechanical tests of the ring - shaped samples fabricated from austenitic steels for materials of fuel assemblies after their exploitation up to arriving of high burning up (leading to damage dose 70 - 94 dpa of cladding materials) at the BN - 600 reactor core [2]. It was happened the situation when cladding of fuel element had parts which showed zero plasticity during tests when damage dose was more than 76 dpa, at the same time fuel element kept tightness up to the 94 dpa. Therefore, it is difficult to use the results of mechanical tests of the ring - shaped samples fabricated from the fuel elements after their exploitation in the reactor to predict safety operating life of fuel elements. There are two reasons for it. Values of plasticity characteristics obtained during tests of the ring - shaped samples are lower than true (see part 2). Stress - deformation states during exploitation and at single - axle elongation of the ring - shaped samples are differed. More exactly, the stress - deformation state arising during exploitation is imitated during tests of tubes by internal pressure. Usually pressure is created by liquid or gas medium during the same tests. It is hard to carry out such tests under hot cell conditions on samples fabricated by remote - control method from irradiated fuel element. It is connected with the following difficulties: to remove fuel from long fuel element samples and to pressurized a supply unit of liquid or gas medium inside short tube samples fabricated from fuel element cladding by remote - control method.

Technique to test samples from thin - walled tubes with small diameter by internal pressure of solid filler was developed in the SB RDIPE [3]. It is possible both to measured specific elongation directly with the help of the technique and to calculate uniform specific elongation, internal pressure of solid filler on sample wall (when fracture have occurred) and tangential stress in a damage area cladding using solid filler compression diagram in approximation of elasticity and plastic deformation theories.

Verification tests of tube and ring - shaped samples fabricated from cladding tubes of Cr16-Ni15-M3 steel fuel elements irradiated up to 75.7 dpa in the BN - 600 reactor were carried out using the technique. The ring - shaped samples with the height 3 mm and the tube samples with the length 15 mm are fabricated both from one and the same tube sections and from non - irradiated tubes. The samples are used at room temperature and at 400 °C.

Test results of the tube and ring - shaped samples are shown in tables 1 and 2. One can see, that specific elongation is higher on the tube samples than on the ring - shaped samples. In particular, minimum value of specific elongation is equal to 0 using test results of the ring - shaped samples at a section of the fuel element located on ~ 400 mm higher than the core bottom (CB). The specific elongation of the tube samples has the value ~ 3.5 % in the same area. Comparison of strength characteristics shows that ultimate strength of the ring - shaped

Table 1

Investigation results of ring-shaped specimens made of the fuel element cladding after their exploitation in the BN-600 reactor at room temperature.

Coordinates from core bottom	δ_u , %	δ_t , %	$R_{0,2}$, MPa	R_B , MPa
non-irradiation	14.0	19.0	761	997
gauze cavity	9.7	16.6	772	1056
390	0.0	0.0	261	261
470	0.9	0.9	713	810
515	0.6	0.6	716	779
820	5.0	7.5	602	879
870	4.0	4.0	641	854
915	5.0	5.9	665	855

Table 2

Investigation results of tube specimens made of the fuel element cladding after their exploitation in the BN-600 reactor at room temperature.

Coordinates from core bottom	δ_u , %	δ_t , %	p , MPa	R_f , MPa
non-irradiation	9	22	53	511
gauze cavity	8	37	32	340
390	2	3	52	426
470	2	6	48	408
515	4	7	48	391
820	5	12	41	358
870	7	10	46	399
915	11	24	33	313

Table 3

Investigation results of ring-shaped specimens made of the fuel element cladding after their exploitation in the BN-600 reactor at 400 °C.

Coordinates from core bottom	δ_u , %	δ_t , %	$R_{0,2}$, MPa	R_B , MPa
non-irradiation	4.0	10.3	584	724
gauze cavity	4.7	7.8	717	877
390	0.0	0.0	151	151
470	0.3	0.3	468	468
515	0.6	0.6	429	517
820	2.2	2.2	493	601
870	0.9	0.9	569	598
15	2.2	2.2	463	645

Table 4

Investigation results of tube specimens made of the fuel element cladding after exploitation in the BN-600 reactor at 400 °C.

Coordinates from core bottom	δ_u , %	δ_t , %	p, MPa	Rf, MPa
gauze cavity	11	31	27	303
390	2	3	46	380
470	2	4	48	382
820	5	9	34	278
870	5	20	33	320
915	4	9	35	283

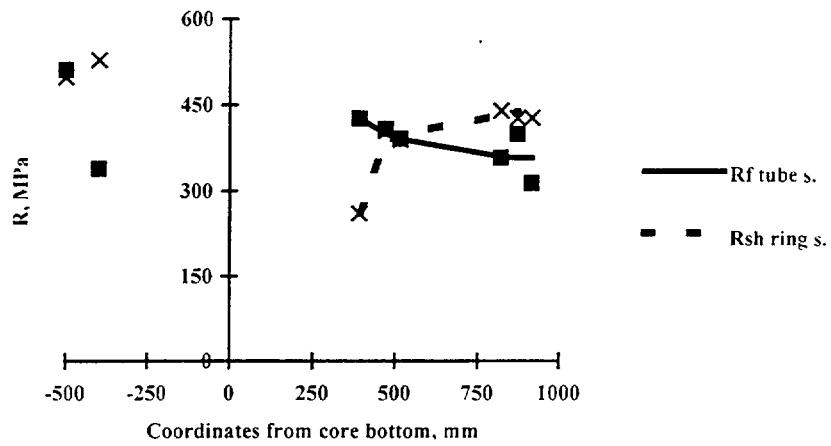
samples both for material of initial state and for most fuel element sections are considerably higher than values of tangential stress (when fracture of the tube samples have occurred). A section with minimum plasticity is expulsion where the ring - shaped samples are fractured at considerably lower stress. The causes of such differences are the following: fracture (during single - axle extension of rings) occur mainly by shear in area of main tangential stresses. At the same time shear component are absent, at least, up to the time while barrel - shaped blister willn't occur. Therefore, comparison of stress (when fracture have occurred) with shear component of fracture stress of the ring - shaped samples will be more correct. Dependence of fuel element section state in the core from strength characteristics for both type of tests are shown in Fig. 3. One can see, that shear component of ultimate strength is close to the value of tangential stress of the tube samples fracture on all range of the fuel element, with the exception of area with the coordinates 400 mm - 500 mm from the core bottom where rings fracture occur at considerably lower shear stresses. View of the tube samples from the brittlest area and from area with high plasticity (the core top) are shown in Fig. 4.

As test results show, both dependence of mechanical properties from fuel element position has analogous character and strength properties relationship obtained on the tube and ring - shaped samples is close at 400 °C (see Table 3 & 4). The fuel element cladding kept plasticity at 400 °C during tests of the tube samples. The minimum value of plasticity is 2.5 %. At the same time the ring - shaped samples have zero plasticity. Plasticity characteristics of the ring - shaped samples are decreased (in 2 times) at 400 °C in comparison with tests at room temperature. The tube samples have close value of specific elongation at the both temperatures, Fig 5. View of the tube samples are shown in Fig. 6 after their tests at 400 °C.

CONCLUSIONS

Carried out investigations results show that tests of the ring - shaped samples irradiated up to high fluence don't give sufficient information to predict residual operating life - time of the fuel elements. More correct information may be obtained from the flat samples expansion tests. However, in order to carry out the tests it is necessary to irradiate material assemblies. It requires additional expenditures. Mechanical properties obtained from that tests don't completely reflect fuel element cladding behavior, so far as stress - deformation state is realized there. The most close to real conditions plasticity characteristics are obtained during

**Strength characteristics of the fuel element cladding
for tube and ring-shaped specimens at 20 °C.**



**Plastisity characteristics of the fuel element cladding
for ring-shaped and tube samples at 20 °C.**

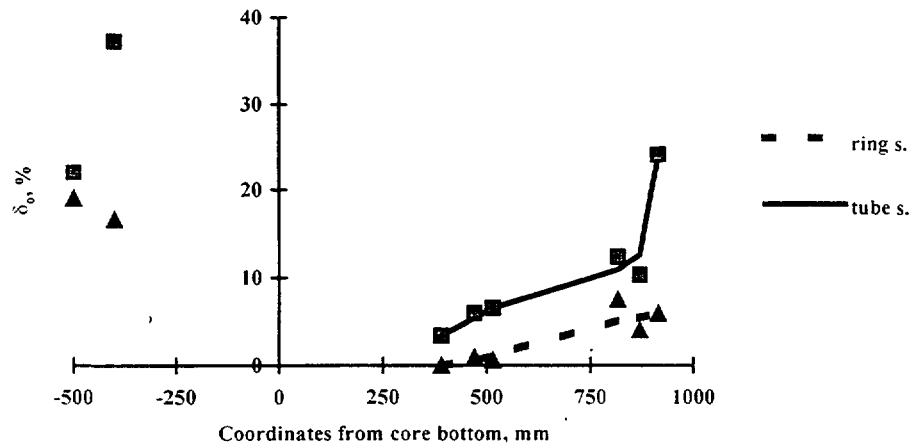
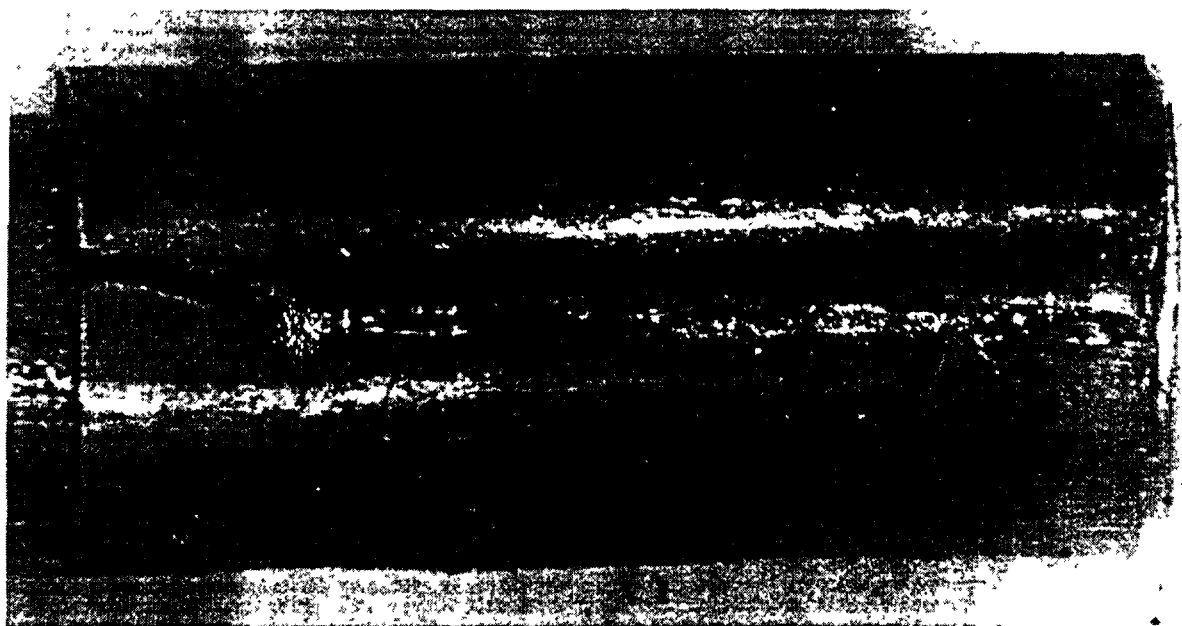


FIG. 3



a

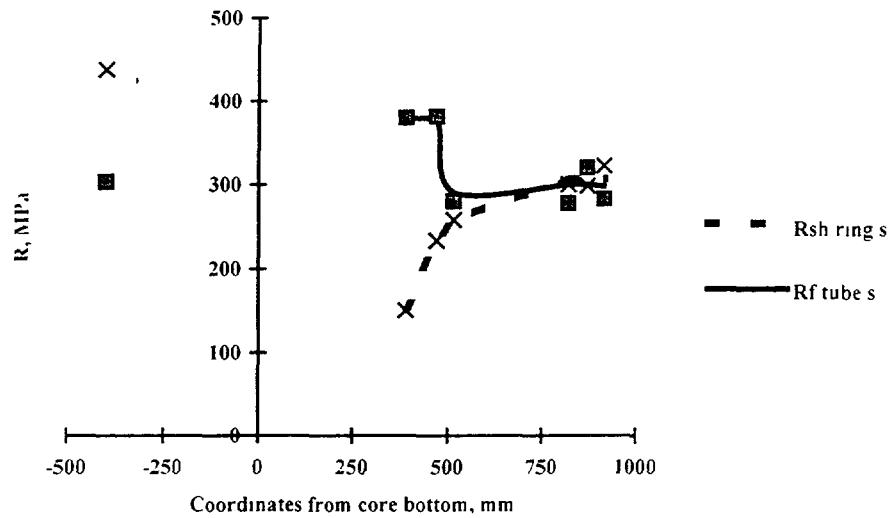


b

Fig.4. Tube specimens appearance after their research by internal pressure at 20 °C:

- a - the specimen from near core center;
- b - the specimen from core top.

**Strength characteristics of the fuel element cladding
for ring-shaped and tube specimens at 400 °C.**



**Plastivity characteristics of the fuel element cladding
for ring-shaped and tube specimens at 400 °C.**

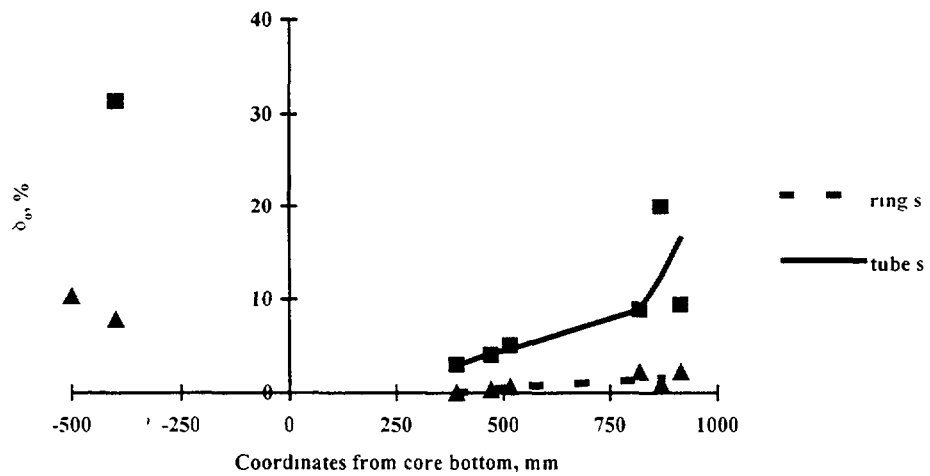
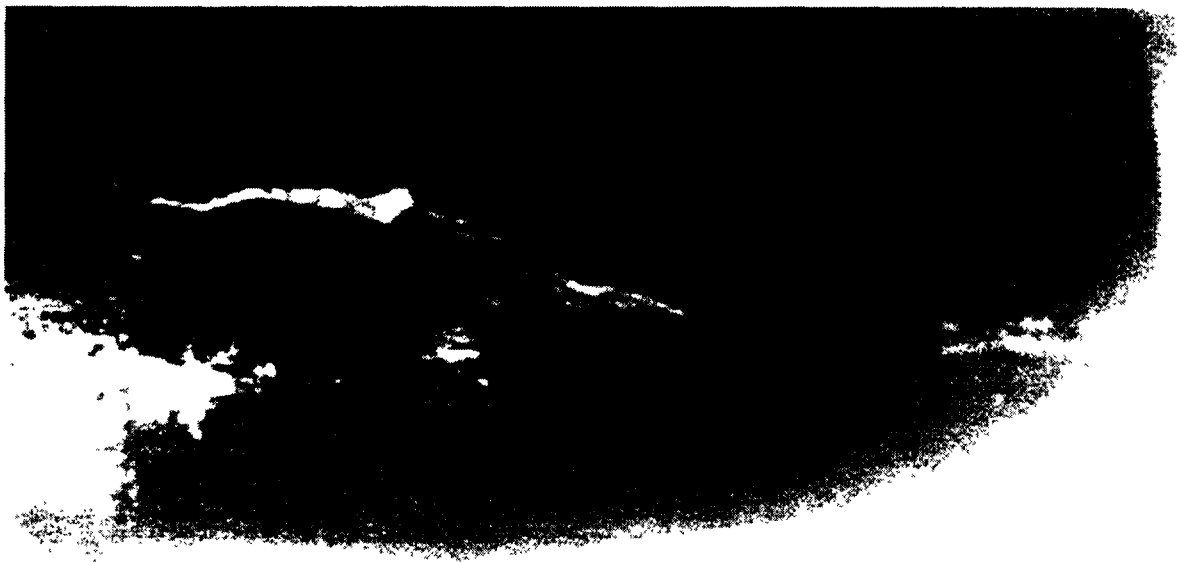


FIG. 5



a



b

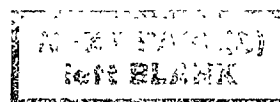
Fig.6. Tube specimens appearance after their research by internal pressure at 400 °C:

- a - the specimen from near core center;
- b - the specimen from core top.

tests of the tube samples fabricated from the fuel elements by internal pressure. But strength characteristics obtained aren't standard mechanical properties (which designers use), such as ultimate strength and conventional yield limit, while the characteristics show ultimate pressures and maximum tangential stresses in the fuel element cladding acceptable during exploitation. Probably, it is suitable now to combine the following techniques: tests of the ring - shaped samples at single - axle expansion and tests of the tube samples by internal pressure carried out in the real fuel elements after their exploitation in commercial reactors. In order to use data obtained correctly it is necessary to carry out fractographic investigation.

REFERENCES

- [1] S.A. Averin, A.V. Kozlov, V.A. Tsigvintsev, E.N. Ushakova, E.A. Medvedeva. The fourth interbranch conference on irradiation material science. Dimitrovgrad. 1995. abstracts. p. 117.
- [2] S.A. Averin, A.V. Kozlov, E.A. Medvedeva, Investigation of structural material of core elements of fast sodium reactor, RAS UrD, Ecaterinburg, 1994, p. 160.
- [3] E.A. Kinerv, A.V. Kozlov, A.V. Agopyan, G.V. Kalashnic, O.S. Korostin. 30 - anniversary of IVV - Complex, abstracts, 1996, p 107.
- [4] A.V. Kozlov, S.A. Averin, L.P. Sinelnikov, A.P. Isakov, Yu. G. Kuznetsov. The fourth interbranch conference on irradiation material science. Dimitrovgrad. 1995. abstracts. p. 187.
- [5] A.V. Kozlov, S.A. Averin, E.N. Shcherbakov, 30 - anniversary of IVV - Complex. abstracts, 1996, p 104.



SWELLING AND IN-PILE CREEP OF NEUTRON IRRADIATED 15Cr15NiTi AUSTENITIC STEELS IN THE TEMPERATURE RANGE OF 400 TO 600°C



XA9848055

R. HÜBNER, K. EHRLICH
Institut für Materialforschung,
Forschungszentrum Karlsruhe,
Karlsruhe, Germany

Presented by E. Materna-Morris

Abstract

A pressurized tube experiment was carried out in the Prototype Fast Reactor (PFR) at Dounreay in order to determine swelling, stress-induced swelling and in-pile creep of different austenitic steels. The tubes were made out of different heats of the commercial German austenitic steel DIN 1.4970 and a number of model plain Fe-15Cr-15Ni stainless steels. Special attention was paid on the influence of minor alloying elements like Si, Ti, degree of Ti/C relation and others. The maximum doses achieved are 106 dpa_{NRT} at 420°C, 81 dpa_{NRT} at 500°C and 61 dpa_{NRT} at 600°C. The hoop stresses of the pressurized tubes were 0, 60 and 120 MPa at all irradiation temperatures. The length and diameter changes of the pressurized capsules have been determined at up to four intermediate stages and after irradiation. Post irradiation examinations by immersion density measurements and transmission electron microscopy (TEM) are partially done.

All alloys exhibited the highest swelling values at 420°C and nearly no swelling at 600°C. The measurements show the large effect of the minor alloying elements upon swelling and in-pile creep. The maximum swelling suppression is achieved for DIN 1.4970 through a high Si-content and an understoichiometric Ti/C relation (understabilization). This yields linear swelling of 1.9% after 106 dpa_{NRT} at 420°C. The formerly observed intercorrelation between swelling and in-pile creep is confirmed up to 106 dpa_{NRT}. It can be described by an equation consisting of a SIPA term (stress induced preferential absorption) and an intercorrelation term similar to the I-creep proposed by Gittus. The estimates of the stress-induced swelling using the Soderberg theorem and the length measurements are compared with the immersion density measurements and results by TEM. The immersion density measurements agree rather good with the length measurements. The stress-induced linear swelling can reach values of 0.8% at 100 dpa_{NRT} and 120 MPa hoop stress. The measurements show an effect of the minor alloying elements on stress-induced swelling similar to the effect on stress-free swelling.

1. INTRODUCTION

The burn-up of a fuel element in a Fast Breeder Reactor is limited by volume swelling and in-pile creep. The improvement of these properties is therefore highly recommended. It is widely accepted that a proper choice of thermo-mechanical treatment and minor alloying elements can be very beneficial. Therefore an irradiation program was initiated some time ago to study the influence of important minor alloying elements on swelling and in-pile creep. This program named PFR-M2 was carried out in the British PFR reactor. First results have already been presented previously [1,2]. After the end of the irradiation the post irradiation examinations have started. First results will be presented for four heats of the German austenitic steel DIN 1.4970.

2. EXPERIMENTAL PROCEDURE

Pressurized capsules were fabricated from 6.0 by 0.38 mm cladding material with a cladding section length of 25.5 mm; the total length of the finished capsules amounts to 28.5 mm including the endplugs, which were resistance-welded to the sections. Argon was used as the filling gas instead of helium gas normally employed in order to achieve a greater weight loss in case of blow out. The filling pressure at room temperature was chosen to yield three different hoop stresses at the irradiation temperature. These were 0, 60 and 120 MPa.

The hoop stresses are calculated according to the thin-wall formula with correction to the ideal gas law as proposed by L'Air Liquide [3]

The capsules were irradiated in the British Prototype Fast Reactor (PFR) in Dounreay in contact with the reactor sodium. The three irradiation temperatures were nominal 420, 500 and 600°C. At certain intervals the samples were withdrawn from the reactor for inspections. Their diameter and length were measured with a 2σ accuracy of ± 2μm. Additionally the weight of the capsules was determined. This reveals the pressure loss of some samples with very fine cracks, which are hardly detected during normal handling in the hot cells. The accumulated doses achieved at the time of the intermediate measurements are given in Table I. The dose is calculated for Fe according to the so-called NRT-model.

Four compositional variations of the commercial German 15Cr15NiTi austenite DIN 1 4970 were examined. These variations are identified as B-, I-, K- and L-lot. The B-lot is a low-Si bearing melt, whereas the K-, L- and I-lot are made from high Si bearing melts. The K- and the L-lot stem from the same heats and differ only by a slightly different solution annealing temperature. The I-lot has a lower Ti-content which results in an understabilized condition. The chemical composition is summarized in Table II.

Only the one-dimensional length and diameter strains were determined in this experiment.

$$\varepsilon_D = \frac{D - D_0}{D_0} = \frac{\Delta D}{D_0} \quad \text{and} \quad \varepsilon_L = \frac{L - L_0}{L_0} = \frac{\Delta L}{L_0} \quad (1)$$

Therefore swelling in this paper means linear swelling which amounts to one third of volume swelling. According to the Soderberg theorem [4,5] the length changes originate solely from swelling as long as no other effects like texture effects occur. The diameter increase of a pressurized tube is then the sum of swelling plus the true creep strain, i.e. the volume conservative strain. The true or total swelling is therefore defined as

$$\varepsilon_{\text{true},s}(\sigma) = \frac{\Delta L}{L_0}(\sigma) = \frac{1}{3} \frac{\Delta V}{V_0}(\sigma) \quad (2)$$

The total swelling is the sum of the stress-free swelling and the stress-induced swelling.

$$\varepsilon_{\text{true},s}(\sigma) = \varepsilon_s(\sigma=0) + \varepsilon_s(\sigma) \quad (3)$$

TABLE I. MAXIMUM ACCUMULATED DOSE AT THE INTERMEDIATE MEASUREMENTS

Irradiation temperature [°C]	Accumulated dose [dpa _{NRT}] at measurement No				
	1	2	3	4	5
420	13	51	74	92	106
500	12	40	60	81	---
600	14	27	40	61	---

TABLE II. COMPOSITION OF THE DIN 1 4970 LOTS (wt%)^a

Alloy	C	Si	Mn	Cr	Ni	Mo	Ti
B-lot	0,083	0,42	1,60	14,92	14,73	1,19	0,47
K-lot	0,086	0,99	1,60	15,06	14,86	1,46	0,49
L-lot	0,086	0,96	1,64	15,15	14,90	1,46	0,50
I-lot	0,089	1,01	1,16	15,15	15,00	1,45	0,31

^a Thermo-mechanical treatment: 1100°C SA + 20% CW, except L-lot: 1120°C SA + 20% CW

With the stress-free swelling being the dimensional changes of a stress-free tube:

$$\varepsilon_s(\sigma=0) = \frac{\Delta D}{D_0}(\sigma=0) = \frac{\Delta L}{L_0}(\sigma=0) \quad (4)$$

The total diametrical strain of a pressurized tube then is the sum of all creep and swelling strains:

$$\varepsilon_{\text{tot}}(\sigma) = \frac{\Delta D}{D_0}(\sigma) = \varepsilon_{\text{true, s}}(\sigma) + \varepsilon_{\text{true, c}}(\sigma) \quad (5)$$

A problem arises for the length measurements. Ideally the length change should equal the amount of swelling. However the influence of the heat-affected zone and the endplugs, for technical reasons all fabricated from the same heat of DIN 1.4970, disturbs the length measurements. Assuming that these influences are the same for both a stressed and an unstressed sample, the stress-induced swelling is determined as the difference of the length increase of these samples:

$$\varepsilon_s(\sigma) = \frac{\Delta L}{L_0}(\sigma) - \frac{\Delta L}{L_0}(\sigma=0) \quad (6)$$

This method should also eliminate axial effects which might be caused by texture induced by the cold drawing.

When the stress-induced induced swelling could not be determined experimentally, the creep strain is defined without regard to the stress-induced swelling. It is called apparent creep as a distinction to the true creep:

$$\varepsilon_{\text{apparent, c}}(\sigma) = \varepsilon_{\text{tot}}(\sigma) - \varepsilon_s(\sigma=0) \quad (7)$$

After the irradiation the tubes are cut into pieces and the density change $\Delta\rho/\rho_0$ is determined by immersion density measurements. From these pieces the samples for the transmission electronmicroscope (TEM) are made. The evaluation of the void diameter and the void concentration yields the volume swelling $\Delta V/V$. This value is not very reliable, since the determination of the TEM-sample thickness is rather inaccurate.

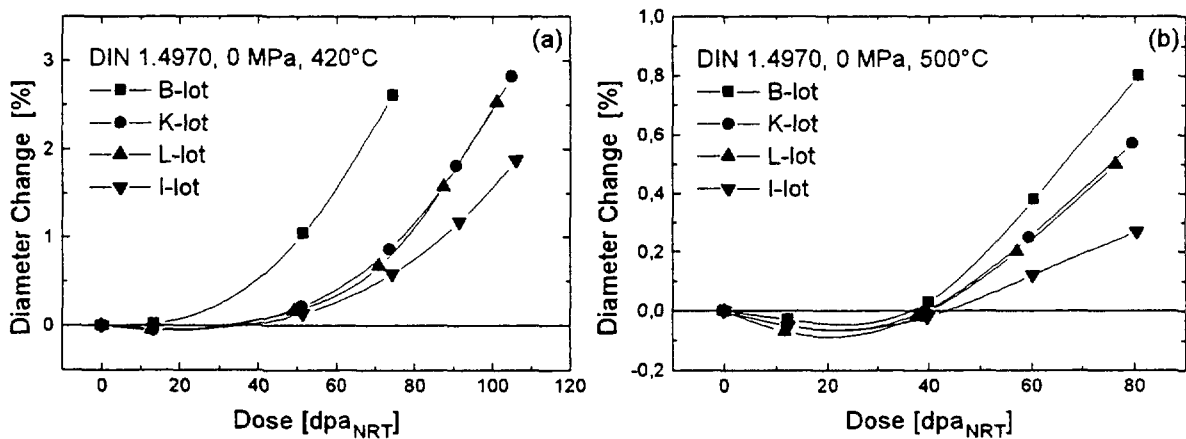


FIG. 1. Dose dependence of stress-free swelling for DIN 1.4970 (a) 420°C (b) 500°C.

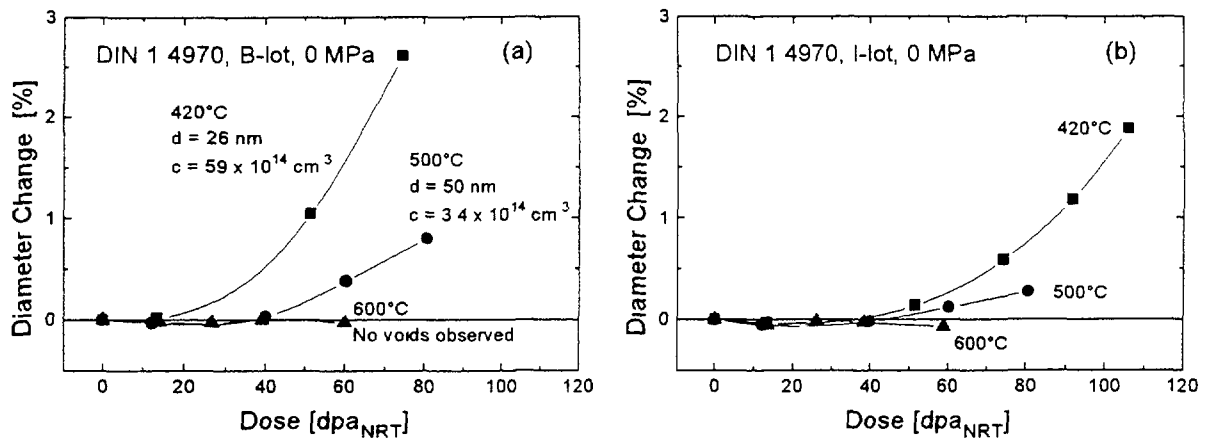


FIG 2 Dose dependence of stress-free swelling at different temperature (a) B-lot (b) I-lot
 d average void diameter, c average void concentration

3 RESULTS

3.1. Stress free swelling

The stress-free swelling has been determined as the diameter change of the stress-free tubes. Figure 1 shows this diameter change for the 4 lots of DIN 1 4970 as a function of dose at 420 and 500°C. It can be seen, that the low Si bearing B-lot shows the highest swelling. It was therefore already withdrawn after the third irradiation campaign. The high Si bearing K- and L-lot show an intermediate swelling. The slightly different solution annealing temperature shows no influence on swelling. The lowest swelling exhibits the high Si and low Ti bearing I-lot. This is in accordance with the results published earlier [2] on model alloys. Most effective in suppressing swelling is the addition of Si. The effect of Ti depends on the C-content. Most effective is understabilization.

The influence of the temperature is shown in Figure 2 for the high and the low swelling lots B and I. The results for the K- and the L-lot are similar. It can be seen that the swelling decreases with increasing temperature. At 600°C there is no swelling detectable up to 61 dpa_{NRT} for all lots. The TEM-analysis of the high swelling B-lot shows that the average void diameter at 500°C is about twice that at 420°C, but the void concentration is nearly 20 times lower.

Some stress-free samples of the B-lot have been irradiated at different reactor positions, so that they experienced different flux. The results of the stress-free swelling of these samples are shown in Figure 3. It can be seen that the swelling is increasing with decreasing flux. The analysis of these data is hampered by the uncertainty of the flux determination at low flux. Also an experimental artifact cannot be excluded.

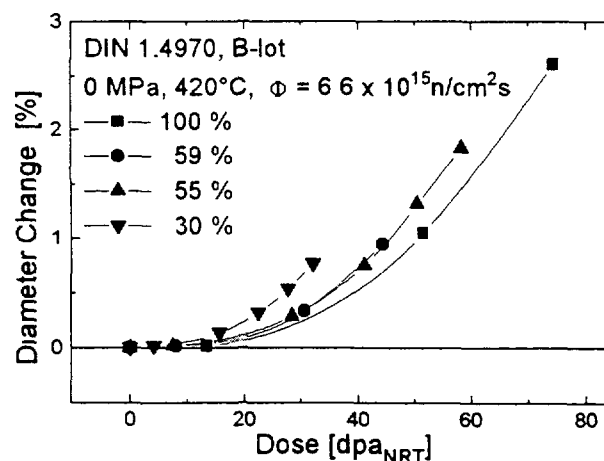


FIG 3 Dose dependence of stress-free swelling for DIN 1 4970 B-lot at different flux levels (in %)

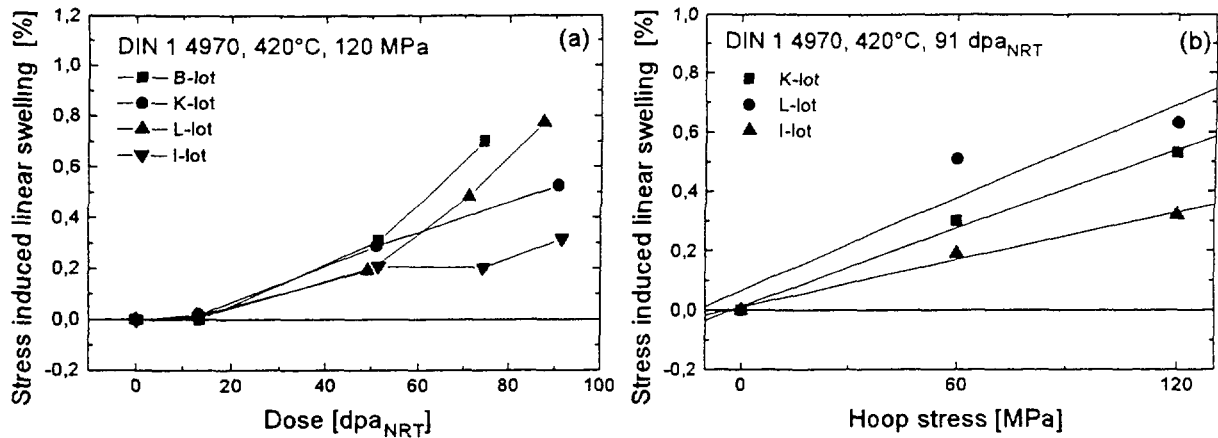


FIG 4 Stress-induced swelling at 420°C for DIN 1 4970 (a) dose dependence (b) stress dependence

3.2. Stress induced swelling

The stress-induced swelling has been determined by length measurement at intermediate doses and by immersion density measurement and TEM-analysis at the end of the irradiation. The results of the length measurements have already been published [1,2]. They can be summarized as follows: The amounts of stress-induced and stress-free swelling show no strong interdependence. Especially the stress-induced swelling exhibits no strong variation despite the large differences in stress-free swelling. This can be seen in Figure 4a. Nevertheless, the ranking according to the swelling resistance is preserved. Astonishing is the difference of stress-induced swelling between the K- and the L-lot, which differ only in a slightly different solution annealing temperature and show no difference in stress-free swelling and in-pile creep. As can be seen in Figure 4b the stress dependence is somewhat linear, but because of the data scatter no firm statement can be made.

The immersion density measurements made after the irradiation confirm the results of the length measurements. The stressed samples show a higher density change than the unstressed ones. To compare the results of the different methods the volume change is calculated out of the density change. The swelling is assumed as one third of the volume change. The stress-induced swelling is then the difference of the swelling of an stressed and an unstressed sample. The results of the I- and the K-lot are plotted in Figure 5. The agreement is similar for the other lots.

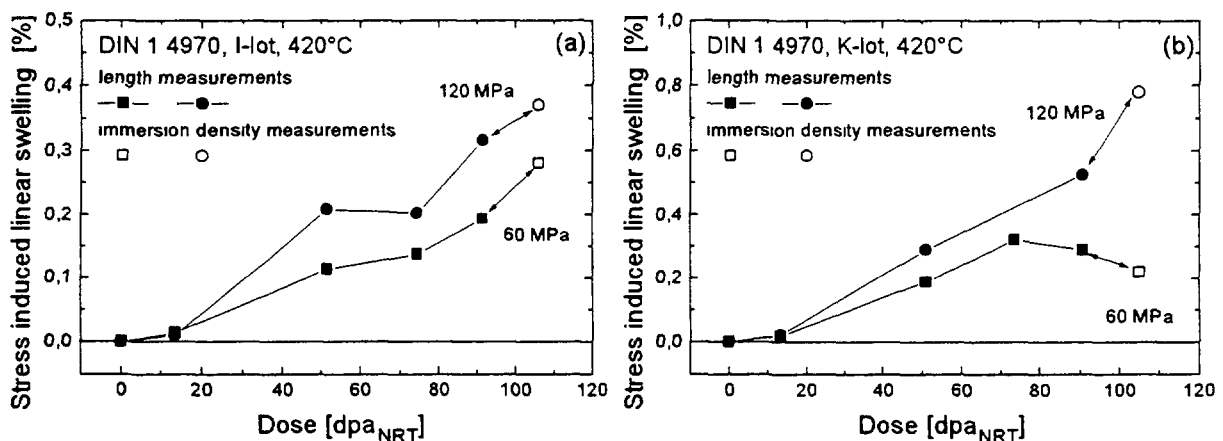


FIG. 5 Dose dependence of stress-induced swelling at 420°C (a) I-lot (b) K-lot

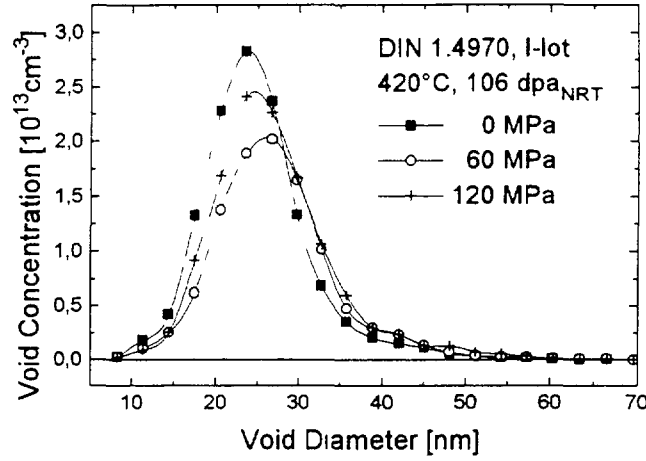


FIG. 6 Influence of stress on void structure at 420°C for DIN 1.4970 I-lot

There are two different mechanisms which could yield a higher swelling in the presence of stress [6]. On the one hand the stress can enhance the void growth. This would lead to bigger voids in a stressed sample compared to an unstressed one. On the other hand the stress can accelerate the void nucleation. This would lead to a higher void concentration. Mathematically these effects can be described as follows ($\Delta V/V_0$: volume change, σ_{hy} : hydrostatic stress)

$$\frac{\Delta V}{V_0}(\sigma_{hy}) = \frac{\Delta V}{V_0}(\sigma_{hy} = 0) \times (1 + A \times \sigma_{hy}) \quad (8)$$

$$\frac{\Delta V}{V_0}(\sigma_{hy}) = \frac{\Delta V}{V_0}(\sigma_{hy} = 0) + B \times \sigma_{hy} \quad (9)$$

Because of the great data scatter, the experimental data can be described with both formulas. The average values of the constants are:

$$\begin{array}{lll} \text{I-lot:} & A = 4 \pm 2 \times 10^{-3} \text{ MPa}^{-1} & B = 15 \pm 0.5 \times 10^{-4} \text{ MPa}^{-1} \\ \text{K-lot:} & A = 6 \pm 3 \times 10^{-3} \text{ MPa}^{-1} & B = 3 \pm 1 \times 10^{-4} \text{ MPa}^{-1} \end{array}$$

Until now only the samples of the I-lot have been examined in the TEM. The results are plotted in Figure 6. The averaged values of the void diameter d and the void concentration c are summarized in Table III. $\Delta V/V$ is the resultant volume swelling.

The effect of stress on the void structure is not straight forward. The 60 MPa sample contains bigger voids with a lower concentration than the unstressed sample. This results in a higher volume swelling. Increasing the stress up to 120 MPa increases the void concentration but results in a similar void diameter than the 60 MPa sample. Nevertheless the mechanism of accelerated void nucleation which yields a higher void concentration can be excluded.

TABLE III. AVERAGE VOID DIAMETER d AND VOID CONCENTRATION c OF DIN 1.4970, I-LOT

σ [MPa]	d [nm]	c [10^{15} cm^{-3}]	$\Delta V/V$ [%]
0	25	3.8	4.4
60	27	3.2	4.9
120	27	3.7	5.6

3.3. In-pile creep

In the earlier publications on this project [1,2] a linear correlation could be established between the total swelling and the true in-pile creep as well as between the stress-free swelling and the apparent creep at 420°C. This relation was applicable for both stresses used in this experiment. The stress-free swelling and the apparent creep correlation was of the form [2]

$$\varepsilon_{\text{apparent},c}(\sigma, \Phi t) = \text{SIPA} \times \sigma \times \Phi t + \text{IC} \times \varepsilon_s(\sigma = 0, \Phi t) \times \sigma^n \quad (10)$$

where

$$\text{SIPA} = 2.5 \times 10^{-6} (\text{dpa}_{\text{NRT}} \text{ MPa})^{-1}$$

$$\text{IC} = 10 \times 10^{-4} (\text{MPa})^{-1.5}$$

$$n = 1.5$$

Φt is the dose in dpa_{NRT}

The first term was formulated according to the theory of stress-induced preferential absorption [7]. While the second term was formulated according to the so-called I-creep model proposed by Gittus [8]. However this model postulates a linear stress dependence, while the results on the total swelling and the true in-pile creep can only be fitted with a stress exponent of 1.5 [1]. The constants SIPA and IC have been determined with the experimental data available after the fourth intermediate measurement which means a maximum dose of 90 dpa_{NRT} .

In Figure 7 the observed values of apparent creep are compared with the values calculated according to Equation (10) and the corresponding constants. The new results obtained after the last irradiation campaign with a maximum dose of 106 dpa_{NRT} are plotted as hollow symbols. It can be seen that these data can be described rather good with the equation and the constants obtained for a maximum dose of 90 dpa_{NRT} .

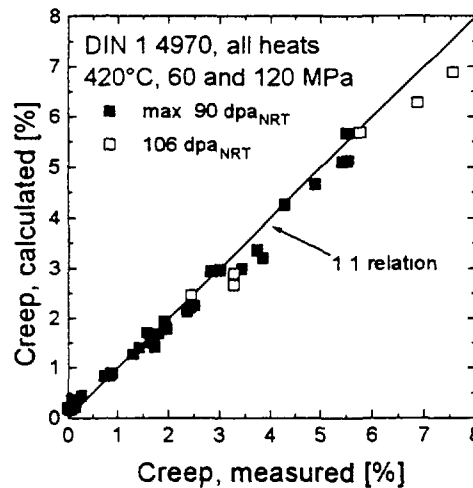


FIG. 7. Comparison of all experimentally measured and according to Equation (10) calculated in-pile creep strains for DIN 1.4970 at 420°C.

4. SUMMARY

The results from this experiment can be summarized as follows:

- The stress-free swelling is strongly affected by minor alloying elements. The best results are obtained with a high Si-content and a slightly understabilization with Ti.
- The swelling decreases with increasing temperature. This is caused by a strongly decreasing void concentration, which exceeds the increasing void diameter. At 600°C no swelling is observed up to 61 dpa_{NRT}.
- The effect of stress-induced swelling is confirmed by immersion density measurements and TEM-analysis. The effect of stress on the void structure is rather complicated, but the accelerated void nucleation can be excluded as the basic mechanism.
- The correlation between swelling and in-pile creep found earlier can be expanded up to 106 dpa_{NRT}. The in-pile creep can be described by a two term equation which adds the SIPA effect and a term similar to the I-creep model but with a stress exponent of 1.5.

REFERENCES

- [1] HERSCHBACH, K., SCHNEIDER, W., BERGMANN, H.-J., „Swelling and in-pile creep behaviour of some 15Cr15NiTi stainless steels in the temperature range 400 to 600°C“, Effects of Radiation on Materials: 14th International Symposium (Vol. II), ASTM STP 1046 (1990) 570-587
- [2] HERSCHBACH, K., SCHNEIDER, W., EHRLICH, K., „Effects of minor alloying elements upon swelling and in-pile creep in model plain Fe-15Cr-15Ni stainless steels and in commercial DIN 1.4970 alloys“, J. Nucl. Mater. **203** (1993) 233-248
- [3] L’AIR LIQUIDE, Division Scientifique, Encyclopedie des Gaz – Gas Encyclopaedie Elsevier, Amsterdam, New York (1976) 92 pp.
- [4] SODERBERG, C. R.; „Interpretation of creep tests on tubes“, Transactions of ASME **63** (1941) 737-748
- [5] NORTON, F. H., SODERBERG, C. R., „Report on tubular creep tests“, Transactions of ASME **64** (1942) 769-777
- [6] HERSCHBACH, K., SCHNEIDER, W., EHRLICH, K., „Bestrahlungsinduziertes Kriechen und Schwellen des austenitischen Werkstoffes Nr. 1.4981 zwischen 400 und 500°C (RIPCEX I)“, J. Nucl. Mater. **101** (1981) 326-335
- [7] HEALD, P. T., SPEIGHT, M. V., „Steady-state irradiation creep“, Phil. Mag. **29** (1974) 1075-1080
- [8] GITTUS, J. H., „Theory of dislocation-creep due to the frenkel defects or interstitialcies produced by the bombardment with energetic particles“, Phil. Mag. **25** (1972) 345-354

V.V. POPOV

Institute of Physics and Power Engineering, State Scientific Center,
Obninsk, Russian Federation

Abstract

The main mechanism of deformation of a fast reactor fuel pin clad under loading is in-pile creep. Depending upon the value of stress and temperature in a clad, two mechanisms of deformation may be realized: intergranular creep and intragranular dislocation creep, respectively at low stresses and at higher stresses. Intergranular creep is accompanied either by formation or growth of pores along grain boundaries (at $T_{irr} > 0.5 T_{melt}$) or by arising and development of cracks at grain triad joints (at higher temperatures). Formation of pores and cracks occurs as the stress exceeds a certain threshold value. The level of failure stresses in the course of reactor operation has been computed in relation to behaviour of an austenitic steel as a fuel pin clad material.

Strength analysis of fast reactor (FR) fuel pins requires knowing of in-pile mechanical properties of fuel pin cladding material and their description in the form of functional relationships to loading and irradiation parameters. Along the length of a fuel pin the cladding temperature varies in a rather large range. For example, if at the coolant inlet into a fuel assembly the cladding is heated up to $\sim 350^\circ\text{C}$, then at the outlet it may have a temperature close to 700°C .

The main mechanism of fuel pin clad deformation under loading is in-pile creep. In-pile experiments show [1] that dependence of clad material creep rate $\dot{\epsilon}_{cr}$ (austenitic steel) on irradiation temperature (T_{irr}) has two characteristic regions (see Fig. 1).

At $T_{irr} \geq 0.5 T_{melt}$ (let us call it region I; T_{melt} - melting temperature) a strong dependence of creep rate on irradiation temperature can be observed. At $T_{irr} < 0.5 T_{melt}$ (region II) this dependence is sufficiently weaker.

The dependence of in-pile creep rate on irradiation temperature may be well described by the law of Arrhenius:

$$\dot{\epsilon}_{CR} \sim \exp \left[-\frac{Q_I}{kT_{irr}} \right] + \exp \left[-\frac{Q_{II}}{kT_{irr}} \right]. \quad (1)$$

Here Q_1 and Q_2 are activation energies of creep process in regions I and II, and k - the Boltzmann constant.

In-pile investigations of influence of the stressed state in fuel pin clad on creep rate show [1],[2], that depending upon the stressed state level in a cladding two mechanisms of deformation may be realized (see Fig. 2,3).

a) At $\sigma \leq \sigma_y$ (T_{melt}, Φ) the cladding deformation occurs by slipping along the grain boundaries; here Φ is the fluence of neutrons with $E > 0.1$ MeV, σ_y - cladding material's limit of elasticity. In this case the dependence

$$\dot{\epsilon}_{CR} \sim \sigma \quad (2)$$

takes place.

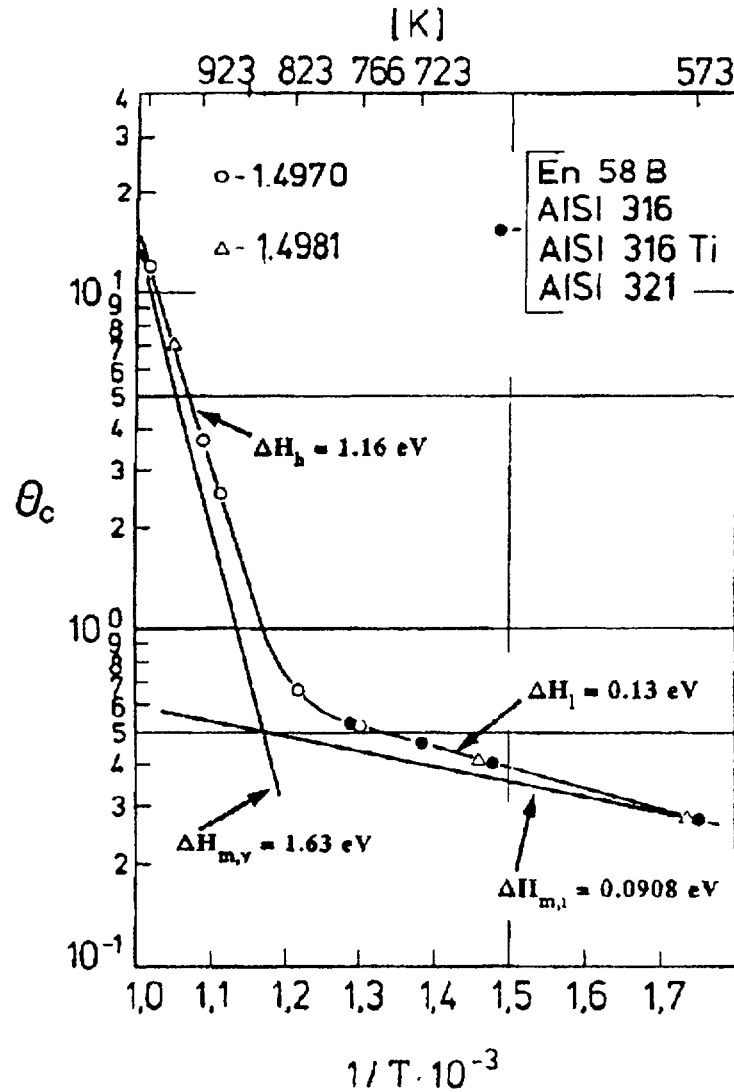


Fig. 1. Dependence of creep rate on testing temperature

b) At $\sigma > \sigma_y(T_m, \Phi)$ the cladding deformation is realized through the mechanism of intragranular dislocation creep, for which the dependence

$$\dot{\epsilon}_{CR} \sim \sigma^n \quad (3)$$

is valid.

If fuel pin cladding deformation is realized through the mechanism of slipping along grain boundaries, one may expect the intergranular nature of cladding failure under insignificant deformation.

Deformation of fuel rod cladding at the expense of intragranular dislocation creep can cause intragranular failure of clad under significant deformation.

Two mechanisms of creep intergranular failure are possible [3]:

- 1) arising of pores along grain boundaries, their growth and coalescence leading to cracking:

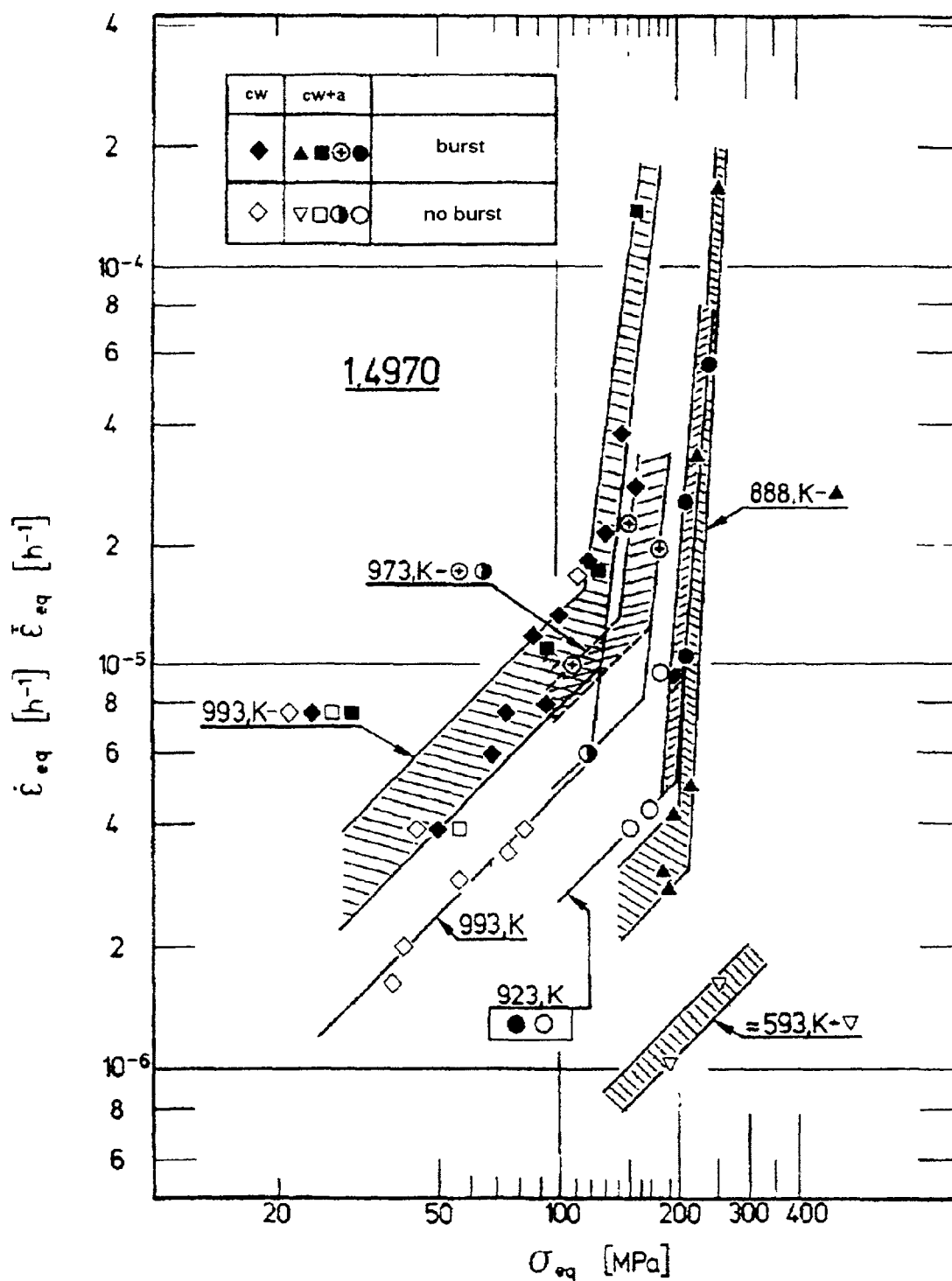


Fig.2. Dependence of irradiation induced creep rate of 1.4970 steel on testing stress

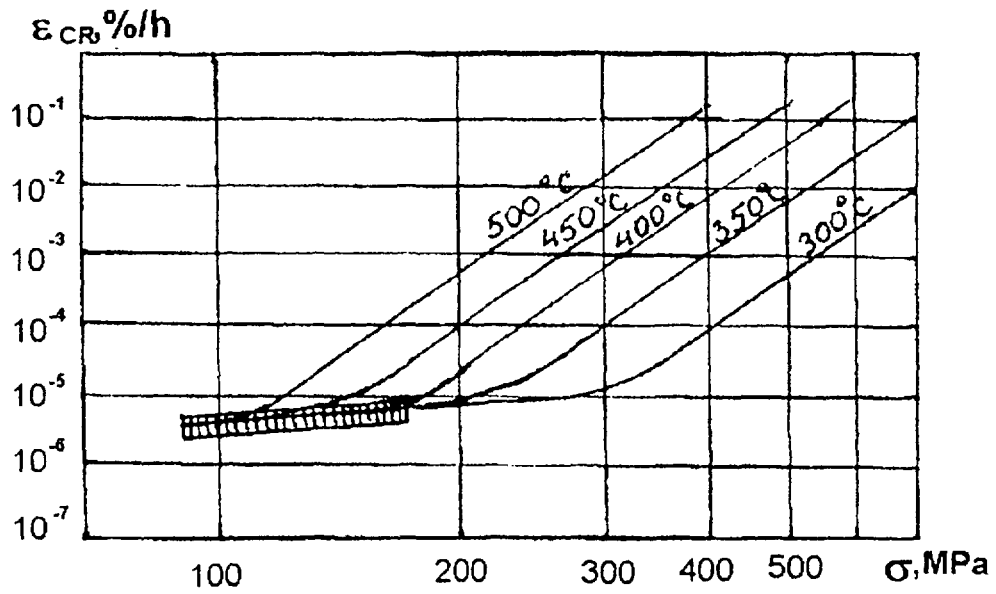


Fig.3. Dependence of creep rate on stress for steel of Cr16Ni15Mo3Nb type

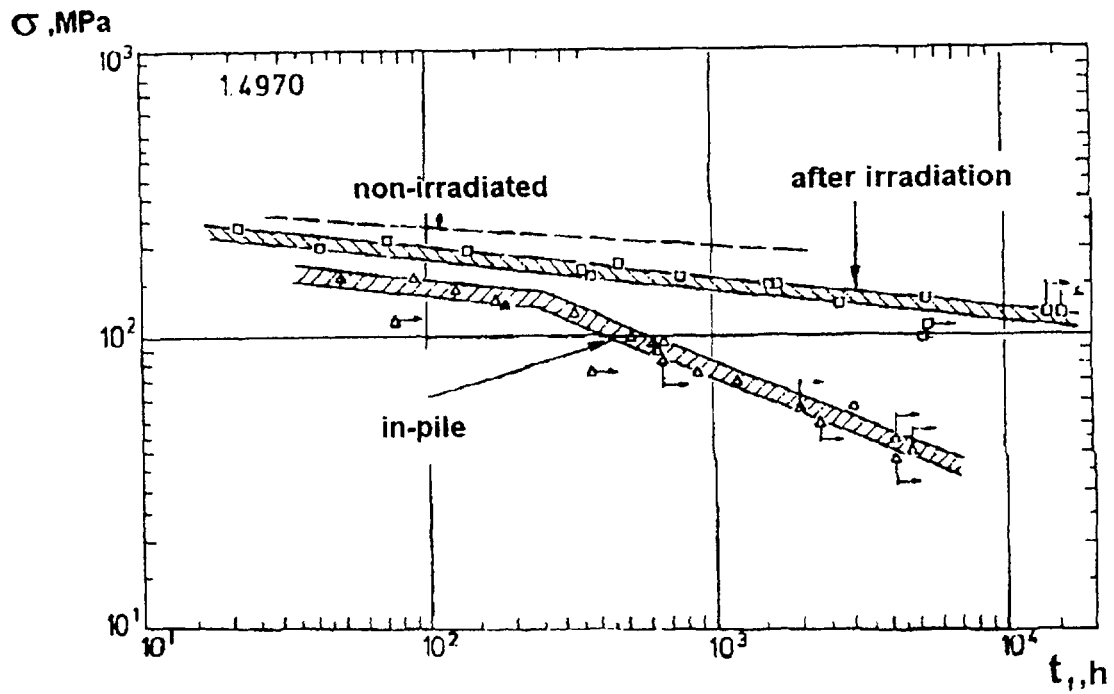


Fig. 4. High temperature of strength 1.4970 steel

2) arising of cracks at joints of grain triads, their growth along boundaries and confluence of cracks formed at different and not very distant joints of grain triads.

The first mechanism may be realized mainly at $T_m > 0,5 T_{melt}$, i.e. in the region I of a fuel pin cladding. Nucleation and growth of pores at grain boundaries occur under the stress

$$\sigma > \sigma_c^{por} \quad , \quad (4)$$

σ_c^{por} is a stress required for formation of a pore under given conditions of irradiation.

Realization of the second mechanism is most probable in the region II of a fuel pin cladding, as at lower temperatures of cladding it is easier to create the required stress concentration at a joint of a grain triad, which is necessary for crack formation, without softening action of grain plastic deformation. This plastic deformation is hindered by hardening effect of irradiation on cladding material at low temperatures. Arising of a crack and its growth from a joint of a grain triad occurs at a stress

$$\sigma > \sigma_c^{cr} \quad , \quad (5)$$

here σ_c^{cr} is a stress required for crack formation at a joint of a grain triad under given conditions of irradiation. The level of stresses σ_c^{cr} is considerably higher than that of σ_c^{por} .

Intergranular creep failure has been investigated in details, -see, e.g., [3]. It may be represented as a process of nucleation of voids in a grain, their growth and coalescence, which lead, as a result of plastic stability loss, to narrowing of partitions, separating them, and, after all, to rupture of these partitions.

As an example of relation between the mechanism of deformation and mechanism of failure let us consider the behavior of austenitic steel 1.4970 under stress at the temperature 720°C, see Fig. 2, 4.

As one can see in Fig.2, transition from dislocational intragranular creep to intergranular creep occurs under the stress $\sigma \approx 130$ MPa. Results relating to in-pile long-term strength and given in Fig. 4 show that transition from intergranular failure to intergranular one occurs under the stress $\sigma \approx 130$ MPa, too, and the mechanism of creep determines the nature of material's failure.

It can be seen in Fig. 4 that the value of limit stress under which pores still arise at grain boundaries may be taken equal to $\sigma_c^{por} \sim 40$ MPa. At lower values of stress, $\sigma < \sigma_c^{por}$, it is difficult, in a reasonable period of time, to achieve failure of fuel pin cladding material.

The value of the plenum volume in a FR fuel pin has been chosen in such a manner that after high burn-ups of fuel ($B \sim 15\%$ of heavy atoms) stresses in a fuel pin cladding caused by pressure of gaseous fission products will not exceed $\sigma \sim 100 - 120$ MPa. Thus a fuel pin cladding operates all the time under conditions of in-pile creep, ensuring the intergranular nature of deformation throughout the entire temperature range along a fuel pin.

Creep rate of cladding material, $\dot{\epsilon}_{CR}$, is a function of stress in cladding, σ , cladding temperature, T_{cl} , and rate of damage dose, \dot{k} . If a cladding of a FR fuel pin is loaded by the swelling fuel (after closing of fuel-cladding gap), the deformation rate of cladding under creep conditions is a function of fuel swelling rate

$$\dot{\epsilon}_{Cl} = f(\dot{S}) \quad (6)$$

here \dot{S} is fuel swelling rate.

Stress in a fuel pin cladding will be determined in this case from the equation:

$$\dot{\epsilon}_{Cl} = \dot{\epsilon}_{CR} \quad . \quad (7)$$

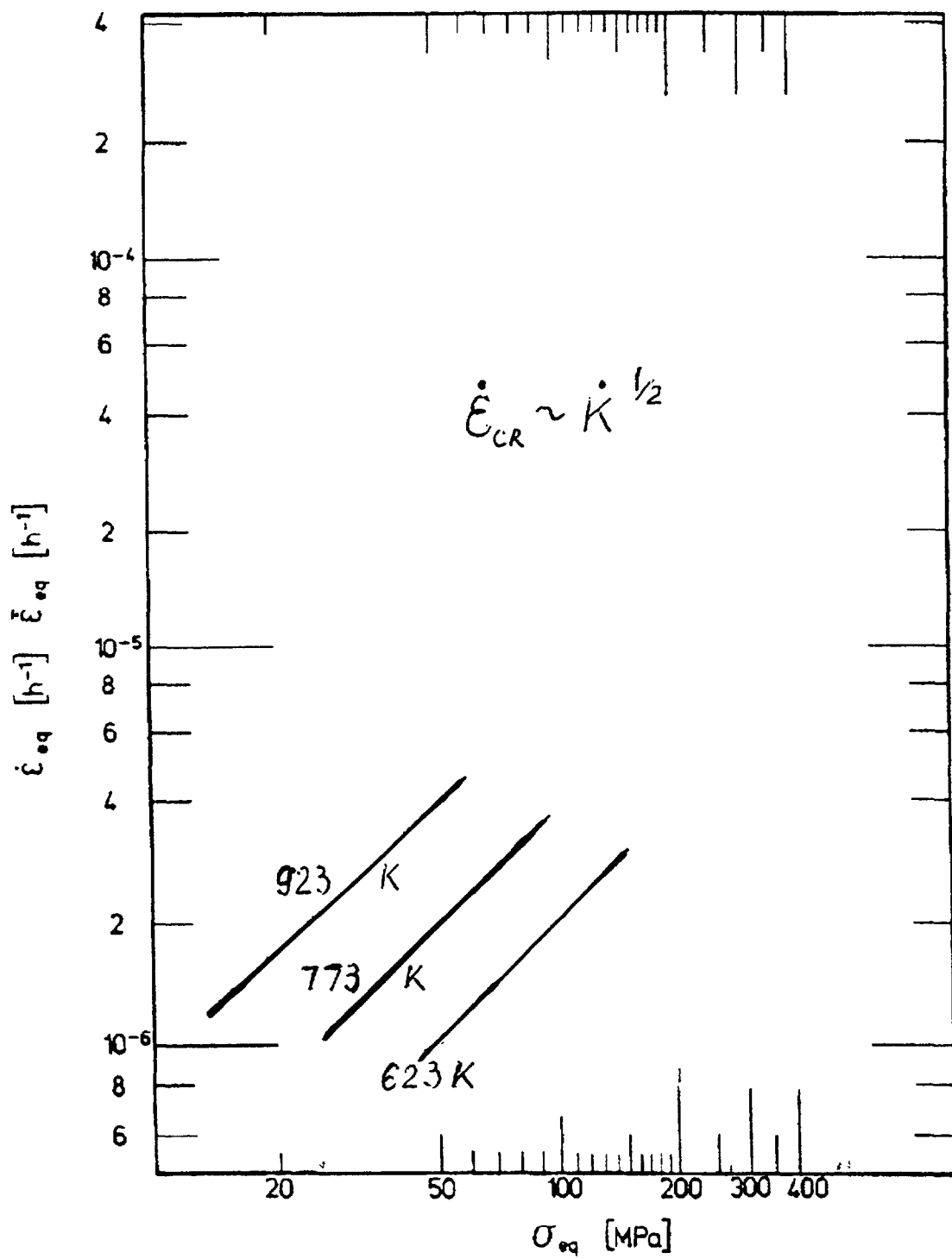


Fig.5. Dependence of irradiation induced creep rate of Cr16Ni15Mo3Nb type on testing stress.

Time to failure (t_f) with intergranular nature of material deformation under creep conditions is usually calculated according to Monkman-Grant relationship [3]

$$t_f \cdot \dot{\epsilon}_{CR}^m = C. \quad (8)$$

Here m and C are certain constants, t_f - time to failure, $\dot{\epsilon}_{CR}$ - steady creep rate of a material under the action of maximal applied stress σ .

Consider now an example of FR fuel pin strength analysis. Data on conditions of cladding irradiation are given in Table 1.

Table 1
FR fuel pin irradiation conditions.

	Top plane	Center plane	Bottom plane
Irradiation temperature, T_{cl} , °C	650	500	350
Rate of damaging dose accumulation, \dot{K} , dpa/h	$3,3 \cdot 10^{-3}$	$6,5 \cdot 10^{-3}$	$3,3 \cdot 10^{-3}$
Stress in fuel pin cladding, σ , MPa:			
at $B^{max} = 10\%$ h.a.	40	40	40
at $B^{max} = 15\%$ h.a.	65	65	65

The analysis of austenitic steels' fracture [1], [2] made it possible to estimate the dependence of cladding material austenitic steel of Cr16Ni15Mo3Nb type rate on applied stress, as well as values of constants m and C in relationship (8) at $T=650$ °C :

$$m \approx 2, C = 6 \cdot 10^{-7}.$$

Analysis of strength in the top plane of the cladding has been carried out for the time interval from $t=11520$ h to $t=17280$ h (maximal swelling, B^{max} , from 10 % h.a. to 15 % h.a.), i.e. $\Delta t=5700$ h. In this period of time the growth of pores at grain boundaries under creep conditions begins, as $\sigma > \sigma_C^{por}$. Determination of cladding creep rate has been carried out in accordance with Fig. 5

At the creep rate which is characteristic for stresses varying from $\sigma=40$ MPa to $\sigma=65$ MPa, the time to cladding failure, according to Fig. 5, is $t_p=2,4 \cdot 10^4 > \Delta t=5760$ h.

Thus in the top plane of cladding there will be no failure during $\Delta t=5700$ h. As in the central and bottom planes of a fuel pin the creep rate is still less than in the uppermost section, there will be no failure owing to pressure of gaseous fission products, too. If in the considered time interval Δt a fuel pin cladding will be loaded isotropically by swelling fuel (UO_2), then cladding deformation rate will be determined as:

$$\dot{\epsilon} = \frac{1}{3} \dot{S} \quad (9)$$

In the top and bottom planes sections of a fuel rod $\dot{S}=4,35 \cdot 10^{-6}$, $\dot{\epsilon}_{cl}=1,45 \cdot 10^{-6}$. In the central plane $\dot{S}=8,7 \cdot 10^{-6} h^{-1}$, $\dot{\epsilon}_c=2,9 \cdot 10^{-6}$. Such rates of a deformation of a cladding cause in it the stresses in the tjp plane $\sigma \sim 80$ MPa.

Thus the main loading factor for the upper planes of a fuel rod cladding is the pressure of gaseous fission products. For the central planes loading by this pressure and loading by fuel swelling are almost the same. For the lower planes loading of cladding by swelling fuel is more dangerous, but the level of stress $\sigma \sim 80$ MPa is not sufficiently high for formation of wedge-like cracks at joints of grain triads under creep condition.

REFERENCES

1. C.Wassilew "Bestrahlungsinduziertes Kriechen und Schwellen-Experimentelle Ergebnisse, Phanomenologische Modelle und Modellegleichungen fur Metalle".- KFK 4668 November 1989 Karlsruhe.
2. A.Ya. Rogosyanov, V.K. Gorbatov, B.V. Samsonov "Creep of Irradiated Austenitic Cr16Ni15Mo3Nb Steels at Temperatures 300-700°C". -Proceedings of the International Conference on Radiation Materials Science, v.8 1990, p.3-6.
3. J.Cadec. Polzuchest i metallicheskh materialov. - Moskwa, "Mir", 1987.
4. K.Miller. Polzuchest i razrusheniye. - Moskva, Metallurgiya, 1986.

A RE-EVALUATION OF HELIUM/dpa AND HYDROGEN/dpa RATIOS FOR FAST REACTOR AND THERMAL REACTOR DATA USED IN FISSION-FUSION CORRELATIONS

F.A. GARNER, L.R. GREENWOOD
Pacific Northwest National Laboratory,
Richland, Washington



B.M. OLIVER
Rockwell International,
Canoga Park, California

United States of America

Abstract

The ^{59}Ni isotope produced by the ^{58}Ni (n, γ) reaction has three highly exothermic reactions, (n, α), (n,p), and (n, γ). These reactions contribute to the displacement damage and two of them can generate significant amounts of helium and hydrogen. The production of helium in EBR-II at high neutron exposure has been measured and found not to include a significant contribution from ^{59}Ni in those core volumes where most material's data were generated. This is in contrast to a significant ^{59}Ni contribution that occurs in the softer below-core areas of FFTF. The often overlooked ^{59}Ni contribution to hydrogen generation is of particular importance when considering neutron spectra with a substantial thermal neutron component, however. Inclusion of the (n,p) and (n, γ) recoil events in the dpa damage calculations requires only a 3% correction to the previously published value, indicating that most of the damage arises from the (n, α) reaction.

1. BACKGROUND

Both helium and hydrogen generated in structural steels by neutron-induced transmutation are receiving renewed attention in both the light water reactor and fusion reactor materials communities. This increased attention is due to the relatively recent discovery that the levels of both gases can be very high for some long-lived components near the core of pressurized water reactors [1,2] and also due to the current focus of the International Thermonuclear Experimental Reactor (ITER) effort on water-cooled designs. Thus, for both ITER and light water reactors, the lower temperatures involved present the possibility that hydrogen may tend to accumulate rather than migrate out of typical stainless steels used in their construction. There are also some indications that hydrogen may exert a stronger effect in the presence of large amounts of helium [3-5], possibly by storage as H_2 in voids and bubbles.

It has been generally accepted that the generation rates of these gases per dpa will be significantly different between fast reactors where most of the irradiation performance data are generated and fusion reactors, which will have much higher initial rates of gas generation. Studies conducted in FFTF-MOTA, however, have shown that the gap between fast reactor and fusion rates for helium production progressively closes as ^{59}Ni is formed and produces helium via a (n, α) reaction, as shown in Fig. 1, especially for irradiations conducted in the core-edge or out-of-core locations [6]. A very significant portion of FFTF irradiations to high neutron exposure was conducted in the below-core basket, where the helium generation rate strongly increases with fluence. Since the ^{59}Ni isotope also has a strong (n,p) cross-section, this means that both the He/dpa and H/dpa ratios will increase with continuing exposure in these near-edge and below-core regions.

Much of the earlier irradiation data was generated in fast reactors such as EBR-II and DFR, which have maximum values of mean neutron energy on the order of 0.8 MeV compared to that in FFTF of ~0.5 MeV. This difference arises from the use of metal fuel in EBR-II and DFR, as

opposed to oxide fuel in FFTF. Therefore, the neutron spectra in EBR-II is not as soft as that in FFTF and will produce lower levels of ^{59}Ni . Also, the out-of-core regions of the EBR-II reactor were not used as extensively as those of FFTF. It was considered prudent, however, to experimentally determine whether the helium/dpa ratio assumed for EBR-II and DFR experiments increased at higher exposure levels in a manner similar to that of FFTF.

This paper will concentrate on three related topics. The first is an experimental determination of helium/dpa ratios across the core of EBR-II. The second topic is a reassessment of the hydrogen generation rate to include the contribution of the ^{59}Ni (n,p) reaction, and the third topic is a reassessment of the consequences of the (n, α), (n,p), and (n, γ) cross sections of ^{59}Ni on the atomic displacement rate.

2. HELIUM MEASUREMENTS AT HIGH NEUTRON EXPOSURE IN EBR-II

Table 1 shows the irradiation conditions chosen, covering eight axial positions from a sequential irradiation in first the AA-7 and then the AA-1 experiments in Row 2 of EBR-II. The AA-7 portion of this experiment was used earlier to determine the dependence of void swelling in Fe-Cr-Ni ternary alloys on dpa, irradiation temperature and composition [7,8].

It is important to note that not only does the neutron flux vary significantly over the small EBR-II core, but the spectral environment also softens as the core edge is approached. Fig. 2 shows the dpa level produced per fast neutron, when energies are measured above 0.1 MeV.

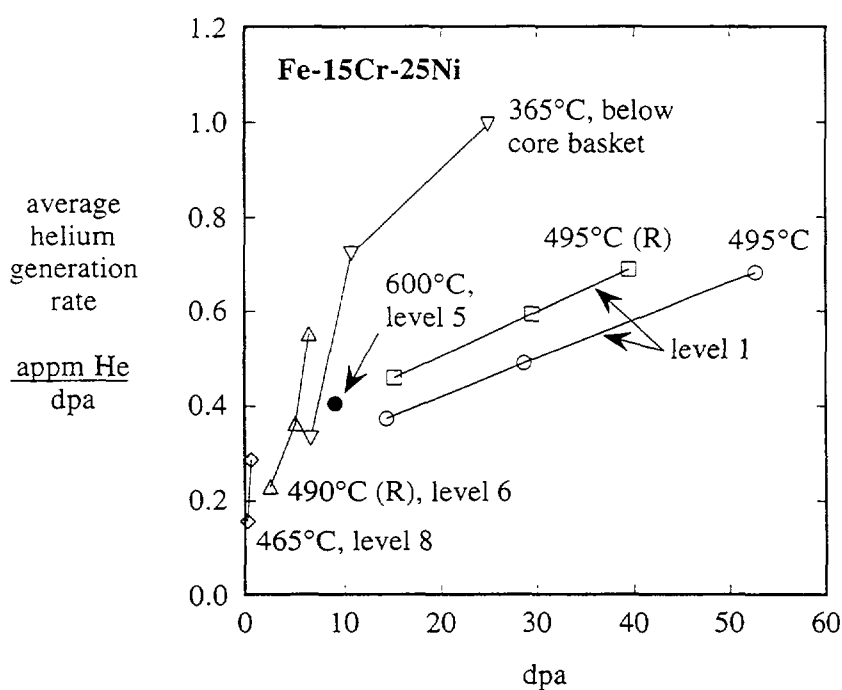


FIGURE 1. Measured helium generation rates for ternary Fe-15Cr-25Ni specimens irradiated in various positions in the FFTF reactor, averaged over the full duration of the various discharges of the experiment, demonstrating the strong effect of ^{59}Ni burn-in [15]. The levels refer to various elevations in the Materials Open Test Assembly (MOTA).

TABLE 1. Irradiation Conditions for Fe-15Cr-XNi Alloys in EBR-II*.

Temperature °C	dpa ⁺	Nominal Nickel Levels, wt%		
		15	45	75
454	76		x	
482	101		x	
538	121		x	
650	130		x	
593	131	x	x	x
510	125		x	
427	108	x	x	x
400	82	x	x	x

- * The relative position in the table also represents the relative axial position in the core, from top to bottom of the irradiation pin.
- + The dpa level chosen represents that calculated for the center of the packet. For the top and bottom packets, this introduces some uncertainty arising from the strong gradients of flux and spectrum at the core edges.

Specimens chosen for helium measurement were Fe-15.0Cr-45.3Ni (wt%) at all eight core axial locations. In addition, Fe-15.6Cr-15.7Ni and Fe-14.6Cr-75.1Ni were also measured, but only at three of the four locations in the bottom half of the core. The latter were added to check that nickel is indeed the dominant source of both high energy (>6 MeV) threshold reactions and low energy (⁵⁹Ni) reactions. The helium measurements were made using isotopic mass dilution with very high accuracy [9,10].

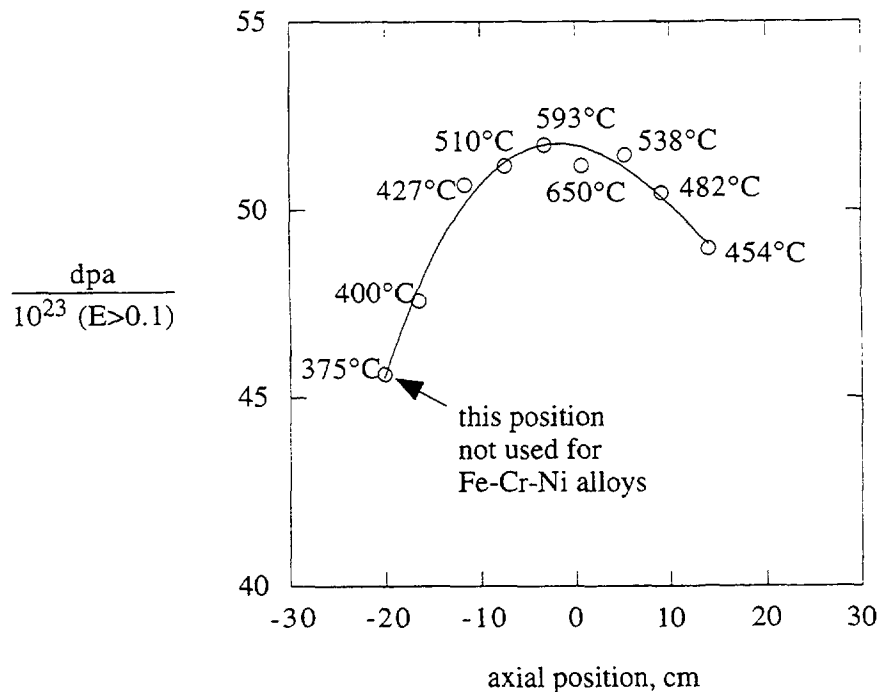


FIGURE 2. Displacements per dpa calculated for Row 2 of EBR-II.

Fig. 3 presents the dependence of helium content on nickel level for the three axial positions where all three alloys were measured. It is clear that helium increases linearly with nickel content at all three dpa levels. The irradiation temperature is not relevant to this determination. When all data are normalized to 15.5% nickel (Fig. 4), it appears that there is a slight increase as one goes from the inside of the core (593°C) toward the outside (400°C). This difference is very small and may reflect only a very slight action of the ^{59}Ni contribution to increase the helium as the high energy reactions involving all three elements (Ni, Fe and Cr) decline as the spectrum softens toward the core edge.

Fig. 5 shows the helium/dpa ratio calculated as a function of core position. With one exception at 400°C, this ratio equals 0.81 ± 0.02 appm He/dpa. The 400°C capsule straddles the lower core boundary and experiences a strong flux gradient along its length. Since the exact placement of the individual specimens in the packet cannot be determined, it may be that the dpa assignment for the measured specimen is too high, thereby producing an artificially lower helium/dpa ratio.

If the dpa levels are accepted without question and the data are plotted vs. dpa, as in Fig. 6a, an apparent intercept of ~16 dpa is found, followed by a steady-state helium/dpa rate of 0.94 appm/dpa. Such a plot implies that ^{59}Ni is playing a significant role, with the intercept reflecting the delay required to breed the ^{59}Ni . In Fig. 6b, however, the 400°C datum is ignored and the data extrapolate back to the origin with a slope of 0.81 appm/dpa.

In order to determine whether Fig. 6a or 6b presents the correct interpretation, another calculation was performed using dosimetry measurements performed on activation foils irradiated to ~11 dpa in Row 3 of EBR-II. Fig. 7 shows that over the bottom half of the core the calculated helium/dpa ratio for Fe-15.0Cr-45.3Ni varies only from 0.81 to 0.89, including both high energy threshold contributions and ^{59}Ni contributions. This implies that Fig. 6b is the correct interpretation.

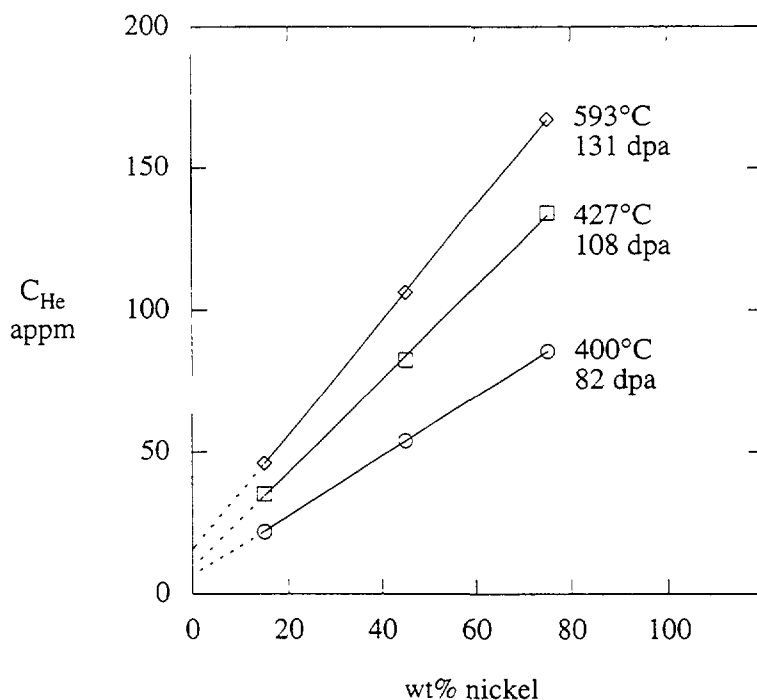


FIGURE 3. Dependence of helium generation on nickel content for Fe-15Cr-XNi alloys at three positions in EBR-II.

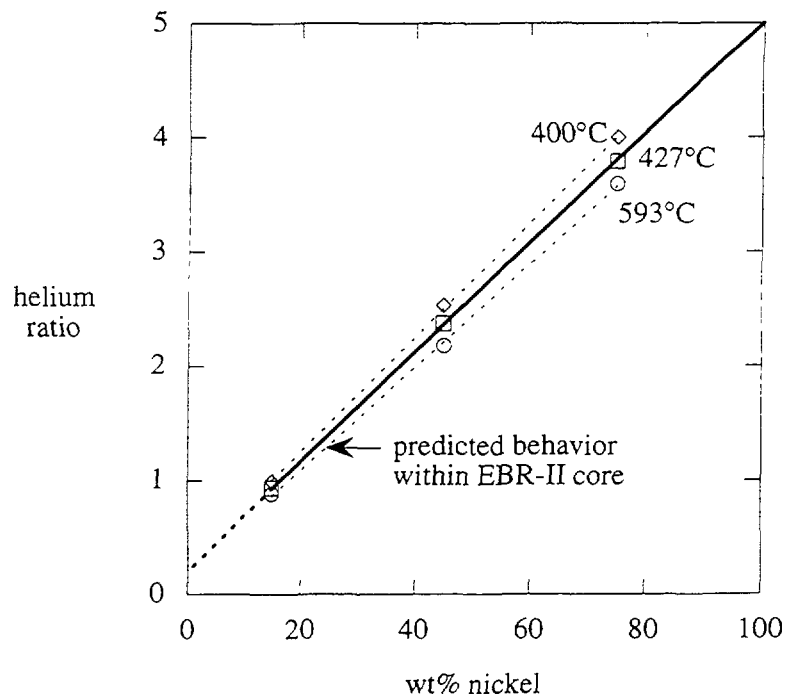


FIGURE 4. Dependence of helium generation on nickel content for Fe-15Cr-Ni alloys normalized to 15.7% nickel.

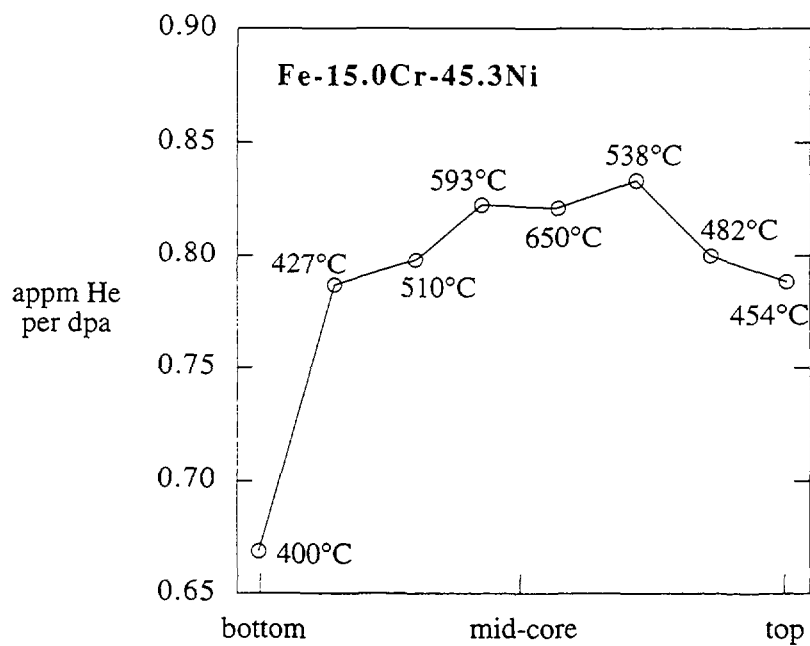


FIGURE 5. Measured helium/dpa ratios for Fe-15Cr-45.3Ni as a function of axial position.

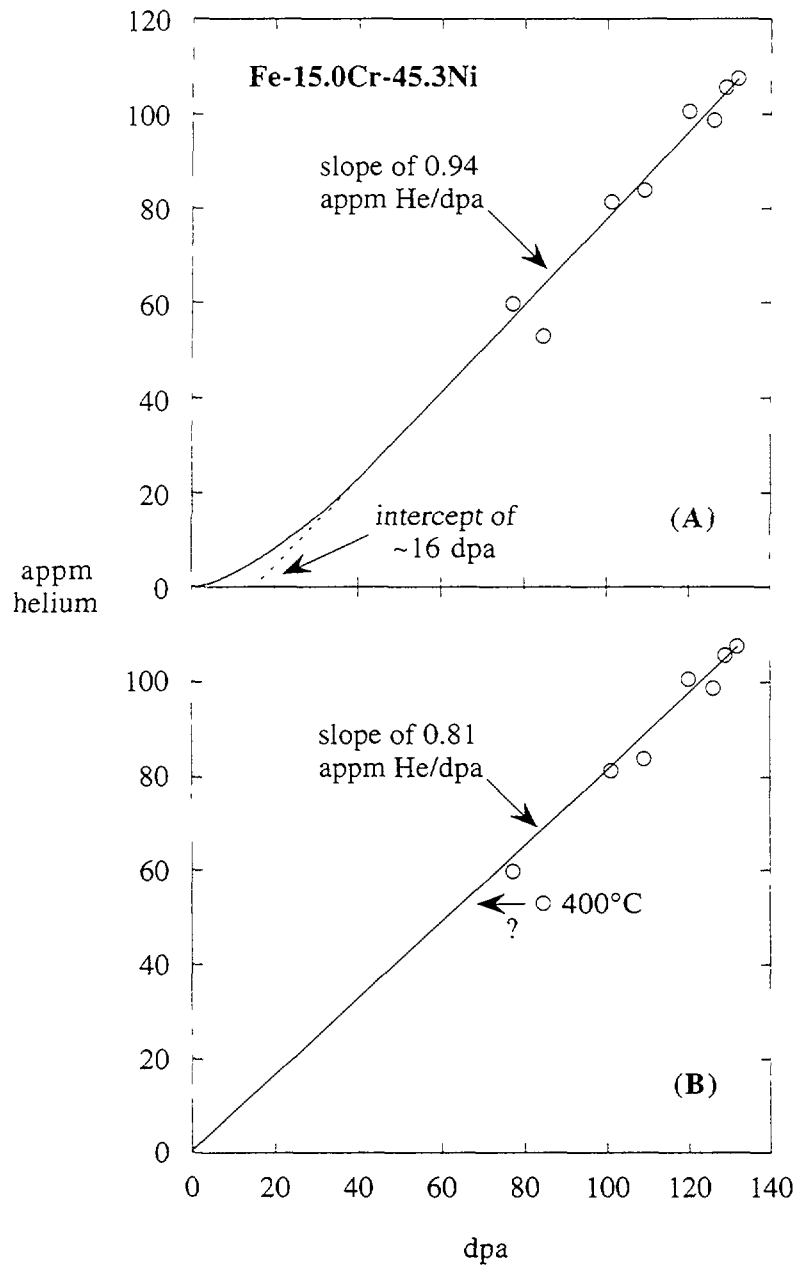


FIGURE 6. Two interpretations of the data, depending on whether the 400°C datum is included.

Table 2 shows the calculated contribution of both helium contributions at three positions for Fe-15Cr-45Ni at 60 dpa. It is obvious that the ^{59}Ni contribution at high fluence levels is only significant far from the core where the mean neutron energies are comparable to those studied in the ^{59}Ni -doping experiments conducted in FFTF [6]. No significant amount of irradiation performance data was generated outside the EBR-II core at such distances, however.

Based on the above data and calculations, it appears that it is not necessary to reconsider any conclusions regarding helium effects based on data generated in EBR-II.

TABLE 2. Helium Generation Calculated for Fe-15Cr-45Ni irradiated in EBR-II to 60 dpa*.

Height**	Fast Neutron Contribution	⁵⁹ Ni Contribution
-15.0 cm#	48.7 appm	0.75 appm
-4.3 cm	51.8	0.17
+37.5 cm	21.3	10.5

* Calculations based on dosimetry measurements at 11 dpa in Row 3

** Measured from core center

-15.0 cm is the core bottom, +15.0 is the core top.

3. HYDROGEN AND HELIUM GENERATION

At low neutron fluences in most materials and neutron spectra, hydrogen and helium are generated solely by fast neutron (n,p) and (n,α) reactions. Since (n,p) reactions have lower fast neutron thresholds (1-2 MeV) than (n,α) reactions (4-6 MeV) in most materials, hydrogen production is typically much larger than helium production. In mixed-spectrum reactors, the well-known ⁵⁸Ni (n,γ) ⁵⁹Ni(n,α) ⁵⁶Fe reaction sequence has been used to simulate fusion-relevant helium-to-dpa generation rates in nickel-bearing alloys [1]. The reaction cross sections, the formula for calculating the helium generation, and the experimental verification in mixed-spectrum reactors have been published previously [11,12]. However, it has generally been overlooked that the competing ⁵⁹Ni(n,p) ⁵⁹Co reaction will also lead to significant increases in the hydrogen generation. The thermal neutron cross sections for the ⁵⁹Ni(n,p) and (n,α) reactions are 2.0 and 12.3 b, respectively, thus leading to about one hydrogen atom for every six helium atoms produced. The

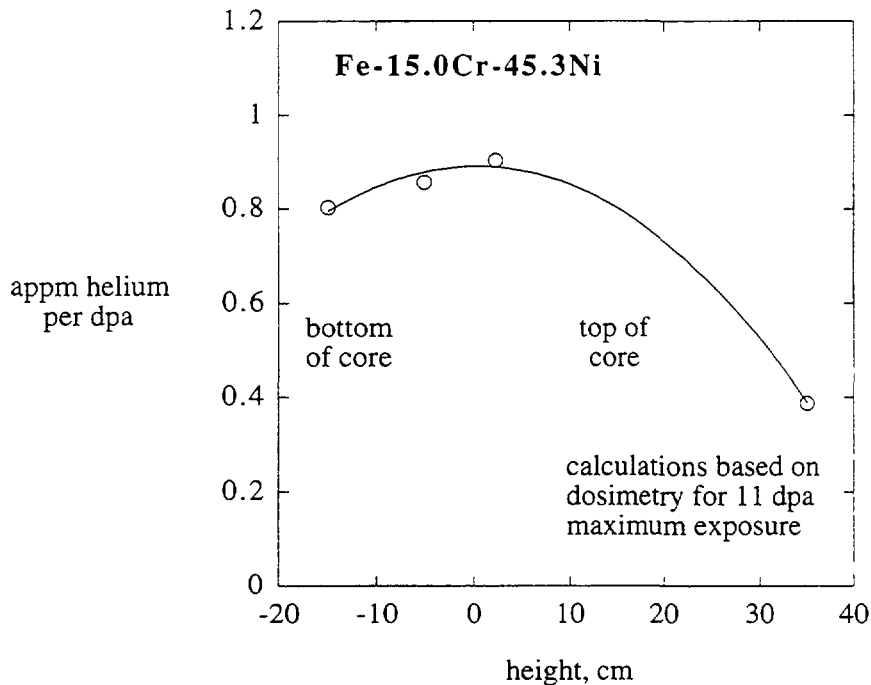


FIGURE 7. Calculated helium/dpa ratios for Fe-15.0Cr-45.3Ni based on dosimetry data from Row 3 of EBR-II at 11 dpa.

energy-dependent (n,p), (n,α), and (n,γ) reaction cross sections for ^{59}Ni are shown in Fig. 8. The large resonance near 0.3 keV produces significant hydrogen and helium at epithermal energies, resulting in enhanced helium and hydrogen production in fast reactors.

The formula for calculating the hydrogen production from this two-step reaction is, as follows:

$$\frac{N(\text{H})}{N_0(^{58}\text{Ni})} = \frac{\sigma_p}{\sigma_T} + \frac{\sigma_p e^{-\sigma_\gamma \phi t}}{(\sigma_\gamma - \sigma_T)} - \frac{\sigma_\gamma \sigma_p e^{-\sigma_\gamma \phi t}}{(\sigma_\gamma - \sigma_T) \sigma_T}$$

where $N(\text{H})$ is the number of hydrogen atoms produced, $N_0(^{58}\text{Ni})$ is the initial number of ^{58}Ni atoms, σ_x refers to the cross sections for the $^{59}\text{Ni}(\text{n,p})$, $^{59}\text{Ni}(\text{n, total absorption})$, and $^{58}\text{Ni}(\text{n,}\gamma)$ reactions as indicated by the subscript, ϕ is the neutron flux, and t is the irradiation time. In a reactor neutron spectrum, the cross sections must be averaged over the entire neutron spectrum and the flux used in the equation is the sum over all neutron energies. To determine the hydrogen content in natural nickel, the ratio of hydrogen to ^{58}Ni atoms must be further multiplied times the abundance of ^{58}Ni of 0.683, and in alloys the nickel content must also be included. It is also important to note that the net hydrogen and helium production in nickel-bearing materials must further take account of the fast (n,p) and (n,α) reactions which will dominate gas production at low neutron fluences. Note that the ^{59}Ni cross sections reverse in Fig. 8 such that at higher neutron energies hydrogen production is much more likely than helium production, as is the case with the stable nickel isotopes.

The above equation predicts that if the neutron spectrum contains a significant thermal component, then ^{58}Ni will be rapidly converted to ^{59}Ni and that hydrogen and helium will subsequently be produced in a non-linear fashion due to the time required for the in-growth of ^{59}Ni . At neutron fluences less than 10^{20} n/cm², the equations can be simplified so that the hydrogen and helium generation are approximately equal to 4.49×10^{-48} cm² and 2.76×10^{-47} cm² times the square of the thermal neutron fluence, respectively, using cross sections from Ref. [13].

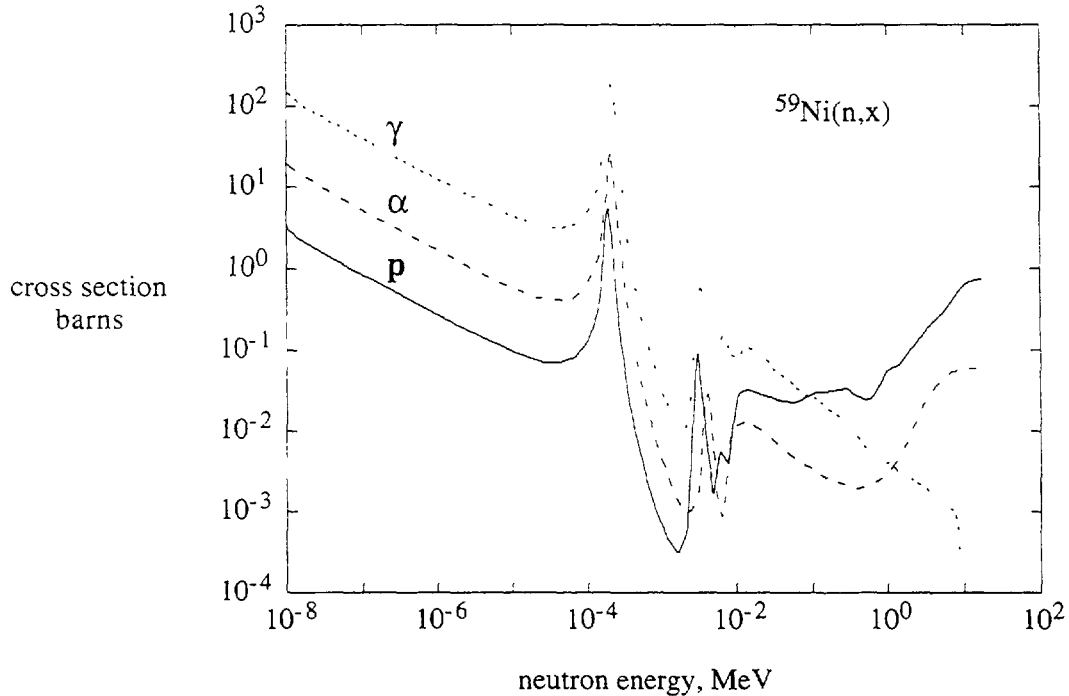


FIGURE 8. Neutron cross sections for the (n,γ), (n,α) and (n,p) reactions of ^{59}Ni .

Depending on the neutron spectrum, the ^{59}Ni contribution to helium generation can be very large or very small. The largest contributions will be in mixed spectra reactors such as the High Flux Isotope Reactor (HFIR) or light water power-generating reactors, as shown in Figs. 9 and 10. The thermal-to-fast neutron ratios for these cases are $\sim 2:1$ (PTP) and $\sim 0.2:1$, respectively.

4. DAMAGE MECHANISMS AND RECOIL EFFECTS

The $^{59}\text{Ni}(n,p)$ and (n,α) reactions are very exothermic, producing both charged particles and heavy atomic recoils which lead to radiation damage. At thermal neutron energies, the (n,p) reaction produces a 1.824 MeV proton and a 0.031 MeV ^{59}Co recoil atom, whereas the (n,α) reaction produces a 4.757 MeV alpha and a 0.340 MeV ^{56}Fe recoil atom. The displacements per atom produced by these reactions can be calculated using the Lindhard energy partition between electronic and nuclear stopping reactions, and assuming the secondary atomic displacements are given by $0.8 T_{\text{dam}}/2E_d$, where T_{dam} is the nuclear stopping energy and E_d is the energy required to displace an atom, which is 40 eV for nickel. The $^{59}\text{Ni}(n,\gamma)$ reaction will also produce a small amount of displacement damage, since the value of T_{dam} is 0.491 keV for this reaction [14]. In a previous publication [12] it was shown that the net displacements per atom (dpa) caused by the $^{59}\text{Ni}(n,\alpha)$ reaction equals 1 dpa for every 567 appm of helium. However, this analysis did not include the weaker contributions of the (n,p) and (n,γ) reactions. Each helium reaction leads to 1762 displacements, whereas the hydrogen and gamma reactions produce 222 and 4.9 displacements, respectively. Weighing by the respective cross sections, all reactions operating on ^{59}Ni result in the corrected relationship of 1 dpa for every 548 appm of helium, a net increase in damage of 3.5%. The

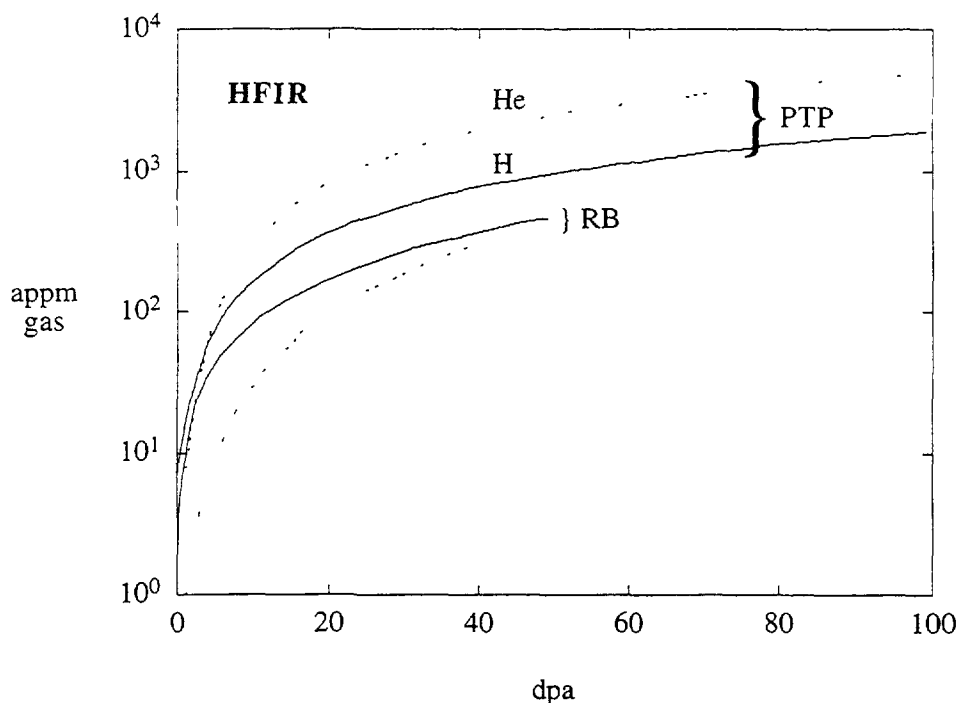


FIGURE 9. Hydrogen and helium production for the Peripheral Target Position (PTP) and Rotating Blanket (RB) positions of HFIR [2]. The late-term decrease in generation rates reflects the progressive burn-out of both ^{58}Ni and ^{59}Ni in the highly thermalized neutron spectra. The RB position has a thermal shield which decreases the ^{59}Ni production, reversing the balance between He and H generation compared to that of the PTP position.

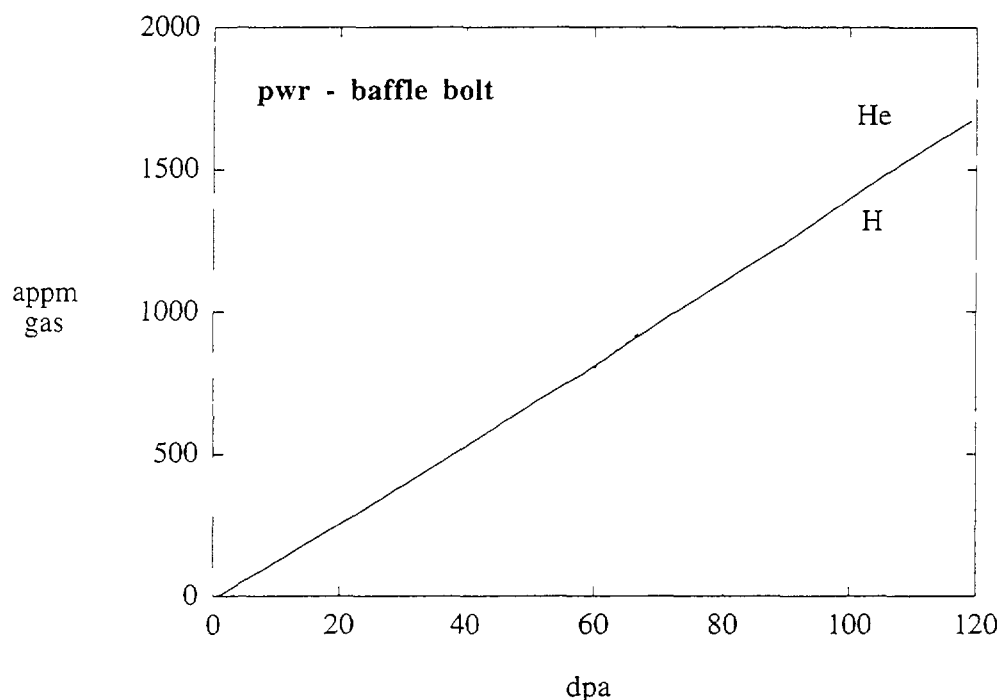


FIGURE 10 Helium and hydrogen production for the mid-core baffle bolt position of a typical pressurized water reactor [2]

equivalent damage ratio for hydrogen is 1 dpa for every 90 appm of hydrogen. The above values are calculated for a thermal neutron spectrum. Energies and displacements will increase somewhat for fast neutron reactions with ^{59}Ni , however, these effects are generally small due to the much lower fast neutron cross sections and the very exothermic nature of the reactions.

The alpha and proton recoils from the ^{59}Ni reactions have ranges of 9.5 and 15.7 μm , respectively, in stainless steel from interactions with thermal neutrons. Since these ranges greatly exceed the scales of both radiation-induced segregation and microstructural inter-sink distances, there is little measurable influence of nickel segregation on the distribution of either transmutant gas atom, except near surfaces where energetic recoils out of the specimen may cause some depletion.

5 CONCLUSIONS

Although the helium/dpa ratios tend to increase due to the progressive build-up of ^{59}Ni in the spectrally-soft regions of FFTF, especially in the below-core basket, a similar process does not contribute significantly in those regions of EBR-II where most high fluence experiments were conducted.

When calculating the hydrogen generated concurrently with helium, however, one must take into account the often overlooked ^{59}Ni (n,p) production contribution, which can be particularly strong in mixed spectra reactors with strong thermal neutron populations. Inclusion of the ^{59}Ni (n,p) and (n, γ) contributions to the displacement rate with that of ^{59}Ni (n, α) requires only a small correction (~3.5%). The combined exothermic contributions of the three ^{59}Ni reactions contributes 1 dpa for every 548 appm of helium, compared to 1 dpa per 567 appm of helium calculated earlier without taking the (n,p) and (n, γ) reactions into account.

REFERENCES

- [1] Garner, F. A., Greenwood, L. R., and Harrod, D. L., "Potential High Fluence Response of Pressure Vessel Internals Constructed from Austenitic Steels", Proceedings Sixth International Symposium on Environmental Degradation in Nuclear Power Systems, Water Reactors, San Diego, CA (1993) pp. 783-790.
- [2] Greenwood, L. R., and Garner, F. A., "Hydrogen Generation Arising from the ^{59}Ni (n,p) reaction and its Impact on Fission-Fusion Correlations", Journal of Nuclear Materials, in press.
- [3] Abramov, E., Solovioff, G., and Eliezer, D., Journal of Nuclear Materials, 212-215 (1994) pp. 1406-1410.
- [4] Kiranov, V. V., Musina, M. V., and Rybin, V. V., Journal of Nuclear Materials, 191-194 (1992) pp. 1318-1322.
- [5] Zuluzhnii, A., Kopytyn, V., and Pestretov, S., Proceedings of All-Union Conference on Radiation Effects on TNR Materials, 2, CRISM (1990) p. 216.
- [6] Garner, F. A., Hamilton, M. L., Greenwood, L. R., Stubbins, J. F., and Oliver, B. M., Effects of Radiation on Materials: 16th International Symposium, ASTM STP 1175, American Society for Testing and Materials, Philadelphia (1993) pp. 921-939.
- [7] Garner, F. A., and Brager, H. R., Effects of Radiation on Materials: 12th International Symposium, ASTM STP 970, American Society for Testing and Materials, Philadelphia (1985) pp. 187-201.
- [8] Garner, F. A. and Kumar, A. S., Radiation-Induced Changes in Microstructure: 13th International Symposium (Part 1), ASTM STP 955, American Society for Testing and Materials, Philadelphia (1987) pp. 289-314.
- [9] Farrar IV, H. and Oliver, B. M., Journal of Vacuum Science Technology, A4 (1986) p. 1740.
- [10] Oliver, B. M., Bradley, J. G. and Farrar IV, H., Geochimica et Cosmochimica Acta, 48 (1984) p. 1759.
- [11] Greenwood, L. R., Kneff, D. W., Skoronski, R. P., and Mann, F. M., Journal of Nuclear Materials, 122-123 (1984) pp. 1002-1006.
- [12] Greenwood, L. R., Journal of Nuclear Materials, 116 (1983) p. 137.
- [13] Mughabghab, S. F., Divadeenam, M. and Holden, N. Z., Neutron Cross Sections, Academic Press (1981).
- [14] Greenwood, L. R., and Smither, R. K., ANL/FPP/TM-197, Argonne National Laboratory (1985).
- [15] Greenwood, L. R., Garner, F. A., and Oliver, B. M., Journal of Nuclear Materials, 212-215 (1994) pp. 492-497.

LIST OF PARTICIPANTS

Abonneau, E.	NOVATOM/FRAMATOM 10 rue Juliette Recamier, F-69006 Lyon, France
Averin, S.	Research and Development Institute of Power Engineering, Sverdlovsk Branch, SB RDIPE 624051 Zarechny, Sverdlovsk Region, Russian Federation
Bailie, J.	British Nuclear Fuels Plc, Sellafield, Seascale, Cumbria, United Kingdom
Baldev, R.	Indira Gandhi Centre for Atomic Research, Kalpakkam 603102, Tamil Nadu, India
Buksha, Yu.	State Scientific Centre Institute of Physics and Power Engineering, 1 Bondarenko Sq., Obninsk, Kaluga Region, 249020, Russian Federation
Fisher, S.	British Nuclear Fuels Plc, Sellafield Seascale, Cumbria, United Kingdom
Garner, F	Pacific Northwest National Laboratory Battelle Boulevard, P.O. Box 999, P8-15 Richland, Washington 99352, United States of America
Govindarajan, S.	Indira Gandhi Centre for Atomic Research Kalpakkam 603102, Tamil Nadu, India
Ioltukhovski, A.	Scientific and Research Institute of Inorganic Materials, (VNIINM), 5 Rogov str., Moscow, 123060, Russian Federation
Karaulov, V.	MAEC, NPP BN-350, 466200 Aktau, Kazakhstan
Khabarov, V.	State Scientific Centre Institute of Physics and Power Engineering, 1 Bondarenko Sq., Obninsk, Kaluga Region, 249020, Russian Federation
Kisly, V.	Research Institute of Atomic Reactors, Dimitrovgrad, 433510, Russian Federation

Kochetkov, L.	State Scientific Centre Institute of Physics and Power Engineering, 1 Bondarenko Sq., Obninsk, Kaluga Region, 249020, Russian Federation
Konobeev, Yu.	State Scientific Centre Institute of Physics and Power Engineering, 1 Bondarenko Sq., Obninsk, Kaluga Region, 249020, Russian Federation
Kozlov, A.	Research and Development Institute of Power Engineering, Sverdlovsk Branch, SB RDIPE 624051 Zarechny, Sverdlovsk Region, Russian Federation
Kuznetsov, V.	Scientific and Research Institute of Inorganic Materials, (VNIINM), 5 Rogov str., Moscow, 123060, Russian Federation
Materna-Morris, E.I.	Forschungszentrum Karlsruhe, Postfach 3640, D-76021 Karlsruhe, Germany
Mitrofanova, N.	Scientific and Research Institute of Inorganic Materials, (VNIINM), 5 Rogov str., Moscow, 123060, Russian Federation
Moseev, L.	State Scientific Centre Institute of Physics and Power Engineering, 1 Bondarenko Sq., Obninsk, Kaluga Region, 249020, Russian Federation
Neustroev V.	Research Institute of Atomic Reactors, Dimitrovgrad, 433510, Russian Federation
Poplavsky V.	State Scientific Centre Institute of Physics and Power Engineering, 1 Bondarenko Sq., Obninsk, Kaluga Region, 249020, Russian Federation
Popov V.	State Scientific Centre Institute of Physics and Power Engineering, 1 Bondarenko Sq., Obninsk, Kaluga Region, 249020, Russian Federation
Porollo, S.	State Scientific Centre Institute of Physics and Power Engineering, 1 Bondarenko Sq., Obninsk, Kaluga Region, 249020, Russian Federation
Rinejski, A.	International Atomic Energy Agency, Wagramer Strasse - 5, P.O. Box 100, A-1400 Vienna, Austria

Staroverov, A.	Experimental Machine Building Bureau (OKBM), 603603 Nizhny Novgorod-74, Russian Federation
Tchuev, V.	NPP BN-600,624 051 Zarechny, Sverdlovsk Region, Russian Federation
Troyanov, V.	State Scientific Centre Institute of Physics and Power Engineering, 1 Bondarenko Sq., Obninsk, Kaluga Region, 249020, Russian Federation
Voevodin V.	National Science Centre Institute of Physics and Technology, Kharkov, Ukraine
Xu Yongli	China Institute of Atomic Energy P.O. Box 275 (53), Beijing, 102413, China
Yarovitsin, V.	State Scientific Centre Institute of Physics and Power Engineering, 1 Bondarenko Sq., Obninsk, Kaluga Region, 249020, Russian Federation
Zabudko, L.	State Scientific Centre Institute of Physics and Power Engineering, 1 Bondarenko Sq., Obninsk, Kaluga Region, 249020, Russian Federation